DRAFT

Performance of Caltrans Asphalt Concrete and Asphalt-Rubber Hot Mix Overlays at Moderate Temperatures—Accelerated Pavement Testing Evaluation

John Harvey, Manuel Bejarano,

Ana Fantoni, Andrew Heath, Hee-Cheol Shin

Prepared for the California Department of Transportation

December, 2000

TABLE OF CONTENTS

LIST OF FIGURES

LIST OF TABLES

1.0 INTRODUCTION AND BACKGROUND

1.1 Caltrans Flexible Pavement Overlay Strategies

Caltrans uses overlays of flexible pavements for both maintenance and rehabilitation. Overlays are the primary rehabilitation strategy for flexible pavements that have cracking or ride quality problems.

Maintenance overlays are typically thinner than rehabilitation overlays, and are intended to improve ride quality, or to seal the surface of the pavement to water. They provide minimal increase in the structural capacity of the pavement and are sometimes referred to as "thin blankets."

Rehabilitation overlays are intended to increase the structural capacity of the pavement to a level necessary to withstand 10 years of expected traffic (traditional rehabilitation designs), or to provide increased structural capacity to the pavement through the application of a standard thickness of overlay (Capital Preventive Maintenance overlays).

Caltrans is currently moving toward a philosophy of "preventative maintenance and rehabilitation," with increased funding in the Capital Preventive Maintenance (CAPM) program. The primary objective of preventive maintenance is to increase the structural capacity of flexible pavements by overlaying pavements exhibiting minor to moderate visible damage before they reach a state of advanced deterioration. Widespread cracking, in which the cracks having lost much of their aggregate interlock, would be considered a state of advanced deterioration.(*1*)

It is generally understood that the cost of restoration of structural capacity to flexible pavements typically increases significantly over the often short period of time between observation of cracking on the surface and a state of advanced deterioration. Once cracking has propagated from the bottom of the asphalt concrete to the surface, rainwater can penetrate the

cracks and infiltrate the asphalt concrete and underlying unbound pavement layers. The interaction of the water with heavy traffic loading is typically responsible for the rapid increase in damage and the increase in cost of structural capacity restoration.

The traditional material used for overlays of flexible pavements is dense graded asphalt concrete (DGAC). Caltrans has also used asphalt-rubber hot mix gap-graded (ARHM-GG) for overlays for approximately the last 20 years.(*2*) Typical thicknesses for Caltrans DGAC and ARHM-GG overlays in each of the maintenance and rehabilitation categories are summarized in Table 1.1.

Table 1.1 Summary of Typical Overlay Thicknesses for Caltrans Overlay Categories (*2, 3*).

Overlay Program Category	Typical DGAC Overlay Thickness	Typical ARHM-GG Overlay Thickness
Maintenance	30 mm (0.1 ft.) or less	30 mm (0.1 ft.) or less
Capital Maintenance (CAPM)	76 mm (0.25 ft.)	45 mm (0.15 ft.)
Rehabilitation	Determined from deflection study	Typically 0.5 to 0.67 times the thickness of DGAC overlay thickness determined from deflection study

Although Caltrans has many years of experience with ARHM-GG overlays, the strategy was not used routinely until 1995. In the period of fiscal years 1995/96 through 1997/98, ARHM-GG was used on 2.4 percent of the lane-km overlaid with contracted maintenance overlays, and 10.8 percent of the lane-km overlaid with CAPM overlays.(*3*) Caltrans information indicates that ARHM-GG was not used for rehabilitation overlays of flexible pavements, at least before fiscal year 98/99.(*4*) Lane-kilometers overlaid and average costs per lane-kilometer for the two types of material over the six fiscal years from 1992/93 to 1997/98 are summarized in Table 1.2.

Table 1.2 Summary of Costs and Extent of Implementation of Caltrans Flexible Pavement Overlay Categories(*3, 4*)

Overlay Program Category	Fiscal Years 92/93 – 94/95				Fiscal Years 95/96 – 97/98			
	Cost per Lane-km		Lane-km Treated		Cost per Lane-km		Lane-km Treated	
	DGAC	ARHM-GG	DGAC	ARHM-GG	DGAC	ARHM-GG	DGAC	ARHM-GG
Maintenance	$ 12,884	N/A	2,577	N/A	$ 12,775	$ 23,887	5,711	138
CAPM	N/A	N/A	N/A	N/A	$ 38,555	$ 27,946	2,901	312
Rehabilitation	$ 129,979	N/A	2,709	N/A	$ 103,079	N/A	2,933	N/A

N/A = not applicable.

In 1993, the average cost of Type A DGAC was $31.5 per ton for quantities of 5,000 tons or more. In the same year, the average cost per ton of ARHM-GG was $56.5 per ton for quantities of 1,000 to 10,000 tons, and $40.8 per ton for 10,000 or more tons. Thus, the cost per ton of ARHM-GG is from 30 to 80 percent more than that of DGAC.(5) The differences in cost per lane-kilometer treated, as shown in Table 1.2, are dependent upon the thickness used (Table 1.1) and the unit costs of the two materials.

Generally, it is anticipated that the unit cost of both DGAC and ARHM-GG materials will go down if sufficient quantities are purchased so that the contractors can obtain greater efficiency through economies of scale. The other major factors influencing the unit costs are labor costs and the costs of raw materials, in this case asphalt, aggregate, and rubber. The influence of job size and economies of scale that contractors can translate into lower costs for Caltrans can be seen in the price break between jobs with 1,000 to 10,000 tons and 10,000 and more tons, as discussed earlier. It can also be seen in the difference in cost per lane-kilometer of ARHM-GG overlays for maintenance and CAPM projects. Although CAPM projects typically use 50 percent more material per lane-kilometer (Table 1.1), the average cost per lane-kilometer for CAPM projects is only increased by 17 percent (Table 1.2).

The key issue for Caltrans design and maintenance engineers is the selection of the most cost effective overlay strategy for each project, with cost effectiveness determined by Life Cycle Cost Analysis (LCCA). To perform LCCA, two types of information are necessary:

- the cost per lane-kilometer of each strategy, incorporating the unit cost of the material and the thickness used, and
- the performance of each strategy, in terms of truck load repetitions to reach a defined failure condition, translated to years.

The cost per lane-kilometer of the strategies is known, and is summarized in Table 1.2 [broken down by individual fiscal years in Reference (*3*)].

A major objective of the work presented in this report is to quantify the relative performance of DGAC and ARHM-GG overlays using accelerated pavement testing with the Heavy Vehicle Simulator. A previous study by the University of California Berkeley Contract Team in 1993 indicated that ARHM-GG overlays placed at half the thickness of DGAC overlays had superior performance with respect to reflection cracking under HVS loading on a flexible pavement with a very thin, cracked surface treatment.(*6*) Caltrans desired that a similar study be repeated on thicker pavement structures, more typical of California pavements, and constructed using California materials and contractors.

1.2 Overlay Distress Mechanisms in California

Fatigue cracking or reflection cracking are the two primary modes of distress that lead to failure of DGAC and ARHM-GG overlays for maintenance, CAPM, or rehabilitation.

1.2.1 Fatigue and Reflection Cracking

Fatigue cracking and reflection cracking are caused by repeated stresses and strains in the overlay. Fatigue cracking of overlays typically begins at the bottom of the overlay, and is caused by repeated tensile strains from traffic loading. Fatigue cracking can begin at the top of the overlay under certain conditions, and this distress mechanism is referred to as "top down fatigue cracking". A fatigue cracking typically begins as longitudinal or transverse cracks in the wheelpath. The longitudinal cracks are eventually connected by transverse cracks, or the transverse cracks are connected with longitudinal cracks after more traffic loading. With continued loading, and the entrance of water and dust, the cracks lose aggregate interlock and individual "cobbles" begin rock independently under traffic. The locations where fatigue cracks begin at the bottom of the asphalt concrete layer are determined by the locations of maximum strains and random variation of the properties of the asphalt concrete.

Reflection cracking is also caused by repeated stresses and strains in the overlay. In this sense, reflection cracking is a form of fatigue. However, reflection cracking is different from fatigue cracking because the locations of the reflection cracks are determined by the locations of existing cracks in the underlying pavement. Stresses and strains are concentrated at existing cracks and those stresses and strains are transferred to the bottom of the overlay at those locations. Reflection cracking is easily identifiable if the crack pattern on the surface of the underlying pavement before the overlay reappears on the surface of the overlay.

Reflection cracking also differs from fatigue cracking with regard to the types of stresses and strains that occur because of the cracked condition of the underlying pavement. Tensile strains and stresses occur as with fatigue cracking, however they can be caused by day to night temperature changes which open and close the cracks, as well as traffic. Shear stresses and

strains also occur at the crack and are transferred to the overlay as traffic loads pass from one side of a transverse crack to the other.

Overlays can develop cracking through either fatigue mechanism, or the reflection mechanism. In general, fatigue cracking will predominate when the overlay is thick relative to the thickness of the cracked existing layer and the existing underlying layer is cracked to the extent that stresses and strains are not concentrated at a few locations. Milling or otherwise breaking up and compacting the existing cracked asphalt concrete will cause it to behave as an unbound granular base, which will not transmit tensile or shear stresses to the bottom of the overlay.

Reflection cracking will predominate when the overlay thickness is thin relative to the thickness of the underlying cracked asphalt concrete and the existing asphalt concrete has distinct cracks but is not completely broken up.

The original development of the current Caltrans overlay design procedure (CTM 356) in the 1950s and 1960s was based on data from relatively thick overlays over relatively thin existing asphalt concrete layers. The assumption is that these overlays would fail by the fatigue mechanism, not reflection cracking. This assumption was probably valid for the majority of those projects. Since that time Caltrans' flexible pavements have become thicker because of increased traffic loading and successive overlays. At this time, the same method is being used to design relatively thin overlays, such as the CAPM and maintenance overlays, over relatively thick existing cracked asphalt concrete layers. Although the method still assumes that fatigue is the primary distress mechanism, it is likely that most of these pavements fail because of reflection cracking. The method has been amended, and a system of overlay thicknesses has been developed that is intended to mitigate reflection cracking. However, the data used to

develop that system is limited, and has not been thoroughly calibrated against actual field performance. The method also does not account for differences in traffic load repetitions or climate region, and thus the two sources of stresses and strains that cause reflection cracking are not included in the method.

1.2.2 Other Overlay Distress Modes

Other distress modes include rutting of the mix, delamination, and "stripping" (damage to and loss of binder adhesion in asphalt bound materials due to exposure to water). Each of these distresses can occur in both DGAC and ARHM-GG overlays. Rutting typically occurs within the first five years after construction if it is going to occur at all, and can be controlled in the mix design process through selection of aggregate gradation and source, asphalt binder properties, binder content, and compaction. A separate report (*7*) describes the rutting performance of the DGAC and ARHM-GG overlays discussed in this report.

Delamination, the loss of adhesion between the overlay and the existing pavement surface, typically occurs when an insufficient tack coat is used to bind the overlay to the existing surface. Delamination can also occur if water is able to penetrate the overlay, through cracks or poor compaction, and becomes trapped between the overlay and the underlying pavement. The trapped water can then cause the tack coat to lose its effectiveness, and can cause stripping at the underside of the overlay. Delamination is controlled through application of a suitable tack coat, and through good compaction of the overlay to reduce its permeability and increase its resistance to cracking.

1.3 Caltrans Overlay Thickness Design

The Caltrans design method for DGAC overlay thickness for structural (rehabilitation) overlays is based on surface deflections and component analysis, and empirical estimates of thickness to retard reflections cracking [California Test Method 356 (*8*)]. The thickness design method for ARHM-GG overlays is based on the DGAC design thickness and other criteria, which are included in a thickness design guide document published by the Caltrans Engineering Service Center.(*9*) The structural and reflection cracking equivalencies of ARHM-GG compared to DGAC have evolved over the years, primarily based on observations of test section performance.(*2*)

Following Caltrans guidelines, the maximum ARHM-GG overlay thickness is 60 mm, and the minimum is 30 mm. ARHM-GG to DGAC equivalence ratios range from 1.5 to 2.0 for structural applications in which fatigue cracking is the expected distress mode, and 1.5 to 2.33 for structural applications in which reflection cracking is the expected distress mode. Inversely, ARHM-GG thicknesses are 0.67 to 0.5 times those of the corresponding DGAC overlay for fatigue cracking, and 0.50 to 0.43 times those of the DGAC overlay for reflection cracking. The structural and reflection cracking ratios are larger if a Stress Absorbing Membrane Interlayer (SAMI) is placed between the existing pavement and the ARHM-GG overlay.

For the comparison performed in this experiment, the thickness ratio of ARHM-GG to DGAC overlays was designed using standard Caltrans procedures for rehabilitation designs (*8*–*10*): the ARHM-GG overlay was half the thickness of the DGAC overlay.

To be selected based on Life Cycle Cost Analysis, ARHM-GG must have better performance than DGAC for the same thickness of overlays, or similar performance when the ARHM-GG overlay is thinner, to offset its higher unit cost. Caltrans uses the same thickness for maintenance overlays (Tables 1.1 and 1.3) regardless of the overlay type. To be cost effective,

the ARHM-GG must therefore have better performance than DGAC. Using the data from Tables 1.1 and 1.2, it can be calculated that the ARHM-GG maintenance overlay must have 90 percent better performance in terms of Net Present Value of future work required in the analysis period to be cost effective (Table 1.3).

Caltrans uses thinner ARHM-GG overlays compared to DGAC overlays for CAPM projects. To be cost effective, the difference in thickness must offset the greater cost of the overlay. Using the data from Tables 1.1 and 1.2, the thickness reduction required to offset the greater initial cost of CAPM projects in terms of Net Present Value of future work required in the analysis period must about 30 percent (Table 1.3). It is assumed that the ratio of costs of CAPM and rehabilitation overlays will be similar for the two material types, which suggests that rehabilitation overlays must also be about 30 percent thinner than DGAC overlays to be cost effective.

The results in Table 1.3 indicate that ARHM-GG is probably as cost effective as DGAC if it provides double the life of same thickness DGAC maintenance overlays, and that ARHM-GG is probably more than cost effective if the current thickness guidelines for CAPM and rehabilitation overlays provide similar performance as current thicknesses of DGAC.

Table 1.3 Comparison of Initial Cost Ratios for Caltrans ARHM-GG and DGAC Overlays.[*]

Overlay Program Category	Initial Cost per Lane-km[†]		Initial Cost Ratio	Current Thickness Ratio[§]
	DGAC	ARHM-GG	ARHM/DGAC	ARHM/DGAC
Maintenance	$ 12,775	$ 23,887	1.9	1.00
CAPM	$ 38,555	$ 27,946	0.7	0.59
Rehabilitation	$ 38,555		0.7[‡]	0.43 to 0.67

[*] The results presented in Table 1.1 are simplistic and are not based on full LCCA with discounted future costs and a reasonable analysis period. They are only intended to provide a rough indication of thickness versus initial cost ratios.
[†] from Table 1.2
[‡] assumed same as CAPM
[§] from Table 1.1

1.4 Caltrans Overlay Mix Design

Selection of optimum binder content in the mix design for DGAC is performed following California Test Method 367.(*8*) The criteria for DGAC binder content selection are minimum value for Hveem stabilometer [CTM 366 (*8*)], 4 percent air-void content under standard kneading compaction [CTM 304, 308 (*8*)], and a "flushing" criterion for which the technician determines whether the mix looks over-asphalted. The minimum Hveem stabilometer value for 19-mm maximum aggregate size DGAC Type A is 37.

Mix design for ARHM-GG is performed following guide documents published by the Caltrans Engineering Service Center. The current criteria are a minimum Hveem stabilometer value of 23, a minimum air-void content of 4 percent under standard kneading compaction, and a minimum 18 percent Voids in the Mineral Aggregate (VMA). The air-void content under laboratory compaction criterion is 3 percent when less than about 35,000 equivalent single axle loads (ESALs) are expected in the 10-year design life of the overlay, or when the maximum ambient air temperature is not expected to exceed 35°C. The air-void content criterion is 5 percent in desert areas where more than about 3,500,000 ESALs are expected in the 10-year design life.(*2*)

In addition to these requirements, allowable binder contents for ARHM-GG are constrained to be within the range of 7.0 to 9.5 percent (by mass of aggregate). Dense graded asphalt rubber hot mix (ARHM-DG) must be within 6.5 and 8.5 percent (by mass of aggregate).(*2*)

These mix design requirements are based on experience gained through a trial and error process over the past 20 years. That process has included many successful applications of ARHM-GG overlays, and a few severe rutting failures of ARHM-GG overlay projects in desert areas with heavy traffic, which lead to the current version of the mix design requirements.

Caltrans has recently been working on performance based specifications for ARHM. In several cases, a performance based mix design procedure developed as part of the Strategic Highway Research Program (SHRP) at the University of California, Berkeley has indicated the need for lower binder contents for ARHM-GG than were recommended using the Caltrans criteria. These cases were primarily in hot desert locations and locations with heavy traffic. The UCB procedure includes the use of the Repeated Simple Shear Test at Constant Height (RSST-CH).

The relatively small proportion of ARHM-GG overlays compared to DGAC overlays is likely due to the following considerations:

- Uncertainty about the relative life cycle costs of ARHM-GG versus DGAC because of the lack of good comparative performance data from typical Caltrans applications, and because the cost per ton including construction of ARHM-GG in place is greater than the cost of DGAC (although the cost data from 1993 indicate that the differential is more than offset by use of reduced thicknesses), and
- Uncertainty about the ability of the Caltrans mix design criteria to prevent rutting failures, in part because ARHM-GG does not meet the criteria for Hveem stabilometer values used for DGAC, despite the performance history which suggests that ARHM-GG typically has adequate rutting performance as used by Caltrans.

It has been suggested that greater use of ARHM-GG as an overlay strategy by Caltrans is warranted, provided that the material can routinely be designed and constructed to provide performance that results in a lower life cycle cost than the DGAC overlay strategy. However, if life cycle costs for ARHM-GG are greater than those for DGAC, then the use of ARHM-GG is

not warranted. ARHM-GG is assumed to be as recyclable as DGAC, although this assumption remains to be proven.

1.5 Objectives

The objective of CAL/APT Goal 3 is to evaluate the long-term and short-term performance of the two overlay strategies. Long-term performance is defined as failure from fatigue cracking, reflection cracking, or rutting of the unbound pavement layers. Short-term performance is defined as failure by rutting of the asphalt bound materials, including the overlay, underlying asphalt concrete, or asphalt treated permeable base (ATPB). Life cycle cost is dependent upon both long-term and short-term performance.

The rutting performance under accelerated pavement testing of the ARHM-GG and DGAC overlays, whose long-term performance is evaluated in this report, was presented in Reference (*7*). Laboratory testing and analysis is currently underway to permit the extrapolation of the accelerated pavement testing results included in this report and Reference (*7*) to various pavement structures, various levels of construction quality, various climates, and various traffic loading scenarios. The results of the laboratory testing and analysis will be included in later reports.

The laboratory test and Heavy Vehicle Simulator (HVS) test experiments for the evaluation of the long-term performance of the overlays strategies were designed to meet the following objectives (*11*):

1. Validation of the existing deflection-based Caltrans thickness design procedures for DGAC and ARHM-GG with respect to fatigue cracking, reflection cracking, and rutting of the unbound layers (depending upon the failure mode that actually occurs in the test sections);

2. Validate mechanistic-empirical procedures for fatigue and unbound layer rutting;
3. Quantify the effective elastic moduli of the various pavement layers;
4. Determine the failure mechanisms of the two overlay strategies at moderate temperatures;
5. Determine the permanent deformation behavior in all the layers at moderate temperatures;
6. Evaluate the flexural stiffness and flexural fatigue cracking resistance of the overlay materials for different temperatures and strain levels by means of laboratory flexural beam testing;
7. Evaluate the shear fatigue resistance and tensile fatigue resistance, and the fatigue resistance under combined shear and tensile loading, using laboratory reflection crack device testing, and
8. Quantify the effects of construction variation on performance at moderate temperatures (long-term performance) from the laboratory testing results and mechanistic analysis.

Results relating to Objectives 1, 3, 4, and 5 are included in this report. Information regarding completion of the remaining objectives will be included in Goal 3 reports that will follow this report. An evaluation of the Caltrans overlay design procedure (CTM 356) with respect to pavement temperatures at the time of deflection measurement, and the correspondence between Dynaflect, Benkelman Beam, and Falling Weight Deflectometer deflections is included in Reference (*10*).

1.6 Scope of this Report

This report presents results from accelerated pavement tests using the Caltrans Heavy Vehicle Simulator (HVS) of DGAC and ARHM-GG overlays placed at the University of California Berkeley Pavement Research Center. The results presented in this report are from four tests conducted at 20°C to evaluate the performance of the two overlay strategies with respect to cracking (fatigue or reflection), and rutting of the unbound pavement layers.

Both overlay strategies were evaluated on previously tested drained and undrained flexible pavement structures. The overlays were placed on existing flexible pavement structures, sections of which were previously tested as part of CAL/APT Goal 1.(*12–16*) The mix designs and thickness designs for the overlays and their construction are included in References (*10, 11*).

2.0 HVS TEST EXPERIMENT DESIGN

The experiment design to evaluate the long-term performance of the Goal 3 overlays for the four HVS test sections included the following variables:

- **Overlay type:** asphalt-rubber hot mix gap-graded (ARHM-GG) and dense graded asphalt concrete (DGAC).
- **Overlay thickness:** the design thickness for the two ARHM-GG overlays was 38 mm. The design thickness for the two DGAC overlays were 62 and 75 mm. The DGAC overlay thicknesses were assumed equal for the experiment design because the 62-mm overlay was placed over a DGAC patch designed to be 12.5 mm thick.
- **Underlying pavement structure:** each overlay type was placed on both a drained flexible structure and an undrained flexible structure.

The matrix of primary experiment variables, associated test section numbers, and the numbers of the underlying previously failed test sections are shown in Table 2.1.

Table 2.1 Matrix of HVS Test Experiment Variables and Test Numbers.

	75-mm Dense Graded Asphalt Concrete (DGAC) Overlay	**38-mm Asphalt Rubber Hot Mix – Gap Graded (ARHM-GG) Overlay**
Drained Structure (with ATPB layer)	514 (over previously failed 500RF)	515 (over previously failed 502CT)
Undrained Structure (no ATPB layer)	517 (over previously failed 501RF)	518 (over previously failed 503RF)

2.1 Layout of Test Sections

The Goal 3 cracking test sections were located on the Richmond Field Station (RFS) pavement structures as shown in Figure 2.1.

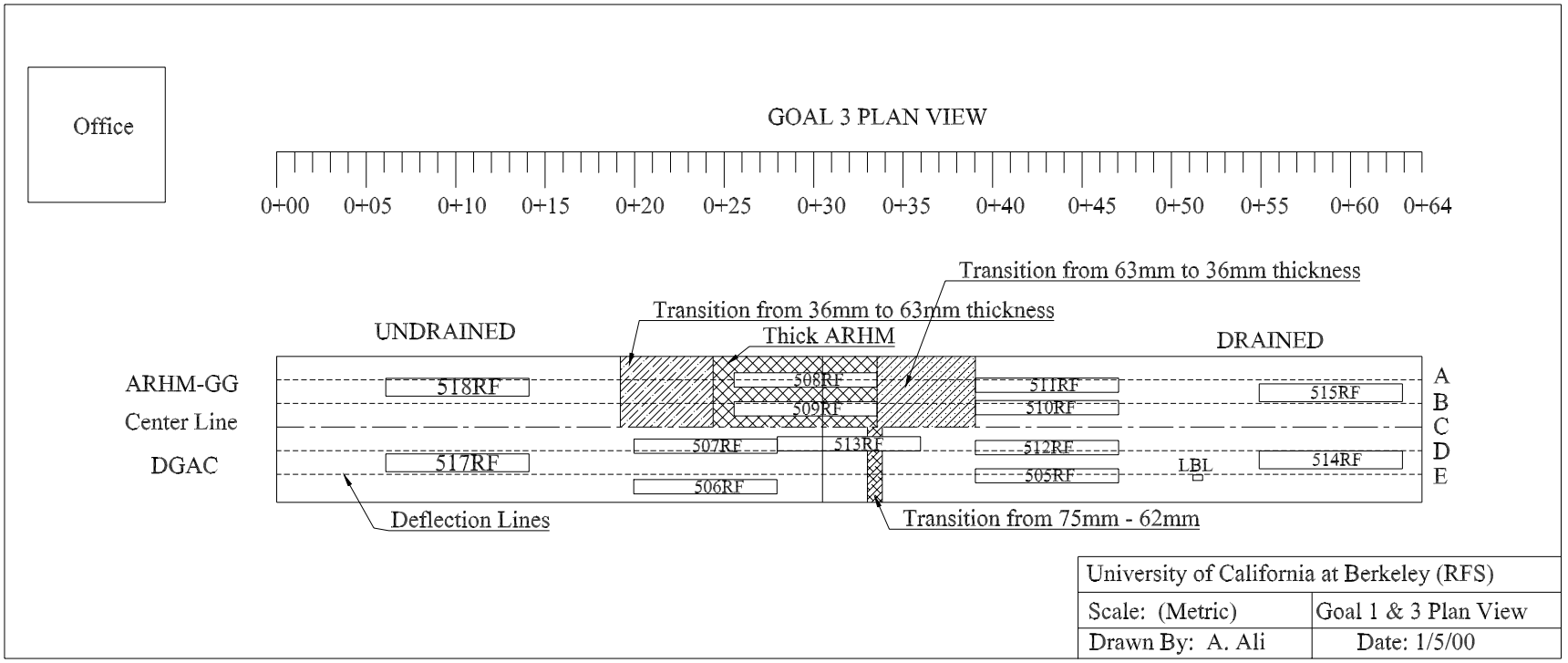

Figure 2.1. Layout of Goal 3 HVS tests sections—Section 514.

2.2 Pavement Structures

The Goal 3 overlays were constructed upon the four previously failed Goal 1 pavement test sections (500RF, 501RF, 502RF, 503RF). The Goal 1 structures included two types: "drained" containing an Asphalt Treated Permeable Base (ATPB) layer, and "undrained" containing no ATPB layer. The drained pavement structures are shown in Figure 2.2, and the undrained structures in Figure 2.3.

The design of the Goal 1 drained and undrained pavement structures is presented in detail in Reference (*12*). The designs of the Goal 3 ARHM-GG and DGAC overlays are presented in detail in References (*10, 11*).

The Goal 1 test sections beneath the Goal 3 test sections had been subjected to substantial trafficking prior to the overlays. The condition of each section at the completion of trafficking is presented in detail in References (*10, 13–16*), and briefly summarized with respect to previous trafficking, cracking, and rut depth in each layer in Tables 2.2, 2.3, and 2.4, respectively.

Table 2.2 Accumulated Trafficking and Equivalent Single Axle Loads (ESALs) at Completion of Goal 1 Trafficking (*11–16*)

	500RF (overlaid by 514)	**501RF (overlaid by 517)**	**502CT (overlaid by 515)**	**503RF (overlaid by 518)**
Repetitions at 40 kN	150,000	150,000	150,000	150,000
Repetitions at 80 kN	50,000	50,000	50,000	50,000
Repetitions at 100 kN	2,372,372	1,226,467	2,473,589	1,711,823
Total Equivalent Single Axle Loads (ESAL)*	112,400,000	58,600,000	117,100,000	81,400,000

*assuming load equivalence exponent of 4.2

Table 2.3 Average Crack Length per Area at Completion of Goal 1 Trafficking (*7*)

Crack Length. m/m^2			
500RF (overlaid by 514)	**501RF (overlaid by 517)**	**502CT (overlaid by 515)**	**503RF (overlaid by 518)**
2.5	9.6	4.0	6.5

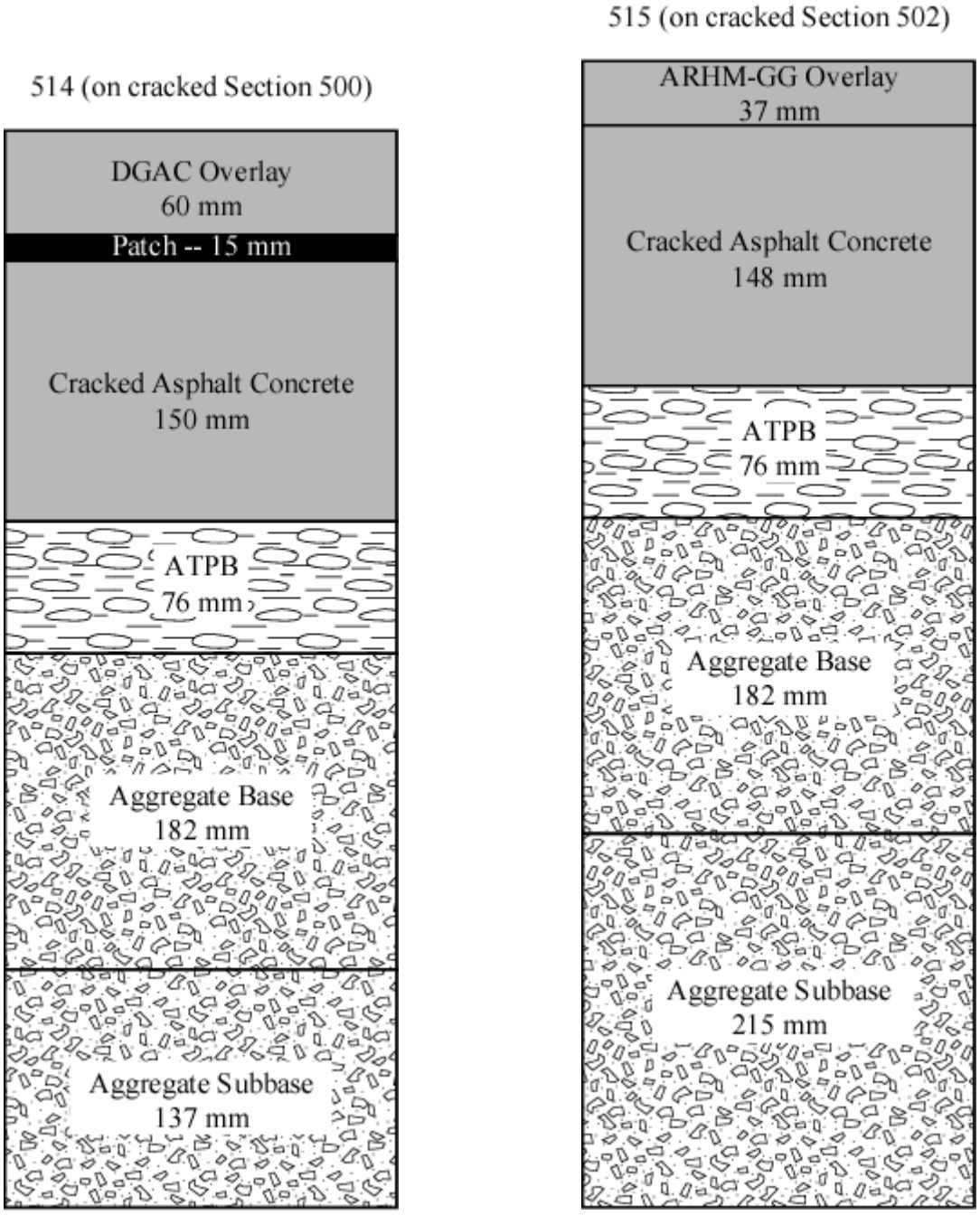

2.2a **2.2b**

Figure 2.2. Design drained pavement structures (Sections 514, 515).

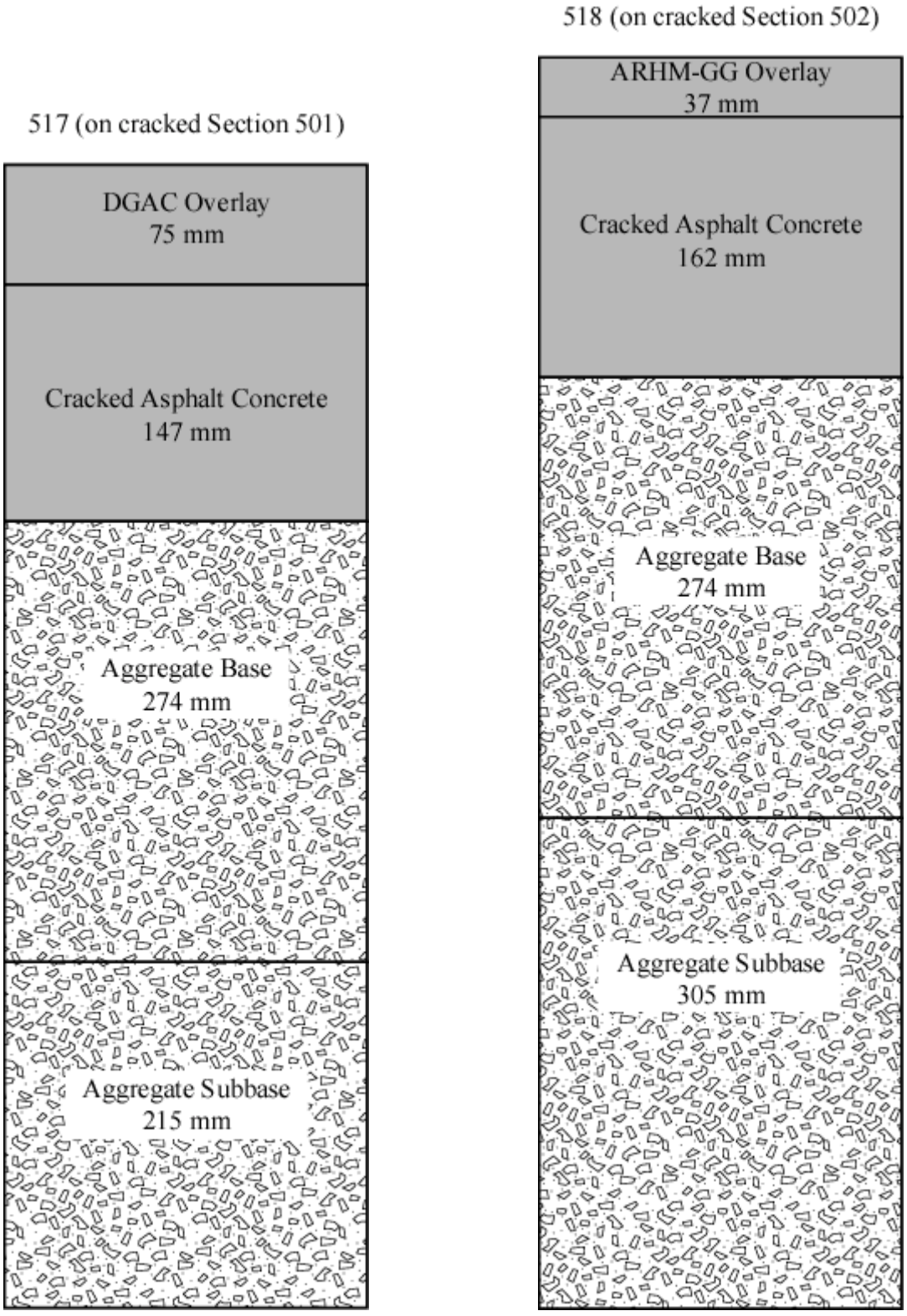

2.3a **2.3b**

Figure 2.3. Design undrained pavement structures (Sections 517, 518).

Table 2.4 Vertical Permanent Deformation in Each Layer at Completion of Goal 1 Trafficking (*10*)

Pavement Layer	Permanent Deformation, percent			
	500RF (overlaid by 514)	**501RF (overlaid by 517)**	**502CT (overlaid by 515)**	**503RF (overlaid by 518)**
Asphalt Concrete	52	52	68*	48
ATPB	7	not used		not used
Aggregate Base	17	26	16	33
Aggregate Subbase	12	11	6	17
Subgrade	12	11	10	2
Final Rut Depth (mm)	*15*	*11*	*14*	*11*

*includes asphalt concrete and ATPB

It can be seen that each of the four test sections beneath the overlay test sections had been subjected to significant trafficking, and that all had a high level of cracking. Limited coring data at the completion of the Goal 1 trafficking indicated that on all four sections, the cracking was in the top lift of the two asphalt concrete lifts (Figures 2.2 and 2.3), and that the bottom of the two lifts remained uncracked. The cores also indicated that all four sections had no bond between the two asphalt concrete lifts. The lack of bonding was attributed to lack of a tack coat between the two lifts during Goal 1 construction, and the fact that all of the Goal 1 trafficking was at moderate temperatures (20°C).(*10*)

2.2.1 Materials

The pavement materials in the rutting test sections are described in detail in previous reports. The materials and construction of the pavement structure beneath the overlays is described in Reference (*12*). The overlay materials and construction are described in Reference (*10*). The material properties important to understanding the cracking performance of the test sections are summarized in the following sections.

2.2.1.1 Overlay Mixes

The ARHM-GG and DGAC materials were specified as follows in the bid documents for the Goal 3 overlays:

> *DGAC shall meet Caltrans Standard Specificatons for 19 mm (3/4 in.) Type A, coarse gradation asphalt concrete.*
>
> *ARHM-GG shall meet Caltrans Standard Special Provisions for 12.5 mm (1/2 in.) Type 2, gap-graded asphalt rubber hot mix. The mix design shall be based on a 4 percent air-void content.*

The mix design aggregate gradations, contract compliance ranges determined following Caltrans standard specifications, and results of extractions from belt samples taken at the plant are shown in Tables 2.5 and 2.6. Both mix design gradations were within Caltrans specifications for target limits.

Table 2.5 Summary of Extracted Gradation and Binder Content for DGAC Overlay Mix (*10*)

	Percent Passing Sieve Size			
Sieve Size (mm)	**Mix Design**	**Permissible Operating Range** †	**Extracted (Average)**	**Extracted (Standard Deviation)**
19	100	90–100	99.8	0.6
12.5	93		95.2	1.9
9.5	73	60–75	76.4	2.6
4.75	50	45–55	52.3	2.0
2.36	39	34–44	36.6	1.5
1.18	27		27.4	1.1
0.60	18	13–23	22.3	1.0
0.30	11		17.2	0.7
0.15	6		9.3	0.5
0.075	5	3–7	6.8	0.3
Binder Content * *(%)*	*5.0–5.3*		*5.1*	*0.1*

* Percent by mass of aggregate

† Per Section 39 Caltrans Standard Specifications)

Table 2.6 Summary of Extracted Gradation, Binder Content and Rubber Content for ARHM-GG Mix.(*10*)

Sieve Size (mm)	Percent Passing Sieve Size			Extracted (Standard Deviation)
	Mix Design	Permissible Operating Range ‡	Extracted (Average)	
19	100	100	100.0	
12.5	98	90–100	97.3	1.2
9.5	85	81–91	84.4	2.6
4.75	33	28–38	34.0	2.5
2.36	21	18–26	22.7	1.8
1.18	15		16.7	1.4
0.60	10	7–15	12.7	1.2
0.30	6		9.2	0.9
0.15	4		6.1	0.8
0.075	3	3–7	4.6	0.6
Binder Content (%)*	*7.6–7.9*		*6.9*	*0.5*
Rubber Content† (%)	21		15.9	3.3

* Percent by mass of aggregate
† Percent by mass of binder
‡ Per applicable Caltrans Special Provisions)

The binder for the DGAC mix was an AR-4000 meeting Caltrans specifications, manufactured by Huntway in Benicia. The PG classification for the DGAC binder is PG 64-16. The binder formulation for the ARHM-GG mix included 76.5 percent (by mass) Shell AR-4000, 2.5 percent Witco cutter oil, 15.75 percent No. 10 mesh crumb rubber, and 5.25 percent high natural rubber. Both of the rubber components were manufactured by BAS. The binder was formulated to meet the appropriate Caltrans special provisions at the time the mix design was developed. The PG classification for the ARHM-GG binder is PG 82-28.(*10*)

The binder contents were selected following Caltrans standard procedures. The binder content for the DGAC mix was selected based on the Caltrans "flushing" criterion. At the design binder content of 5.3 percent (by mass of aggregate), the Hveem stabilometer value was 42 and the air-void content under standard kneading compaction was 5.5 percent. The Caltrans

minimum permissible Hveem stabilometer value is 37 for this mix. By Caltrans criteria, the DGAC overlay mix should have a low probability of rutting in the field.

The binder content for the ARHM-GG mix was selected based on the Caltrans criterion for air-void content under standard kneading compaction. At the design binder content of 7.9 percent (by mass of aggregate), the Hveem stabilometer value was 23 and the air-void content under standard kneading compaction was 4.0 percent.(*10*)

The extracted aggregate gradations indicate that the constructed gradations were within nearly all of the Caltrans specification operating ranges (Tables 2.5, 2.6). The DGAC mix was somewhat coarser than the target gradations for the coarse sizes, and finer than the targets for the fine sizes (Table 2.5, Figure 2.4). The ARHM-GG gradation nearly matched the target value for all sizes (Table 2.6, Figure 2.4).

The extracted binder contents from the DGAC mix were within the mix design range. The extracted binder contents from the ARHM-GG mix had much greater variability, and were below the mix design range. Assuming that there were no difficulties with the extraction process for asphalt-rubber binders, the average binder content was found to be 0.7 to 1.0 percent less than the target range (by mass of aggregate).

2.2.1.2 Goal 1 Asphalt Concrete Mix

The Goal 1 asphalt concrete mix designs, and the results of previous laboratory tests on field cores and laboratory compacted specimens are summarized in Reference (*12*). The same asphalt concrete mix was used for the top and bottom lifts of the Goal 1 structures. The mix met all Caltrans standard specifications for Type A, 19-mm maximum size, coarse gradation mix (Figure 2.4). The aggregate sources and asphalt source were not the same as those used for the DGAC overlay mix, and the two mixes were produced by different plants.

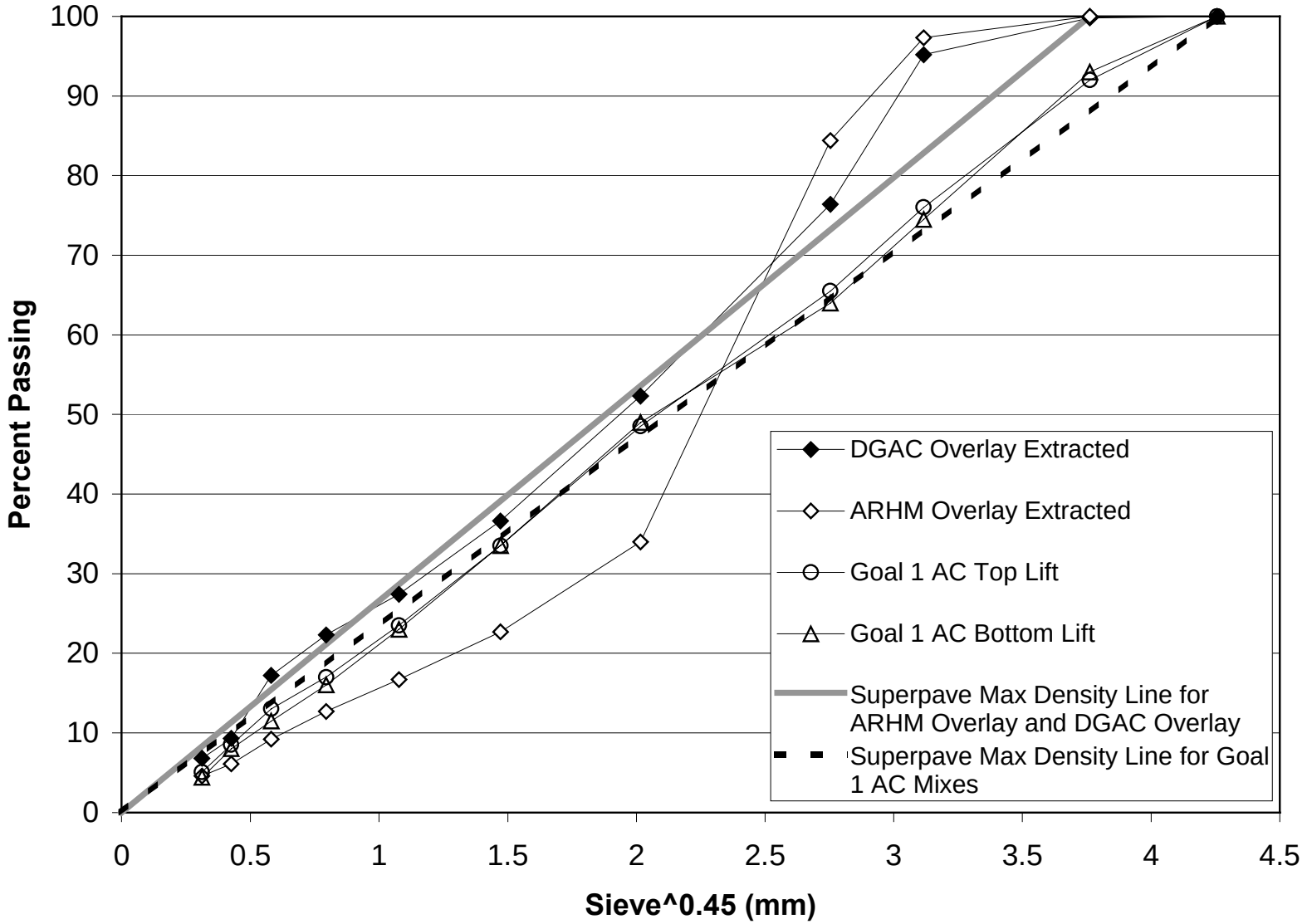

Figure 2.4. Target and actual aggregate gradations for DGAC and ARHM-GG overlay mixes, from extractions.

The asphalt binder met Caltrans requirements for AR-4000 and was produced by the Shell refinery at Benicia. The binder content selected following Caltrans test methods was 4.9 percent by mass of aggregate, and the mix design recommended range was 4.6 to 4.9 percent. The binder content was selected based on the Caltrans "flushing" criterion. The Hveem stabilometer value at 4.9 percent asphalt content was 47, and the air-void content under standard kneading compaction was 4.4 percent. Mix design target gradations, the Caltrans operating ranges, and gradation analyses from extraction and plant belt samples are shown in Table 2.7.

Table 2.7 Summary of Extracted Gradation and Binder Content for Goal 1 Asphalt Concrete Mix (*12*).

Sieve Size (mm)	**Percent Passing Sieve Size**				**Top Lift Extracted (Standard Deviation)**	**Bottom Lift Extracted (Standard Deviation)**
	Mix Design	**Permissible Operating Range** *	**Top Lift Extracted (Average)**	**Bottom Lift Extracted**‡ **(Average)**		
25	100	100	100.0	100.0	0.0	0.0
19	99	90–100	92.0	93.0	7.1	1.4
12.5	80		76.0	74.5	8.5	0.7
9.5	67	60–75	65.5	64.0	4.9	2.8
4.75	49	45–55	48.5	49.0	4.9	2.8
2.36	33	29–39	33.5	33.5	3.5	2.1
1.18	22		23.5	23.0	2.1	1.4
0.60	14	10–20	17	16.0	1.4	1.4
0.30	9		13	11.5	1.4	0.7
0.15	6		8.5	8.0	0.7	0.0
0.075	3	3–7	5.1	4.4	0.1	0.6
Binder Content (%)†	*4.6–4.9*		*5.25*	*4.8*		

* Per Section 39 Caltrans Standard Specifications)
† Percent by mass of aggregate
‡ Aggregate gradations include plant belt samples and extracted values

It can be seen that the aggregate gradations obtained from the mix were all within the permissible operating ranges. The asphalt contents obtained from extractions on the top lift of asphalt concrete are somewhat higher than the recommended range from the mix design.

Despite the high asphalt contents, stabilometer tests on material collected from the top lift during construction were found to have typical values ranging from 46 to 48. The asphalt contents from extractions on the bottom lift are within the recommended range. Stabilometer test values on site samples of the bottom lift averaged 46. The minimum Hveem stabilometer value permitted by Caltrans for this mix is 37. These results indicate that by Caltrans criteria, the Goal 1 mix should have a low probability of rutting in the field.

2.2.1.3 Underlying Materials

The asphalt treated permeable base (ATPB) material under some of the HVS rutting sections meets Caltrans standard specifications. Cores and slabs taken from the rutting test sections showed no signs of stripping or other damage. The aggregate base (AB) material meets all Caltrans standard specifications for Class 2 Aggregate Base. R-value tests of the AB had values ranging from 78 to 83. The aggregate base relative density at the time of compaction ranged from 99 to 103 percent and the water contents were at or just below the optimum water content. The Caltrans standard specification requires 95 percent relative compaction.(*12*)

The aggregate subbase (ASB) met all requirements for Caltrans Class 2 Aggregate Subbase. R-value tests of five samples ranged from 55 to 82, averaging 70 with a standard deviation of 10. The relative density of the ASB ranged from 95 to 100 percent. The Caltrans standard specification requires 95 percent relative compaction. The top two meters of the subgrade soil are a high plasticity clay, with a USCS classification of CH, and an AASHTO classification of A-7-6. The liquid limit ranges from 39 to 55 and the plasticity index from 27 to 41. R-value tests of the subgrade produced values ranging from 4 to 30. The relative compaction of the subgrade ranged from 91 to 98 percent, averaging about 95 percent. Caltrans standard specifications require a minimum average relative compaction of 95 percent. The

groundwater table is at depths of approximately 3.5 to 4.8 m below the surface of the subbase.(*8, 12*)

2.3 HVS Test Program

2.3.1 Loading

2.3.1.1 Traffic Distribution and Speed

The HVS test sections were 8 m in length. Pavement performance in the 1-m lengths at each end of the trafficked section (the "turnaround zone") were not included in the performance evaluations because the HVS wheel speed varies in these areas. All trafficking had a wander pattern distributed across a 1-m width. The resulting distribution of passes is shown in Figure 2.5. This is the same wander pattern used on the underlying Goal 1 test sections.

All four of the test sections were trafficked in the bi-directional mode, with the wheel loading the test section in both directions.

The wheel speed was approximately 7.5 km/hr. (4.7 mph) in one direction and 6.8 km/hr. (4.2 mph) in the other direction. The wheel speed of the HVS is much slower than typical free-flowing highway traffic. Because longer slower speeds and the corresponding longer loading times result in more damage than do shorter loading times, the HVS testing was performed under more severe conditions than would be expected on a free-flowing highway. The HVS wheel speed is more typical of slow-moving, heavily congested traffic on an urban freeway, or congested traffic on a highway or city street.

Tire contact area information from a previous study completed for CAL/APT by the Council for Scientific and Industrial Research of the Republic of South Africa (CSIR) was used

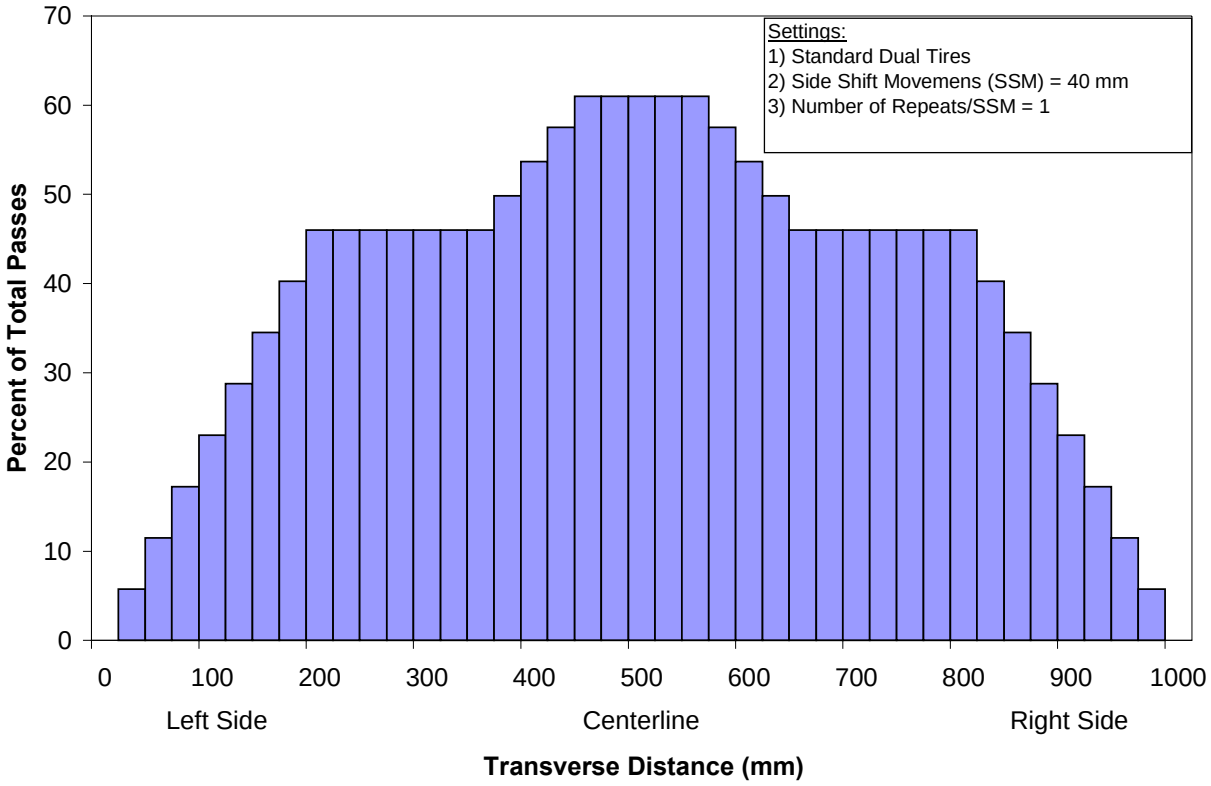

Figure 2.5. HVS traffic wander distribution for all four test sections.

to calculate the contact load duration for the tire type used in the study. The calculations were made using the average HVS wheel speed in both directions. Results are shown in Table 2.8.

Table 2.8 Calculated Surface Contact Durations for Tire/Wheel Types Included in Study, Assuming Average Bi-directional Wheel Speed (*17*)

Tire/Wheel Type	Load* (kN)	Inflation Pressure (kPa)	Contact width* (mm)	Contact length (mm)	Contact Duration (seconds)
Dual radial	20	720	200	190	0.09
Dual radial	40	720	200	295	0.15
Dual radial	50	720	200	328	0.17

* for dual tires, load and width of one tire

2.3.1.2 Tire, Wheel and Loads

Radial tires on dual wheels currently make up most of the commercial truck tires operating on United States highways. A recent study has found that 97 to 99 percent of all commercial truck wheels in the United States are duals, excluding steering axles.(*18*) A recent study of trucks entering Oregon found that less than one percent of tires on commercial trucks were bias-ply, with the remainder being radials.(*19*)

Goodyear G159A, 11R22.5, Load Range G tires on 11-cm wide rims were used in this study. The tire tread consists of six plies of steel cord with a sidewall of one ply of steel cord. The maximum dual load rating is 25.64 kN (5,750 lbs.) at a cold inflation pressure of 723 kPa (105 psi).

The initial test load used on each test section was 40 kN on the dual, or 20 kN on each tire, at the rated inflation pressure. The load was increased to 80 kN on the dual when rutting, and deflections had reached a steady rate of increase under the 40 kN load. The load was increased to 100 kN on the dual once rutting and deflections had stabilized under the 80 kN load. The majority of loading was applied at 100 kN, as reported in Table 2.9.

Table 2.9 Repetitions at Each Load Level

Load on Dual	Section			
	514 (DGAC/drained)	515 (ARHM-GG/drained)	517 (DGAC/undrained)	518 (ARHM-GG/undrained)
	Repetitions*	Repetitions	Repetitions	Repetitions
40 kN	172,000	128,000	148,000	116,000
80 kN	145,000	218,000	179,000	110,000
100 kN	1,350,000	2,065,000	2,019,000	1,406,000

* Values are rounded to the nearest thousand.

2.3.2 Pavement Instrumentation and Methods of Monitoring

Instrumentation of the test sections consisted of the following:

- Multi-Depth Deflectometers (MDD): used to measure elastic vertical deflections and permanent vertical deformations at various levels in the pavement structure relative to a reference deep in the subgrade;
- Road Surface Deflectometer (RSD): used to measure elastic vertical deflections at the surface of the pavement;
- Thermocouples: used to measure temperatures at various depths in the asphalt bound materials;
- Profilometer and Straight Edge: used to measure the transverse profile of the pavement surface to determine permanent deformation;
- Digital Crack Images: used to measure surface cracking;
- Nuclear Density Gage: used to measure the density and water content of the unbound layers at the completion of trafficking, inside and outside the trafficked area;
- Nuclear Hydroprobe: used to measure water contents in the unbound layers just outside the trafficked area during testing of the section; and
- Trenches and Cores: used at the end of trafficking to determine pavement thicknesses and water contents, air-void contents of asphalt bound materials inside and outside the trafficked area at the completion of the test, and to observe the condition of each pavement layer.

The instrumentation is described in detail in Reference (*11, 12, 14*)

In the months after HVS trafficking of the four test sections was completed, cores were taken and trenches were dug to destructively evaluate the performance of the test sections. The

test sections were not subjected to any traffic, high temperatures, or water exposure from the time trafficking was completed to the time coring and trenching were completed.

Locations of MDDs, thermocouples, profilometer measurements, hydroprobe measurements, and trenching and coring locations for all Goal 3 test sections are shown in Figures 2.6–2.9.

2.3.2.1 Multi-Depth Deflectometers (MDD)

MDDs were installed in the pavement sections to allow measurement of both elastic deflection and permanent deformation at in-depth positions. The MDD consists of Linear Variable DisplacementTransducers (LVDTs) fixed to the pavement at various depths. The deflections and deformations measured by the MDDs are relative to an anchor point located 3 or more meters below the pavement surface, at which depth no deflection is assumed to occur.

Two sets of MDDs were installed before testing of the Goal 1 sections on the centerline of the sections at positions 4 and 12. These MDDs were connected to the data acquisition system with cables installed underneath the overlays. Two additional MDDs were installed after the construction of the overlays at positions 6 and 10.

The outputs from an MDD are influence lines of deflection at the selected depths within the pavement under the moving HVS load at a creep speed of about 2 to 3 kph, and the permanent deformation of the pavement versus load repetitions. MDD measurements can be used to:

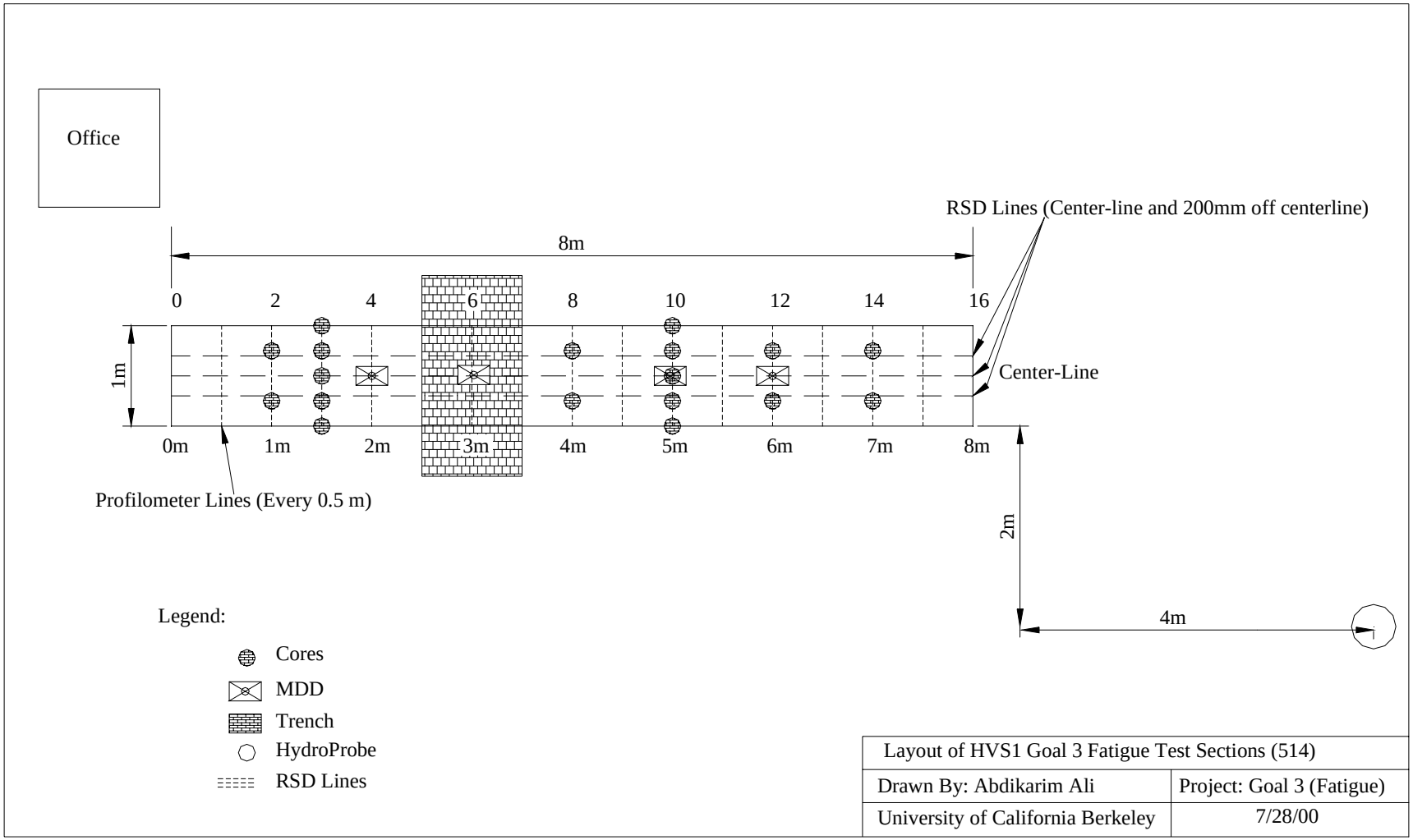

Figure 2.6. Locations of instrumentation, data collection points, and trenches and cores on Section 514 (drained, DGAC overlay).

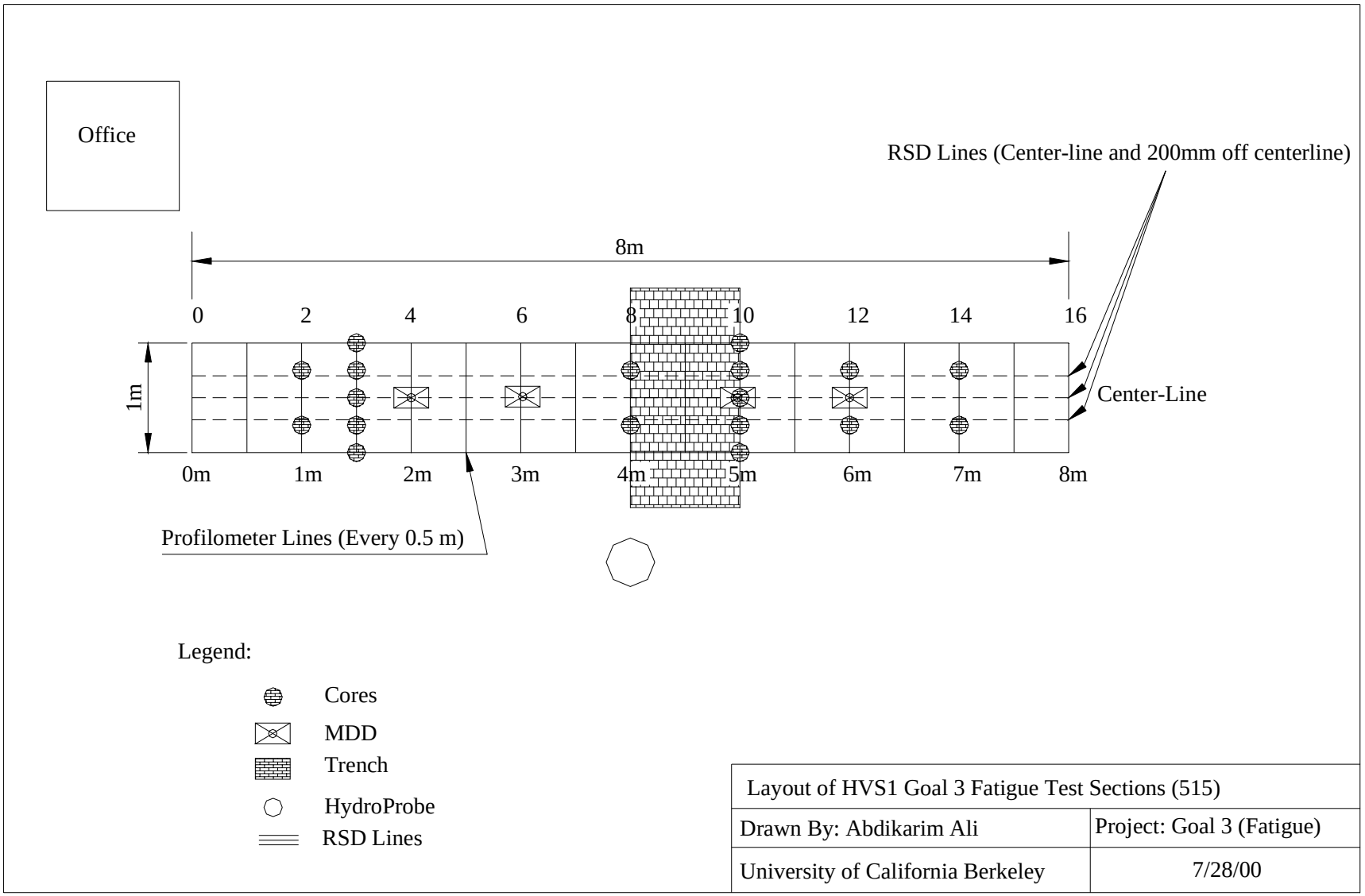

Figure 2.7. Locations of instrumentation, data collection points, and trenches and cores on Section 515 (drained, ARHM-GG overlay).

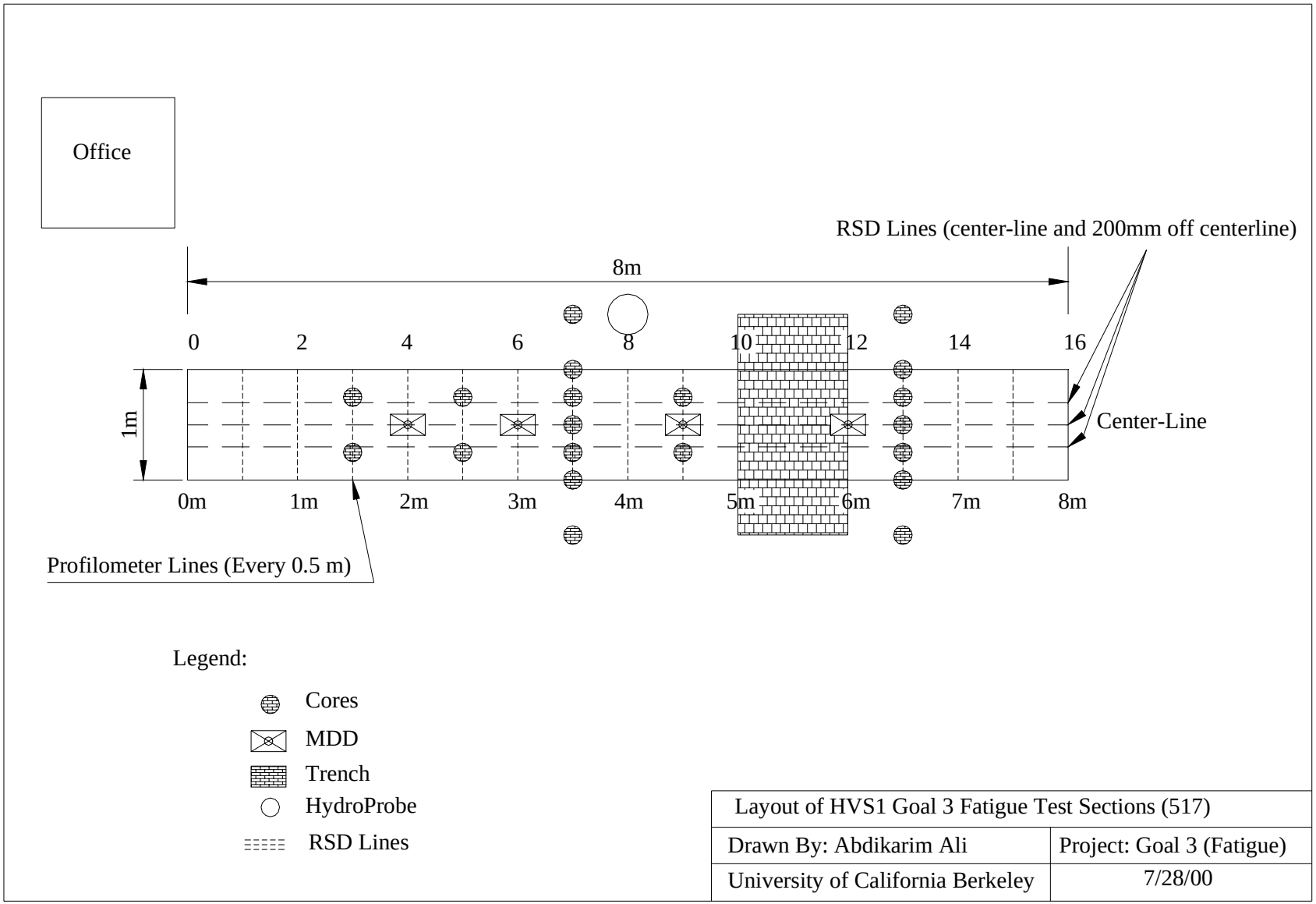

Figure 2.8. Locations of instrumentation, data collection points, and trenches and cores on Section 517 (undrained, DGAC overlay).

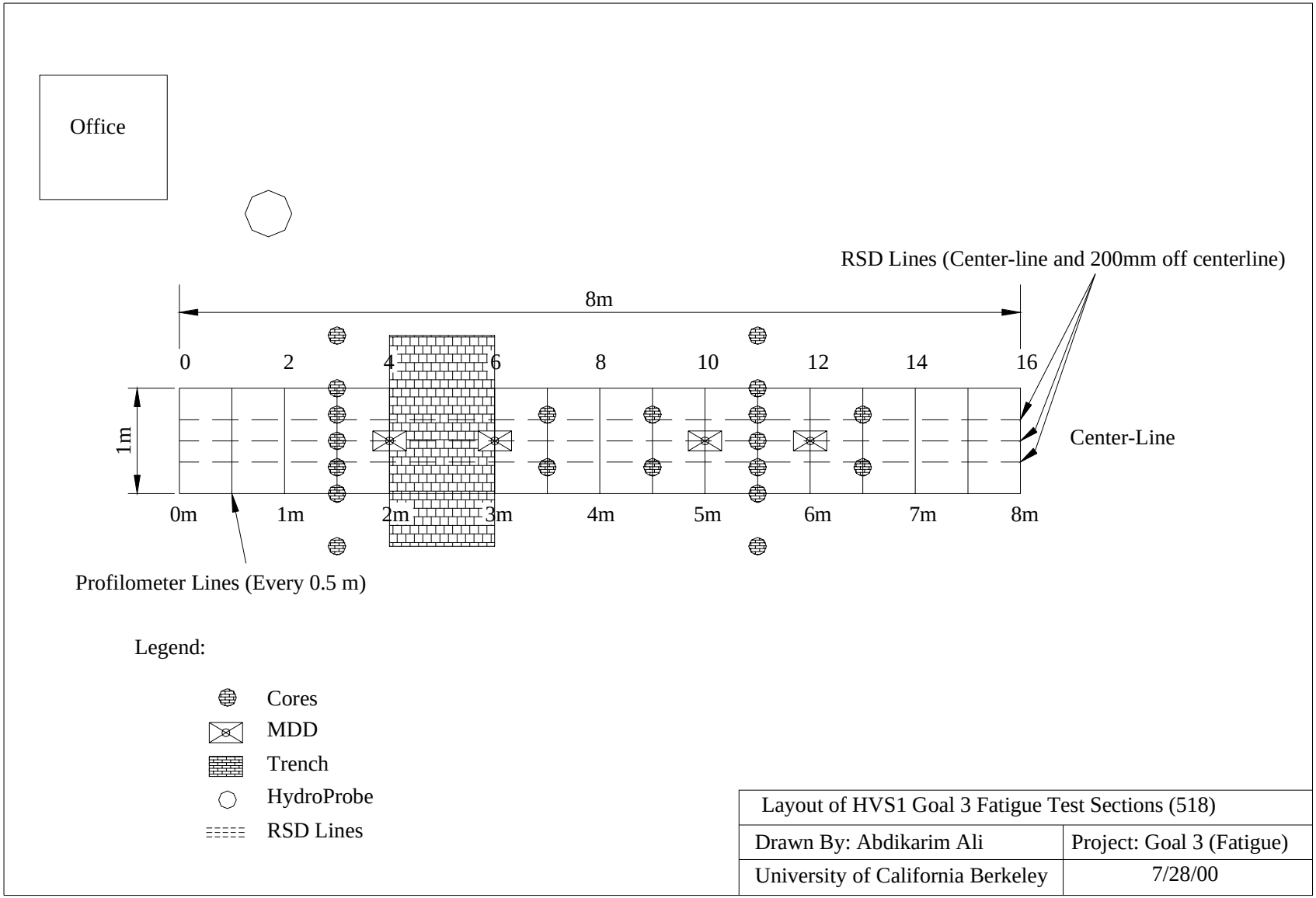

Figure 2.9. Locations of instrumentation, data collection points, and trenches and cores on Section 518 (undrained, ARHM-GG overlay).

- characterize the behavior of the full pavement system,
- monitor changes in the stiffness of the various layers in the pavement with time,
- backcalculate effective E moduli (stiffness) of the various layers,
- determine stress dependency of pavement layers (non-linear elastic behavior), and
- determine the permanent deformation (compression) of all pavement layers.

The depths of installation of the MDDs are shown in Figures 2.10 and 2.11 for the drained sections, and Figures 2.12 and 2.13 for the undrained sections.

2.3.2.2 Road Surface Deflectometer (RSD)

The Road Surface Deflectometer measures the elastic surface deflection of a pavement under the action of a wheel load. The RSD is essentially a modification of the Benkelman Beam. The output from the RSD is an elastic surface deflection curve, which can be used to:

- characterize pavement behavior,
- backcalculate effective elastic moduli (stiffness),
- monitor changes in the stiffness of the pavement with number of load/stress repetitions over time, and
- determine stress dependency of pavement layers (non-linear elastic behavior).

During an HVS test, the RSD measuring points on the pavement are clearly marked to ensure that the deflection is measured at the same point each time.

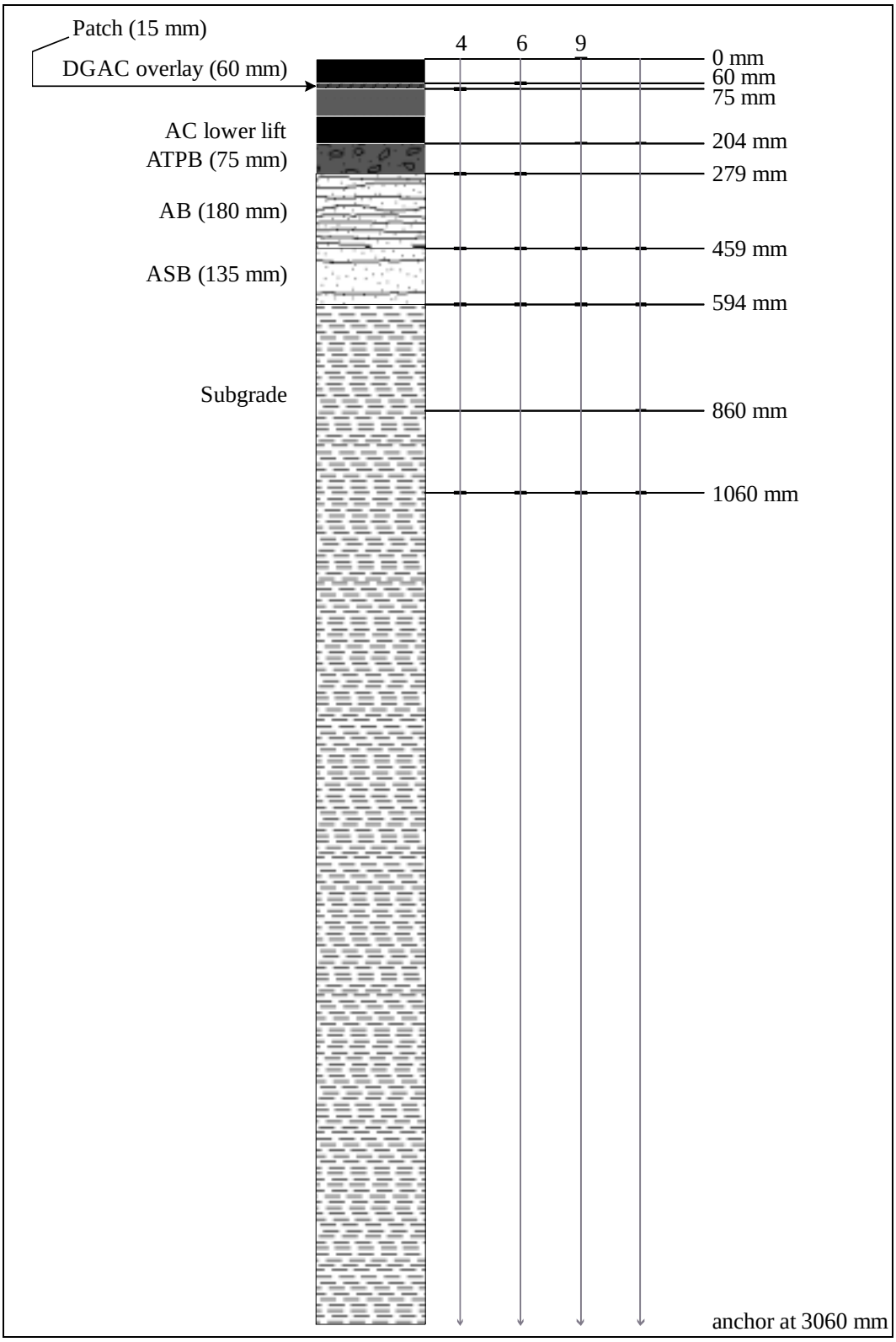

Figure 2.10. Installation depths for MDDs in Section 514 (drained, DGAC overlay).

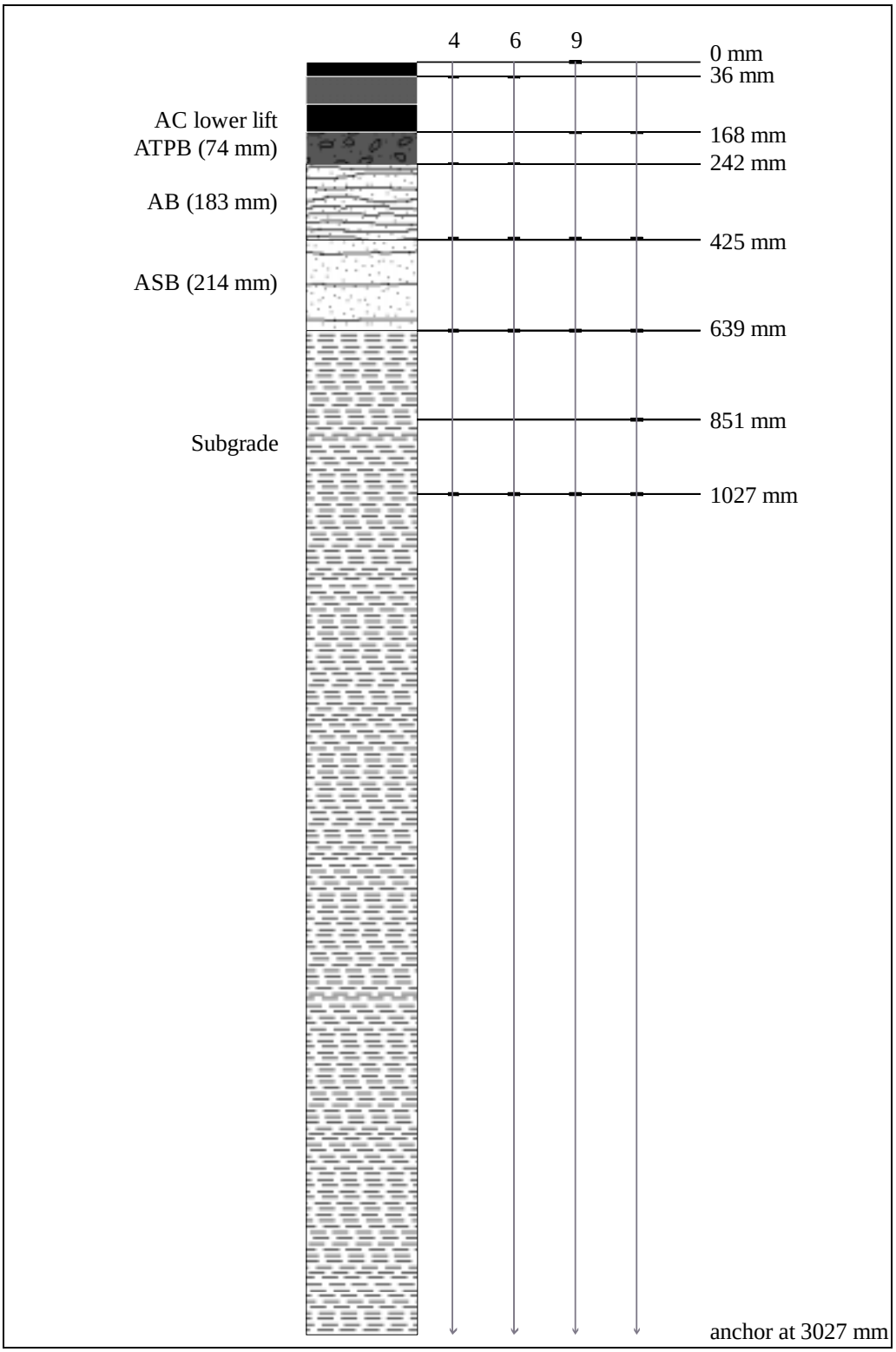

Figure 2.11. Installation depths for MDDs in Section 515 (drained, ARHM-GG overlay).

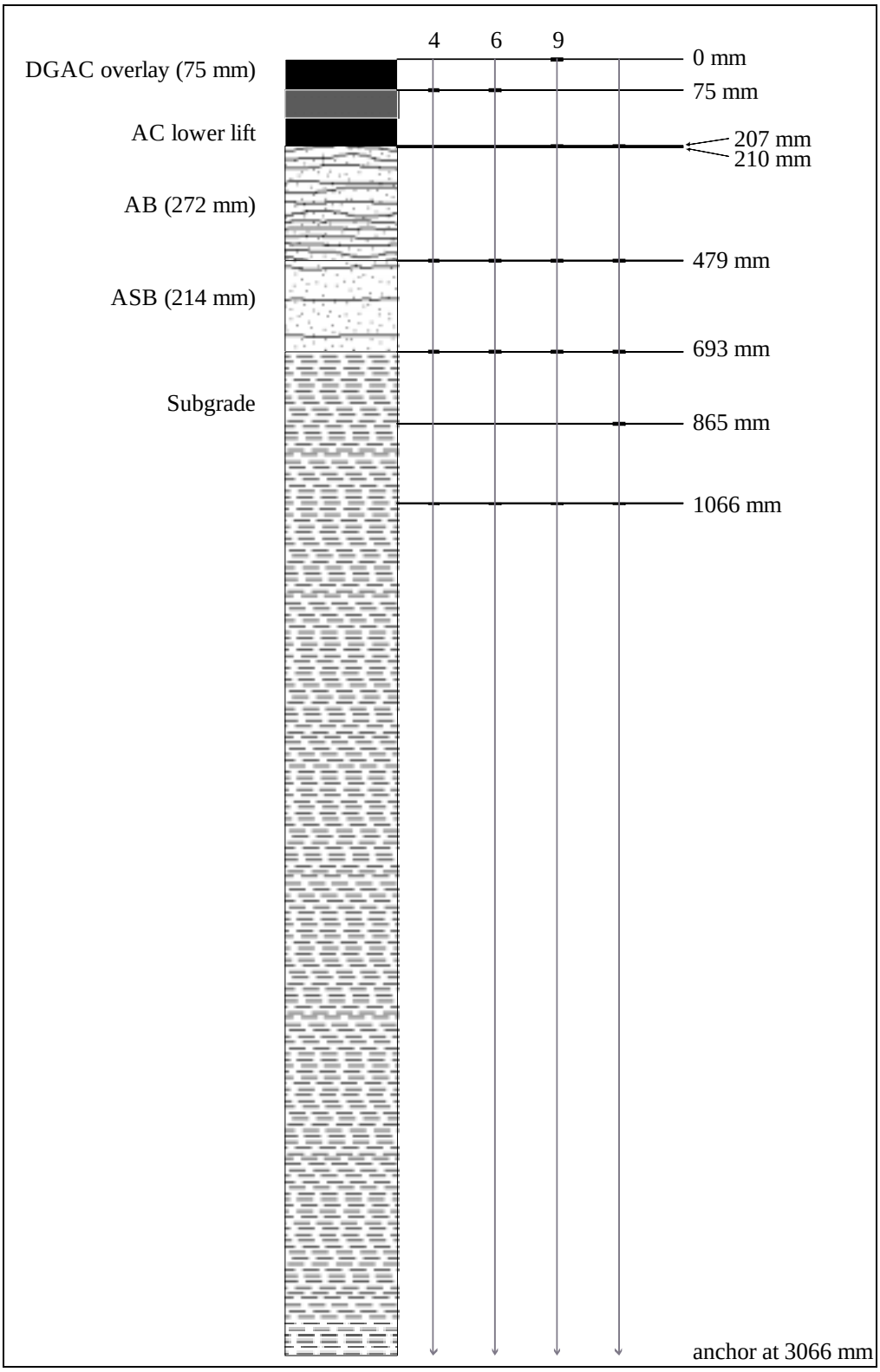

Figure 2.12. Installation depths for MDDs in Section 517 (undrained, DGAC overlay).

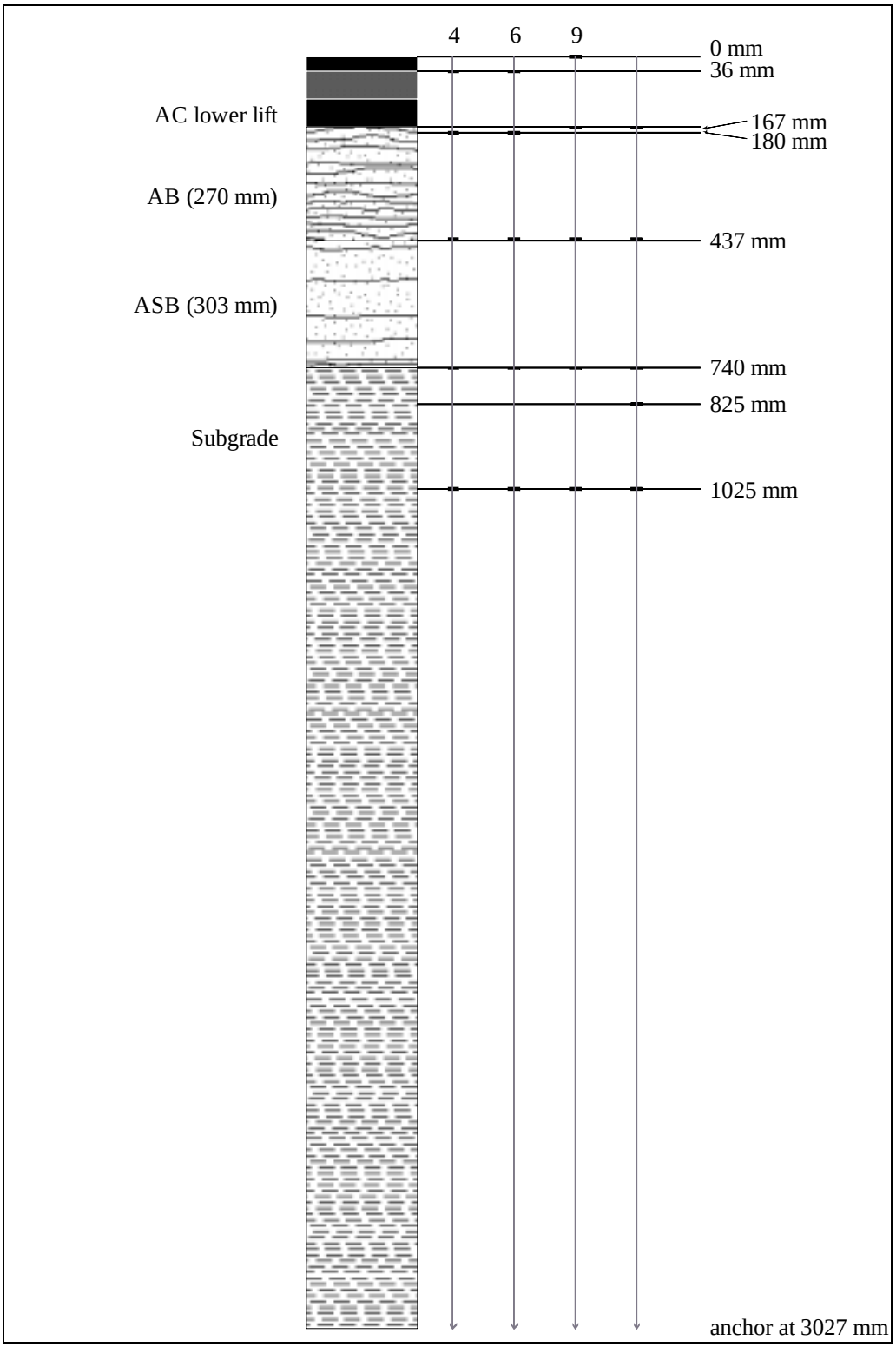

Figure 2.13. Installation depths for MDDs in Section 518 (undrained, ARHM-GG overlay).

2.3.2.3 Thermocouples

Sets of three to five Type K thermocouples were installed just outside of the wheelpath, at one or two locations on each side of each test section. The locations were offset along the length of the section (see Figures 2.6–2.9). The thermocouples in each set were placed at different depths in the pavement, including at the surface, at the bottom of the asphalt treated layers, and in the ATPB layer where applicable.

Thermocouples are installed by drilling a hole in the asphalt concrete approximately 10 mm in diameter. The thermocouples are then wrapped around a wooden dowel at the desired depths and taped in place. They were then placed in the hole hammered into place.

2.3.2.4 Profilometer and Straight Edge

The laser profilometer and data acquisition system developed by CSIR was used to measure pavement surface profile as rutting developed.

Profiles were taken transverse to the wheel path, at locations every 0.5 m along the wheel path (see Figures 2.6–2.9). Maximum rut depth from the profiles obtained from the laser profilometer was defined as the difference between the highest point in the profile and lowest point. On all sections "humps" of material developed at the sides of the wheel path as material as trafficking progressed.

A straight edge was used in the early stages of the experiment to measure maximum rut depth, as an independent check of the laser profilometer. It was found that the maximum rut depth found using both instruments was quite similar, and use of the straight edge was abandoned.

2.3.2.5 Digital Crack Images

Crack monitoring was an essential part of data collection for the test sections because fatigue distress in an asphalt pavement manifests itself in the form of surface cracks. Crack monitoring included visual inspection of the test pavement, direct measurement of crack length, photographic documentation of the cracking progress, and coring to examine the propagation of cracks with depth. The system of digital image analysis developed at UCB (*20*) was employed to measure the process of cracking in asphalt pavements.

The surface of the pavement was regularly scanned for the first surface cracks from the beginning of trafficking, and regular inspection of crack development was made from that point through the end of the test. On all of the test sections, the observed cracks were very narrow ("hairline") cracks and at times difficult to detect visually. It is presumed therefore that operator error will result in fewer cracks being detected than actually exist. However, the influence of operator error is greatly diminished with the implementation of a digital method of crack observation and analysis method.

The lack of expansion, spalling, and other factors that would lead to the deterioration of the hairline cracks observed on the pavement surface can likely be attributed to two factors:

- lack of rainfall and mineral particles on the surface of the test pavement, and
- lack of cracking in the bottom lift of asphalt concrete.

A detailed discussion of these factors is in the Reference (*13*).

The process of digitally analyzing crack propagation is as follows:

- The test section is marked with a lumber crayon as with visual inspection, and then photographed in 1 × 0.5 m sections with a medium-format (60 × 70 mm negative) or high-resolution digital camera.

- The photographs are then digitized (or downloaded, in the case of the digital camera), adjusted to remove parallax and perspective distortion, and then recombined to create a composite two-dimensional image of the test section.
- The cracks from these composite images are then traced in Optimas (*21*) and the images are calibrated to the real-life dimensions of the test section.
- Crack statistics can then be calculated and the analysis introduced to a spreadsheet for analysis.

With this method, starting with the first crack photos, an overlay is created from the traced cracks. This overlay is then placed over the next set of crack photos. Then, when the crack image of the second set is traced, cracks which appear to have decreased in length, or with portions missing or undetected by the technicians performing crack monitoring, can be traced via the overlay along with the new cracks which were detected. The crack trace from this image is then used as an overlay for the next set of crack photos creating a cumulative assessment of crack progress. This process is then repeated through all the sets of crack photos until the end of the test.

It was found that all the cracks which may have disappeared and reappeared later, or which shortened and then lengthened again, were doing so in exactly the same locations and would without exception progress over the duration of the test though they may have been undetected during some crack inspections. Verification of this phenomenon is only possible through the use of digital techniques. Most often, the overlays matched successive crack photos exactly. On occasion, camera perspective could cause some uncorrectable distortion which would offset the overlays slightly. However, this offset was never more than 2 cm in the calibrated image, an error of 0.25 percent.

After completion of trafficking, the digital image of cracking on the surface of the overlays was compared with the digital crack image from the underlying previous test section. The results of this comparison were used to determine whether the cracking in the overlays was reflection cracking, or if the two crack images had cracks in different locations.

2.3.2.6 Nuclear Density Gage

The layer densities and water contents were measured with a nuclear density gage at the completion of trafficking for comparison with the original compaction using both backscatter and in-depth probe techniques. The air-void contents of the overlays could not be measured in the wheelpath because the surface rut made it impossible to place the gauge on a flat surface.

2.3.2.7 Nuclear Hydroprobe

The nuclear hydroprobe was used to monitor water contents in the unbound layers at four locations outside the test sections. The hydroprobe contains a nuclear source and a particle detector mounted on a probe. The probe is inserted into a pre-drilled measurement hole lined with aluminum tubing. The device is calibrated using an identical aluminum lining placed inside a large barrel filled with the compacted material obtained from the unbound layers of the pavement over a range of water contents.

The measurement locations were as follows:

- between Sections 514 and 515;
- between Sections 517 and 518;
- about 3 m from Section 518, away from Section 517; and
- about 3 m from Section 514, away from Section 515.

2.3.2.8 Trenches and Cores

After completion of all of the HVS rutting tests on the overlays, a trench was dug across the wheelpath at one location on each test section, as shown in Figures 2.6–2.9. The first stage of trenching was to cut the trench edges using a diamond blade saw. The trenches were cut wide enough to include sections of the pavement not influenced by the HVS loading, the humps at the sides of the wheel path, and the wheel paths. After waiting several weeks to permit the sections to dry out, the asphalt bound layers were removed in slabs. The slabs were saved to provide material for additional cores if needed. The thickness of the asphalt bound layers, including the overlays and both lifts of Goal 1 asphalt concrete, were measured on the cut face at the sides of the trench at 25-mm intervals.

Photographs were taken of the trench with the asphalt bound layers removed. The laser profilometer was then placed in the trench on the exposed surface of the aggregate base layer, and the profile of the base was taken. The aggregate base was then excavated to the top of the aggregate subbase, and the thickness of the aggregate base was measured at various transverse points across the trench.

Cores were taken at several locations along the wheel path (see Figures 2.6–2.9). Cores were taken outside the temperature-controlled area of the HVS test, inside the temperature-controlled area but outside the area influenced by the HVS trafficking, in the "humps," and in the wheel path. Cores were taken in all three humps and both wheel paths on the dual wheel sections.

2.3.2.9 Data Collection Schedule

Air and pavement temperatures were recorded hourly. Temperatures included in this report are only those recorded when the HVS was trafficking. All other data was collected at

various intervals, more frequently at the beginning of trafficking and after each time the load was increased, and with diminishing frequency afterward.

2.3.3 Test Section Failure Criteria

The criteria for failure and termination of HVS trafficking were:

- Cracking density of 2.5 m/m^2 or more, or
- Surface relative rut depth of 12.5 mm or more.

The crack density criteria is based on the minimum cracking density on the Goal 1 test sections (section 500RF), which is used as a reference criteria. This cracking density has previously been identified by a Caltrans pavement condition surveyor as corresponding to a crack density that would be considered failure by Caltrans criteria.(*13*) The surface rutting criteria is also taken from Caltrans condition survey guidelines.

2.3.4 Environmental Conditions

2.3.4.1 Temperature

The target temperature for each test section was 20ºC at a depth of 50 mm. To heat the test section pavements to the target temperatures, a set of banked reflectors fitted with infrared lamps and resistance-heating elements was used. A kerosene fired air heater was also used for a few hours at the beginning of each test to bring the air temperature from ambient conditions to just below the target temperature. HVS trafficking was not begun until temperatures had stabilized throughout the asphalt concrete layer, as determined from thermocouples. In some cases, heating continued for more than 12 hours before trafficking was begun.

Once the target temperature had been reached, it was maintained by a control system that turned the lamps and heating elements on or off whenever the temperature measured by the thermocouple at 50 mm depth was more than two degrees (C) from the target. The curved shape of the reflectors and channelized traffic pattern, which precluded side-shift movement of the beam, created an enclosed space over the test section that helped to maintain heat in the pavement.

2.3.4.2 Moisture Conditions

The test sections are inside a building, so no rainfall was permitted to reach the pavement. The subgrade consists of the native material and is connected to the natural water table,(*12*) which permits changes in the water contents of the unbound materials. The water table is typically located approximately 3 to 5 meters (see Section 2.2.1.3) below the surface of the pavement and fluctuates seasonally.

No additional water was applied to the surface of the pavement during trafficking.

3.0 DATA SUMMARY: TEMPERATURE, PERMANENT DEFORMATION, ELASTIC DEFLECTIONS, AND CRACKING

This chapter provides a summary and a brief discussion of the data collected before, during, and after HVS trafficking. The pavement response and performance interpretation is discussed in Chapter 4.

3.1 Temperature

All of the test sections are inside a large pole and sheet metal building which somewhat moderates air temperature. The HVS was fitted with a temperature control box and closed loop control system to maintain the pavement at a constant temperature for the four tests described in this report.

3.1.1 Air Temperature

Figures 3.1–3.4 show average daily air temperatures in the test building and in the temperature control box surrounding the pavement test sections. The daily average temperatures were calculated from hourly temperatures recorded during testing. The average air temperatures in the building show significant warming and cooling trends. Progressive warming trends occurred from January to June and cooling trends from September to December. Sections 514 and 517 were tested during the warming trends and Sections 515 and 518 during the cooling trends.

The temperature control box significantly reduced the effect of the ambient air temperature changes inside the building, leading to more uniform average air temperatures inside the temperature control box.

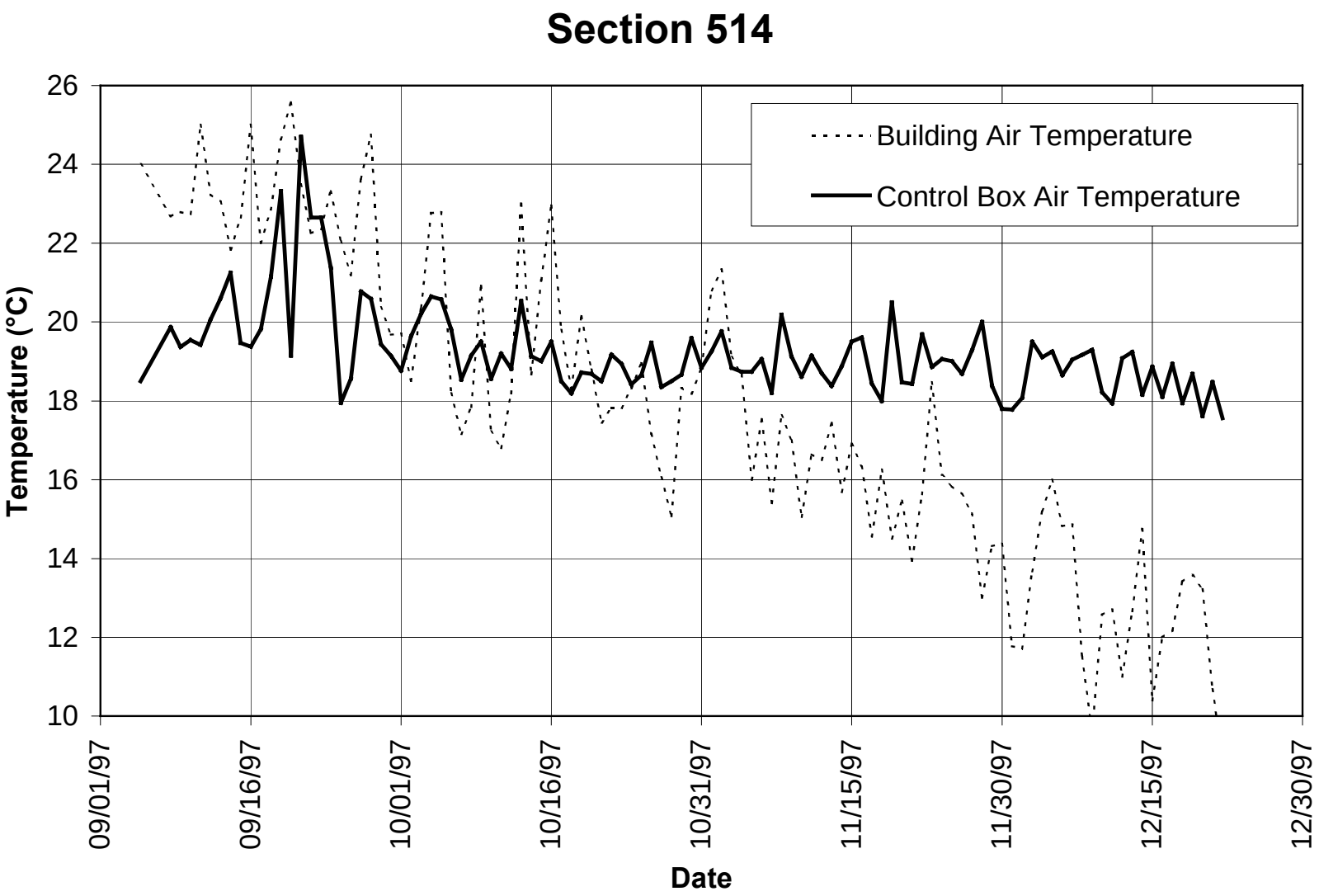

Figure 3.1. Average daily air temperatures for Section 514 (drained, DGAC overlay).

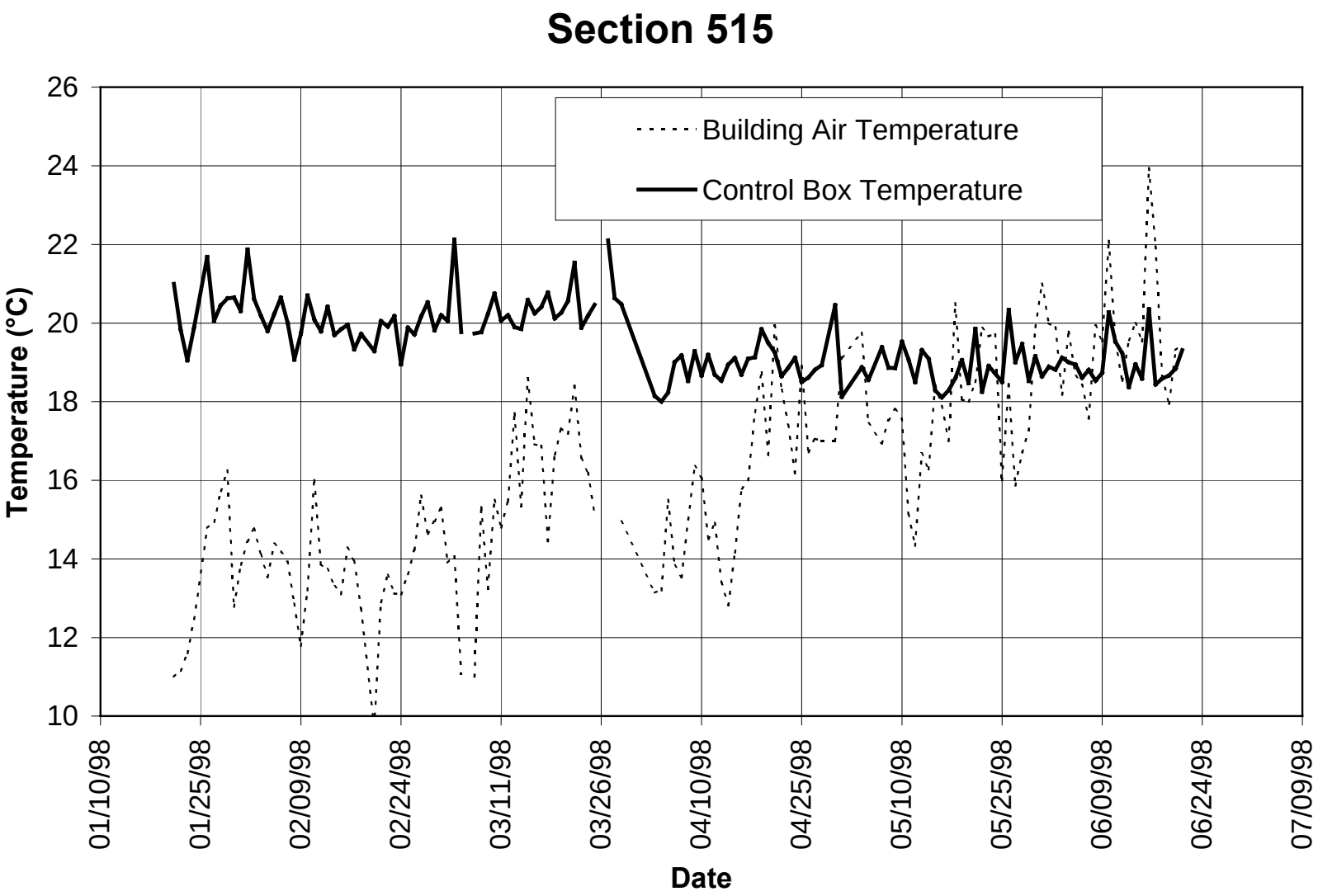

Figure 3.2. Average daily air temperatures for Section 515 (drained, ARHM-GG overlay).

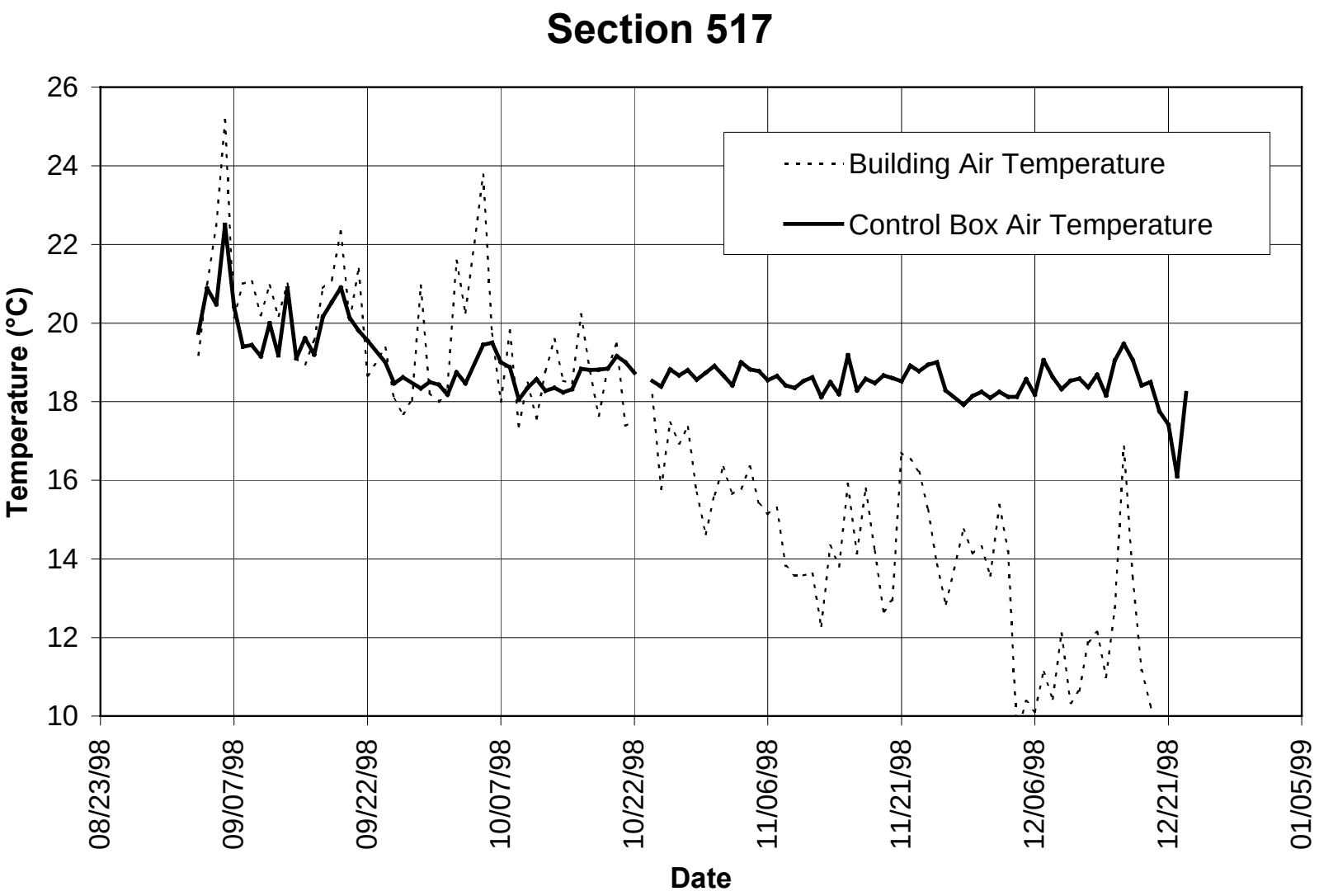

Figure 3.3. Average daily air temperatures for Section 517 (undrained, DGAC overlay).

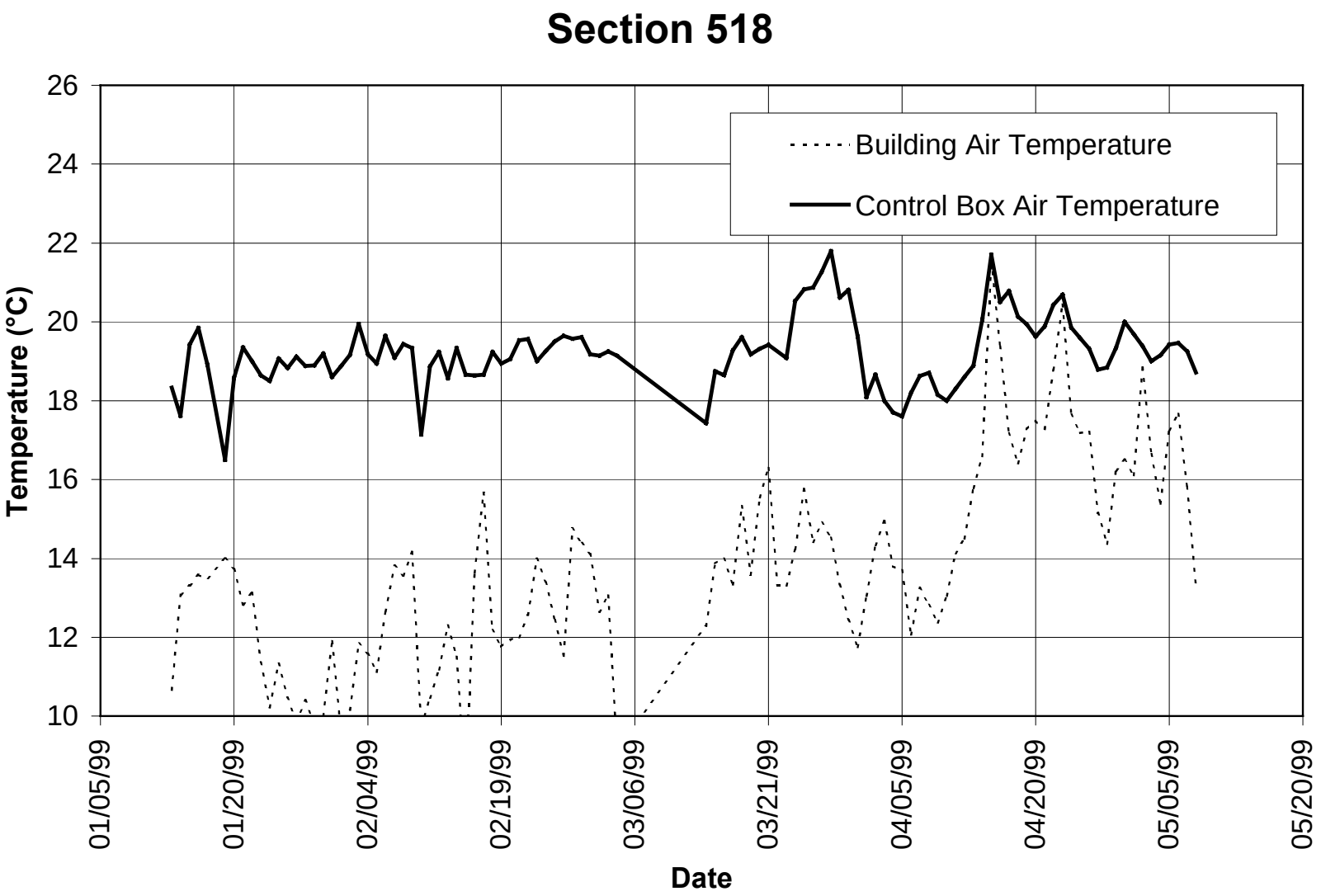

Figure 3.4. Average daily air temperatures for Section 518 (undrained, ARHM-GG overlay).

Table 3.1 presents a summary of average air temperatures in the building and inside the temperature control box for the four tests. For all tests, average air temperatures in the building and in the control box were 16.0ºC and 19.2ºC, respectively.

Table 3.1 Daily Average Temperatures

Test Section		Period		Air Temperature (ºC)			
				Building		Control Box	
		Start	Finish	Average	Standard Deviation	Average	Standard Deviation
Drained	514 DGAC	Late Summer 1997	Late Fall 1997	17.8	4.0	19.2	1.1
	515 ARHM-GG	Winter 1998	Late Spring 1998	16.2	2.6	19.5	0.9
Undrained	517 DGAC	Late Summer 19998	Late Fall 1998	16.2	4.0	18.8	0.8
	518 ARHM-GG	Winter 1999	Late Spring 1999	13.8	2.5	19.2	0.9

3.1.2 Asphalt Concrete Layer Temperatures

Daily average pavement temperatures for the four test sections are presented in Figures 3.5–3.8. Asphalt concrete temperatures were recorded in the overlay, top and bottom lifts of the asphalt concrete, and ATPB layers. Asphalt concrete temperatures were fairly uniform and varied slightly with temperature adjustments in the temperature control box. In general, daily average temperatures in the asphalt concrete layers were approximately 1.5 to 3.6 percent higher than the daily average air temperatures inside the temperature control box.

Asphalt concrete temperatures across the various asphalt concrete layers were within approximately ±1ºC of the pavement surface temperature.

Asphalt concrete temperature gradients in Sections 515 and 518 were somewhat influenced by the temperature adjustments in the temperature control box, which were made to minimize variations in ambient air temperature. From winter to mid-spring, pavement

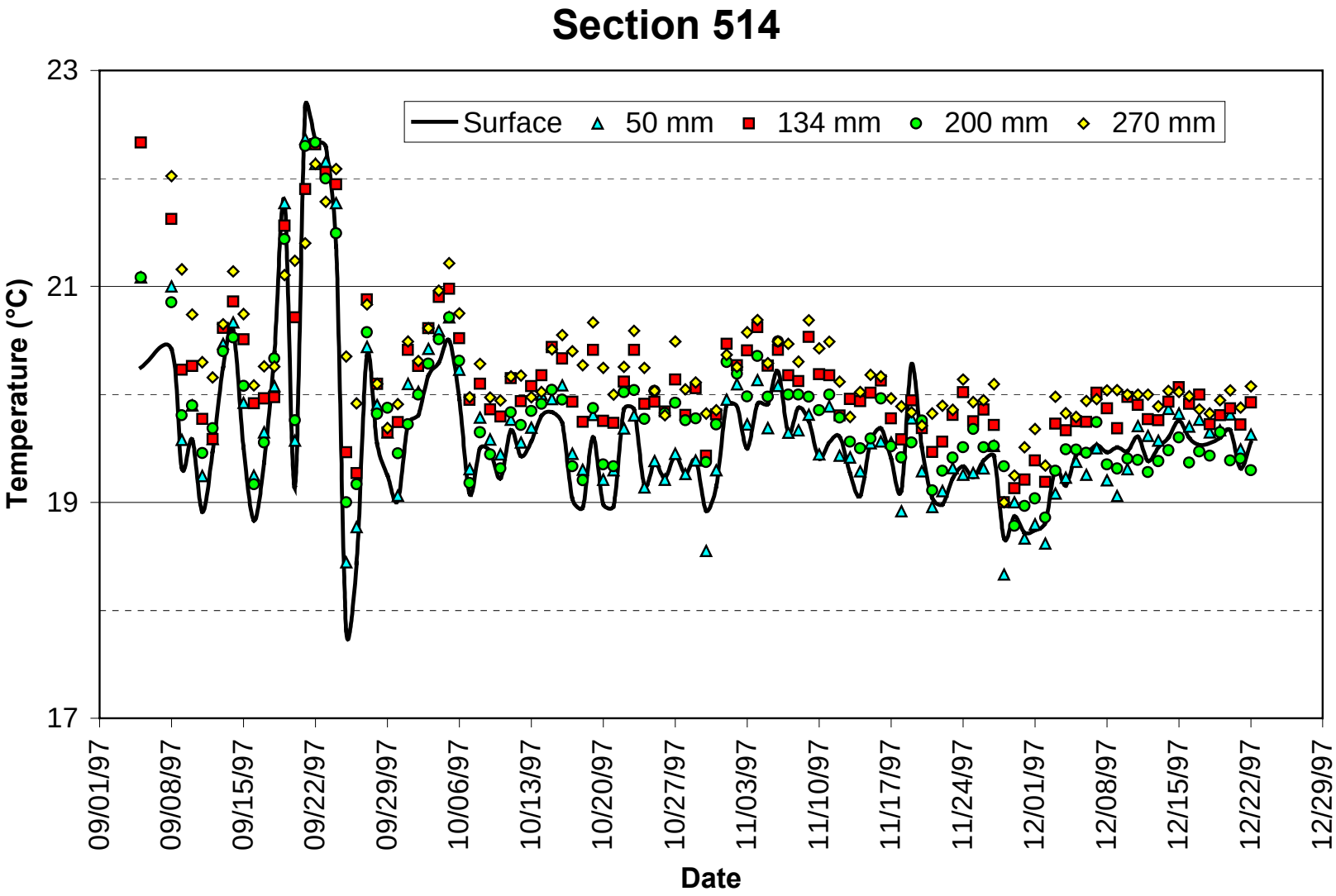

Figure 3.5. Average daily pavement temperatures in Section 514 (drained, DGAC overlay).

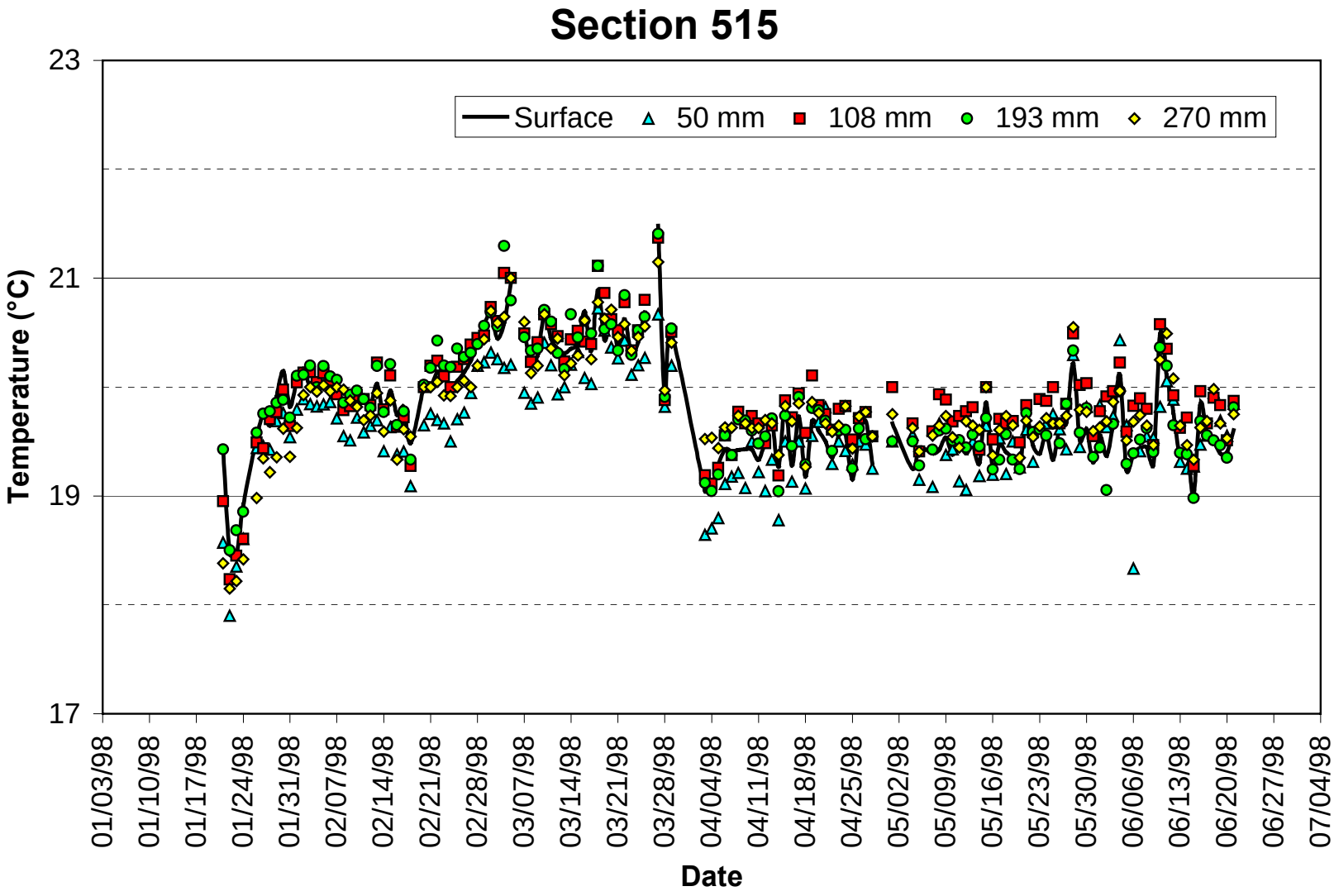

Figure 3.6. Average daily pavement temperatures in Section 515 (drained, ARHM-GG overlay.

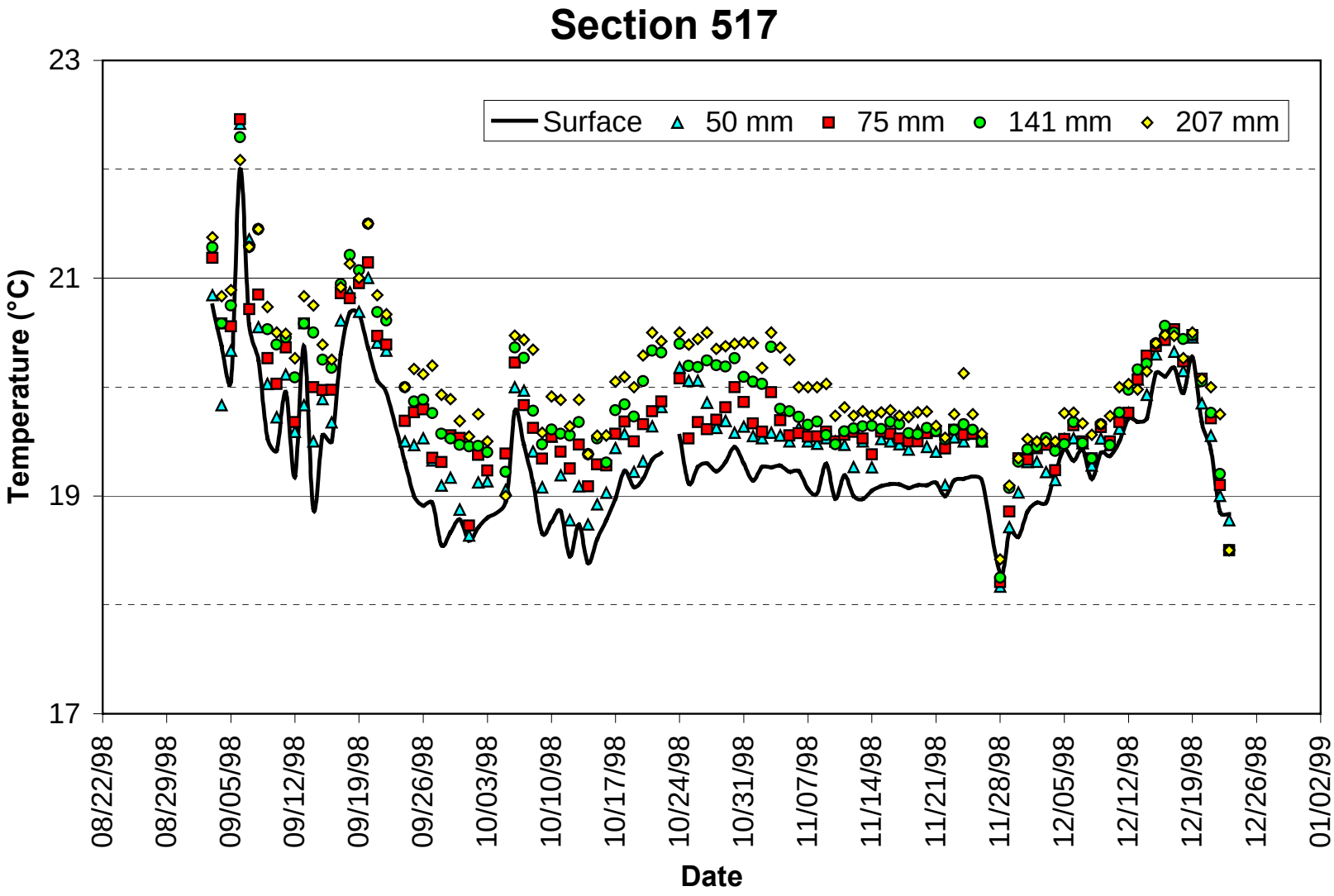

Figure 3.7. Average daily pavement temperatures in Section 517 (undrained, DGAC overlay).

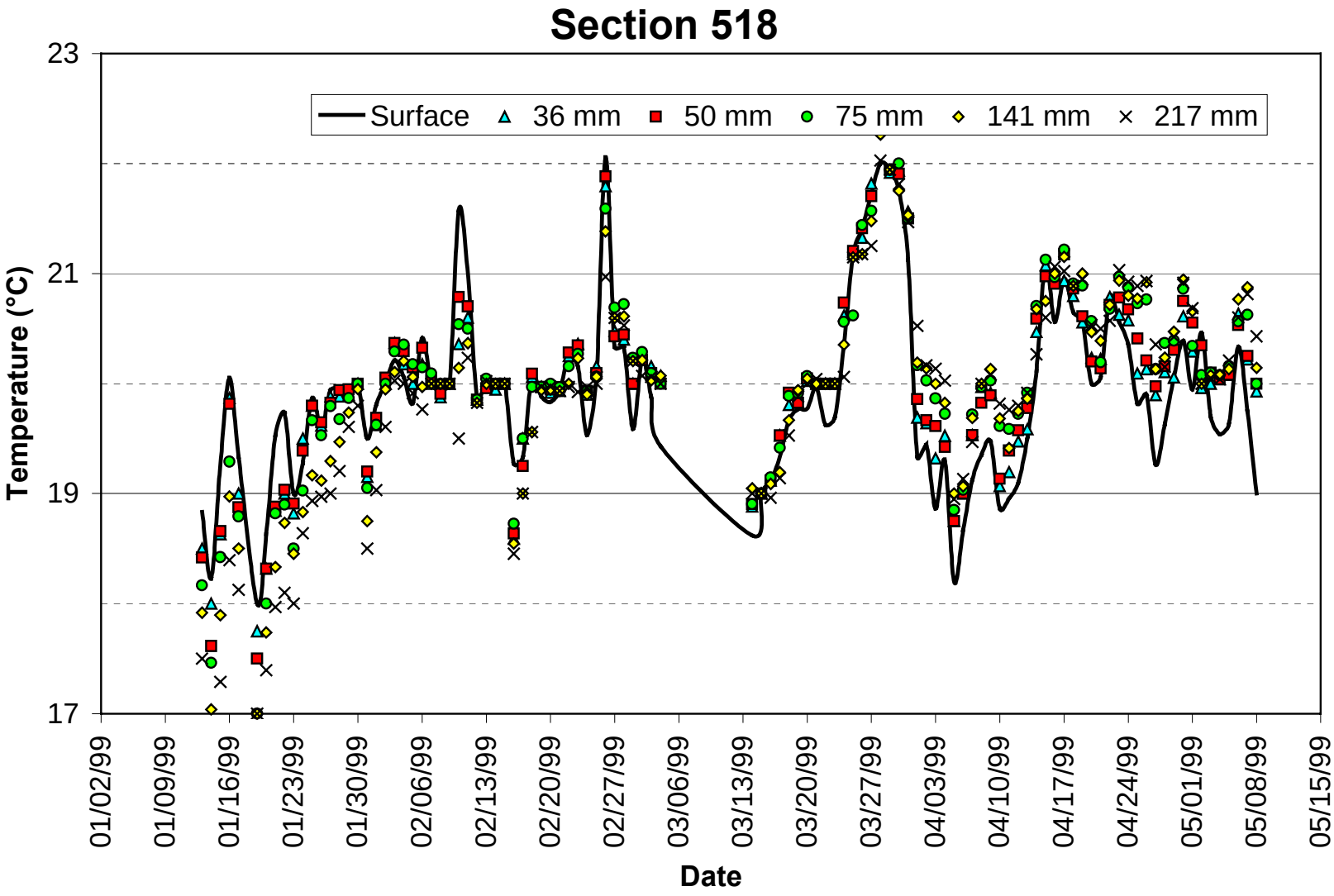

Figure 3.8. Average daily pavement temperatures in Section 518 (undrained, ARHM-GG overlay).

temperatures in Sections 515 and 518 decreased with depth. After mid-spring, pavement temperatures increased with depth.

For all test sections, average asphalt concrete temperatures were 19.9°C with a standard deviation of 0.7°C. Figures 3.9 and 3.10 summarize average asphalt concrete temperatures and standard deviation with depth. The figure shows that the target temperature of 20ºC at a depth of 50 mm was uniformly maintained within standard deviations of less than 1ºC.

3.2 Rainfall and Moisture Contents of Untreated Materials

Figures 3.11 and 3.12 show the monthly precipitation data collected at the National Weather Service Richmond Weather Station and the moisture content of the unbound layers. Dry and rainy seasons are clearly defined. The dry season included the months of June through September and the rainy season the months of October through May. The precipitation during the rainy season of 1997-1998 was significantly larger than that of 1998-1999.

The aggregate base, subbase, and subgrade moisture contents shown in Figures 3.11 and 3.12 are the average moisture contents monitored at four stations around the test sections as described Section 2.3.2.7. Figure 3.11 shows that the average moisture content of the aggregate base and subbase were not affected by precipitation. On the other hand, the variation of the subgrade moisture contents (Figure 3.12) approximately follows the precipitation trends.

A maximum of 5 percent reduction in subgrade moisture content occurred between the end of the rainy season and beginning of the dry season in 1998, which corresponds to the final phase of testing of Section 515 (100-kN traffic load) and the initial phase of testing of Section 517 (40-kN traffic load). It would be expected that these sections should have reduced elastic deflections and permanent deformations in the subgrade during these loading phases.

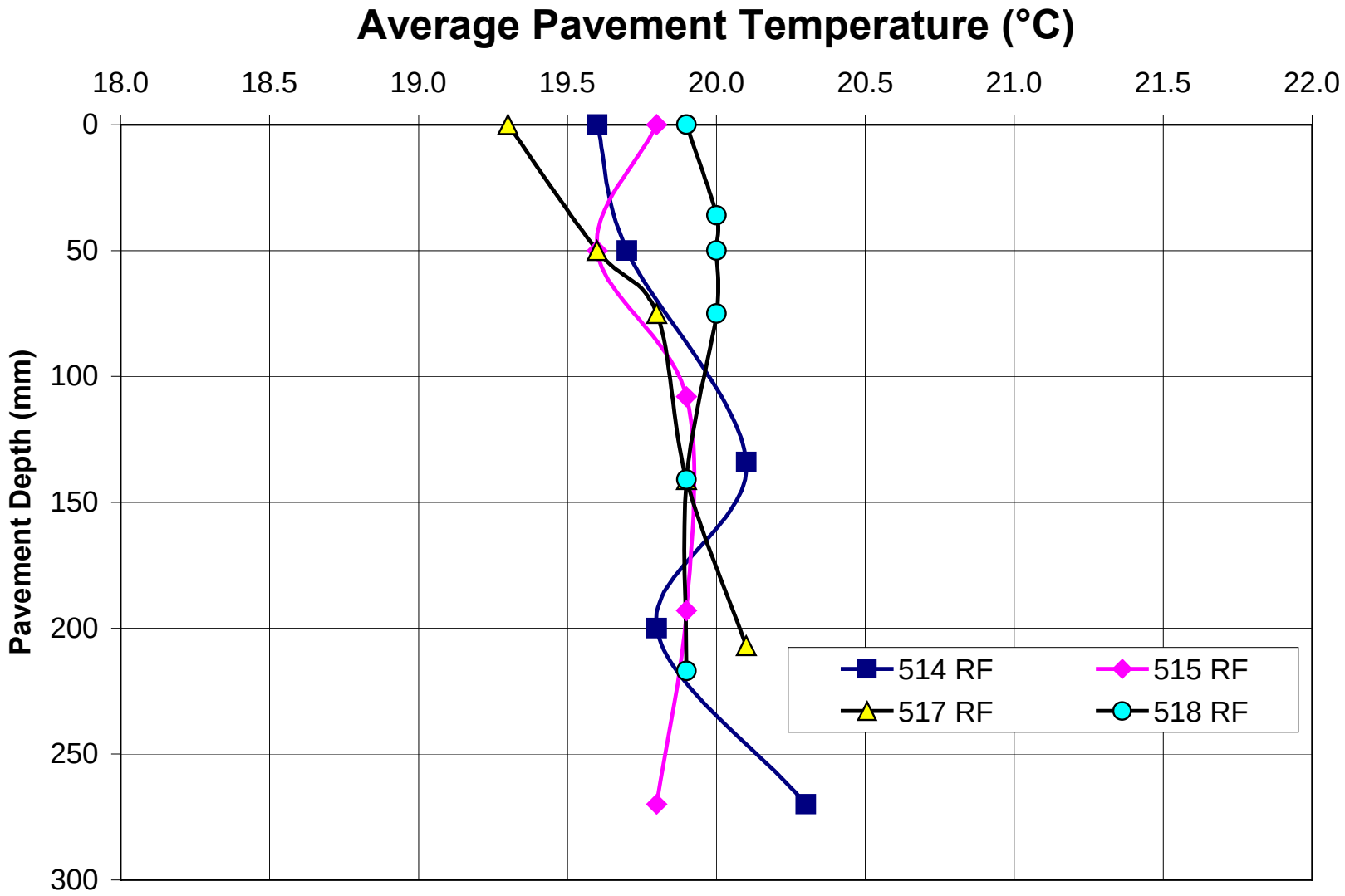

Figure 3.9. Asphalt concrete temperature gradients.

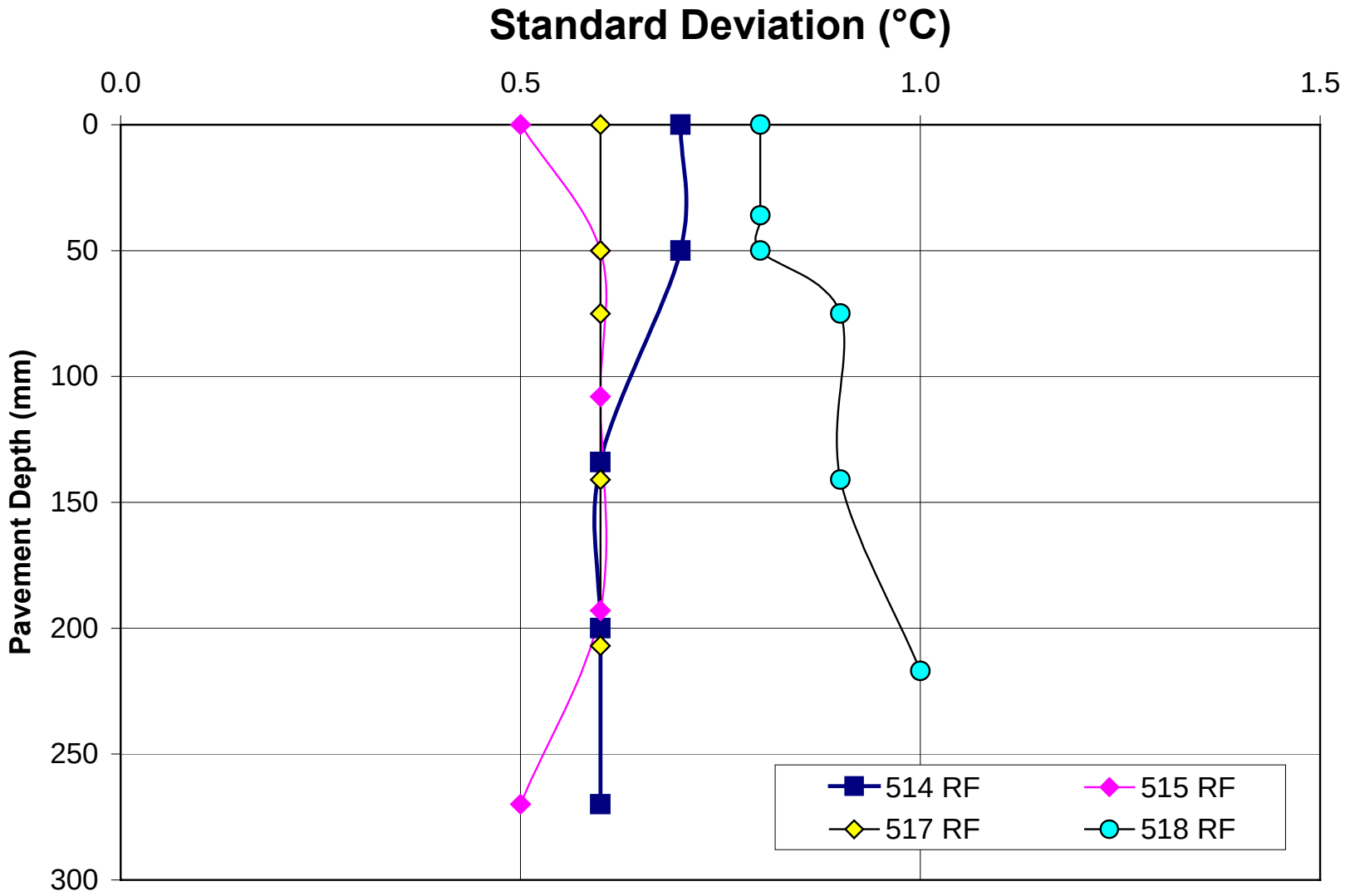

Figure 3.10. Asphalt concrete temperature standard deviation.

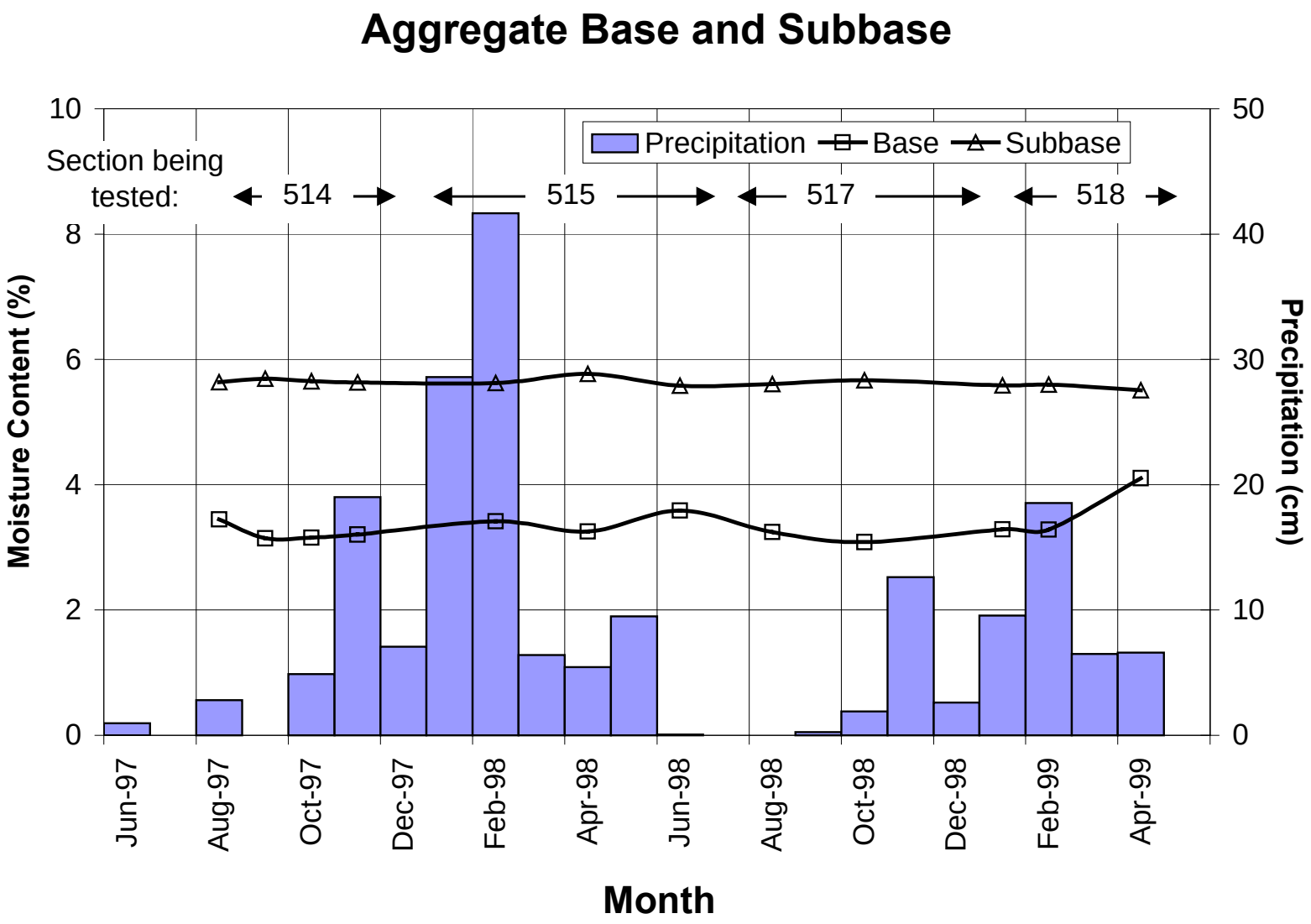

Figure 3.11. Average aggregate base and subbase layer moisture contents and precipitation over the course of testing.

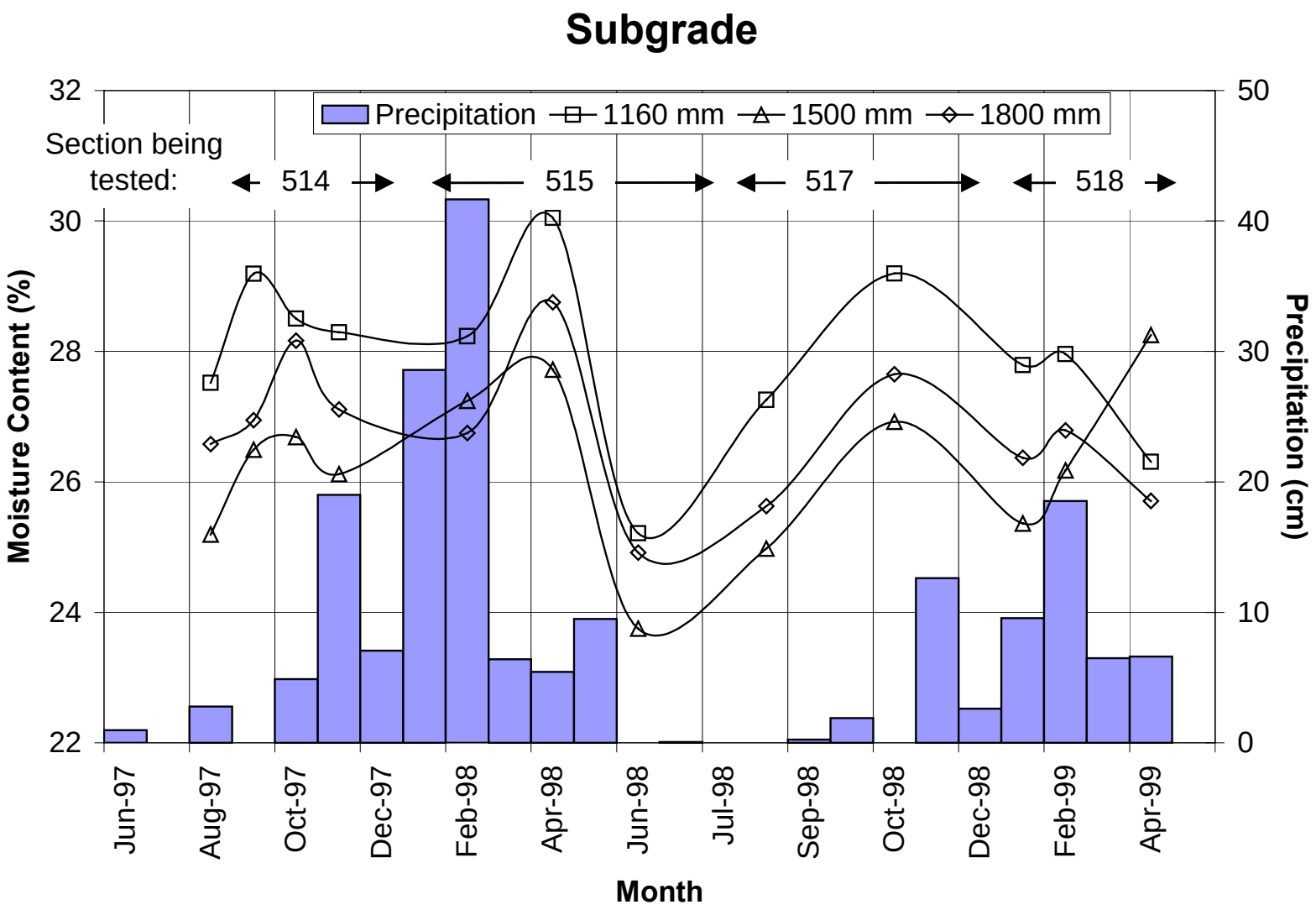

Figure 3.12. Average subgrade layer moisture contents and precipitation over the course of testing.

Table 3.2 shows average moisture contents at the four monitoring stations. Regardless of the 5 percent reduction in subgrade moisture content during May 1998, the fact that the test sections were located inside a building significantly reduced the variation of moisture contents in the untreated materials due to rainfall.

Table 3.2 Average Hydro-Probe Moisture Contents in Unbound Materials

Layer	Moisture Content, percent					
	Monitoring Station					
	N-CL	N-E	S-CL	S-W	Average	Standard Deviation
AB	3.6	2.6	3.6	3.1	3.3	0.5
ASB	5.6	5.7	5.6	5.7	5.6	0.1
SG1	27.6	29.4	27.1	28.8	28.1	1.6
SG2	25.3	26.0	25.8	27.7	26.2	1.8
SG3	26.6	26.5	27.0	28.5	26.9	1.7

3.3 Permanent Deformation Results

The laser profilometer was used to obtain surface profiles and monitor permanent deformation at the surface of the test sections. The MDDs were used to monitor in-depth pavement layer deformation.

3.3.1 Surface Rutting Measured with the Laser Profilometer

Figures 3.13–3.16 show average accumulated rut depth and average maximum rut depth measured with the laser profilometer for all four test sections. The average accumulated rut depth is the average of all profilometer readings from all points measured within the section, excluding the 1-m turnaround stations at each end of the sections. The average maximum rut depth is the maximum of the 256 data readings per measuring station averaged through the 13 data collection stations (Station 2 through Station 14, inclusive). Figures 3.13–3.16 show that

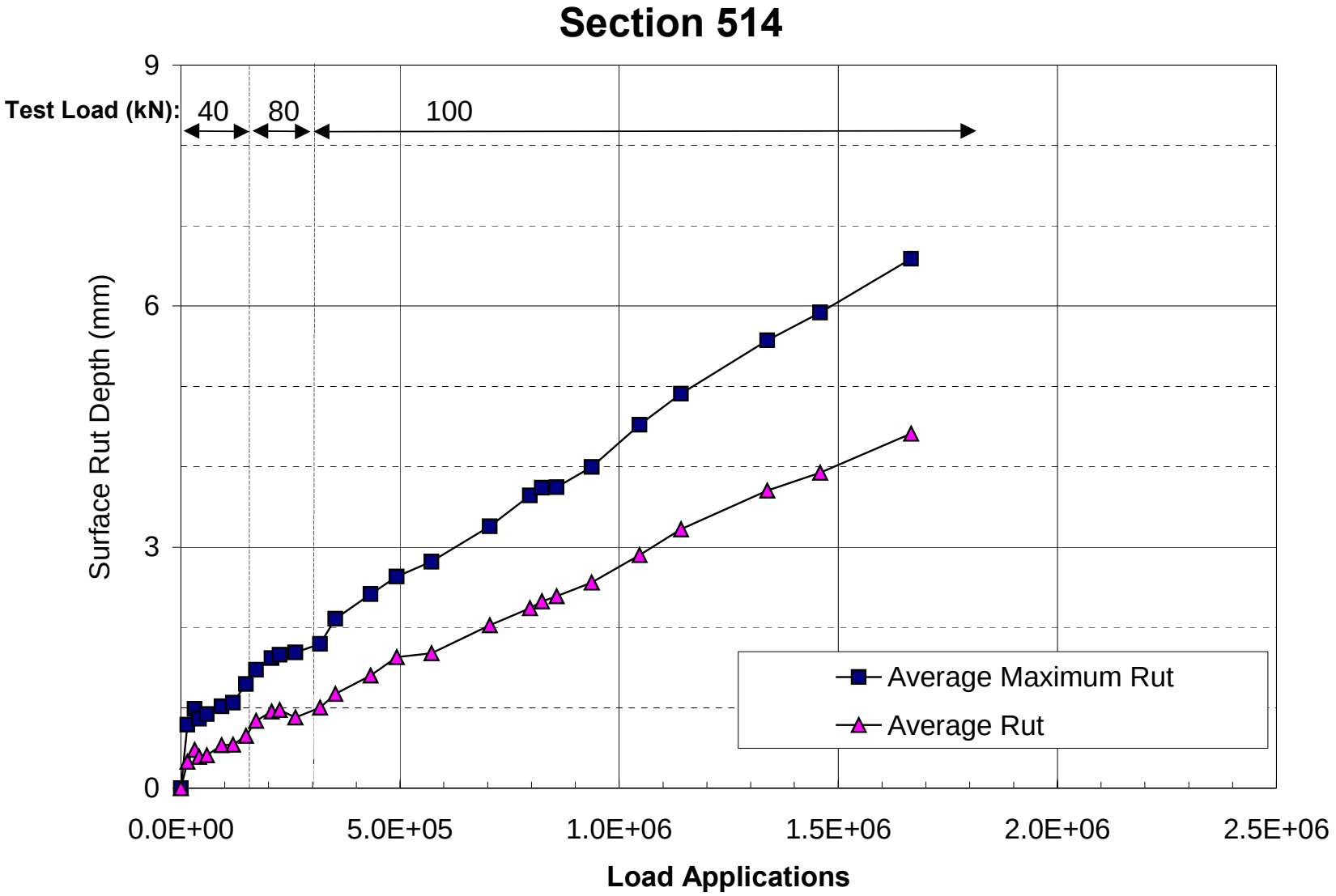

Figure 3.13. Surface rutting in Section 514 (drained, DGAC overlay).

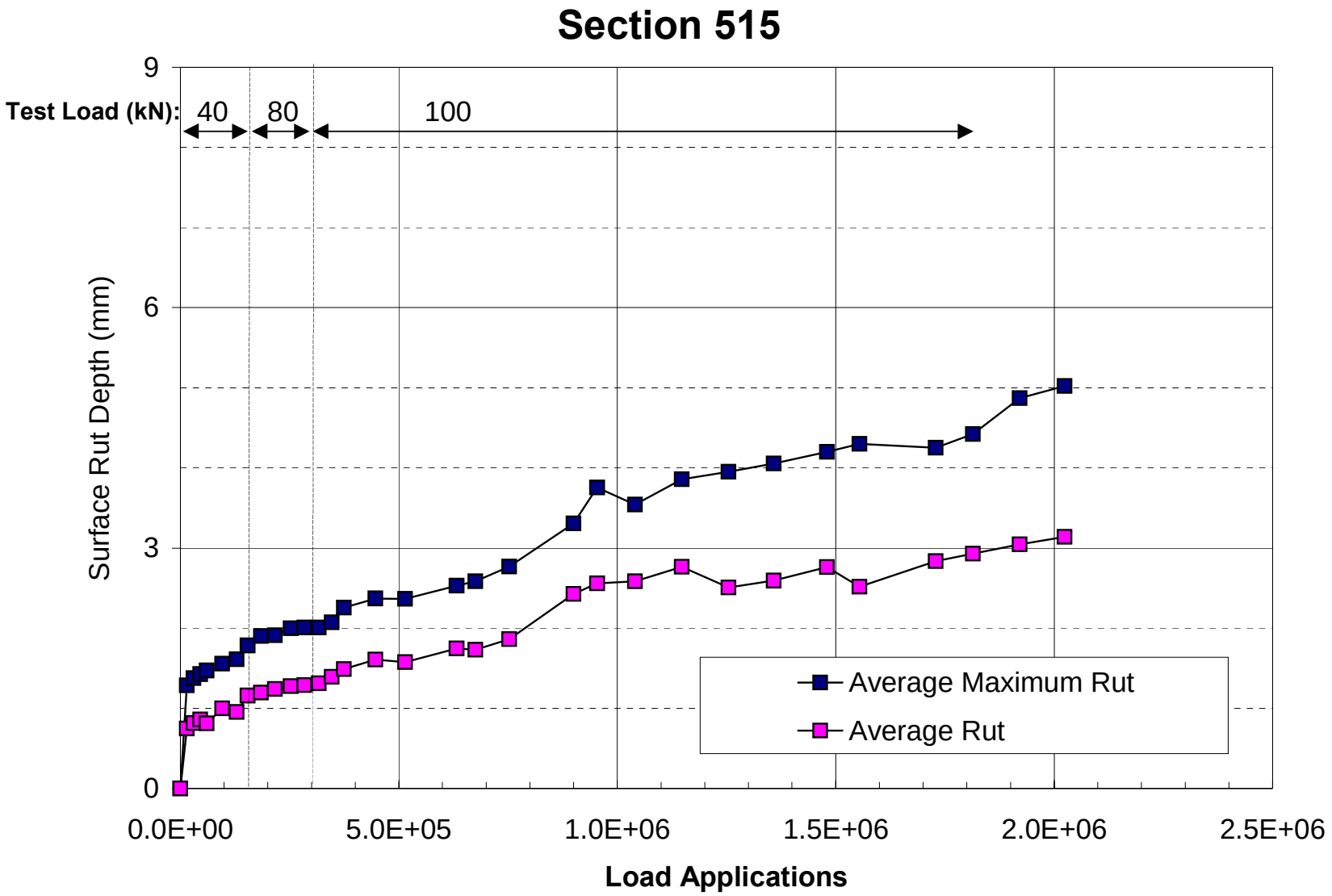

Figure 3.14. Surface rutting in Section 515 (drained, ARHM-GG overlay).

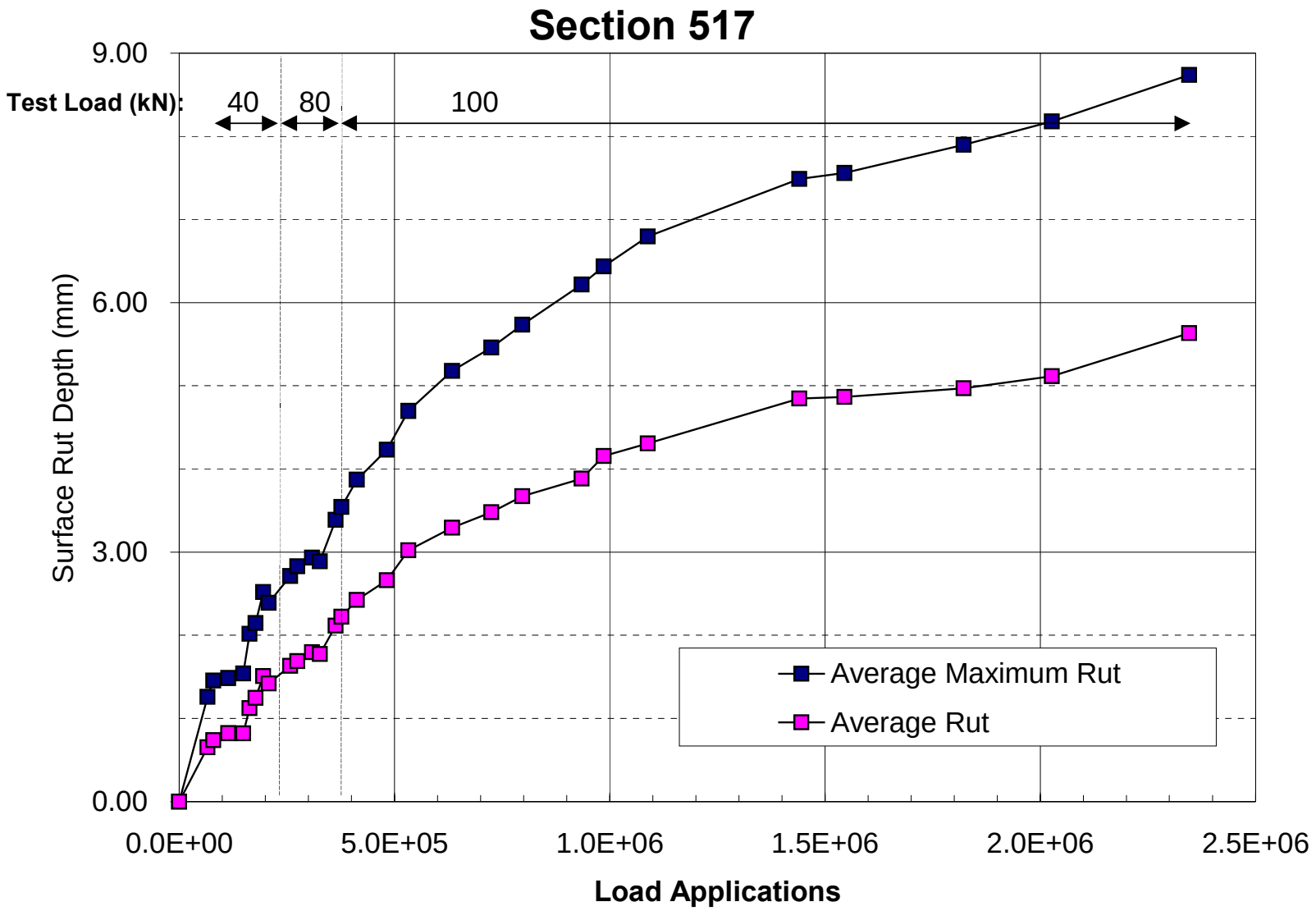

Figure 3.15. Surface rutting in Section 517 (undrained, DGAC overlay).

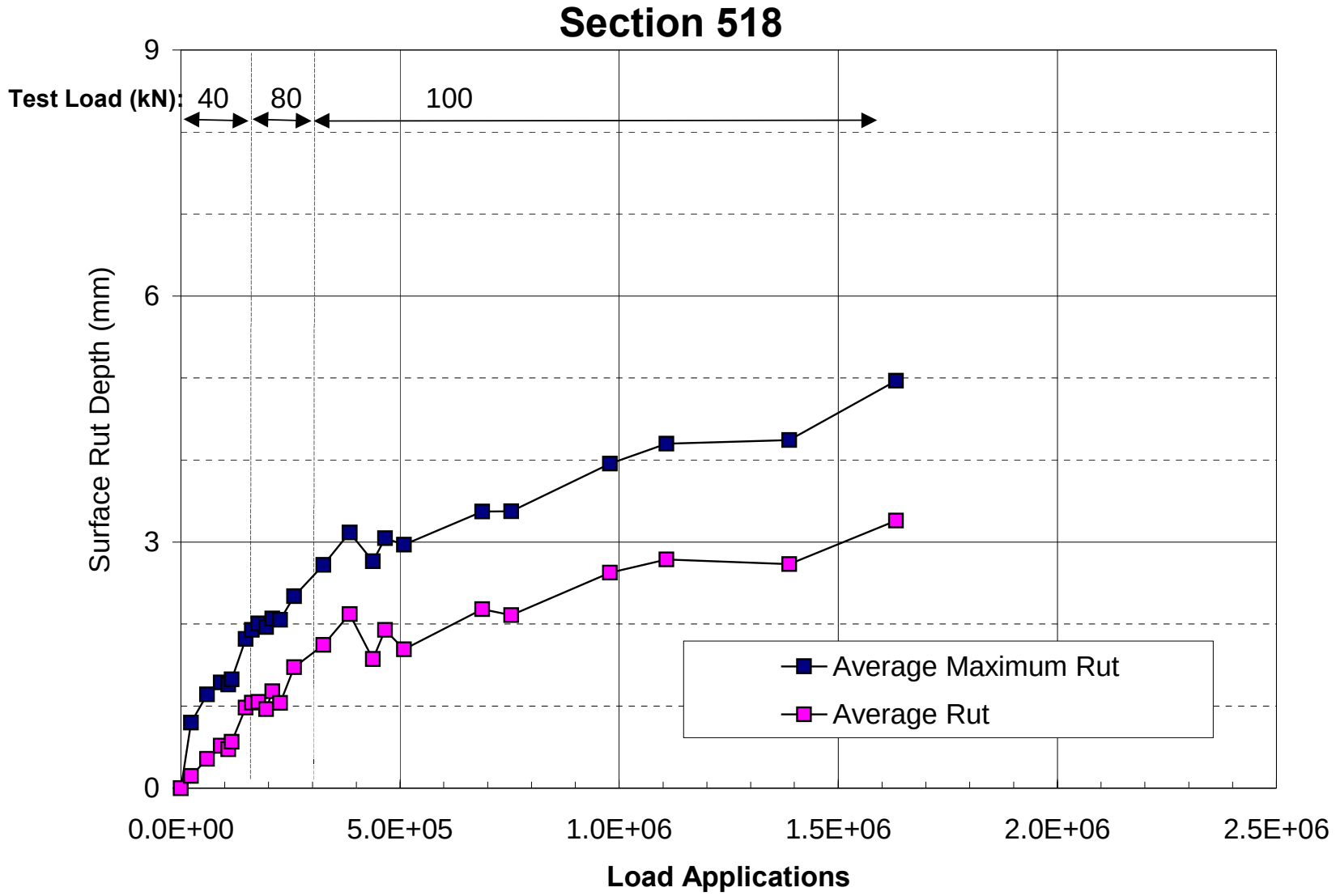

Figure 3.16. Surface rutting in Section 518 (undrained, ARHM-GG overlay).

the sections with the DGAC overlay (Sections 514 and 517) had more rutting than the sections with the ARHM-GG overlay (Sections 515 and 518).

After 1.6 million load applications, the sections with the DGAC overlay (Sections 514 and 517) had accumulated surface rut depths that were about 52 percent greater than the accumulated rut depths in sections with the ARHM-GG overlay (Sections 515 and 518).

Table 3.3 shows maximum rut depths at levels of load application. These levels of load application correspond approximately to the end of traffic of the 40-, 80-, and 100-kN traffic loads for all four test sections. Table 3.3 shows that up to the completion of 310 thousand load applications, no significant difference was observed between the two overlay strategies. However, after 310 thousand load applications, the sections with the ARHM-GG overlay exhibited less deformation than the sections with DGAC overlays. The data also show that for a given overlay strategy, the undrained sections had slightly larger rut depths than the drained sections.

Table 3.3 Average Maximum Rut Depths

Section		Accumulated Surface Rutting (mm) at Three Levels of Traffic of Load Application		
		145,000	**310,000**	**1'600,000**
Drained	514 DGAC	0.7	1.0	4.4
	515 ARHM-GG	1.2	1.3	2.8
Undrained	517 DGAC	0.8	1.8	4.9
	518 ARHM-GG	1.0	1.5	3.3

Figures 3.13–3.16 also show the embedding phase during which the pavement surface undergoes a significant increase in surface rutting. Embedding phases were present during the first HVS traffic repetitions at each of the 40-, 80-, and 100-kN loads. After the embedding phase, a decrease in rut depth accumulation with load applications was observed. The embedding phase under the 100-kN traffic load in Section 517 was significantly larger than for the other sections.

Figures 3.17–3.20 show rut depth distribution at the end of HVS testing for all four sections. The data distribution shows that all the sections had "humps" of uplifted material of less than 3 mm height at the sides of the traffic areas. Large rut depths developed along the centerline of the section. The centerline received more load applications than other areas of the section due to the traffic pattern applied (see Figure 2.5). Fairly uniform rut depths were obtained for the sections with the ARHM-GG overlay (Sections 515 and 518) and less uniform for the section with the DGAC overlay (Sections 514 and 517).

Compared to the DGAC overlay, the rutting performance of the ARHM-GG overlay is surprising considering its high air-void content. Section 3.3.5 discusses air-void contents of the overlay strategies.

3.3.2 In-Depth Permanent Deformation of the Drained Sections Measured with the MDD

3.3.2.1 Section 514 (DGAC)

Figures 3.21–3.24 show in-depth MDD permanent deformation data and surface rutting profilometer data recorded at Stations 4, 6, 10, and 12. The data show that most of the rutting occurred within the asphalt-bound layers. The MDDs located at Station 10 recorded the highest rut depth in the section. The surface measurements recorded with this MDD are in good agreement with the profilometer data obtained at the same station.

Table 3.4 presents the average permanent deformation contribution of each layer to surface rutting. Data are presented for average readings at Stations 4 and 6 and at Stations 10 and 12 because MDDs were installed at different layer interfaces as described in the Goal 3 test plan. Table 3.4 shows that at Stations 4 and 6, 78 percent of the surface rutting occurred in the asphalt-bound layers (DGAC overlay, AC patch, asphalt concrete, ATPB) with approximately 50

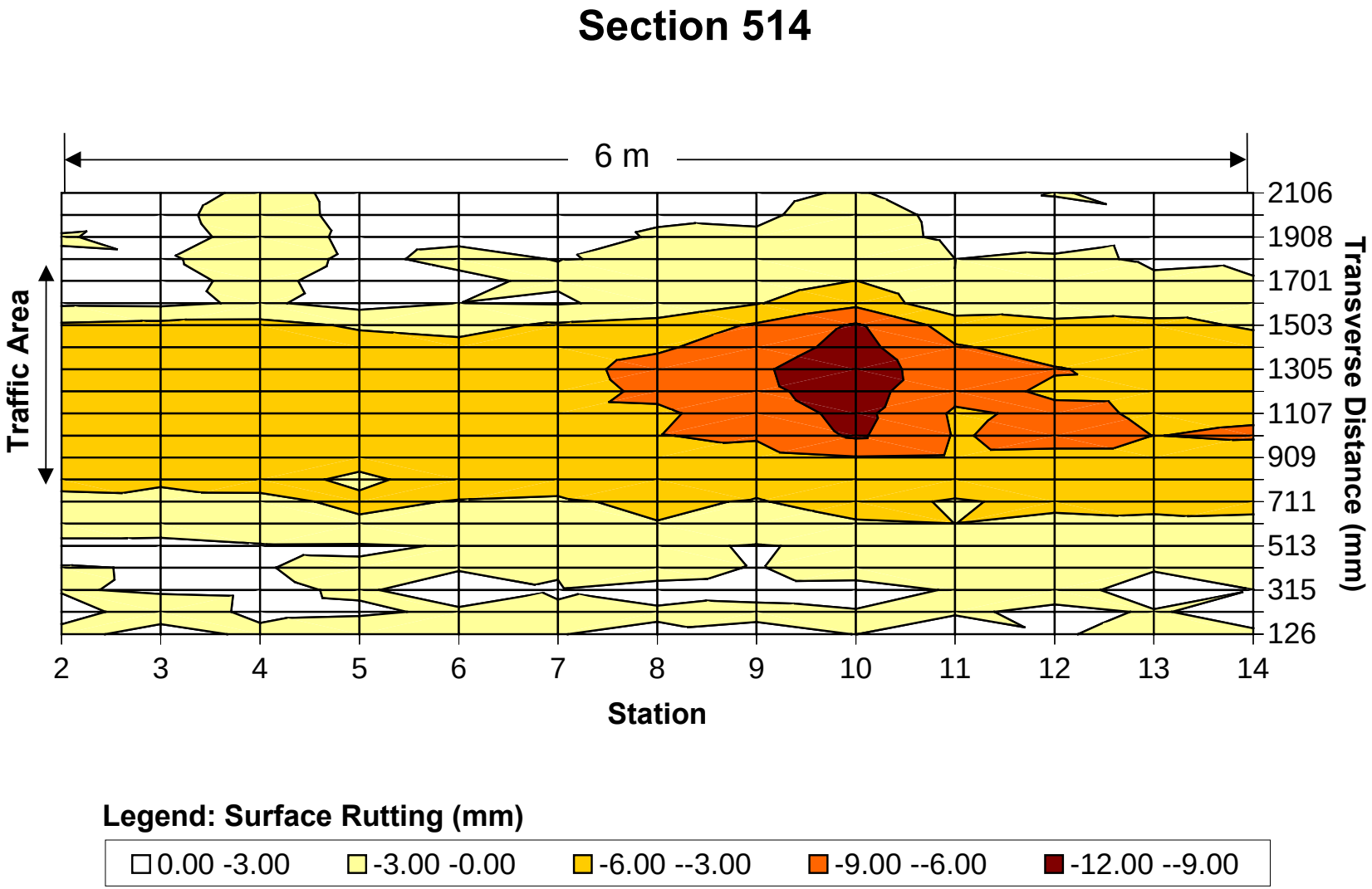

Figure 3.17. Rut depth distribution after HVS testing in Section 514 (drained, DGAC overlay).

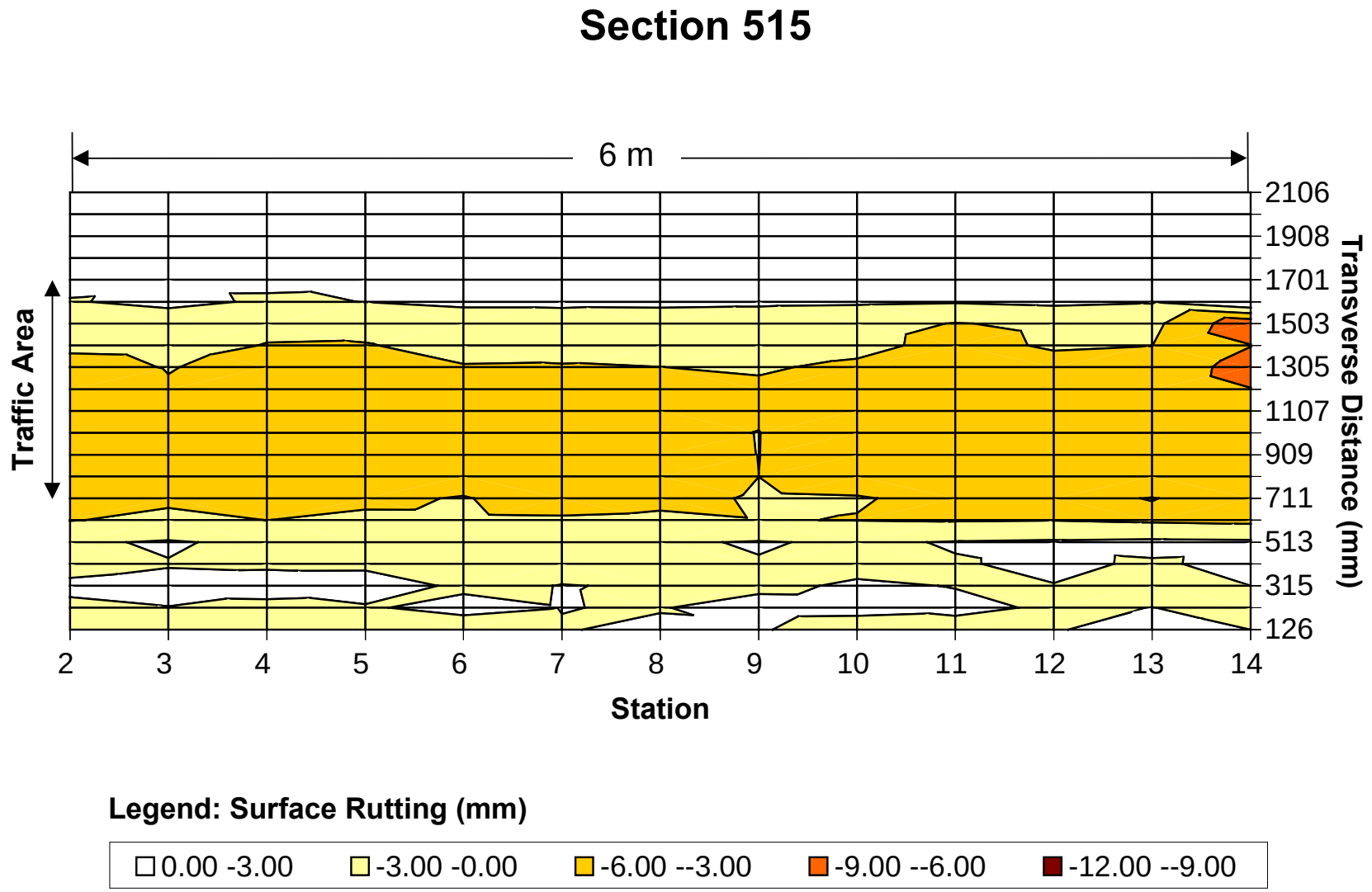

Figure 3.18. Rut depth distribution after HVS testing in Section 515 (drained, ARHM-GG overlay).

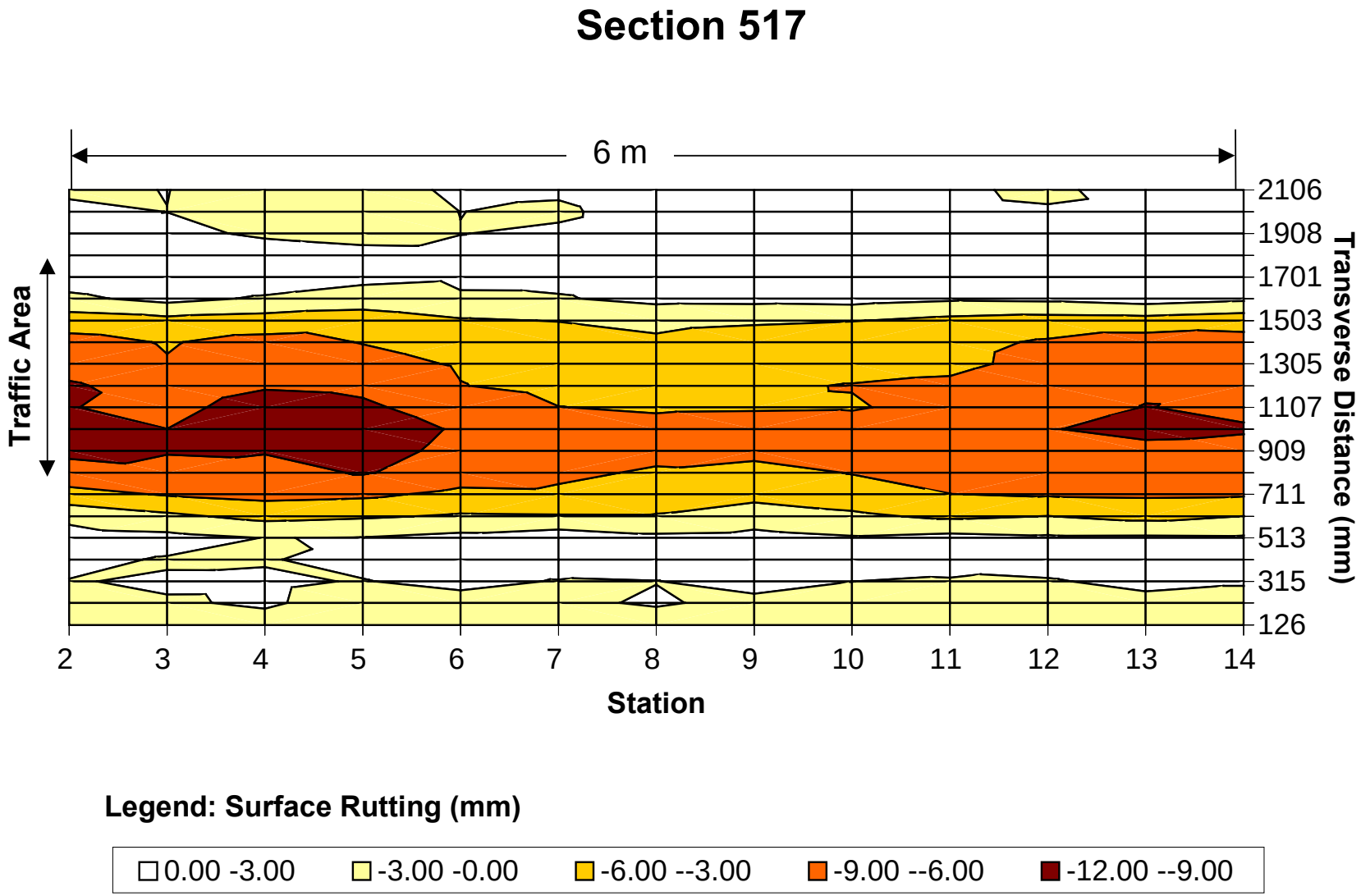

Figure 3.19. Rut depth distribution after HVS testing in Section 517 (undrained, DGAC overlay).

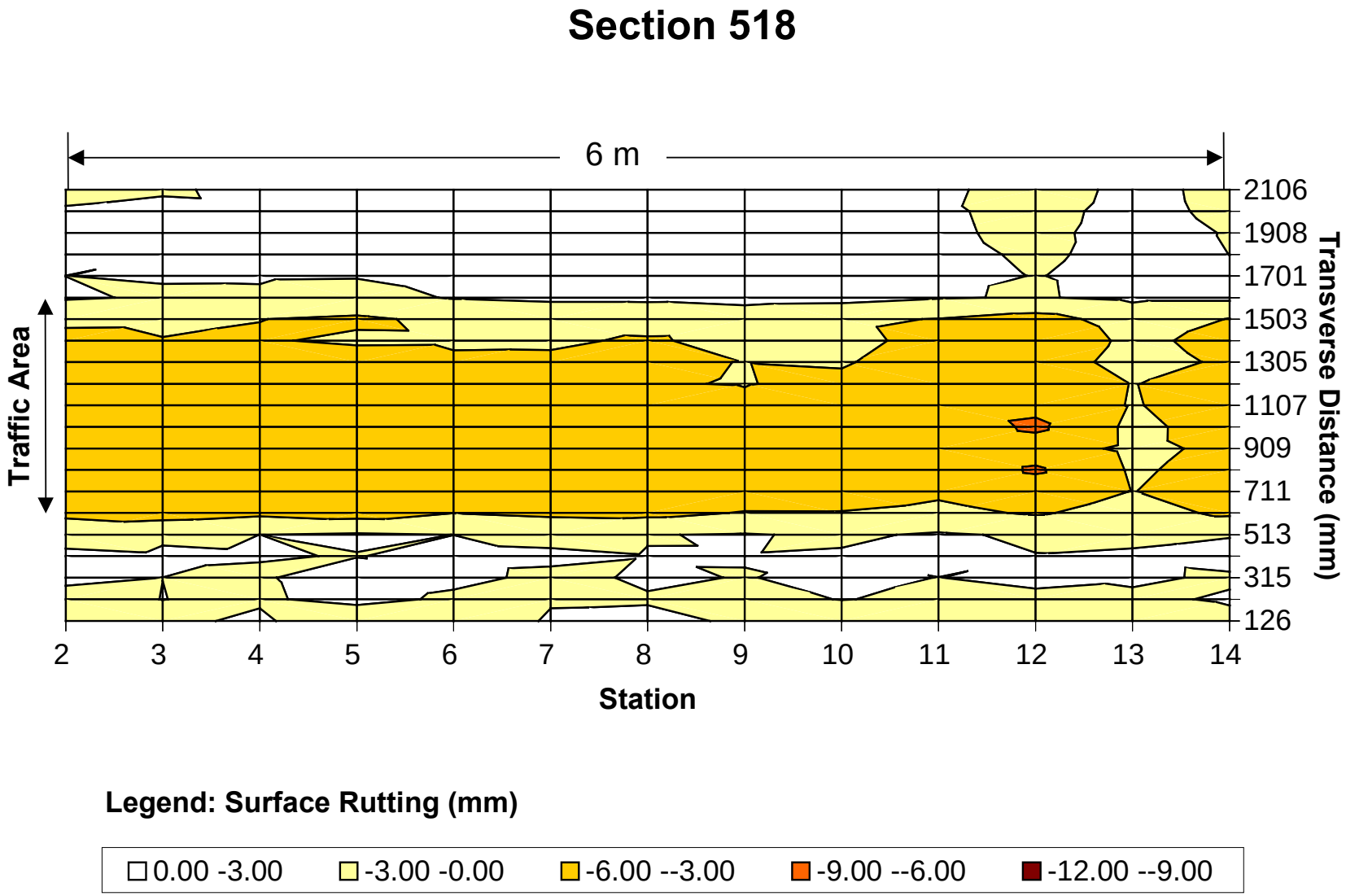

Figure 3.20. Rut depth distribution after HVS testing in Section 518 (undrained, ARHM-GG overlay).

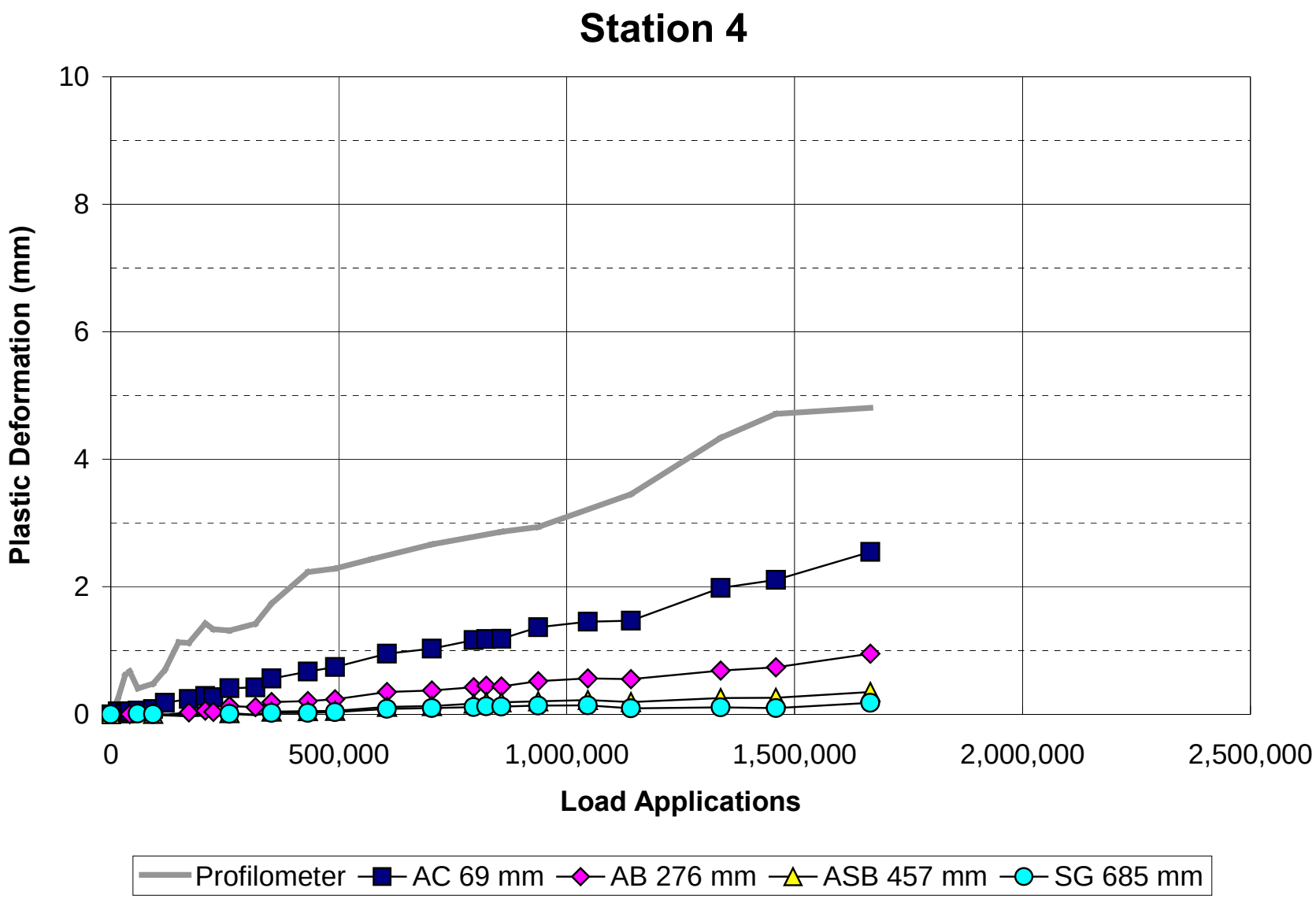

Figure 3.21. In-depth permanent deformation at Station 4, Section 514 (drained, DGAC overlay).

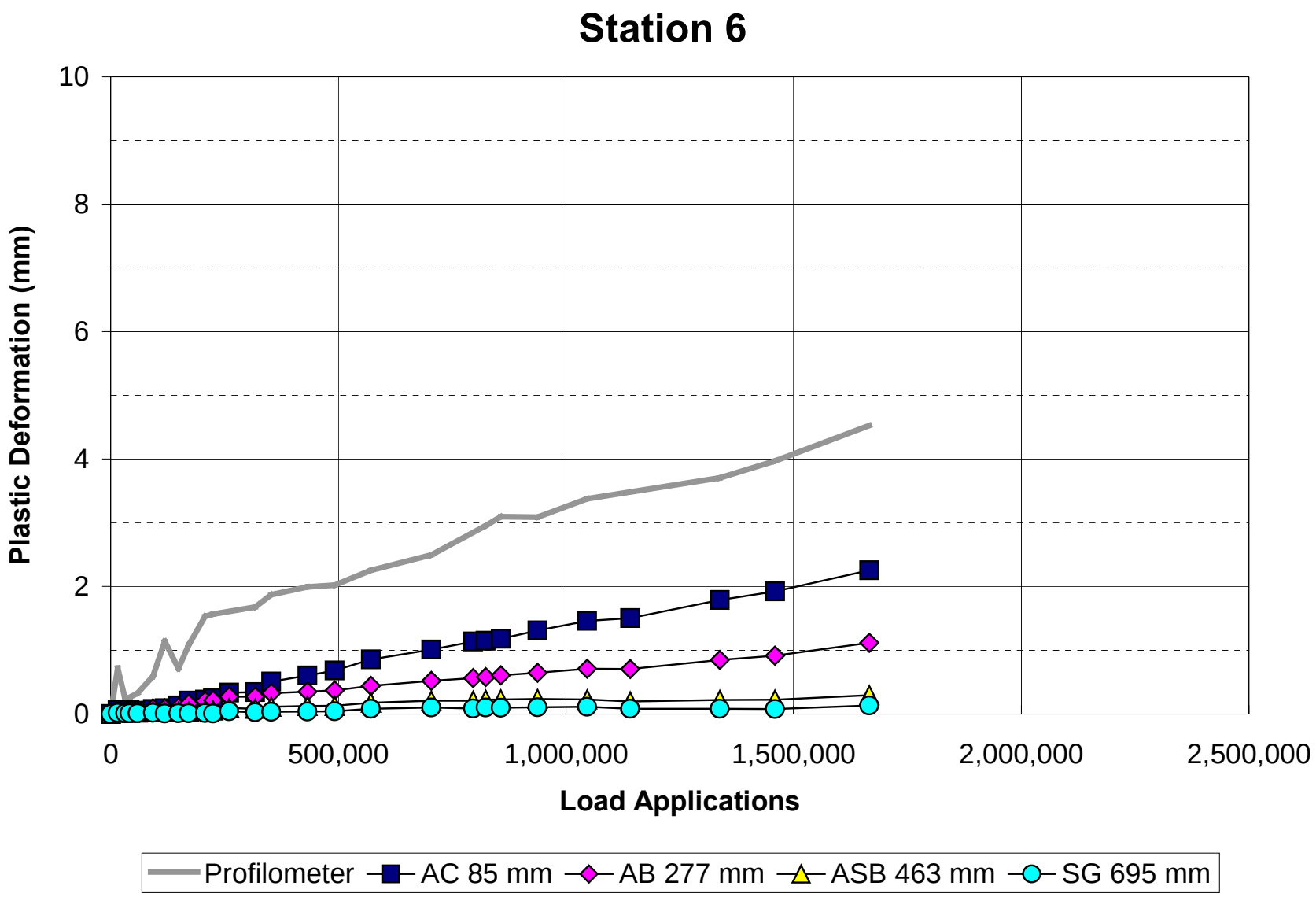

Figure 3.22. In-depth permanent deformation at Station 6, Section 514 (drained, DGAC overlay).

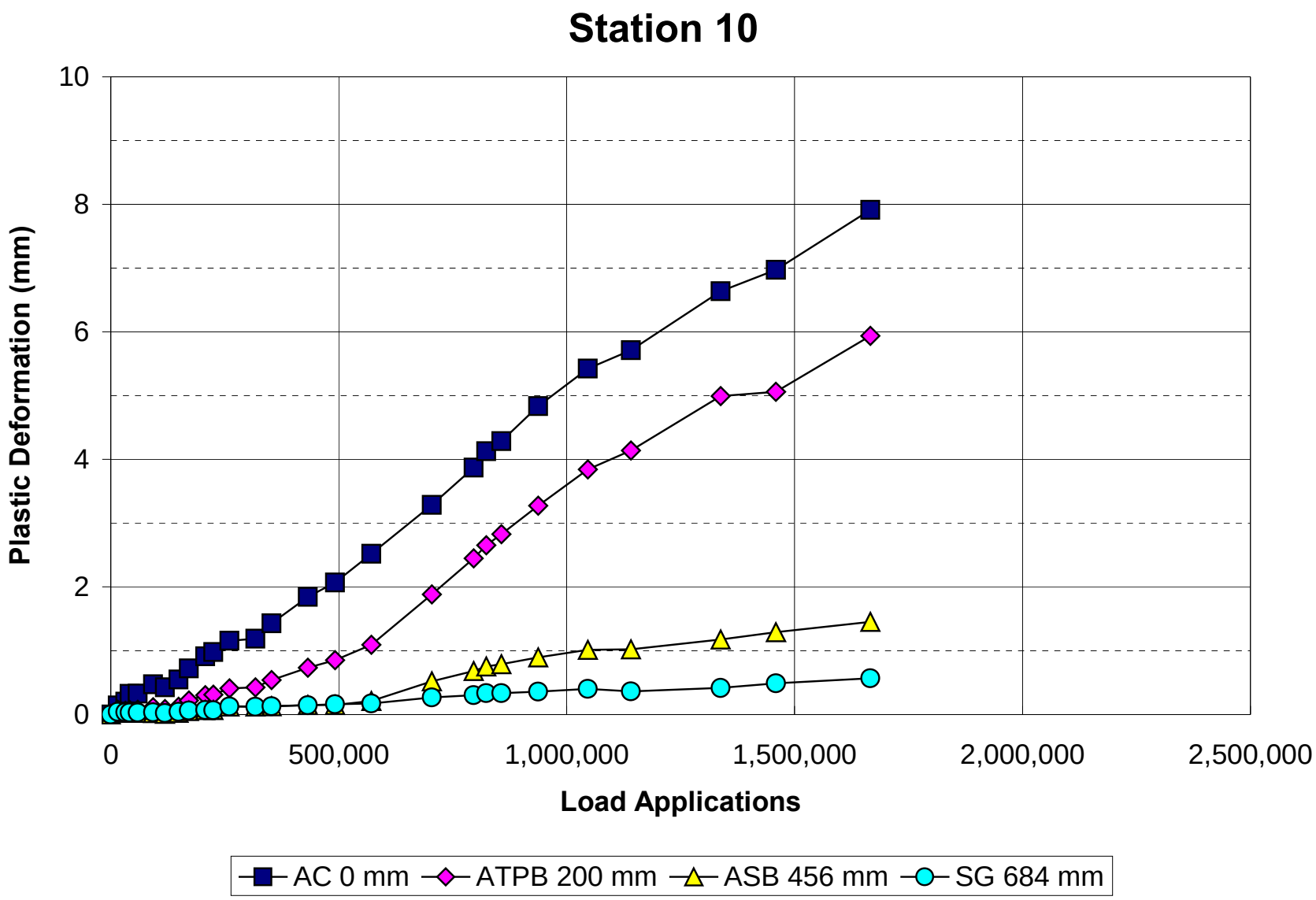

Figure 3.23. In-depth permanent deformation at Station 10, Section 514 (drained, DGAC overlay).

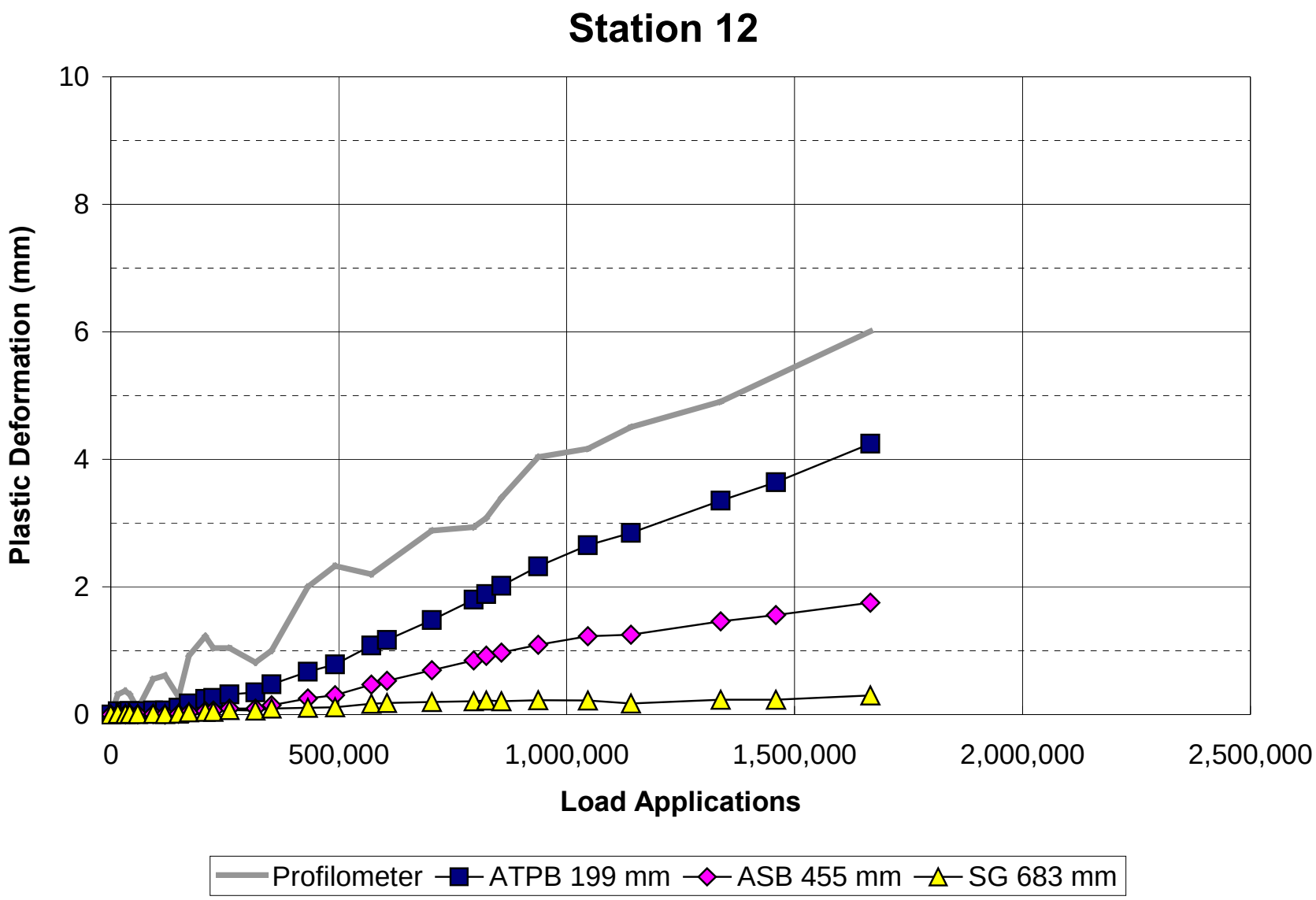

Figure 3.24. In-depth permanent deformation at Station 12, Section 514 (drained, DGAC overlay).

percent occurring in the DGAC overlay. Rutting contribution of the unbound layers was about 22 percent, with about 3 percent attributed to the subgrade. Data at Stations 10 and 12 show that the contribution of both the DGAC overlay and old AC were approximately 37 percent. A rutting contribution of 45 percent is attributed to the ATPB and AB layers around this location.

Table 3.4 Average Rutting Contribution of Pavement Layers in Section 514

Pavement Layer	MDDs 4 and 6			MDDs 10 and 12		
	Permanent Deformation on Top of Layer (mm)	**Contribution (percent)**	**Permanent Deformation per Layer Thickness (10^{-2} mm)**	**Permanent Deformation on Top of Layer (mm)**	**Contribution (percent)**	**Permanent Deformation per Layer Thickness (10^{-2} mm)**
DGAC Overlay + Patch	4.7	48.6	2.7	8.1	37.0	0.9
AC	2.4	29.3	0.7	n/a*	n/a	n/a
ATPB	n/a	n/a	n/a	5.1	45.4	0.8
Base	1.0	15.2	0.4	n/a	n/a	n/a
Subbase	0.3	3.5	0.1	1.4	10.6	0.2
Subgrade	0.2	3.4	n/a	0.6	7.0	n/a
Total		***100.0***			***100.0***	

* n/a indicates that an MDD was not present at this layer and location

Rutting contributions of the ASB and SG varied among Stations 4 and 6 and Stations 10 and 12, but in all cases the combined rutting contribution of these two layers was less than 17 percent of the total rut depth. The differences in rutting contributions can be due to construction variability possibly related to thickness and layer density.

There are indications that the ATPB may have contributed to rutting out of proportion with its 75-mm thickness. The thickness of this layer is too small to measure rutting using the MDD. However, when combined with aggregate base or the asphalt concrete, the rutting contribution of the combined layers increases indicating that the ATPB may be responsible. However, the trenching data presented in 3.3.6 indicates that the aggregate base rather than the ATPB is responsible for the increased permanent deformation.

3.3.2.2 Section 515 (ARHM-GG)

Figures 3.25–3.28 show surface and in-depth permanent deformation data monitored at Stations 4, 6, 10, and 12. The figures show that significant rutting occurred in the asphalt-bound layers, and in particular in the ATPB layer. The average rutting contributions of the layers are presented in Table 3.5. The average contribution of the bound layers is approximately 78 percent, with about 40 percent attributed to the ATPB. Rutting contribution of the unbound layers was 22 percent, with about 6 percent attributed to the subgrade.

Table 3.5 Average Rutting Contribution of Pavement Layers in Section 515

Pavement Layer	MDD Location*	Permanent Deformation Measured at Top of Layer (mm)	Contribution (percent)	Permanent Deformation per Layer Thickness (10^{-2} mm)
ARHM-GG Overlay	10	4.0	24.9	2.5
AC	4, 6	3.0	13.2	0.4
ATPB	10	2.5	40.3	2.5
Base	4, 6	0.9	7.6	0.2
Subbase	4, 6, 12	0.6	8.0	0.2
Subgrade	6, 10	0.2	6.0	
Total			***100.0***	

* MDDs were positioned at different depths for different locations on the test section. If more than one MDD was located at a given layer, the average deformation is presented.

3.3.3 In-Depth Permanent Deformation of the Undrained Sections

3.3.3.1 Section 517 (DGAC)

Figures 3.29–3.31 show surface and in-depth permanent deformation data monitored at Stations 4, 6, and 9. The data show that the DGAC overlay significantly contributed to surface rutting. Table 3.6 shows that more than 54 percent of the surface rutting occurred in the asphalt-bound layers with 42 percent attributed to the DGAC overlay. The rutting contribution of the

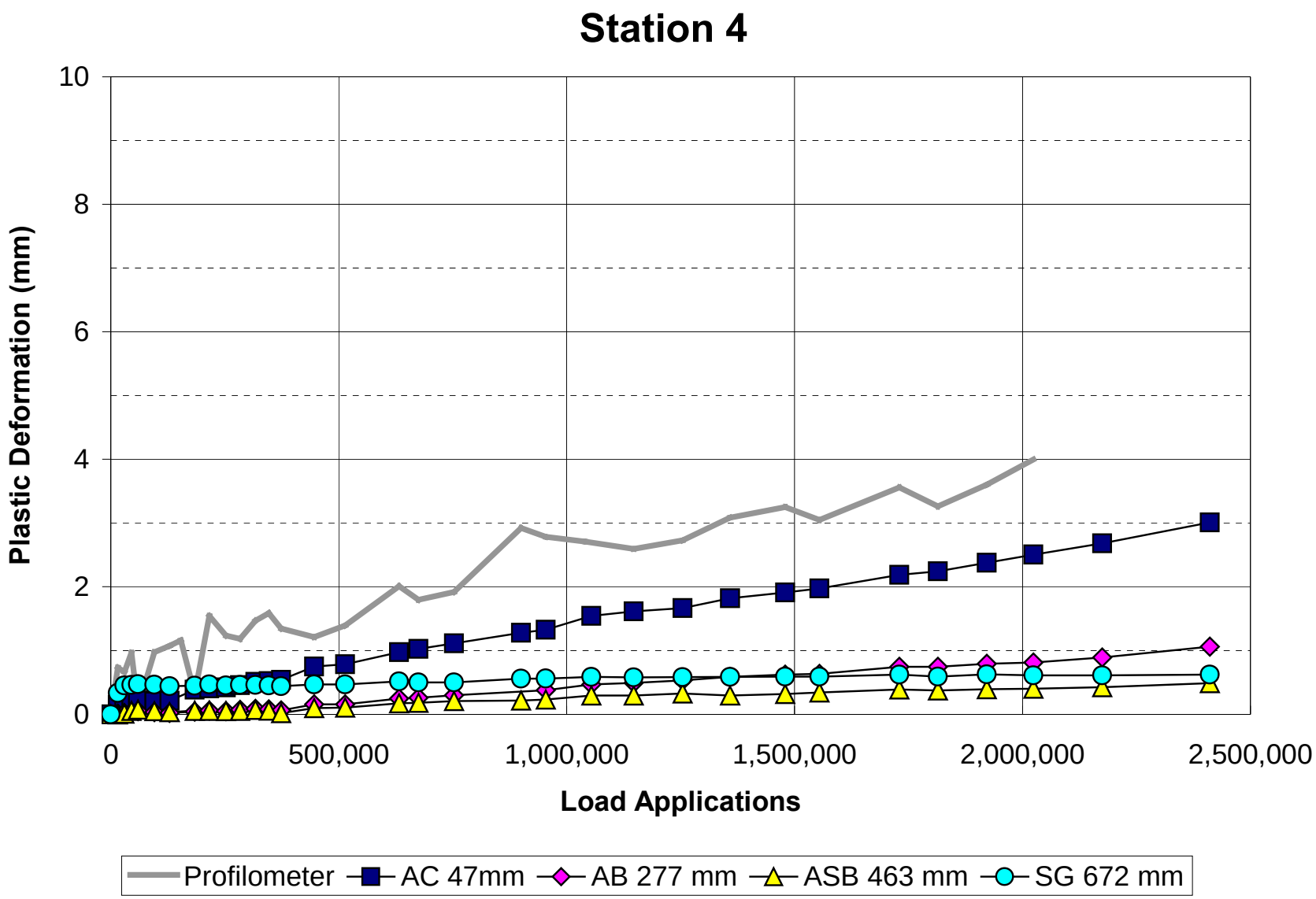

Figure 3.25. In-depth permanent deformation at Station 4, Section 515 (drained, ARHM-GG overlay).

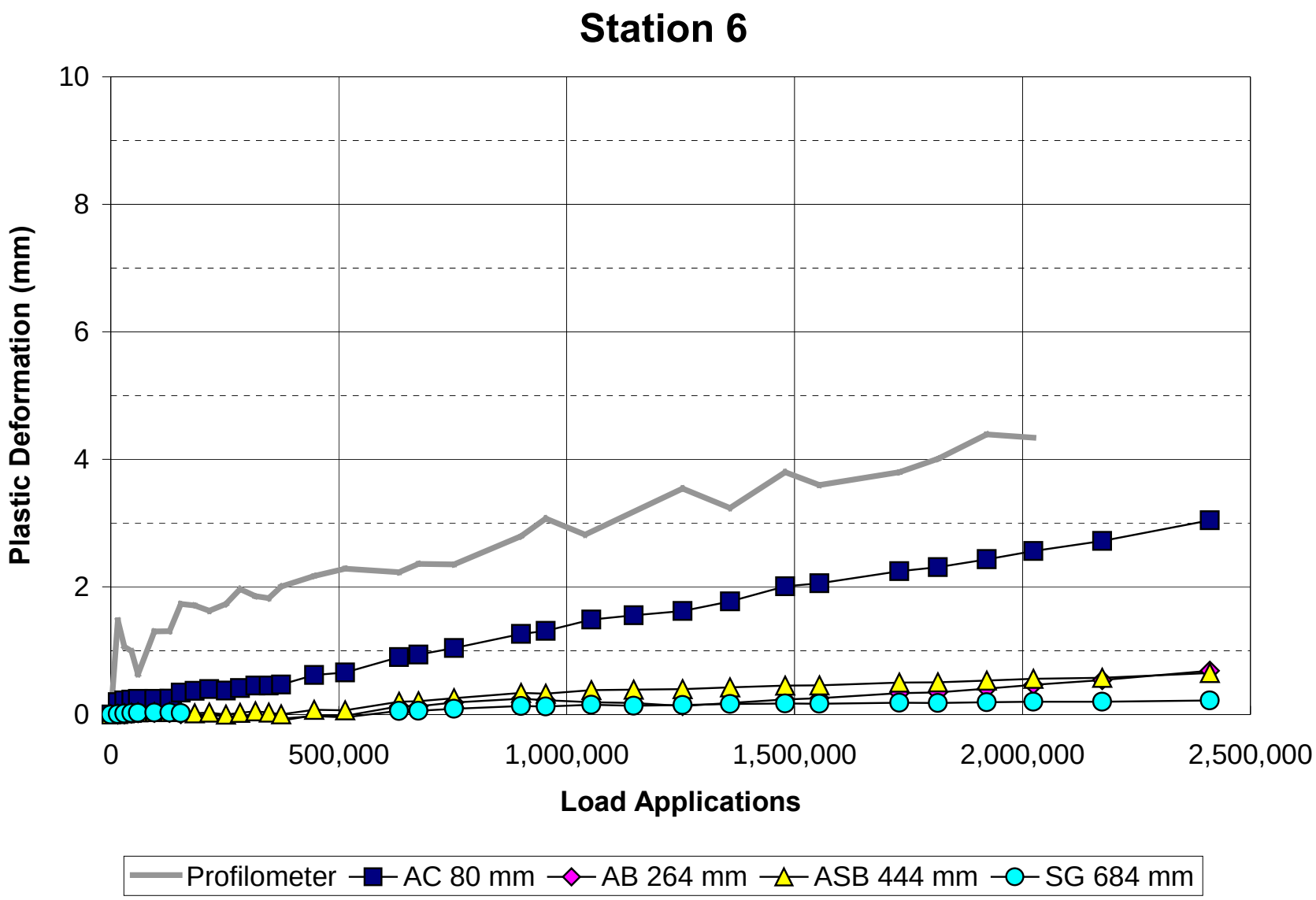

Figure 3.26. In-depth permanent deformation at Station 6, Section 515 (drained, ARHM-GG overlay).

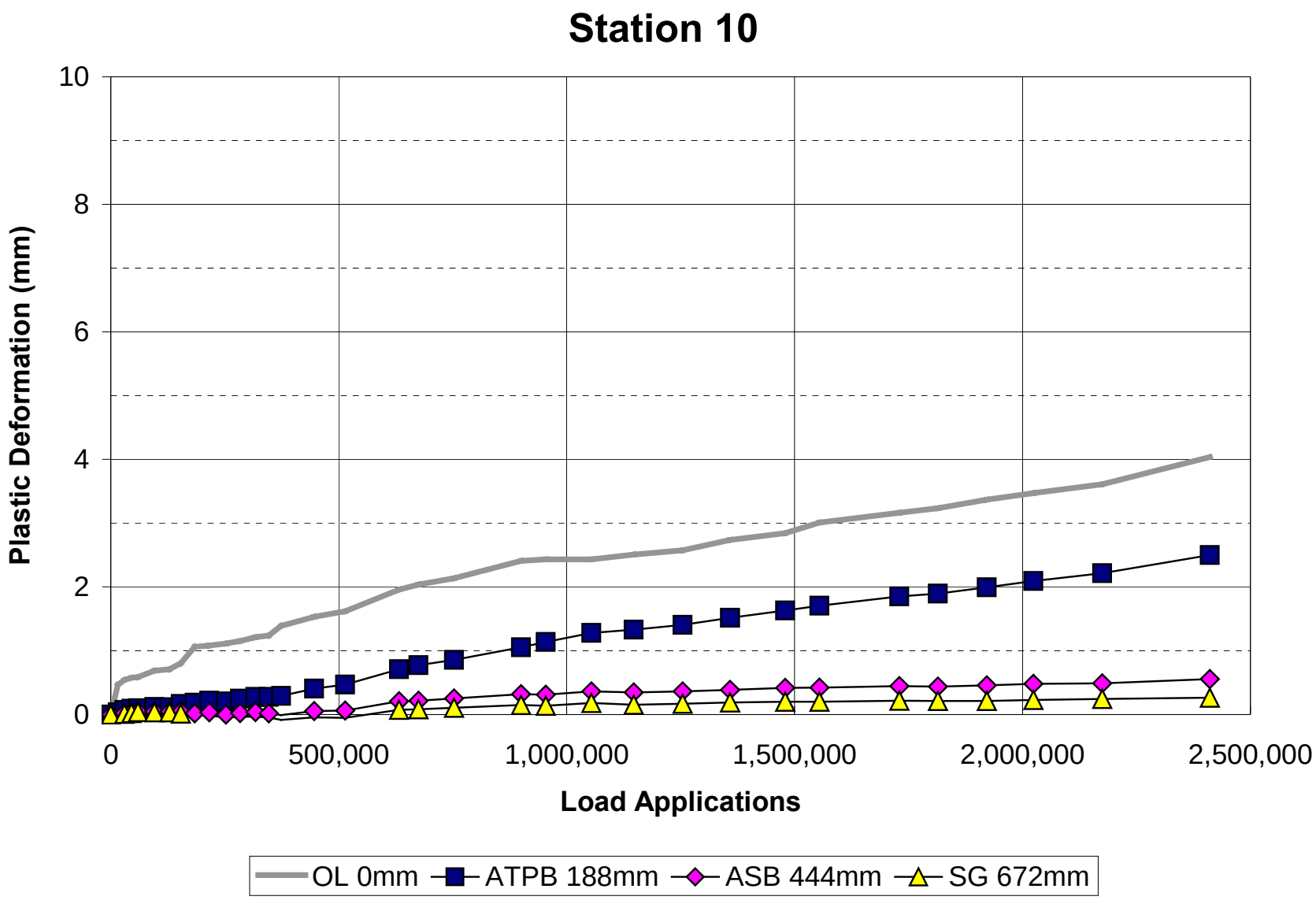

Figure 3.27. In-depth permanent deformation at Station 10, Section 515 (drained, ARHM-GG overlay).

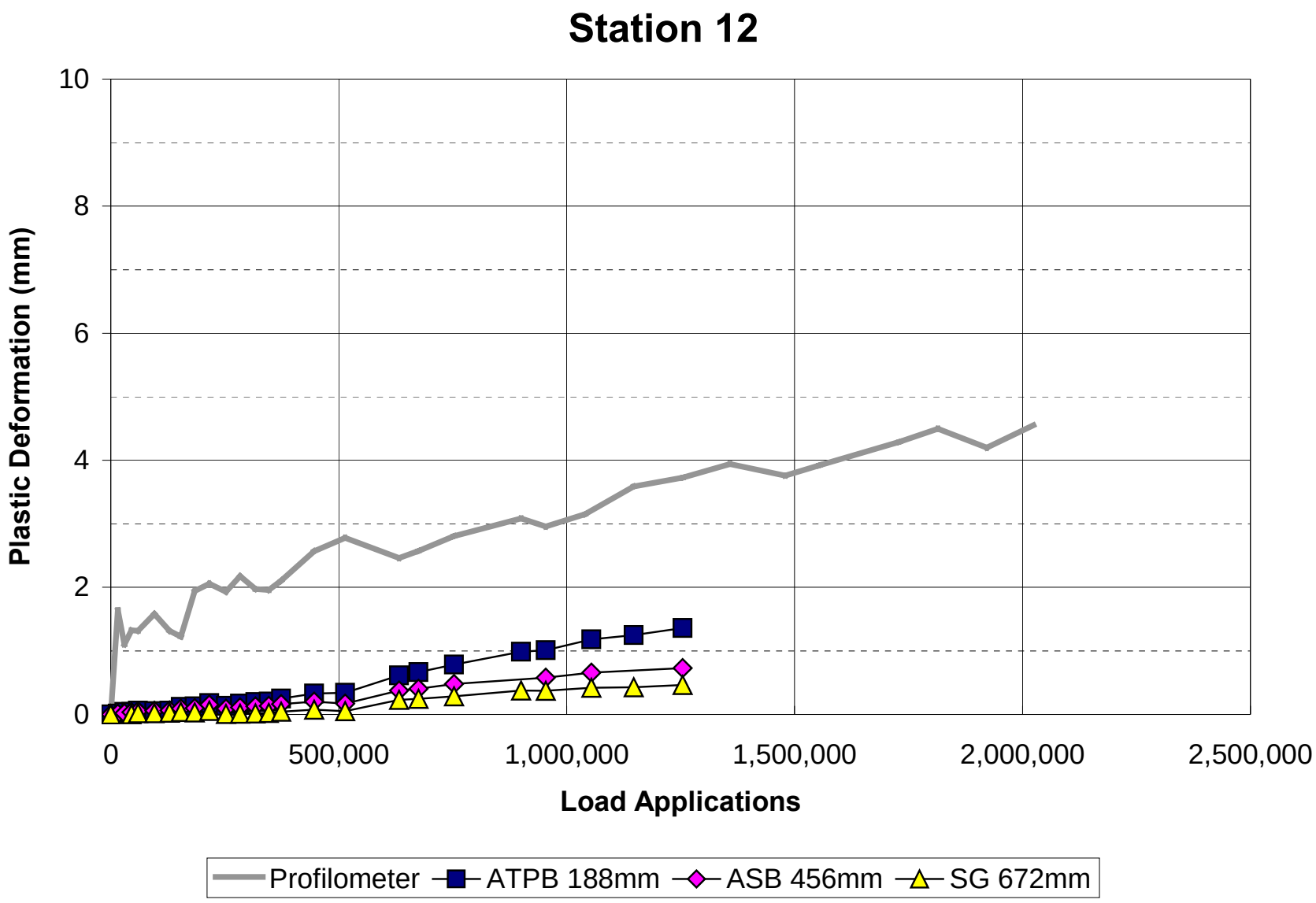

Figure 3.28. In-depth permanent deformation at Station 12, Section 515 (drained, ARHM-GG overlay).

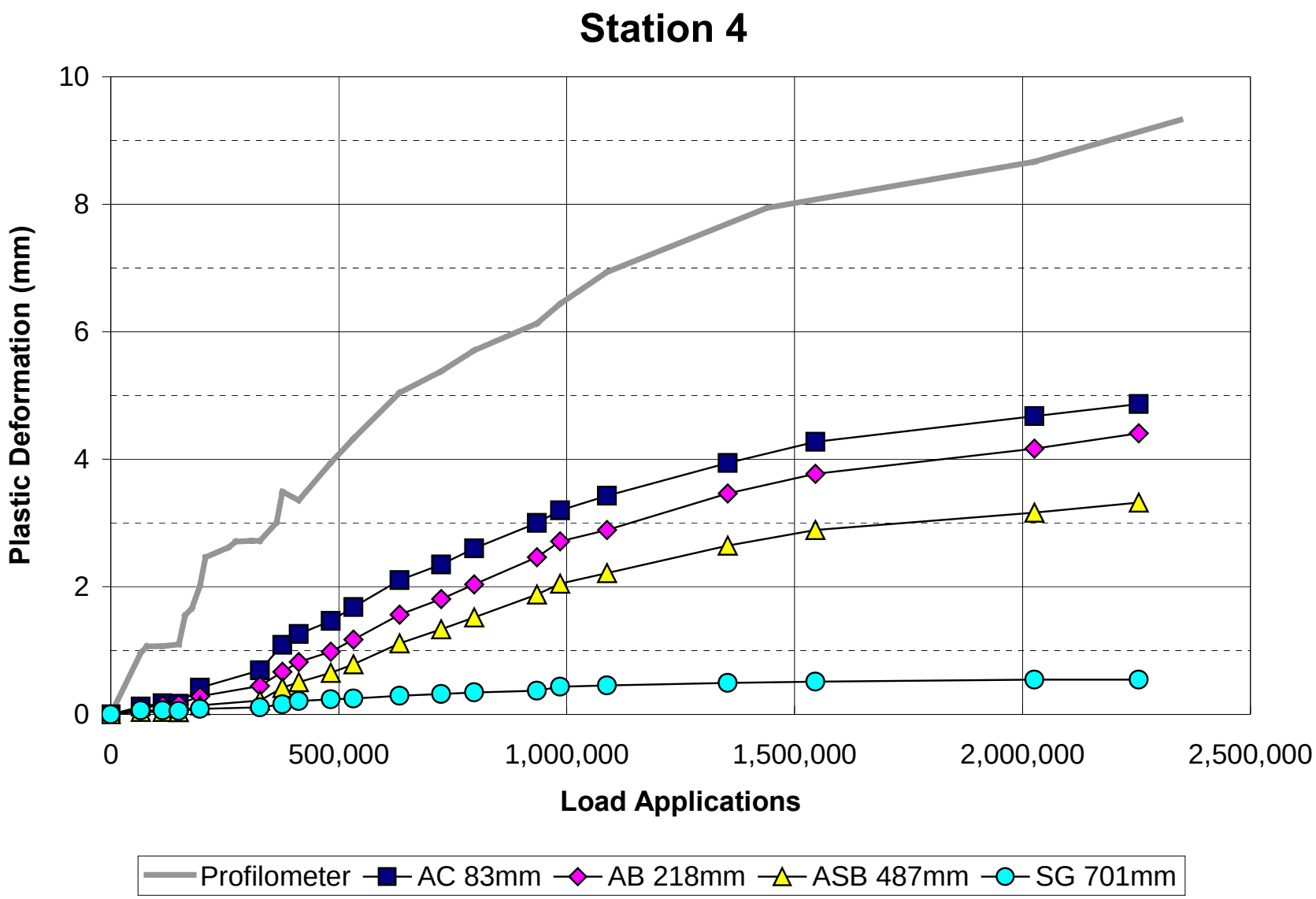

Figure 3.29. In-depth permanent deformation at Station 4, Section 517 (undrained, DGAC overlay).

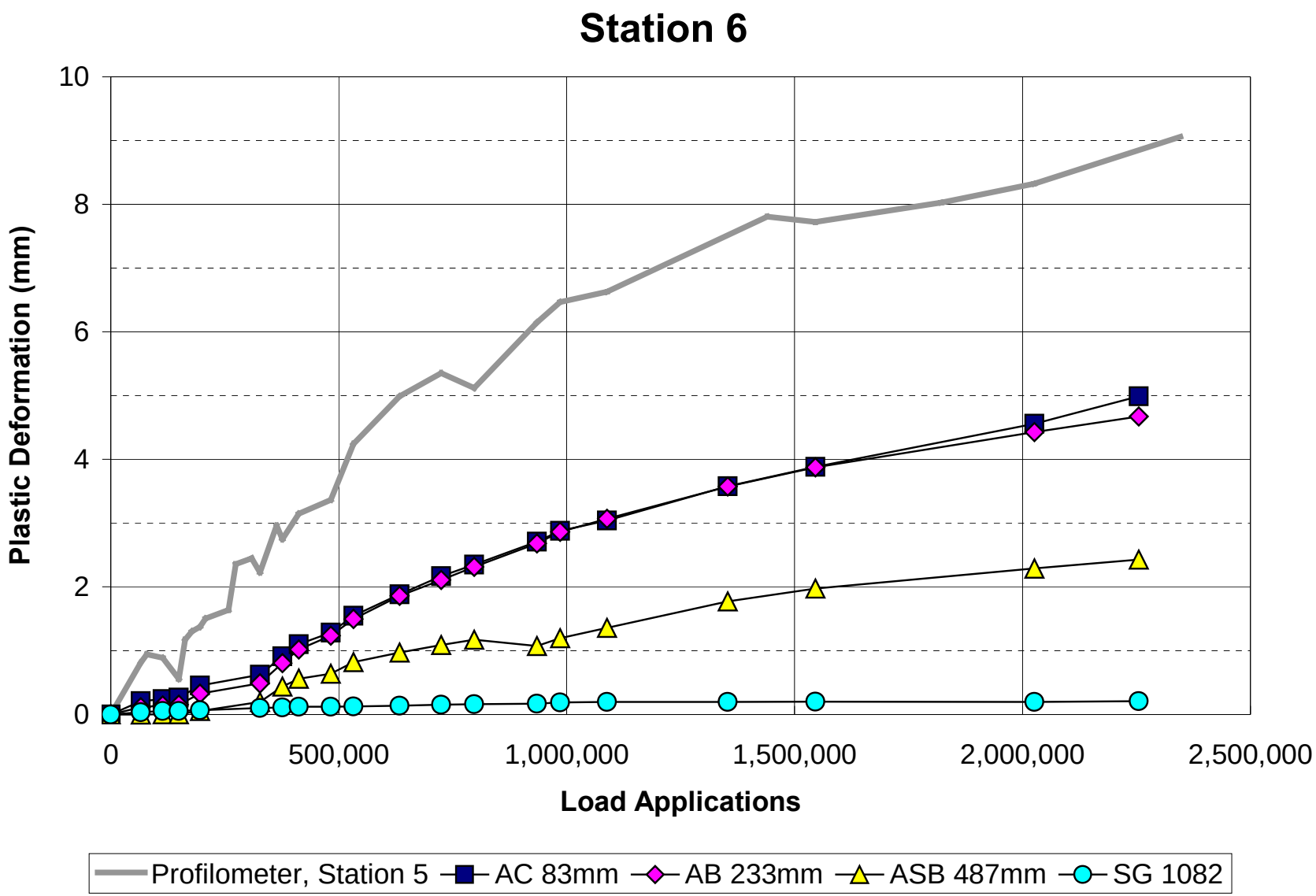

Figure 3.30. In-depth permanent deformation at Station 6, Section 517 (undrained, DGAC overlay).

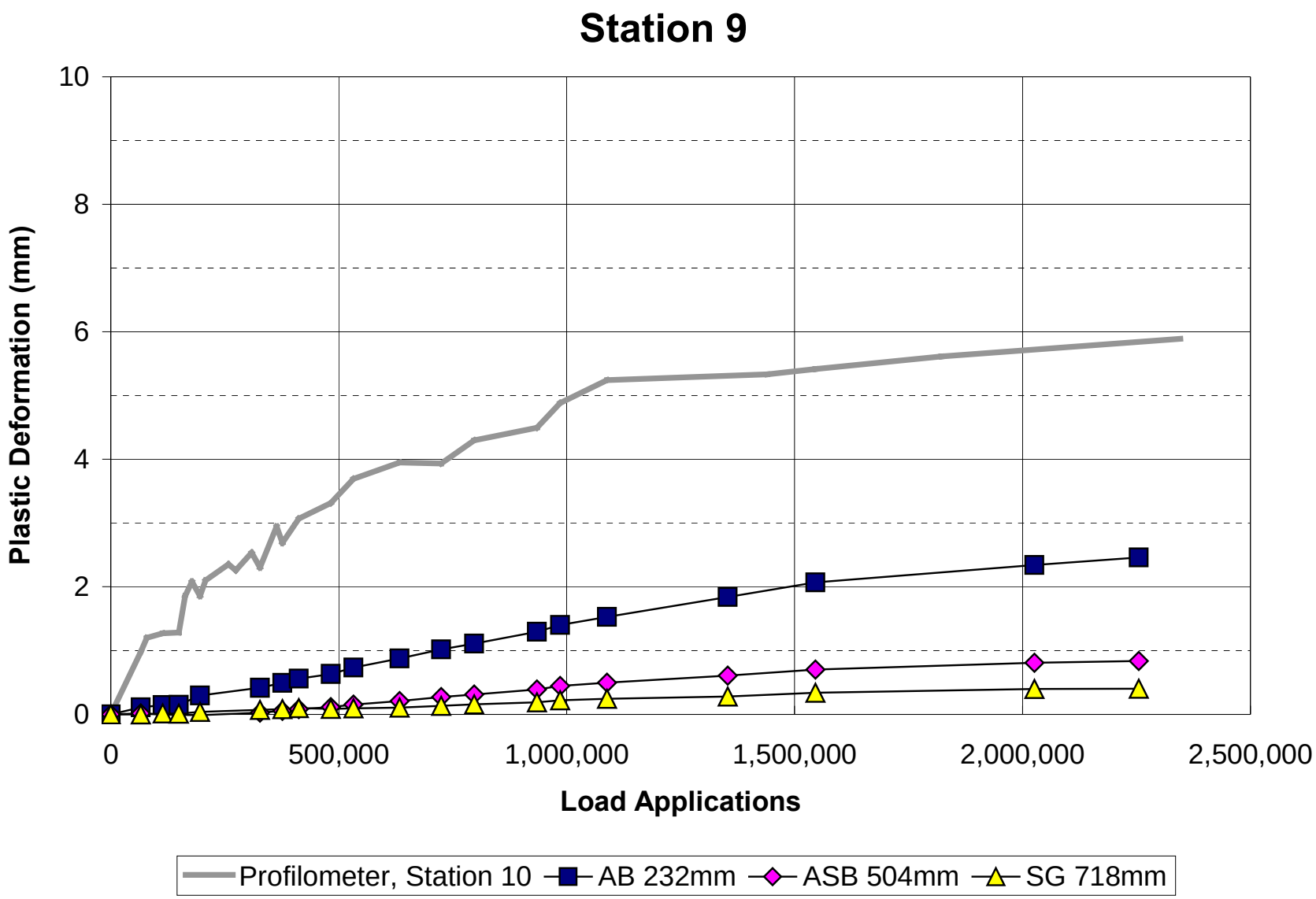

Figure 3.31. In-depth permanent deformation at Station 9, Section 517 (undrained, DGAC overlay).

unbound layers was 47 percent, which is larger than the rutting contributions of the unbound layers in the drained sections.

Table 3.6 Average Rutting Contribution of Pavement Layers in Section 517

Pavement Layer	MDD Location*	Permanent Deformation Measured at Top of Layer (mm)	Contribution (percent)	Permanent Deformation per Layer Thickness (10^{-2} mm)
DGAC Overlay	9	8.4	41.2	1.4
AC	4, 6	4.9	12.9	0.5
Base	4, 6, 9	3.9	22.5	NA
Subbase	4, 6, 9, 12	2.0	17.8	0.7
Subgrade	4, 9	0.5	5.6	0.2
Total			***100.0***	

* MDDs were positioned at different depths for different locations on the test section. If more than one MDD was located at a given layer, the average deformation is presented.

3.3.3.2 Section 518 ARHM-GG

Figures 3.32 and 3.33 show surface and in-depth permanent deformation data recorded at Stations 6 and 10. The data indicate a larger contribution of the unbound layers to the total surface rutting compared to the other sections. Table 3.7 shows that approximately 35 percent of the surface rut is attributable to the ARHM-GG overlay and AC layer. The unbound layers contributed approximately 63 percent of the total surface rutting. As in Section 517, the rutting contribution of the unbound layers is larger than the rutting contribution of the unbound layers in the drained sections. This is due to the additional protection provided to the unbound layers by the stiffer ATPB, and to the AB being deeper below the surface in the drained sections.

Most of the increase in rutting in the unbound layers in Section 518 occurred in the aggregate subbase and subgrade combined, rather than in the aggregate base as with Section 517.

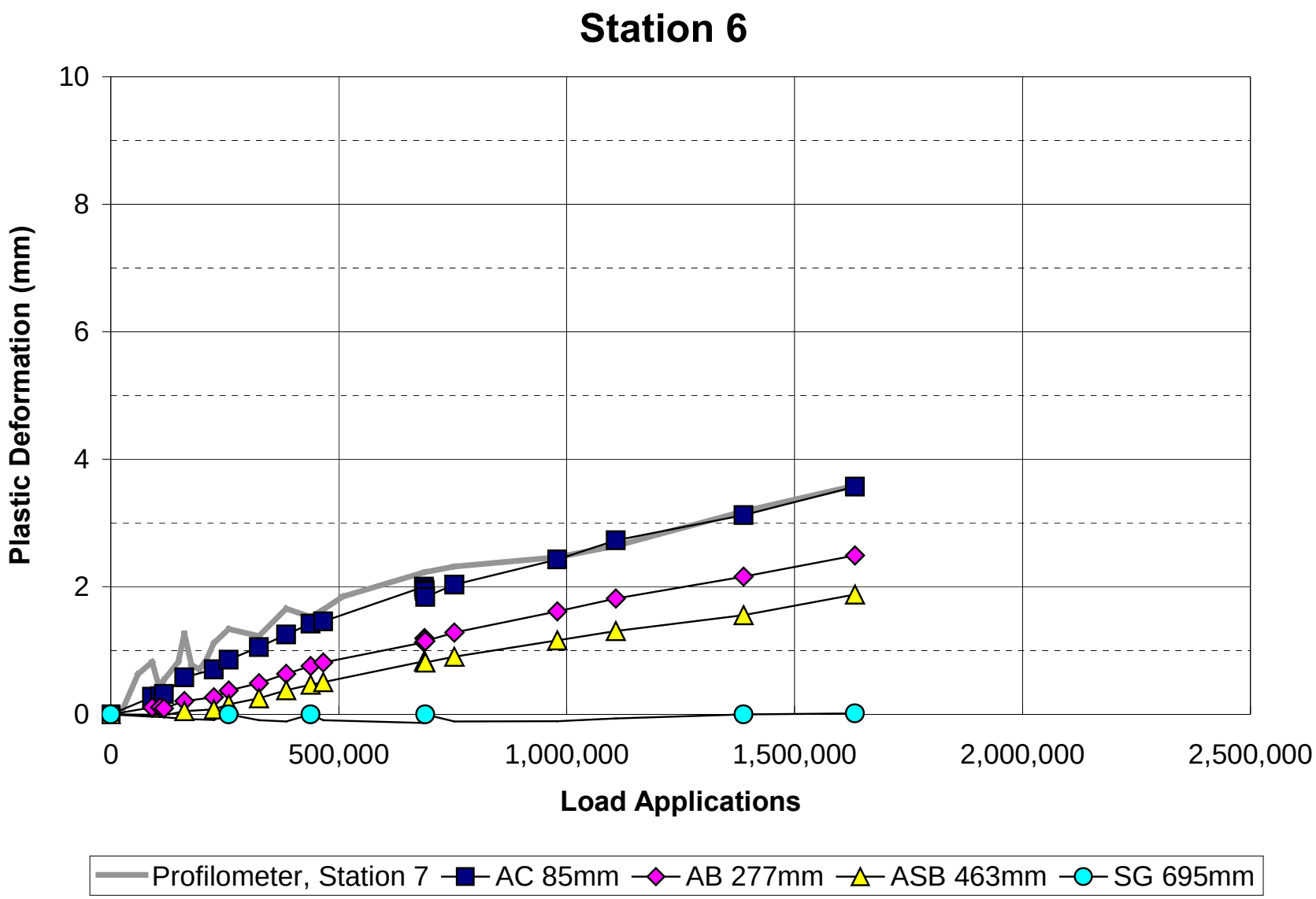

Figure 3.32. In-depth permanent deformation at Station 6, Section 518 (undrained, ARHM-GG overlay).

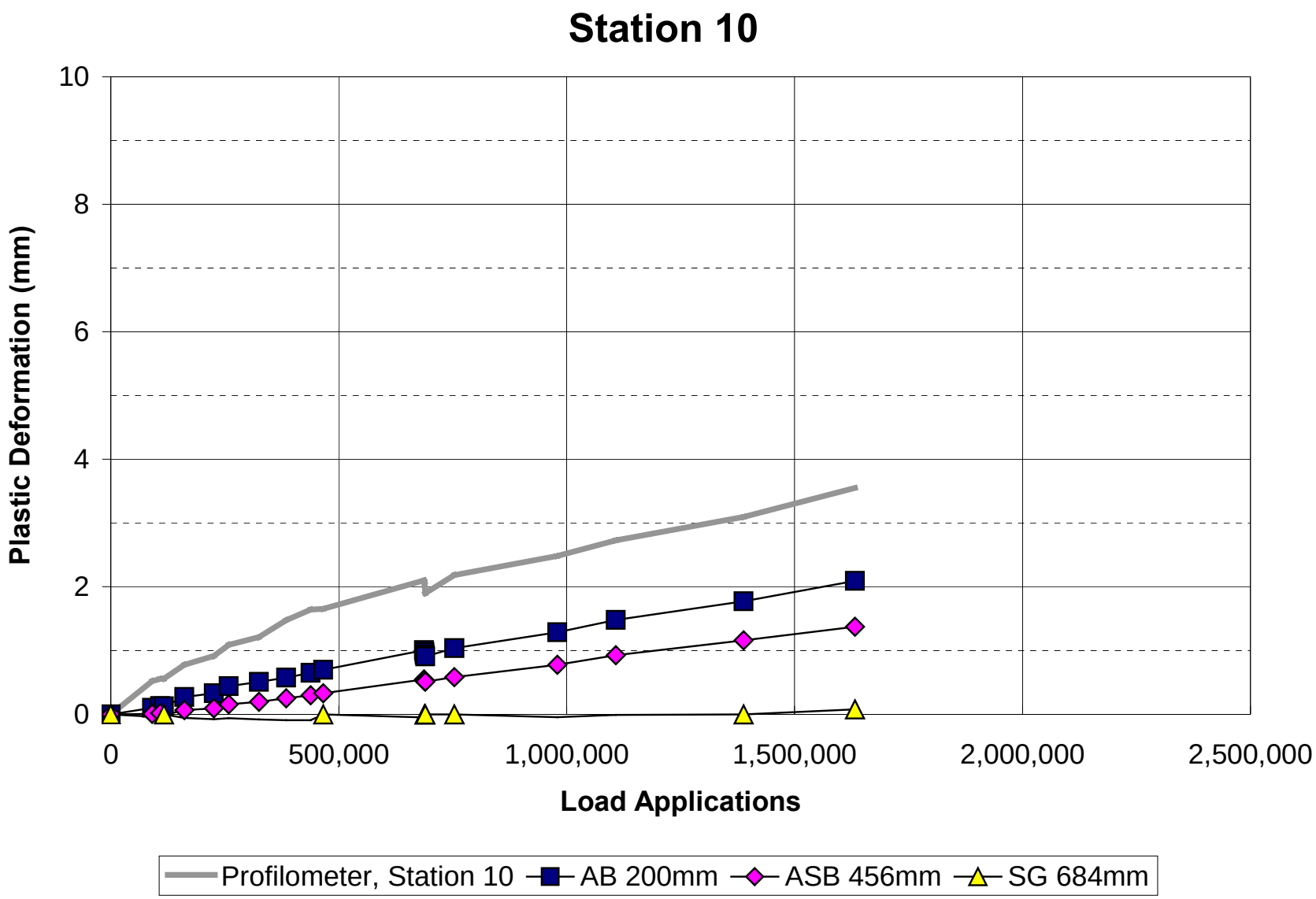

Figure 3.33. In-depth permanent deformation at Station 10, Section 518 (undrained, ARHM-GG overlay).

Table 3.7 Average Rutting Contribution of Pavement Layers in Section 518

Pavement Layer	MDD Location*	Permanent Deformation Measured at Top of Layer (mm)	Contribution (percent)	Permanent Deformation per Layer Thickness (10^{-2} mm)
ARHM-GG overlay and AC combined	6, 10	3.6	35.4	0.8
Base	6, 10	2.3	18.7	0.32
Subbase	6, 10	1.6	45.9	0.37
Subgrade		N/A	N/A	
Total			***100.0***	

* MDDs were positioned at different depths for different locations on the test section. If more than one MDD was located at a given layer, the average deformation is presented.

3.3.4 Comparison of Goal 3 and Goal 1 Tests

Table 3.8 summarizes rut depths of the Goal 1 and Goal 3 tests at the end of HVS testing. The rut depths obtained in the overlay tests (Goal 3) are less than those obtained before the sections were overlaid (Goal 1), particularly in the unbound layers. Figures 3.34–3.37 show that the permanent deformation of the unbound layers during the Goal 3 HVS traffic is a continuation of the permanent deformation pattern of the Goal 1 HVS traffic. The results are important when addressing the rutting potential of pavements in need of rehabilitation. When considering the rutting potential of rehabilitated sections, the previous traffic applications in the various pavement layers must be considered.

Table 3.8 Comparison of Rutting Contribution of Pavement Layers at the Completion of HVS Trafficking

Layer	Drained				Undrained			
	514 DGAC		515 ARHM-GG		517 DGAC		518 ARHM-GG	
	Goal 1	Goal 3	Goal 1	Goal 3	Goal 1	Goal 3	Goal 1	Goal 3
Asphalt Bound	8.9	5.0	9.5	3.0	5.7	4.1	5.3	2.7
Base and Subbase	4.3	1.0	3.1	0.6	4.1	3.0	5.5	1.9
Subgrade	1.8	0.3	1.4	0.6	1.2	0.4	0.2	0.3

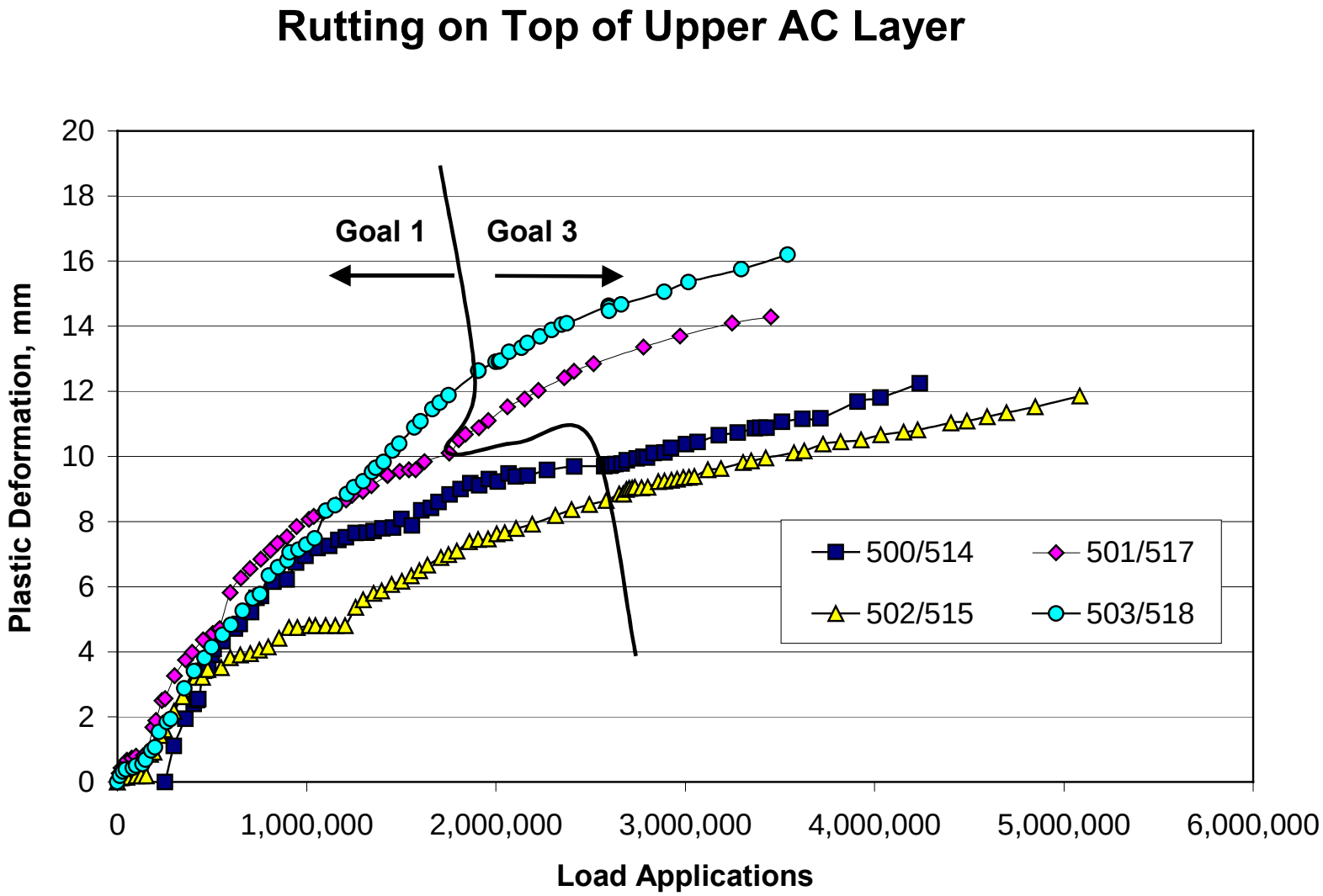

Figure 3.34. Rutting in top of upper AC layer for Goal 1 and Goal 3 sections.

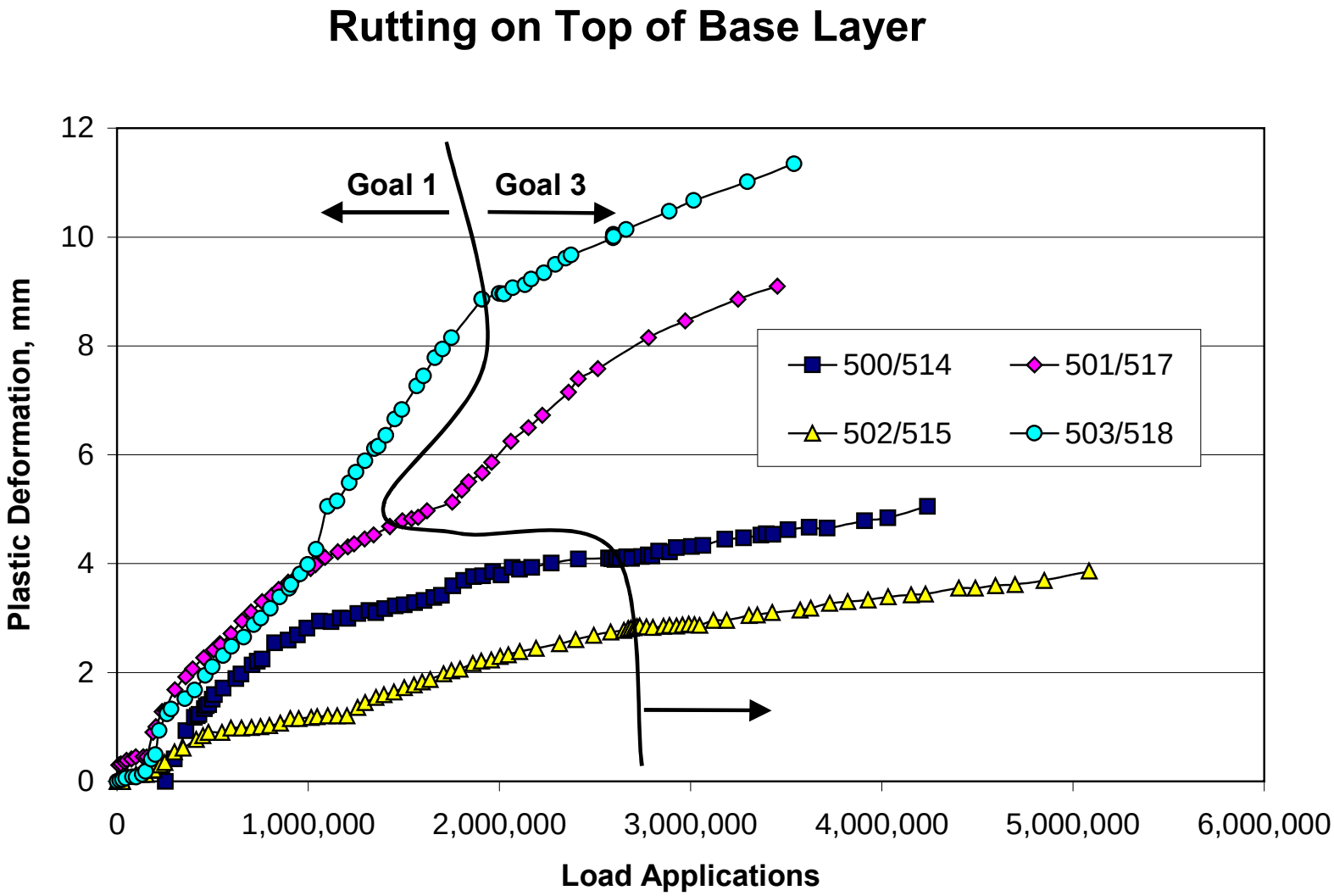

Figure 3.35. Rutting in top of AB layer for Goal 1 and Goal 3 sections.

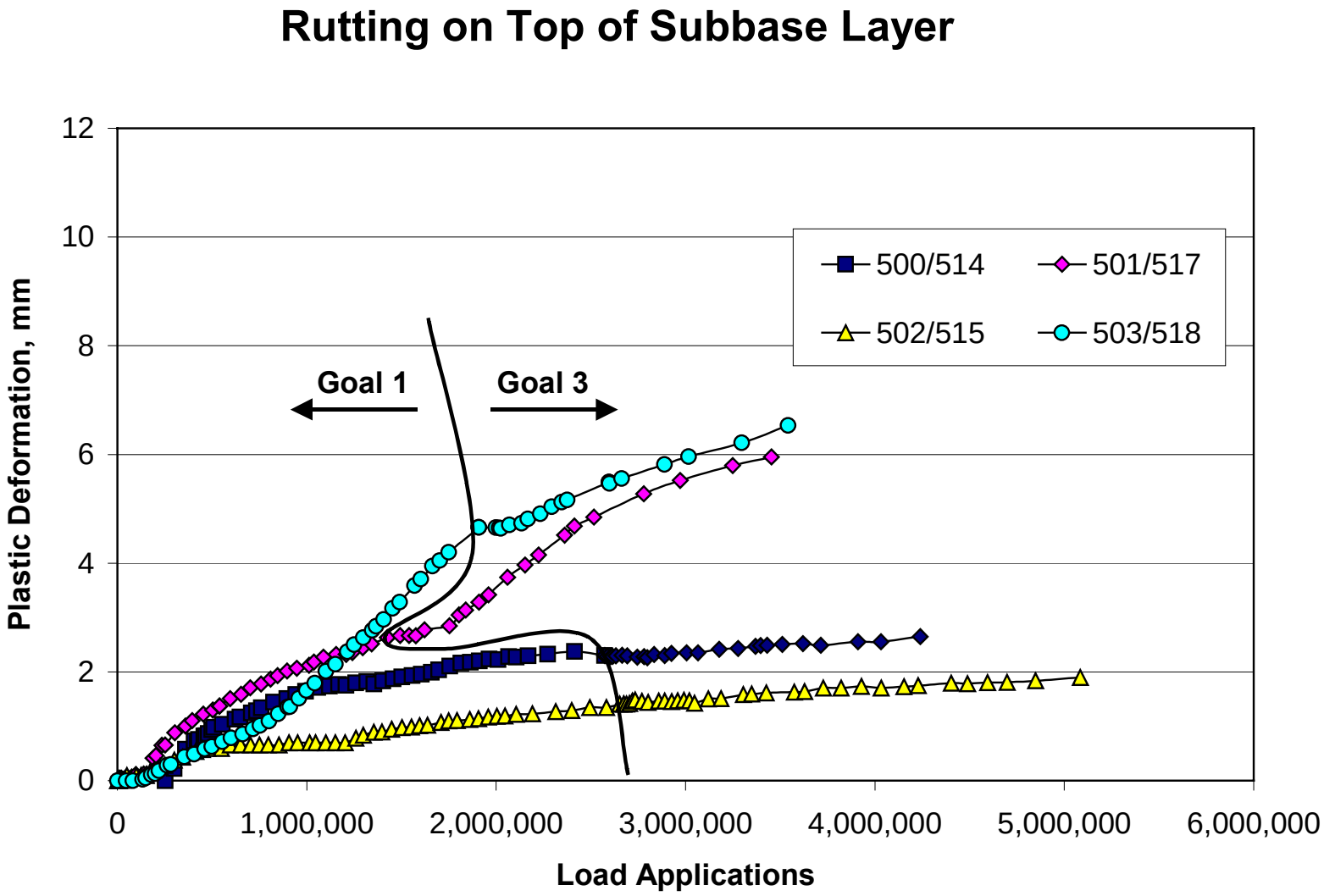

Figure 3.36. Rutting in top of ASB layer for Goal 1 and Goal 3 sections.

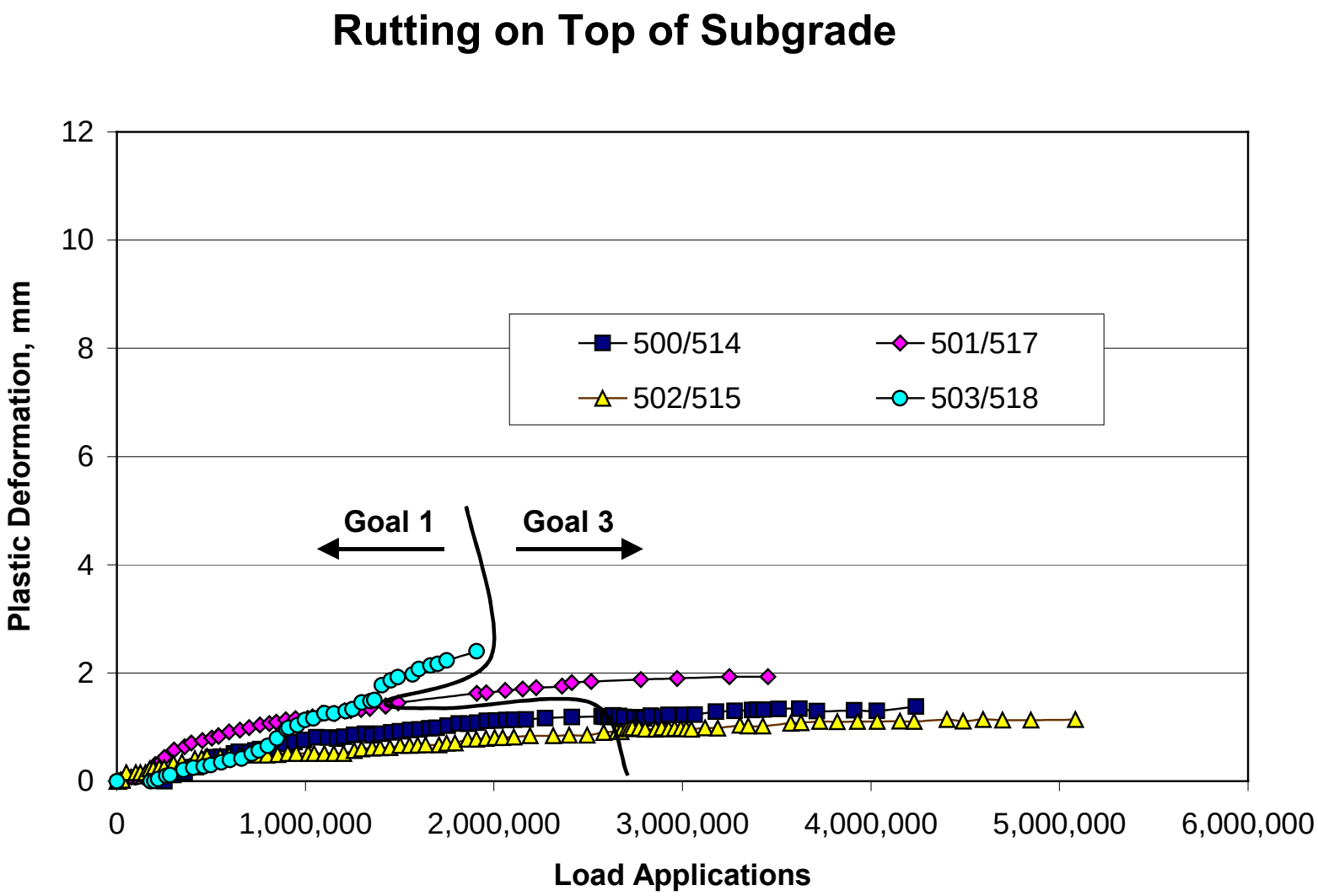

Figure 3.37. Rutting in top of subgrade for Goal 1 and Goal 3 sections.

3.3.5 Air-Void Contents from Extracted Cores

Cores of 150 mm diameter were extracted from Sections 514, 517, and 518 eight months after traffic on Section 518 was completed. Air-void contents for Sections 515 were measured from 400 × 170 mm rectangular slabs removed from the section. Air-void contents were measured using AASHTO T-275 Method A.

Figures 3.38 to 3.39 present air-void content data for the overlays and other bound layers for Sections 514, 517, and 518. Table 3.9 summarizes air-void content data for three distinct areas in the test sections: 1) *traffic* areas, i.e., the areas within the width of the section excluding the turnaround zones; 2) *hump* areas, i.e., the regions of uplifted material at the sides of the traffic areas; and 3) *non-traffic* areas, i.e., the areas located outside of the section and beyond the hump areas. The air-voids contents in the traffic and hump areas can be used to gage the compaction of the mixes under trafficking. Air-void contents in the non-trafficked areas can be used to gage the initial variability of air-void contents in all the bound layers.

Table 3.9 Average Air-Void Contents in Test Sections

Layer	Air Void Content, percent											
	514 DGAC			515 ARHM-GG*		517 DGAC			518 ARHM-GG			
	Traffic	Hump	Non-Traffic	Traffic Hump	Non-Traffic	Traffic	Hump	Non-Traffic	Traffic	Hump	Non-Traffic	
Overlay	7.2	7.9	7.6	8.6	9.1	5.4	6.8	6.8	12.3	15.2	14.7	
AC Top Lift	3.7	6.1	6.3	N/A	N/A	4.4	5.7	5.7	4.4	6.1	5.2	
AC Bottom Lift	2.5	4.0	3.7	2.5	3.4	5.6	6.2	5.9	3.4	3.7	4.5	
ATPB	21.1	21.0	21.2	N/A	N/A							

* Air void contents for section 515 were obtained from 400 by 170 mm rectangular slabs. All others were obtained from 150 mm diameter cores.

The data show that lower air-void contents were obtained for all bound layers within the trafficked area. For the overlays, initial air voids were higher for the ARHM-GG (ranging from 9.1 to 14.7 percent) than for the DGAC (ranging from 6.8 to 7.6 percent). The rutting

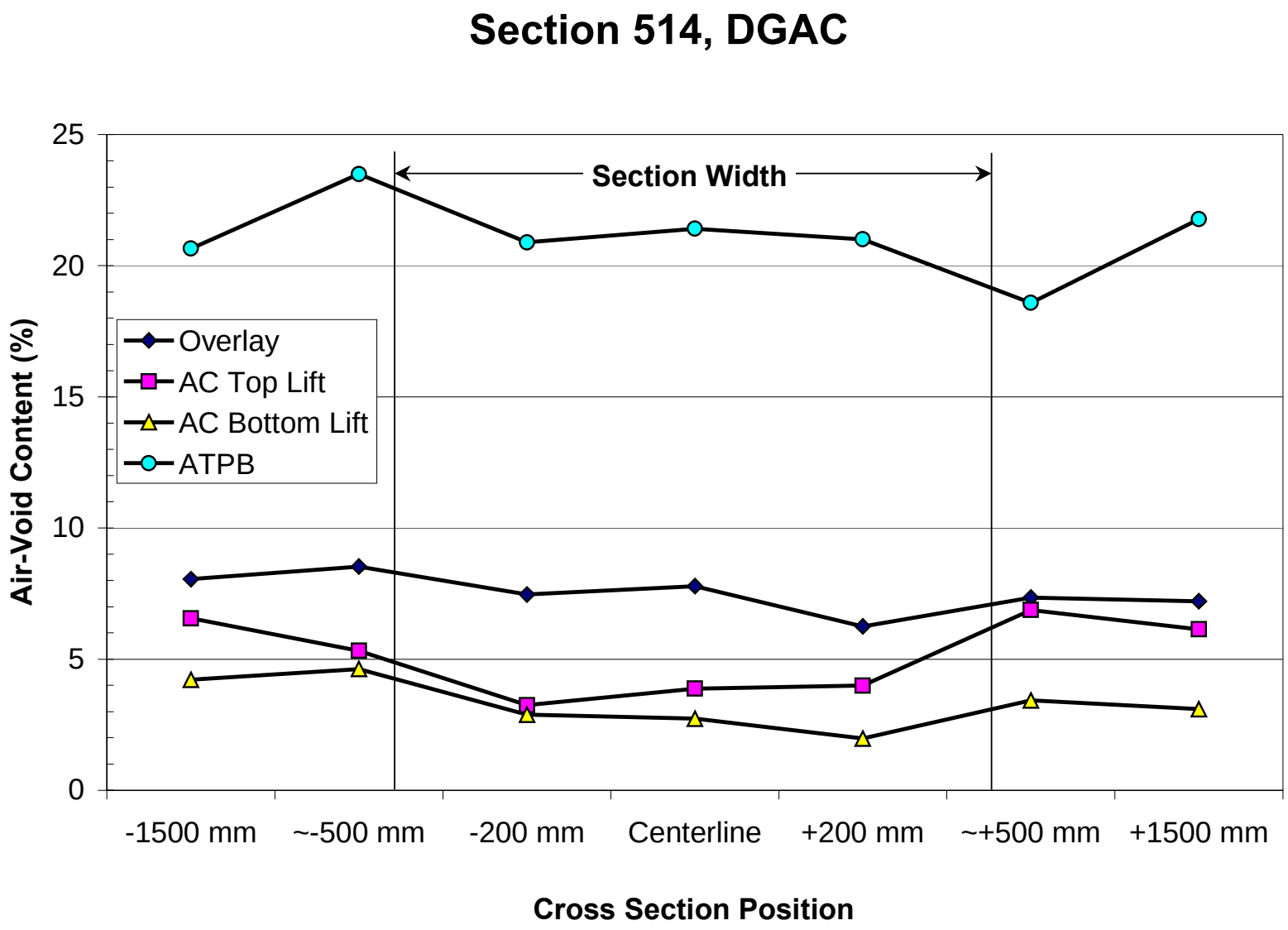

Figure 3.38. Air-void contents from extracted cores, Section 514 (drained, ARHM-GG overlay).

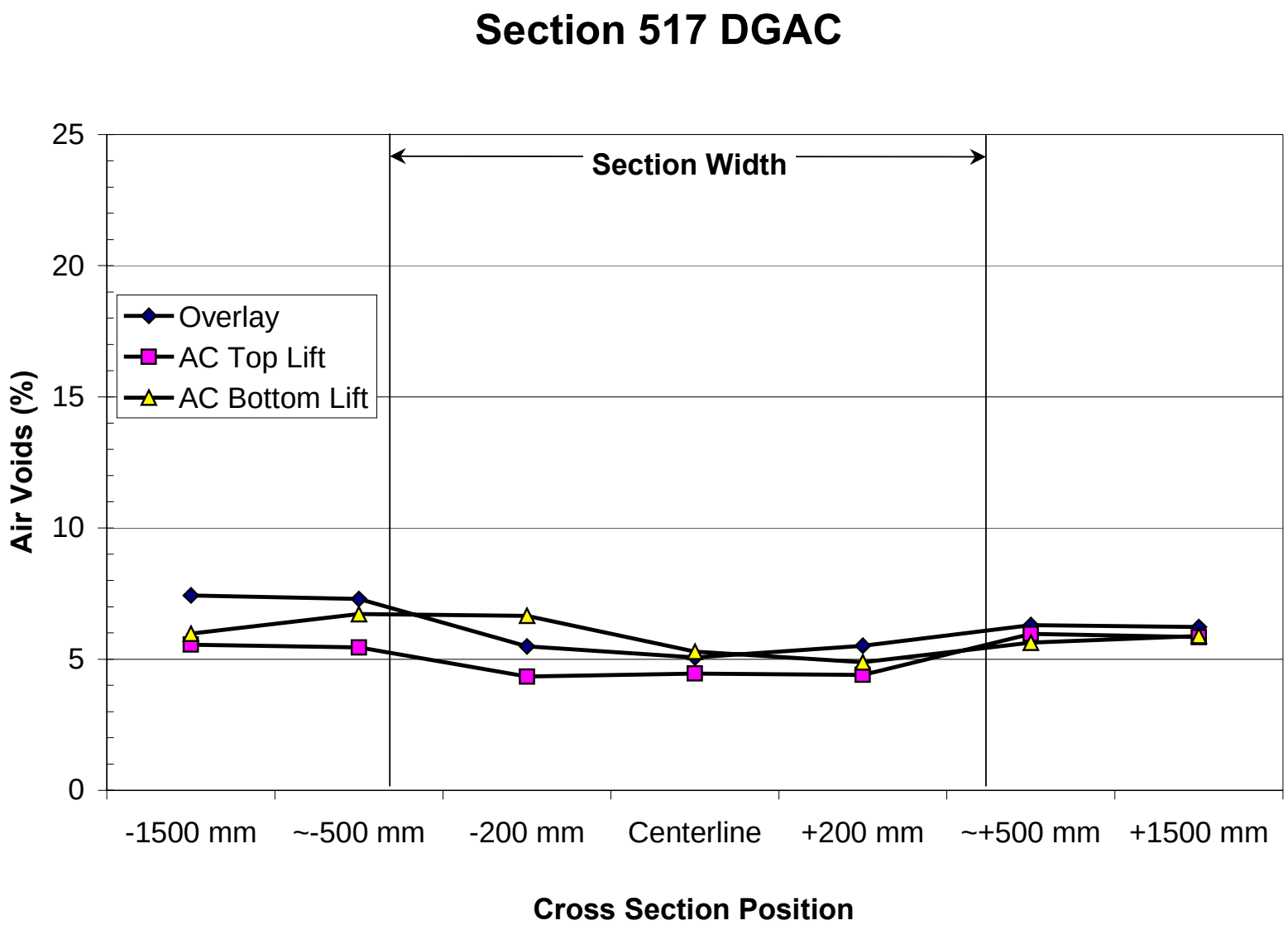

Figure 3.39 Air-void contents from extracted cores, Section 517 (undrained, DGAC overlay).

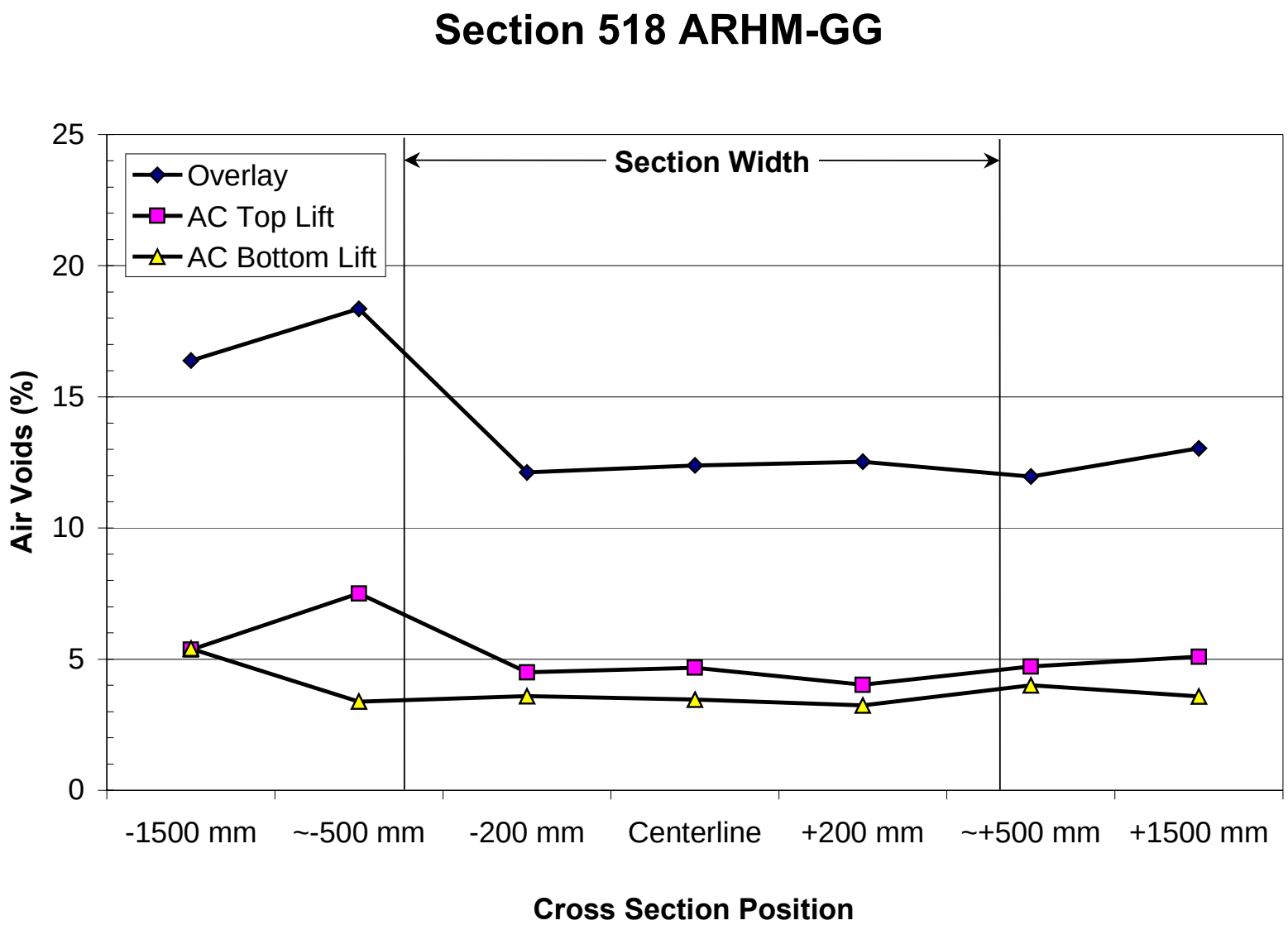

Figure 3.40. Air-void contents from extracted cores, Section 518 (undrained, ARHM-GG overlay).

performance of the ARHM-GG overlay can be significantly influenced by the required overlay thickness regardless of the high air-void content.

For all other bound layers, the data from the non-trafficked areas indicate the variability in air-void content. Initial air-void contents in the top asphalt concrete lift varied from 5.2 to 6.3 percent, and in the bottom AC lift from 3.7 to 5.9 percent.

3.3.6 Trench Data

After the completion of HVS trafficking on the various test sections, trenches were dug in each of the test sections in order to facilitate direct observation of the thickness and permanent deformation of the various pavement layers. Figures 3.41–3.48 show profile data at the interface of each layer at the completion of HVS testing. The profiles show that the subbase thickness varied considerably among the four sections. Subbase thickness also varied along the width of the pavement in Sections 514, 517, and 518. Differences in subbase thickness were anticipated and reported in previous CAL/APT reports (*13–16*).

Table 3.10 shows the average layer thicknesses measured in the trenches inside and outside the traffic area compared to the assumed thicknesses used for previous analyses. The ATPB layer in the drained sections was 20 to 30 mm thinner than the design 76-mm thickness, and the AB layer was approximately 25 mm thinner than the design thickness of 182 mm. All other thicknesses are reasonably similar to the design thicknesses.

Based on the profiles, permanent deformation was estimated for each pavement layer, as presented in Table 3.11. The plastic deformation of the AC, ATPB, and unbound layers is the total permanent deformation accumulated during the Goal 1 and Goal 3 HVS tests. Due to variability in subbase thickness and interface roughness, it was difficult to calculate permanent deformation of the subbase and subgrade layers by direct observation of the trenched sections.

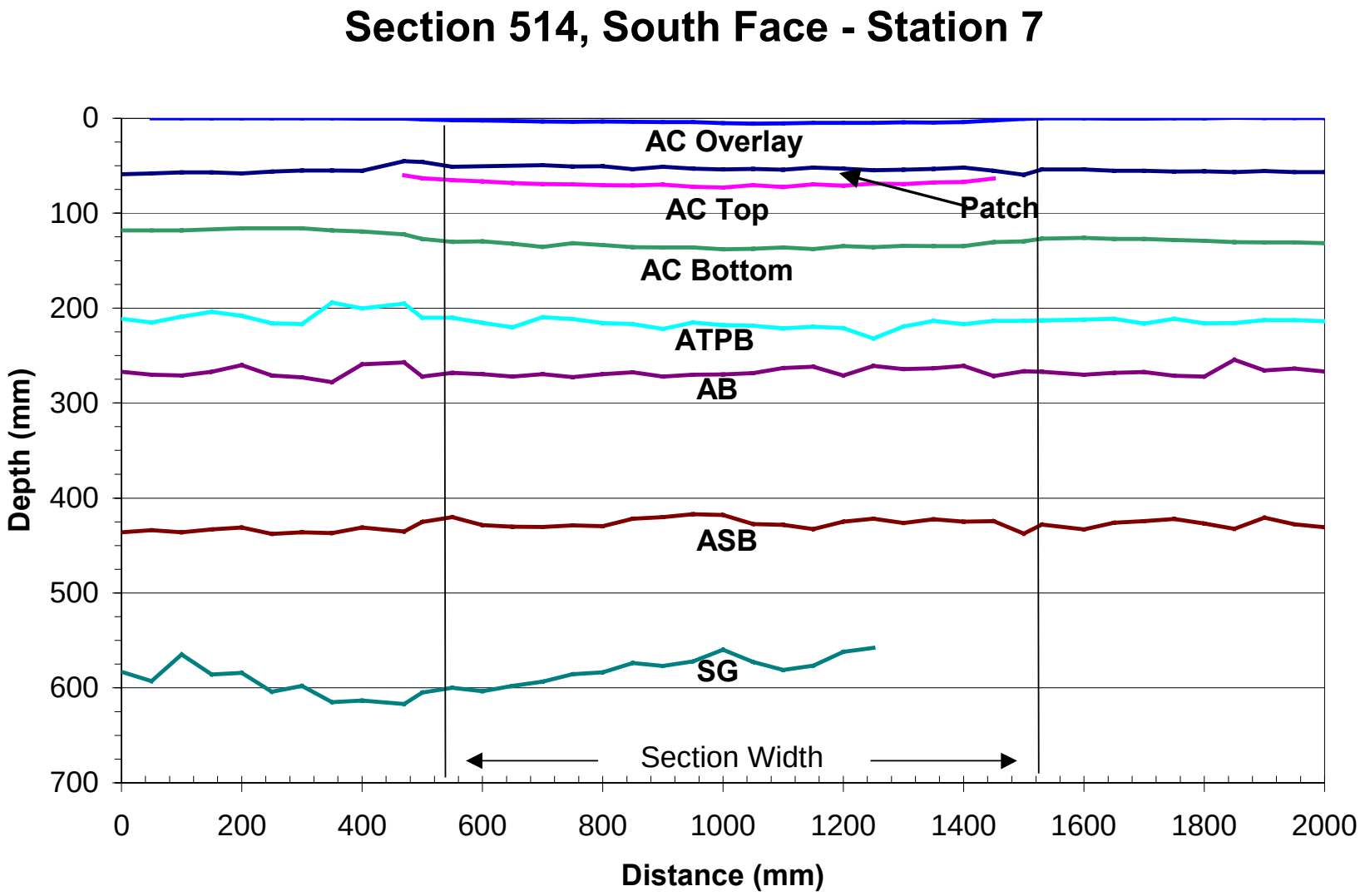

Figure 3.41. Test pit data for Section 500/514, north face of pit at Station 5.

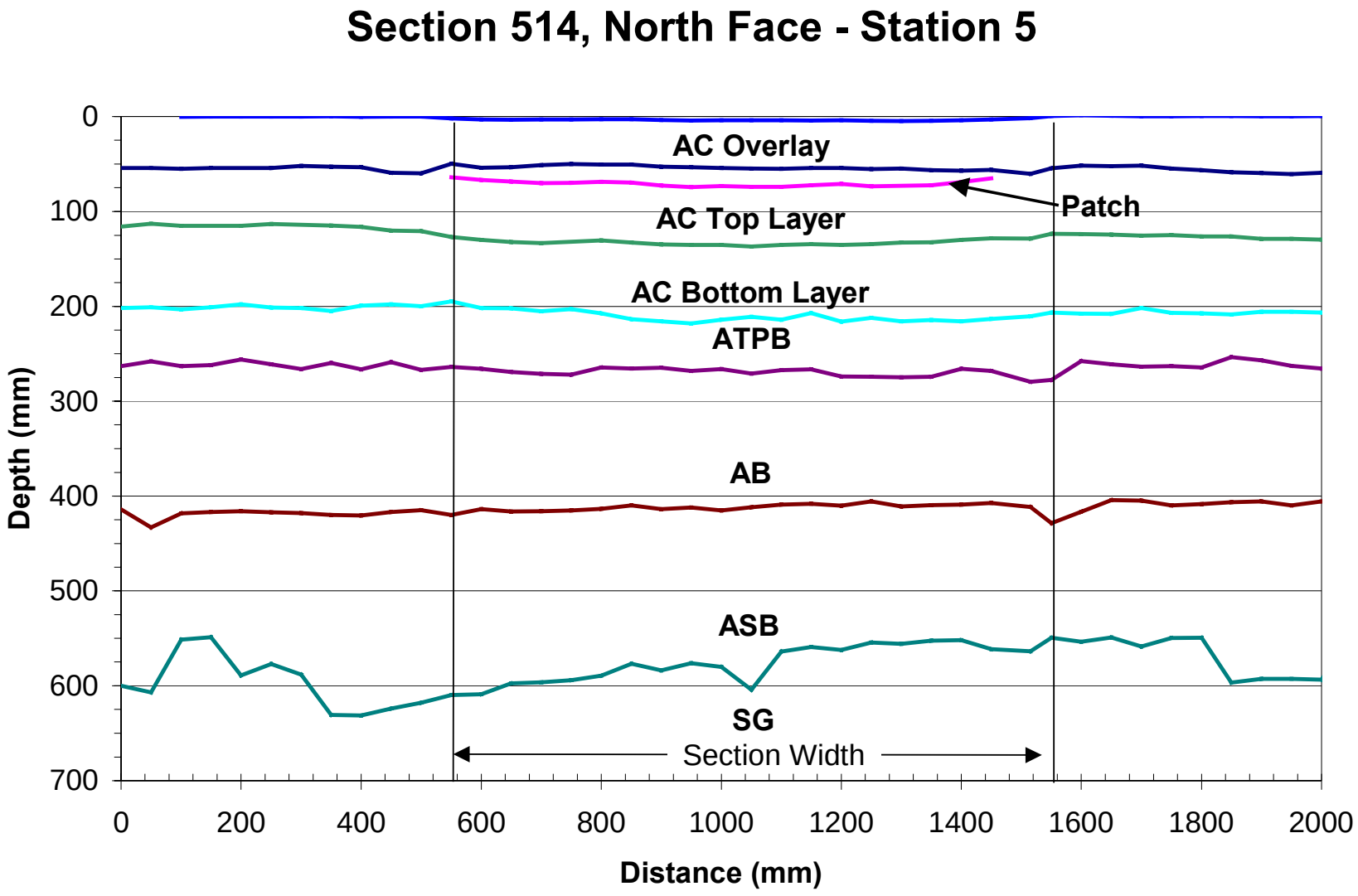

Figure 3.42. Test pit data for Section 500/514, south face of pit at Station 7.

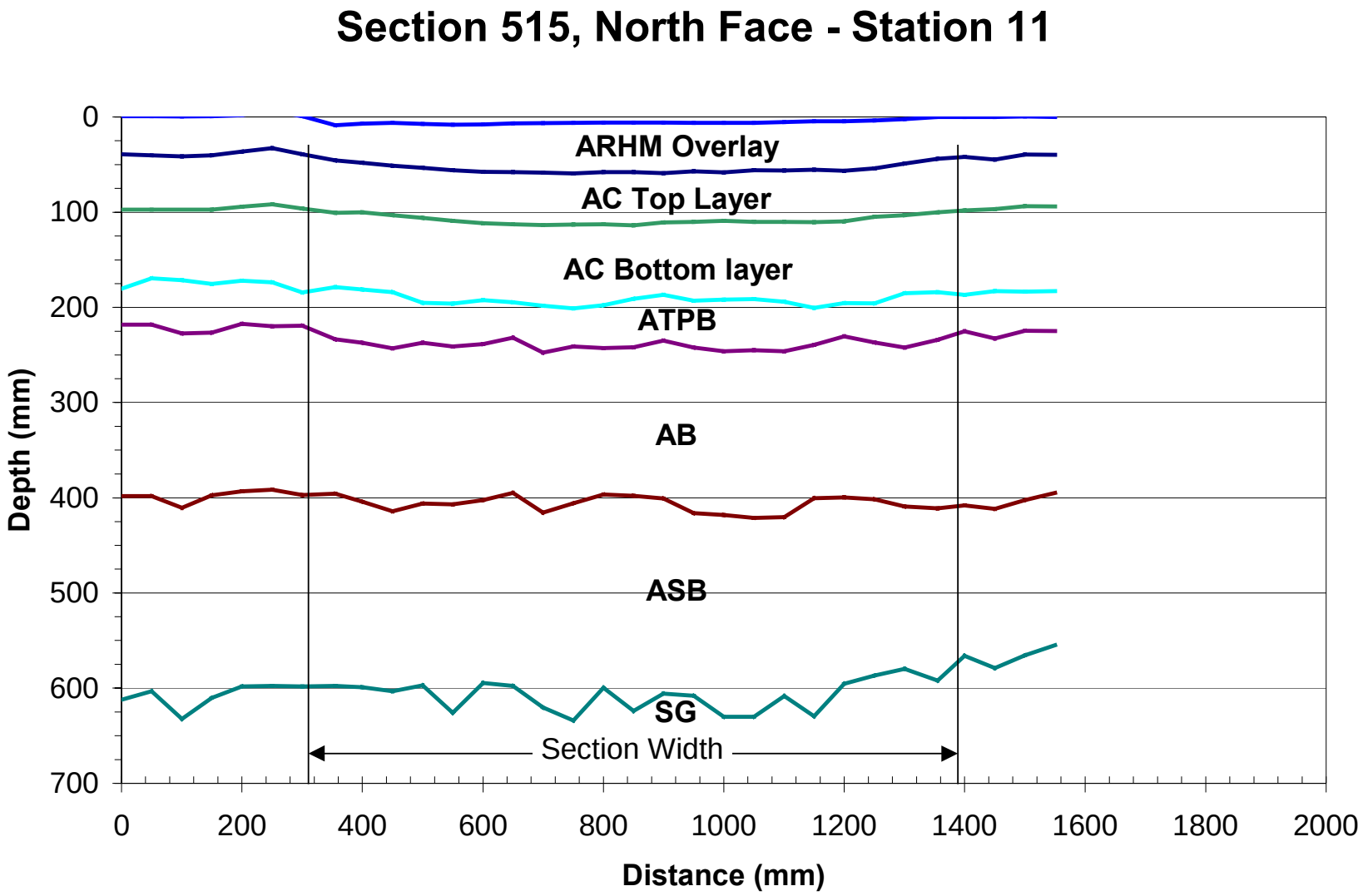

Figure 3.43. Test pit data for Section 502/515, north face of pit at Station 11.

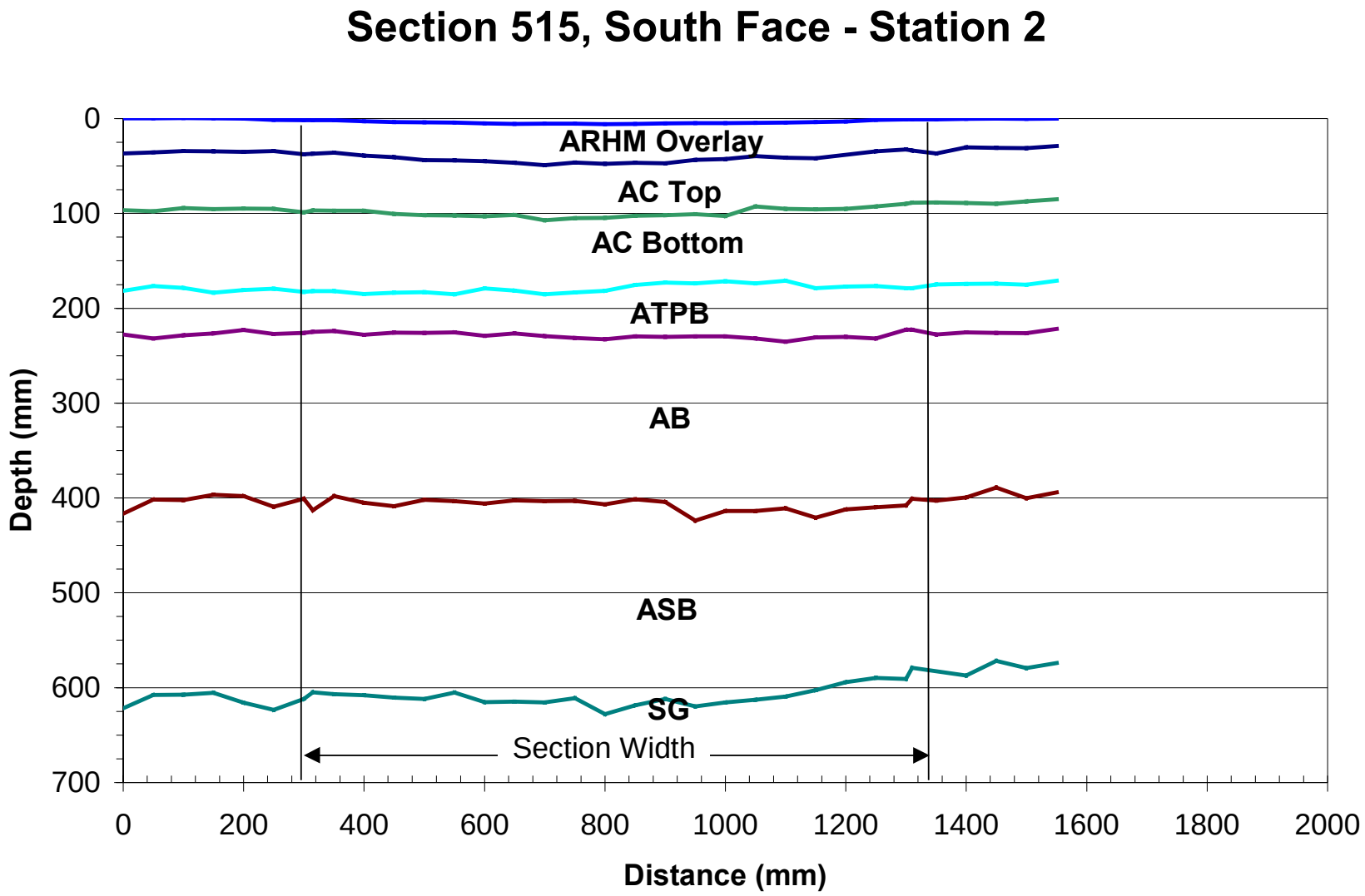

Figure 3.44. Test pit data for Section 502/515, south face of pit at Station 2.

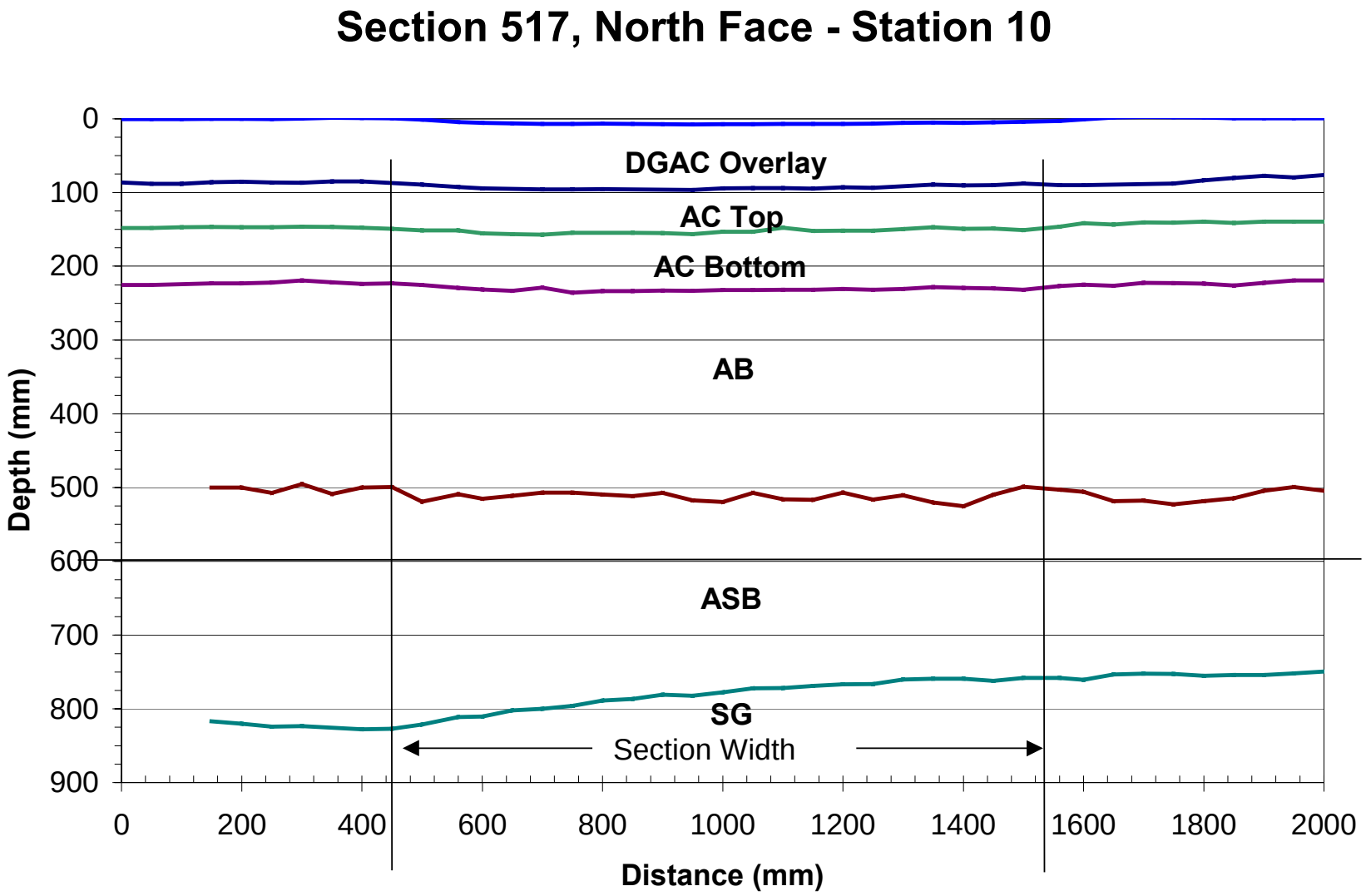

Figure 3.45. Test pit data for Section 501/517, north face of pit at Station 10.

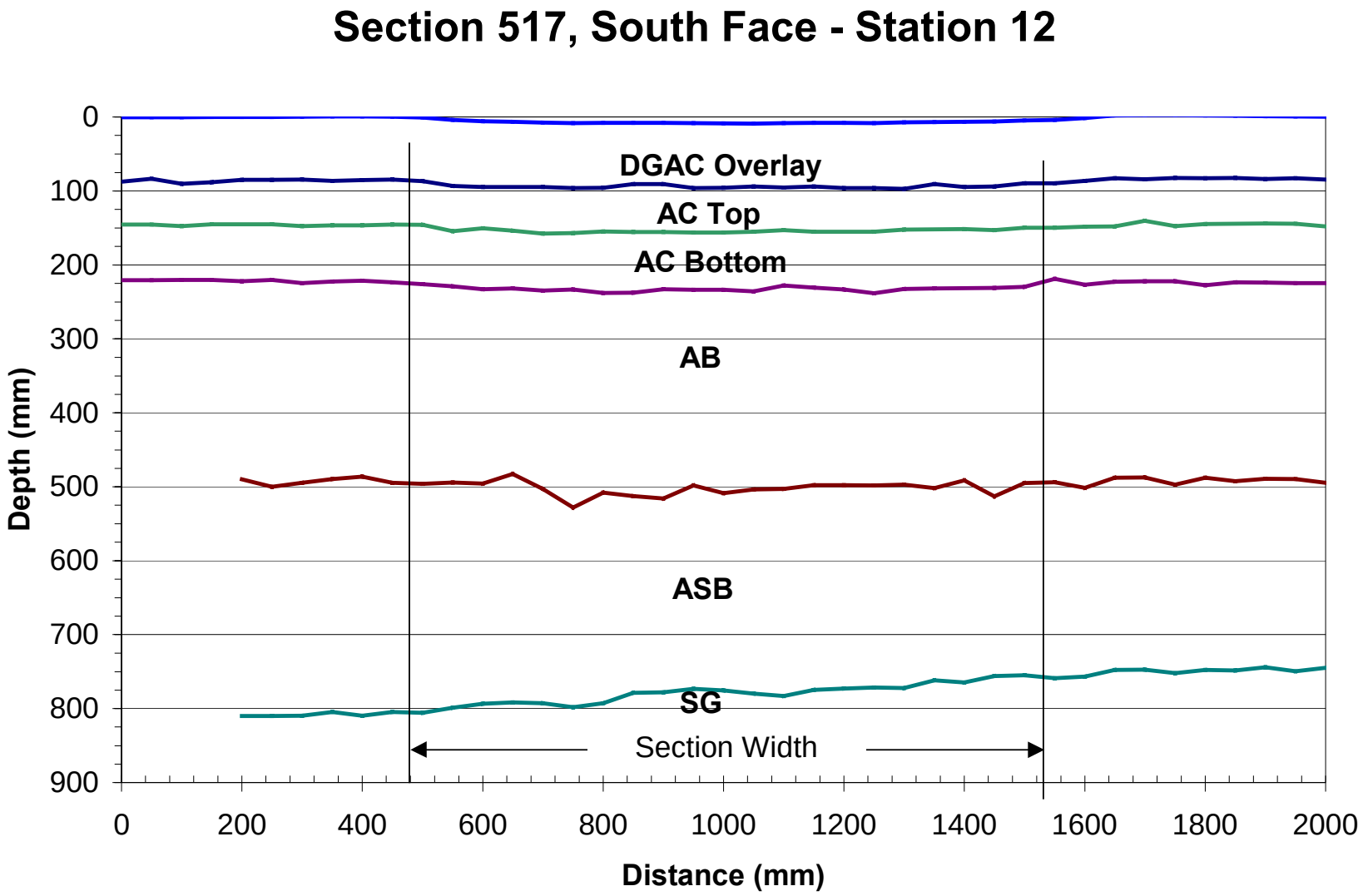

Figure 3.46. Test pit data for Section 501/517, south face of pit at Station 12.

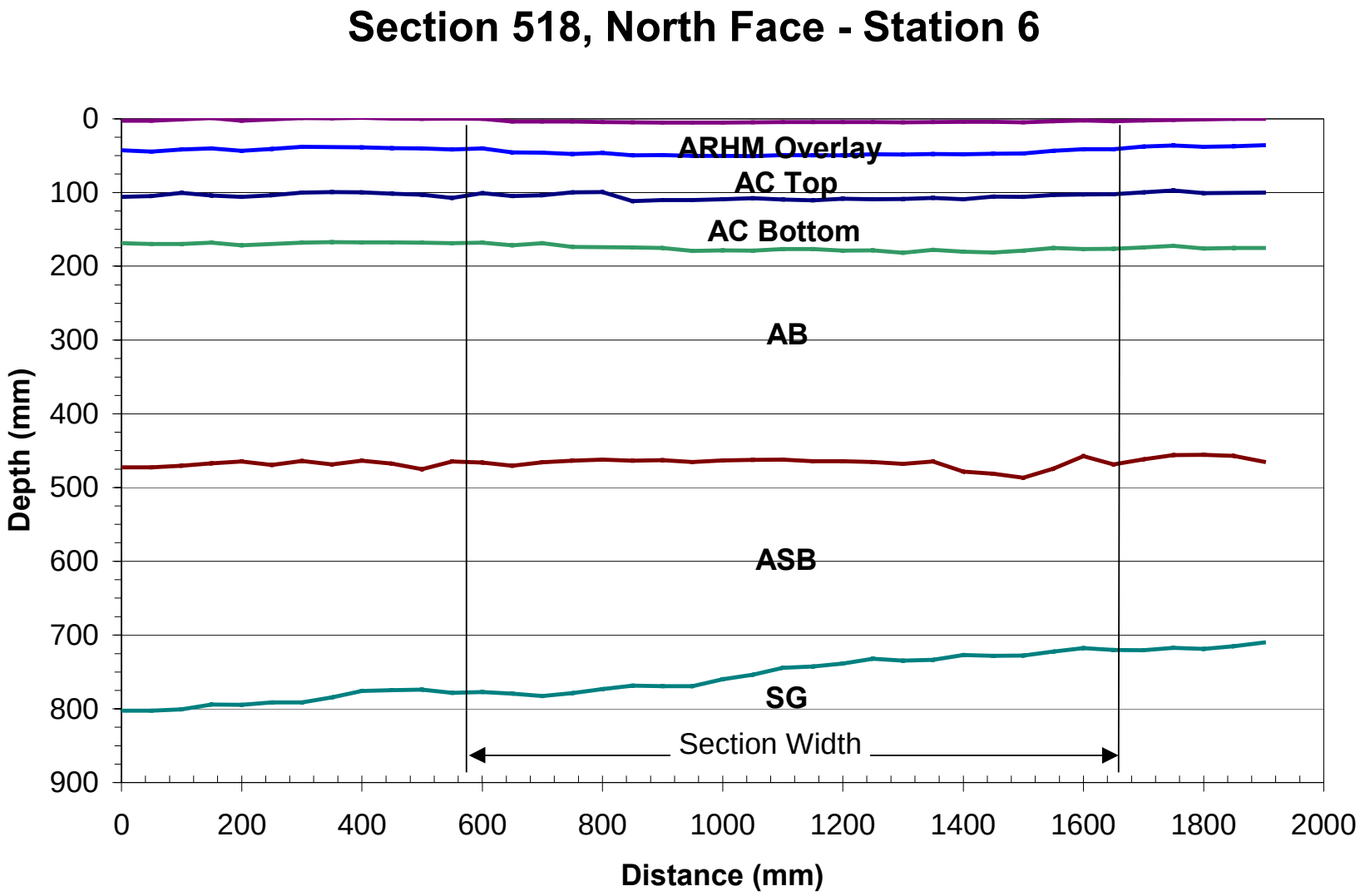

Figure 3.47. Test pit data for Section 503/518, north face of pit at Station 6.

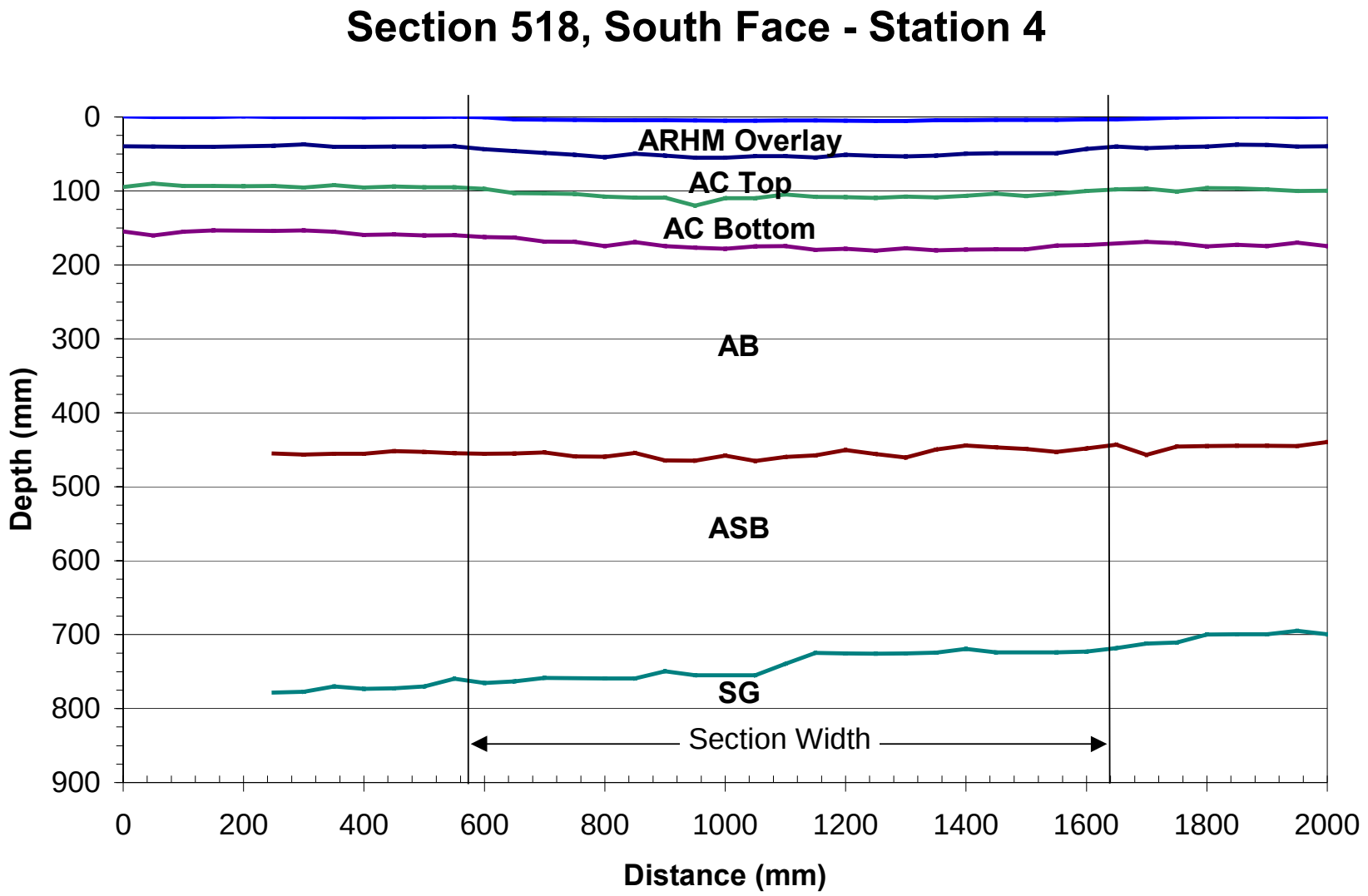

Figure 3.48. Test pit data for Section 503/518, south face of pit at Station 4.

Table 3.10 Comparison of Design and Field Thicknesses in Sections

Section	Layer	Layer Thickness (mm)		
		Design	Inside	Outside
Section 514	DGAC Overlay	60	50.0	55.9
	Patch to fill rut	15	15.0	
	Asphalt Concrete	129	144.4	151.6
	ATPB	75	55.6	56.8
	Aggregate Base	180	151.3	157.9
	Aggregate Subbase	135	161.4	159.1
	Total Thickness	594	577.7	581.3
Section 515	ARHM-GG Overlay	38	43.4	37.2
	Asphalt Concrete	131	137.3	141.3
	ATPB	75	48.6	46.7
	Aggregate Base	183	173.1	175.8
	Aggregate Subbase	214	200.6	195.2
	Total Thickness	641	603.0	596.2
Section 517	DGAC Overlay	75	87.0	84.9
	Asphalt Concrete	132	138.6	138.3
	Aggregate Base	272	274.8	215.7
	Aggregate Subbase	214	269.4	249.4
	Total Thickness	693	769.8	688.3
Section 518	ARHM-GG Overlay	38	45.6	38.8
	Asphalt Concrete	131	126.4	126.8
	Aggregate Base	270	285.0	292.3
	Aggregate Subbase	303	294.9	294.8
	Total Thickness	742	751.9	752.7

Table 3.11 Plastic Deformation in Layer Measured Directly in Test Trench

	Plastic Deformation in Layer (mm)			
	Drained		Undrained	
Layer	514 DGAC	515 ARHM-GG	517 DGAC	518 ARHM-GG
Overlay	4.6	5.6	7.7	4.9
AC	4.7	3.5	2.8	4.8
ATPB	5.9	6.5	N.A.	N.A.
Unbound	3.5	4.4	8.0	6.6
Total Surface	*5.1*	*7.3*	*8.1*	*5.5*

Table 3.11 shows that the asphalt-bound layers accumulated a significant amount of permanent deformation. The trench data also indicate that the ATPB did not significantly contribute to the surface rutting as assumed using the MDD data (see Sections 3.3.2.1 and 3.3.2.2). Due to the assumptions of a thicker ATPB, it is possible that the permanent deformation recorded for the ATPB was actually accumulated in the AB layer.

The permanent deformation on top of the base layer was difficult to estimate due to the roughness of the interface between this layer and the layer above. However, average values indicate that higher permanent deformation occurred on top of the aggregate base in the undrained sections than in the drained sections.

3.3.7 Summary of Permanent Deformation Data

In general, in-depth permanent deformation data and direct observation data from the test trenches show that for the drained sections, approximately 78 percent of the rutting measured from the surface of the sections occurred in the asphalt-bound layers (with little contribution from the ATPB), 17 percent occurred in the granular base and subbase layers, and 5 percent occurred in the subgrade.

For the undrained sections, approximately 54 percent of the rutting measured from the surface of the sections occurred in the asphalt-bound layers, 40 percent in the base and subbase, and 6 percent in the subgrade. The total contribution of the subgrade to surface rutting was not significant.

Analysis of layer permanent deformation based on MDD data requires actual or measured layer thicknesses to draw proper conclusions. The information based on design thicknesses was inaccurate with regard to the actual thickness of the ATPB.

It is apparent from direct observation of the pavement layers (trenches) and the MDD data that much of the rutting occurred in the ATPB and/or at the top of the aggregate base (AB). The location of the MDD module in the ATPB, in the AB, or exactly at the interface is critical to determine where the rutting occurred. By assuming a thicker ATPB layer, the permanent deformation estimated for this layer is actually the permanent deformation of the ATPB layer plus a portion of the permanent deformation occurring in the AB layer. This analysis would conclude that the ATPB significantly contributed to surface rutting rather than the AB layer.

3.4 Elastic Deflection Results

Elastic deflections in the pavement sections were measured with the Road Surface Deflectometer (RSD) and Multi-Depth Deflectometers (MDDs). Figures 3.49 and 3.50 show typical deflection basins obtained with these instruments.

Note: Surface and in-depth deflection data presented in the following sections are peak values of the deflection basins.

3.4.1 Surface Deflection Data

Surface elastic deflections were monitored using the RSD along the centerline of the sections at Stations 4, 6, 8, 10, and 12 under the 40-, 80-, and 100-kN test loads. Figures 3.51–3.54 show average deflection data ± one standard deviation for the 40- and 100-kN test loads. The figures show the progressive increase of surface deflection with HVS traffic, with most of the increase occurring under the 80- and 100-kN traffic loads. The variability of surface deflections along the sections is also evident in figures. At the completion of HVS trafficking, the highest elastic deflections were obtained on Section 514 (drained/DGAC) followed by

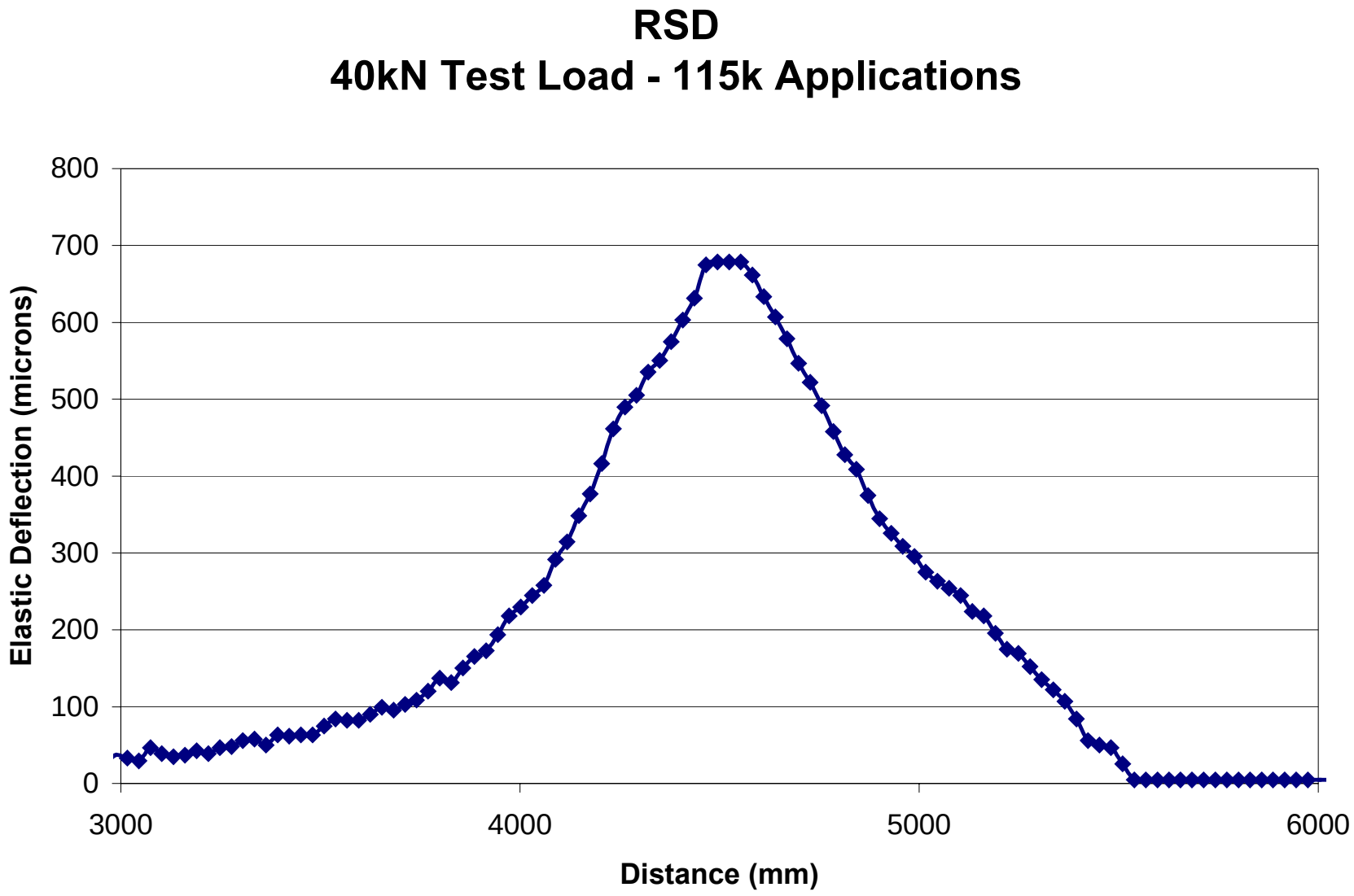

Figure 3.49. Typical RSD deflection basin.

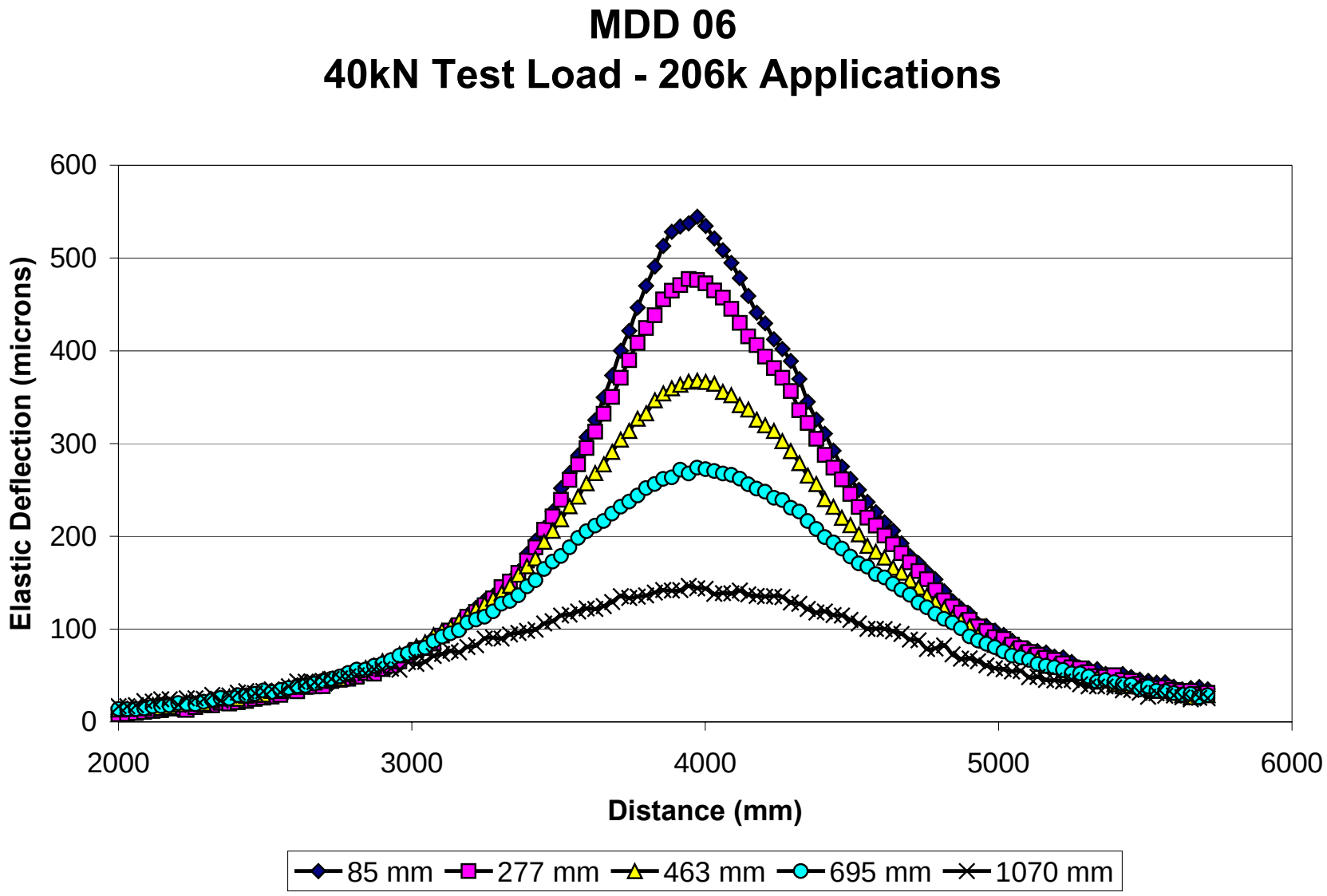

Figure 3.50. Typical MDD deflection basins.

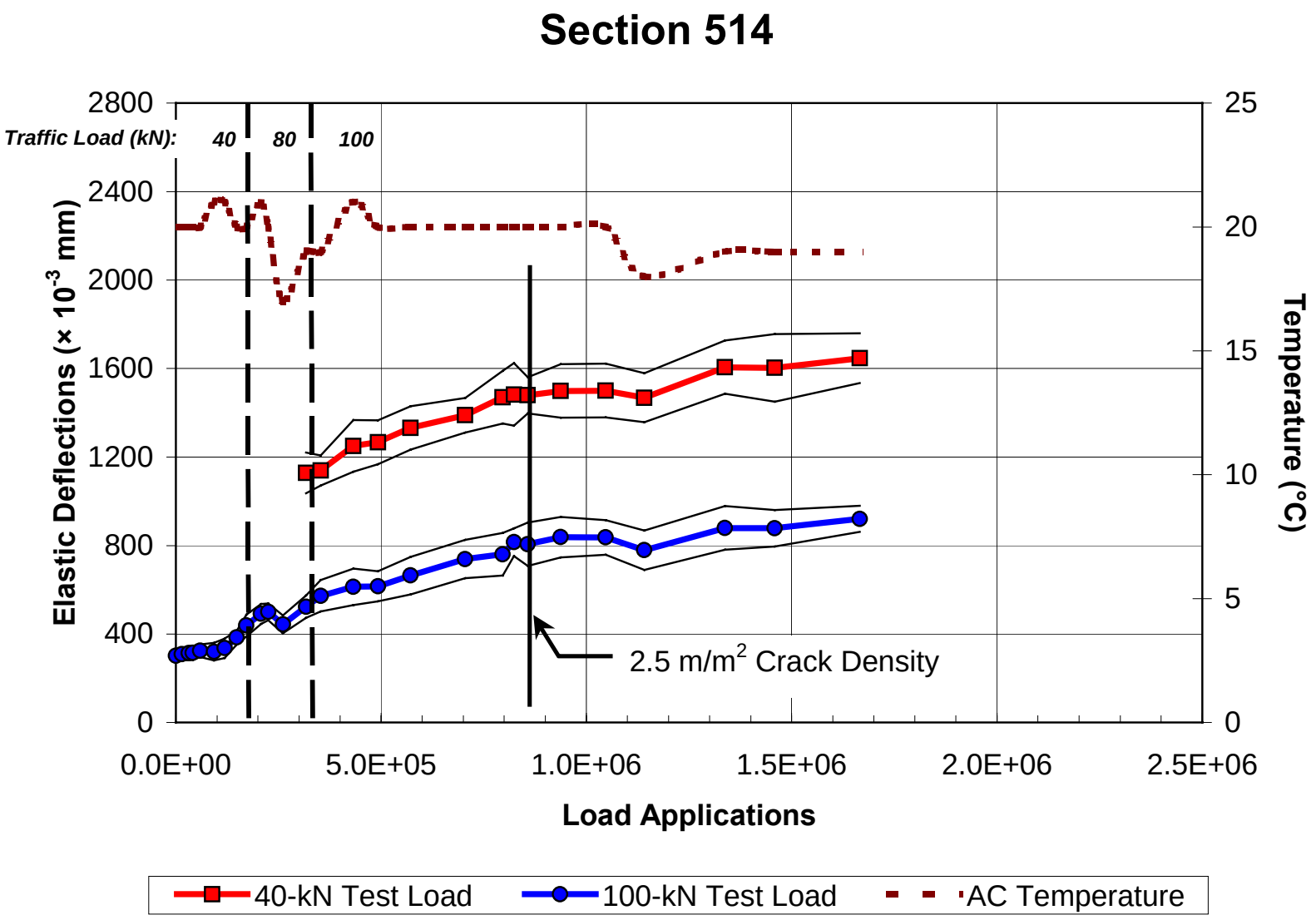

Figure 3.51. RSD surface deflections for Section 514 (drained, DGAC overlay).

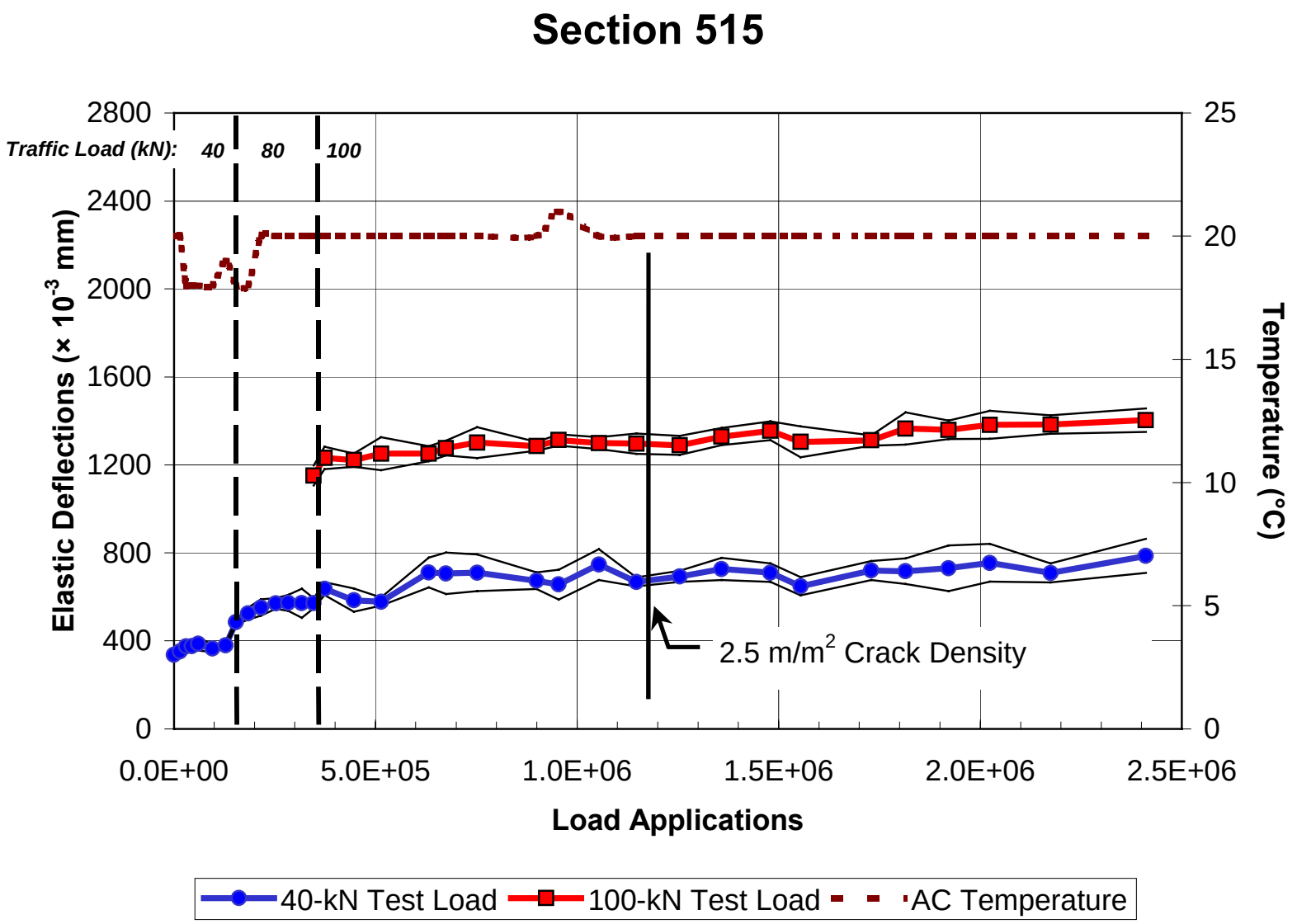

Figure 3.52. RSD surface deflections in for Section 515 (drained, ARHM-GG overlay).

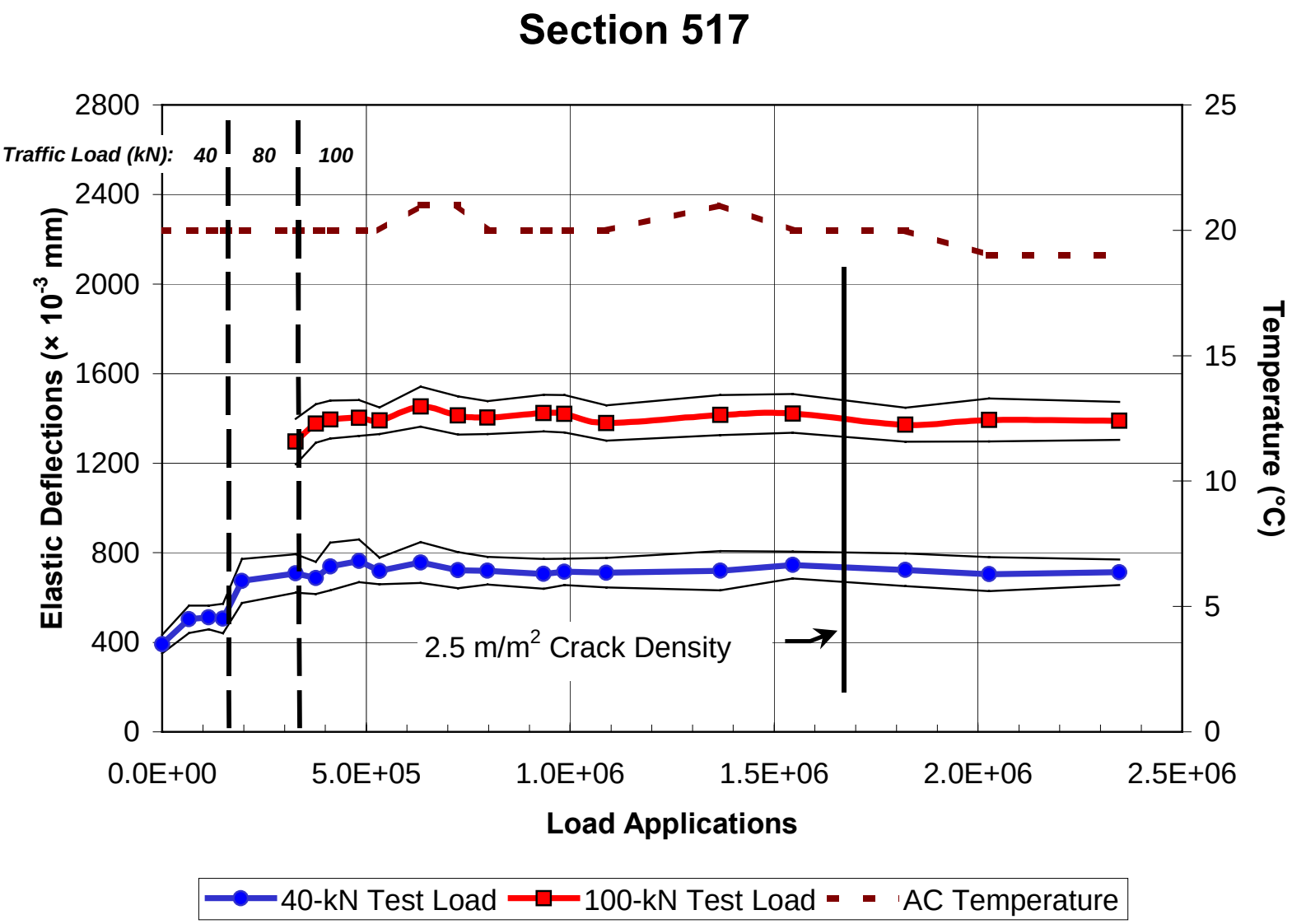

Figure 3.53. RSD surface deflections for Section 517 (undrained, DGAC overlay).

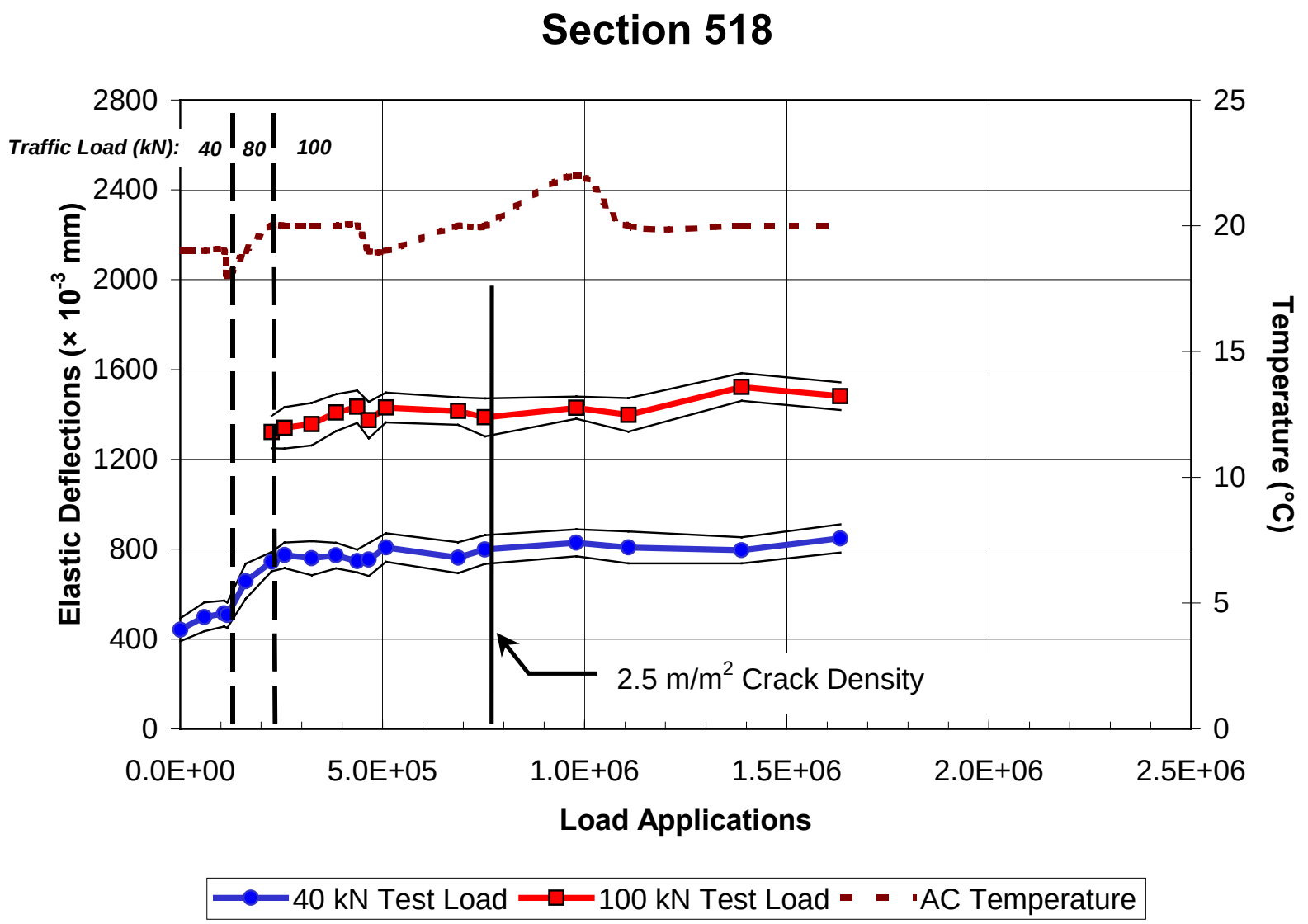

Figure 3.54. RSD surface deflections for Section 518 (undrained, ARHM-GG).

Section 518 (undrained/ARHM-GG), Section 515 (drained/ARHM-GG), and Section 517 (undrained/DGAC), respectively.

Coefficients of variability (standard deviation/mean × 100 percent) under the three test loads are summarized in Table 3.12. The table shows that the sections with the DGAC overlay (Sections 514 and 517) had slightly larger variability than the sections with the ARHM-GG overlay (Sections 515 and 518). The variability in each section could be due to layer thickness variations, material homogeneity, asphalt concrete temperature, and bonding between the top and bottom AC layers.

Table 3.12 Average Coefficient of Variation of Surface Deflections

Test Load (kN)	Average Coefficient of Variation of Surface Deflections (percent)			
	Pavement Sections			
	Drained		Undrained	
	514 DGAC	515 ARHM-GG	517 DGAC	518 ARHM-GG
40	10.4	6.9	10.8	9.0
80	7.4	3.7	7.7	6.2
100	7.7	3.5	6.0	5.3

Figure 3.55 shows the results from RSD measurements taken at the completion of HVS trafficking. Figure 3.56 plots the level of bonding (bonded or unbonded) between the top and bottom AC lifts for all sections obtained from extracted cores or removed slabs. There was considerable variability in the RSD data: lower RSD deflections were obtained where the two AC lifts were bonded and higher deflections where the two AC lifts where not bonded.

3.4.1.1 Comparison of Goal 1 and Goal 3

Figure 3.57 compares surface elastic deflection among the Goal 1 and Goal 3 programs under the 40-kN test load. The figure shows that both overlay strategies used for Goal 3

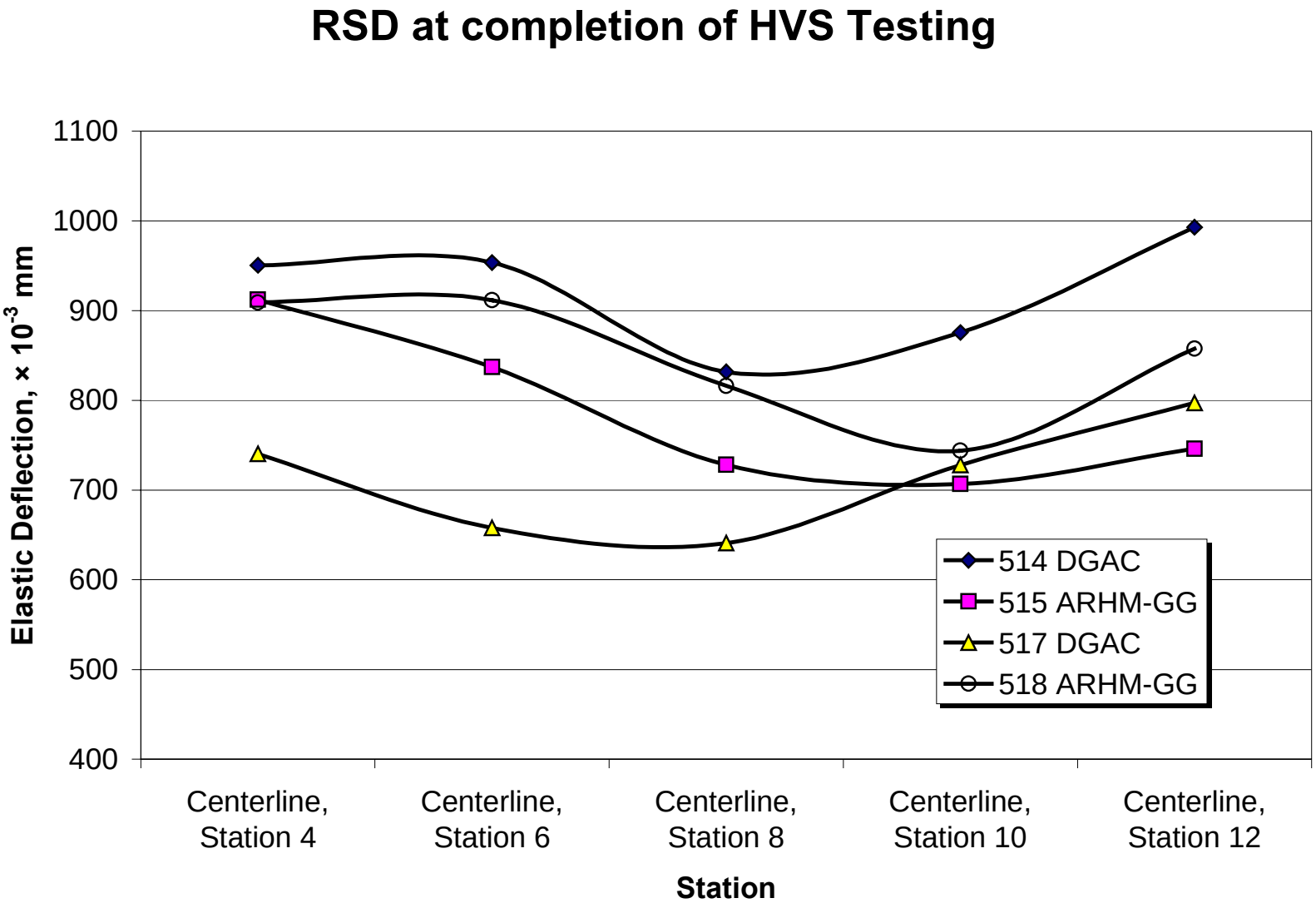

Figure 3.55. Longitudinal variation of RSD deflections for all sections.

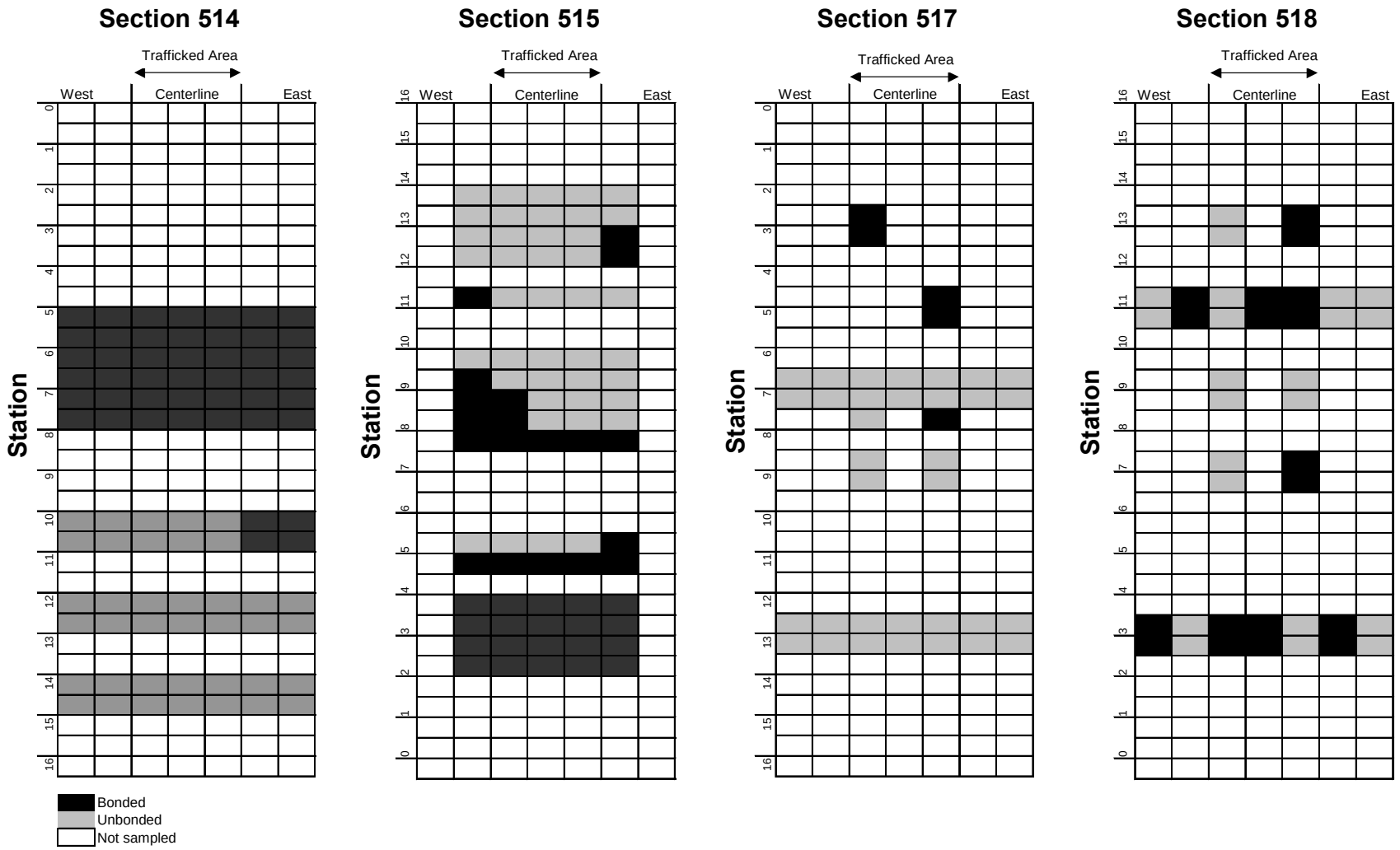

Figure 3.56. Level of bonding between top and bottom AC lifts.

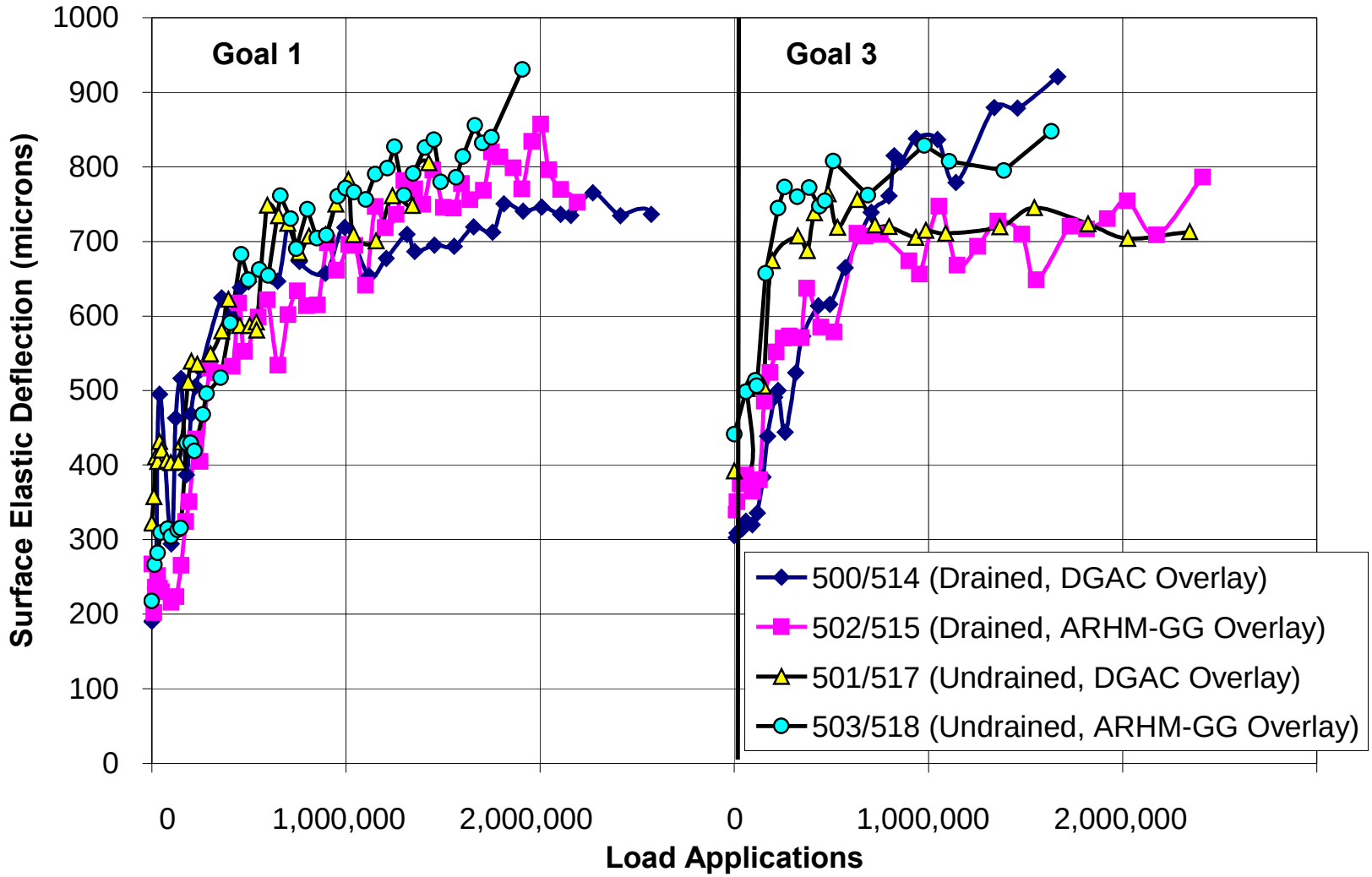

Figure 3.57. Comparison of Goal 1 and Goal 3 RSD deflections under the 40-kN test load.

significantly reduced the elastic deflections obtained at the completion of Goal 1 HVS trafficking.

Table 3.13 presents average elastic deflections at various stages under the 40-kN test load. The data show that both overlay strategies produced a similar reduction in elastic deflections. Average reductions were 58 percent and 46% for the drained and undrained sections, respectively. The results are surprising considering that the ARHM-GG overlay was half the thickness, poorly compacted, and less stiff than the DGAC overlay

Table 3.13 Average Elastic Deflection under 40 kN Test Load

Stage of Testing	**Elastic Deflections in Test Sections (microns)**			
	514	**515**	**517**	**518**
Before Overlay	703	878	805	930
Beginning of 40-kN Traffic Loading	306	344	447	470
Beginning of 100-kN Traffic Loading	548	604	697	758
Completion of Traffic Loading	900	747	708	821

3.4.1.2 Centerline versus Offset

Figures 3.58–3.61 compare average RSD data obtained from the centerline of the pavement section and from offset positions 200 mm from the centerline. The figures show that under the test loads, surface deflections at the offset points were lower than those at the centerline, indicating more severe damage along the traffic centerline than towards the edges of the test sections. This result is to be expected because more loads are applied at points near the centerline due to traffic wander.

Table 3.14 summarizes the reduction in elastic deflection at the offset points compared to the centerline. The table shows that the offset deflections are within one standard deviation of the variability of the centerline deflections (see Table 3.12). Therefore, no significant benefit is obtained by analyzing pavement deflections at locations other than the centerline.

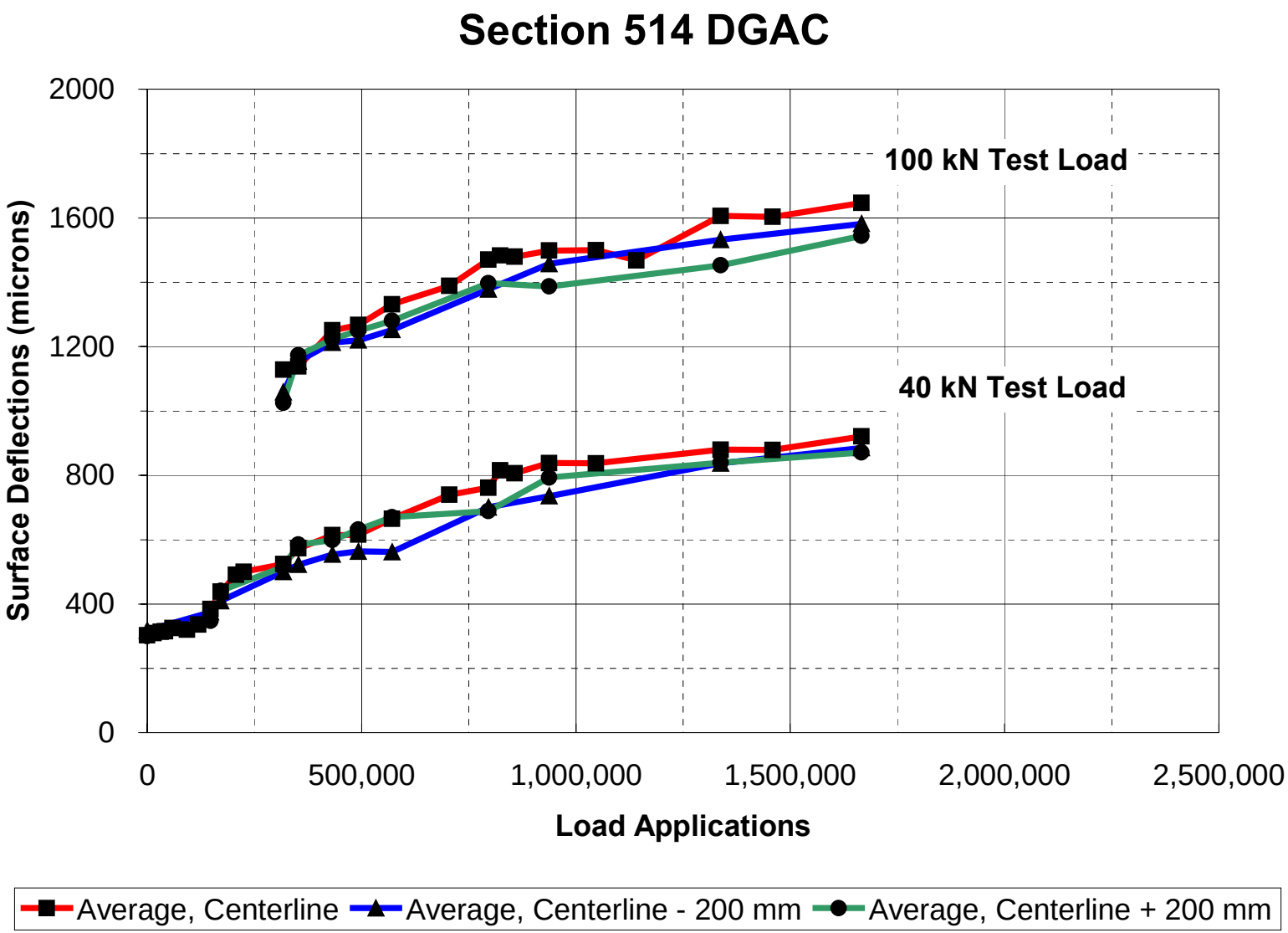

Figure 3.58. Centerline and offset elastic deflections for Section 514 (drained, DGAC overlay).

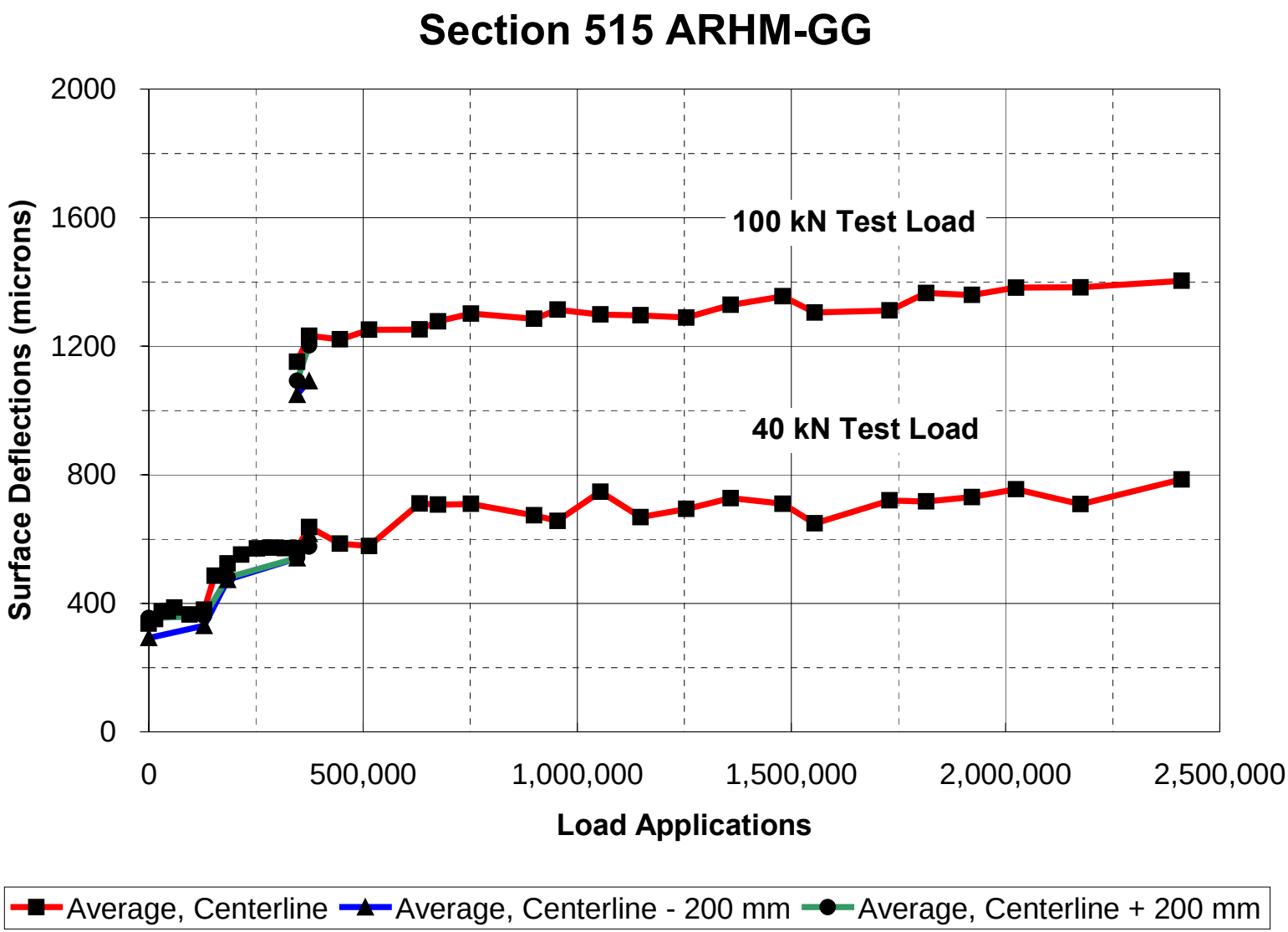

Figure 3.59. Centerline and offset elastic deflections for Section 515 (drained, ARHM-GG overlay).

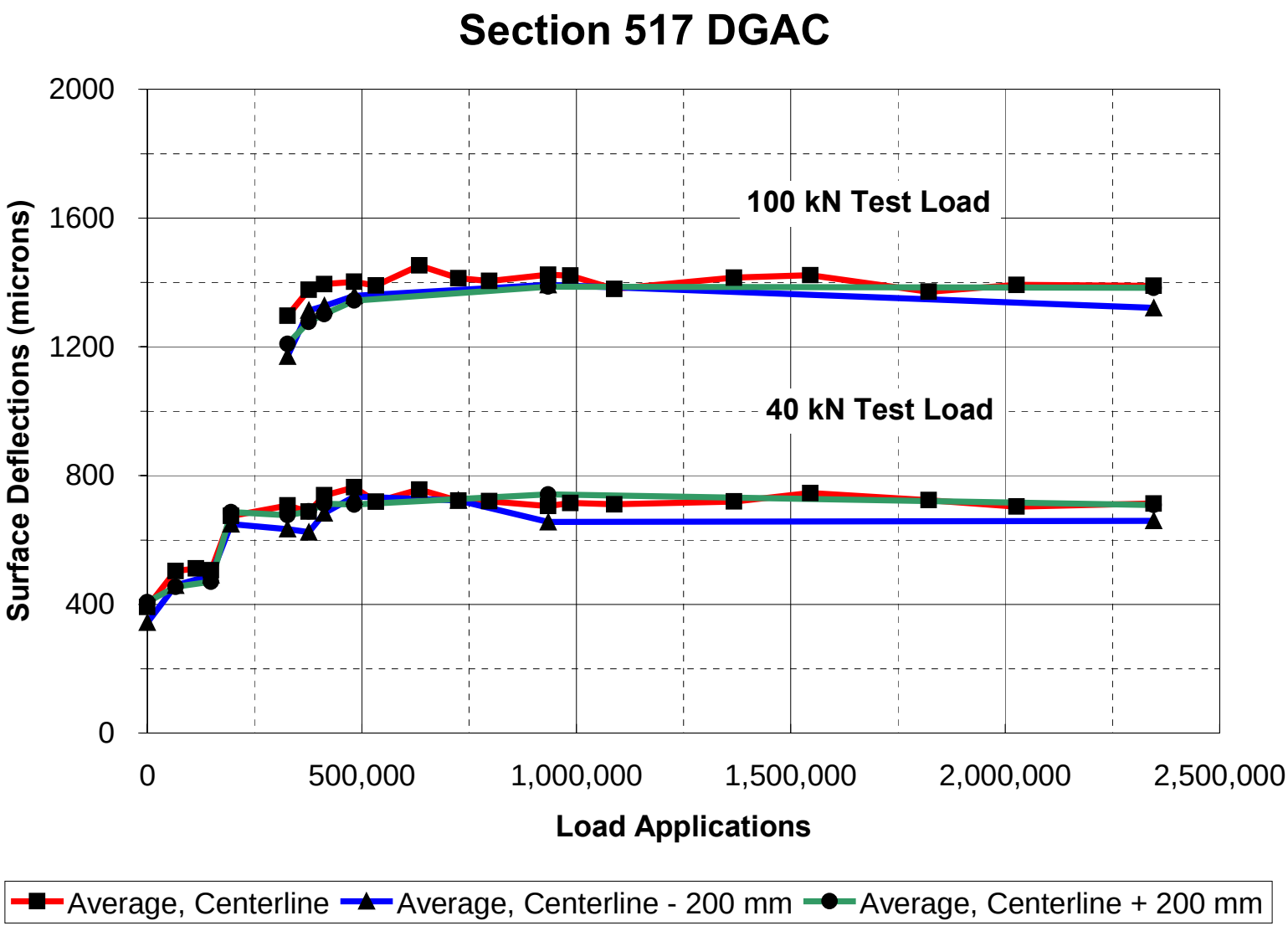

Figure 3.60. Centerline and offset elastic deflections for Section 517 (undrained, DGAC overlay).

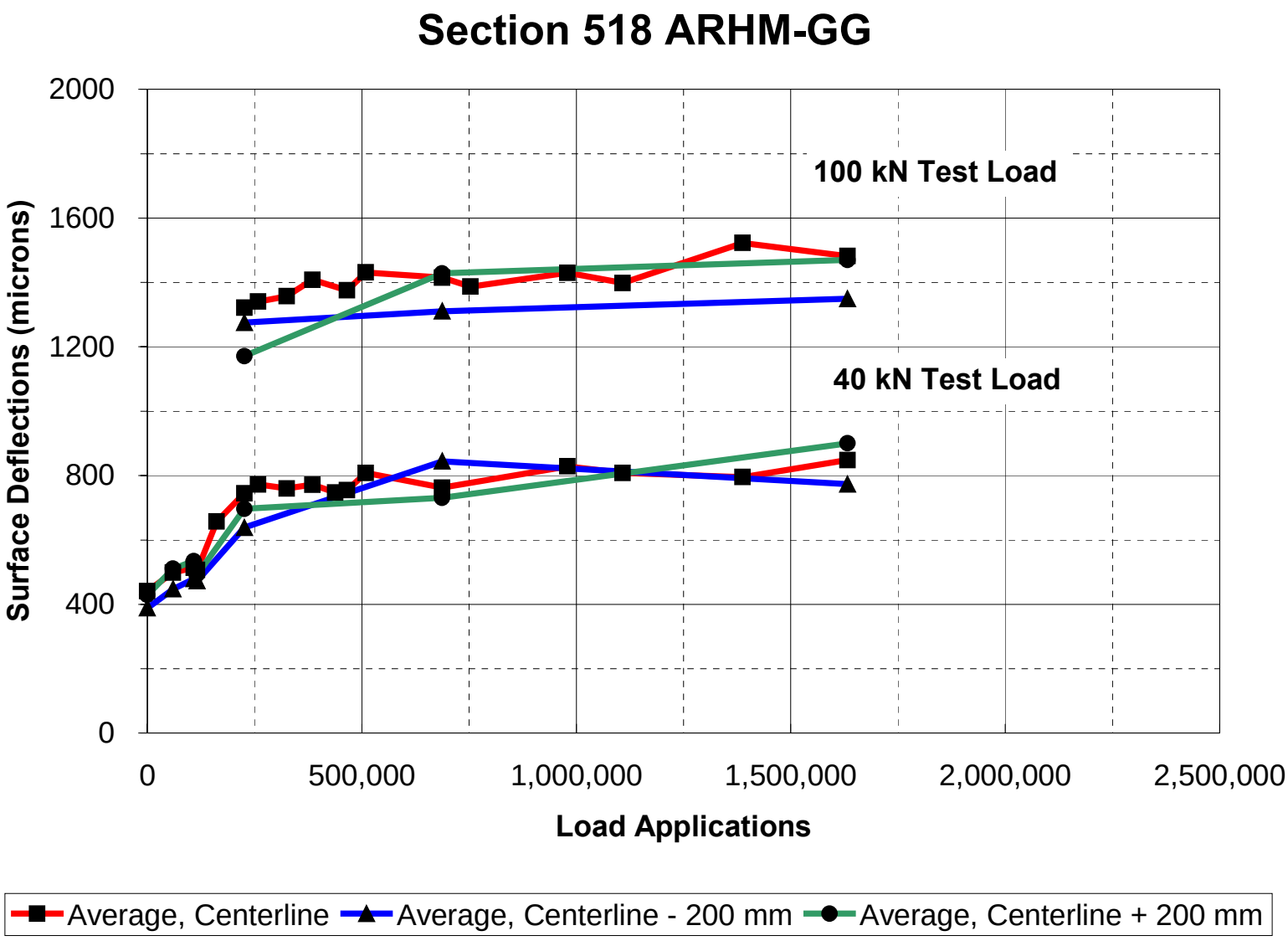

Figure 3.61. Centerline and offset elastic deflections for Section 518 (undrained, ARHM-GG overlay).

Table 3.14 Reduction in Elastic Deflection at Offset Points from Centerline

Reduction in Deflection, Centerline versus 200-mm Offset Points (percent)			
Pavement Sections			
Drained		Undrained	
514 DGAC	515 ARHM-GG	517 DGAC	518 ARHM-GG
4.0	6.8	4.8	4.2

3.4.1.3 RSD versus MDD

Surface deflections were also monitored using the MDDs positioned at Station 10 on each section. Figures 3.62–3.65 compare MDD to RSD data for the drained and undrained sections. For sections 515, 517, and 518, deflections measured with the MDDs were 4 to 5.5 percent higher than deflections measured with the RSD. The excellent agreement between the two devices in the three aforementioned sections indicates the usefulness of the RSD device in defining the uniformity of the sections and checking the MDD results.

For Section 514, MDD results were 16 percent lower than RSD data. The reason for the difference is not clear. A possible reason is the rigid ring supporting the MDD at the surface may have constrained the vertical movement of this MDD.

3.4.2 In-Depth Pavement Deflections in the Drained Sections

In-depth elastic deflection data for the 40-kN and 100-kN test loads are presented in Figures 3.66–3.73 for Section 514, and in Figures 3.74–3.79 for Section 515. The data show a progressive increase in elastic deflection with traffic loading for all pavement layers and the subgrade. The data also show the influence of pavement temperature on the in-depth elastic deflections. As presented in Table 3.1, pavement temperatures were more uniform for Section 515 than for Section 514. Subgrade water content variations, discussed in Section 3.2, did not significantly influence the in-depth elastic deflections. In Section 515, the subgrade water

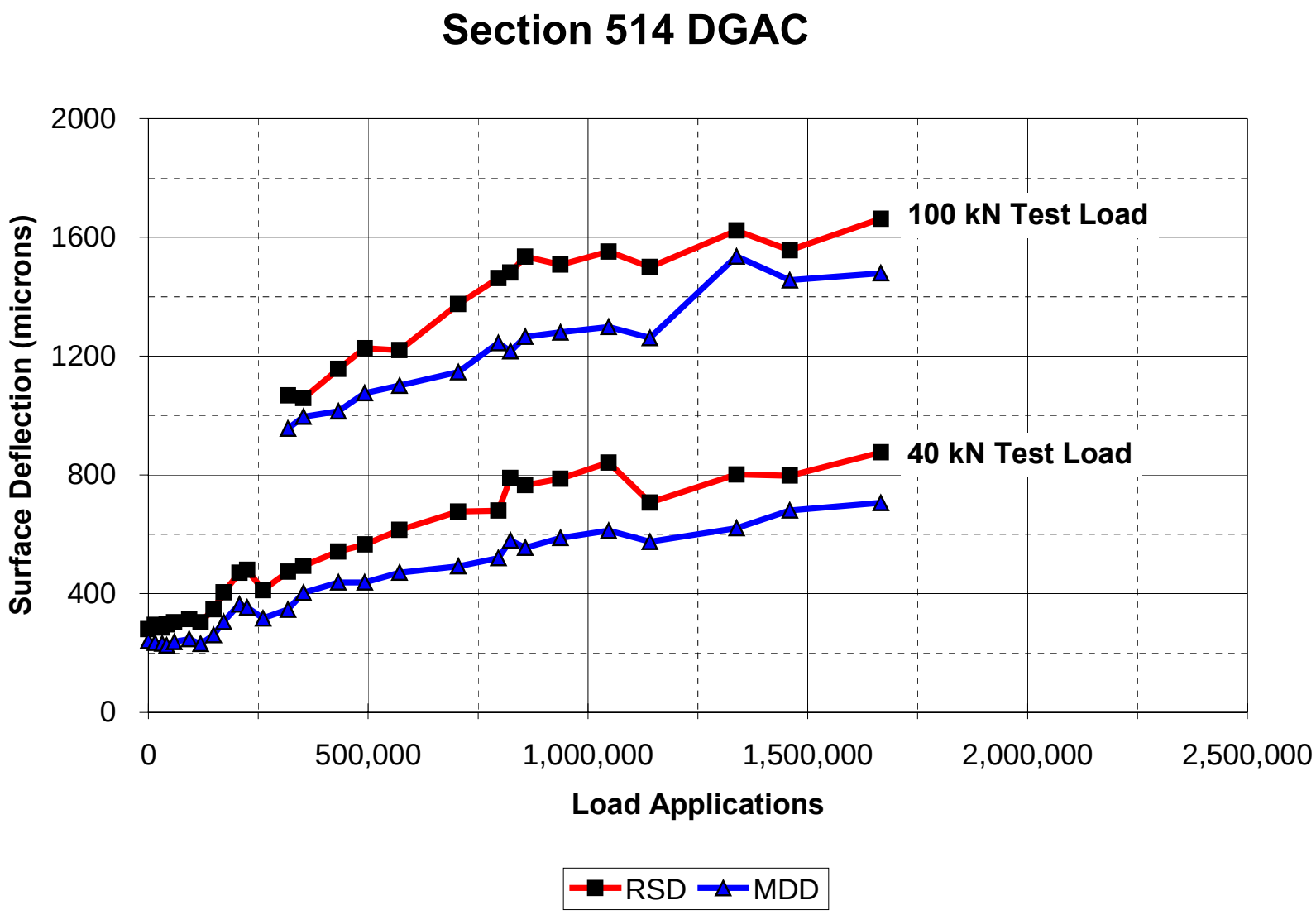

Figure 3.62. MDD and RSD surface deflections in Section 514 (drained, DGAC overlay).

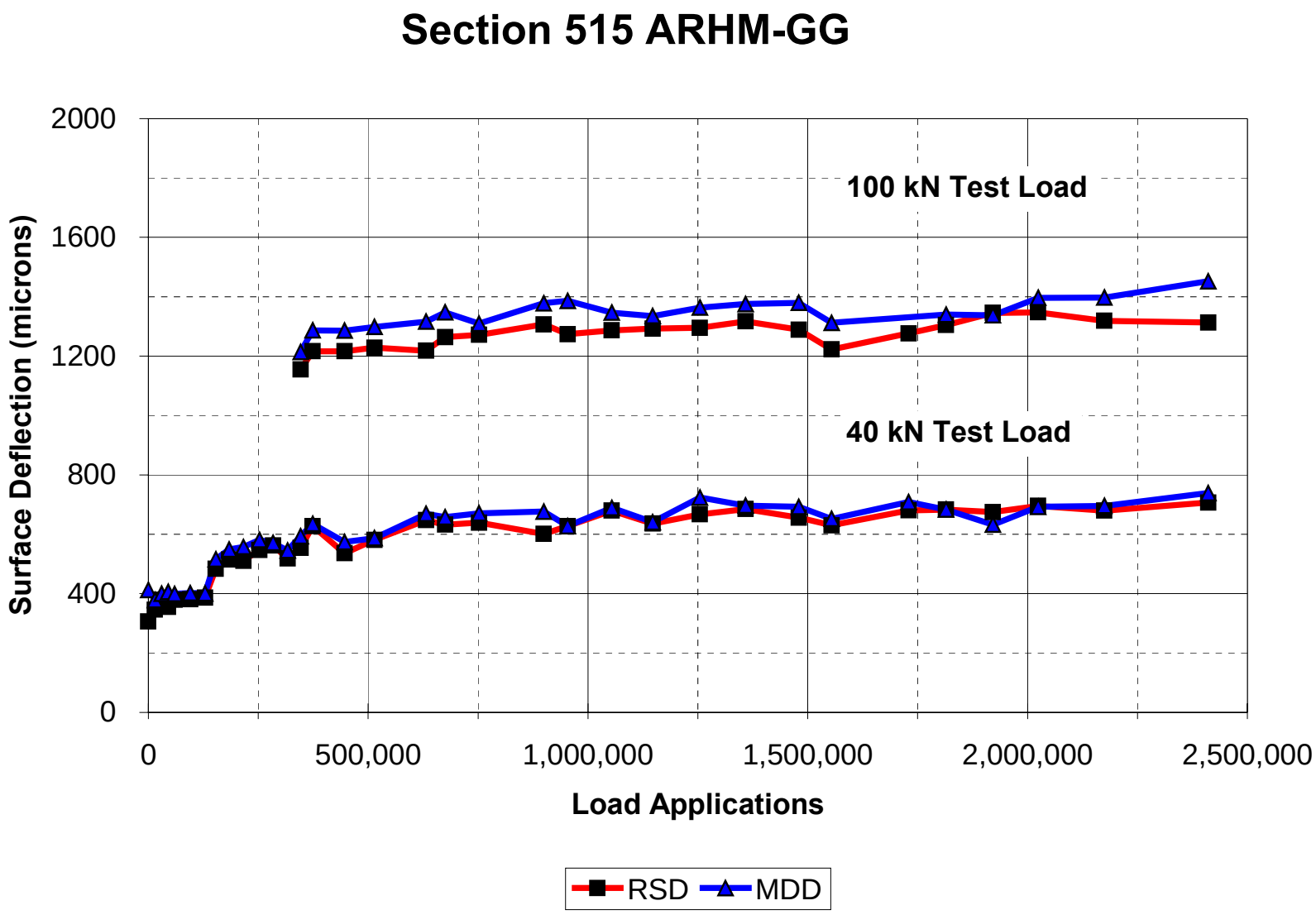

Figure 3.63. MDD and RSD surface deflections in Section 515 (drained, ARHM-GG overlay).

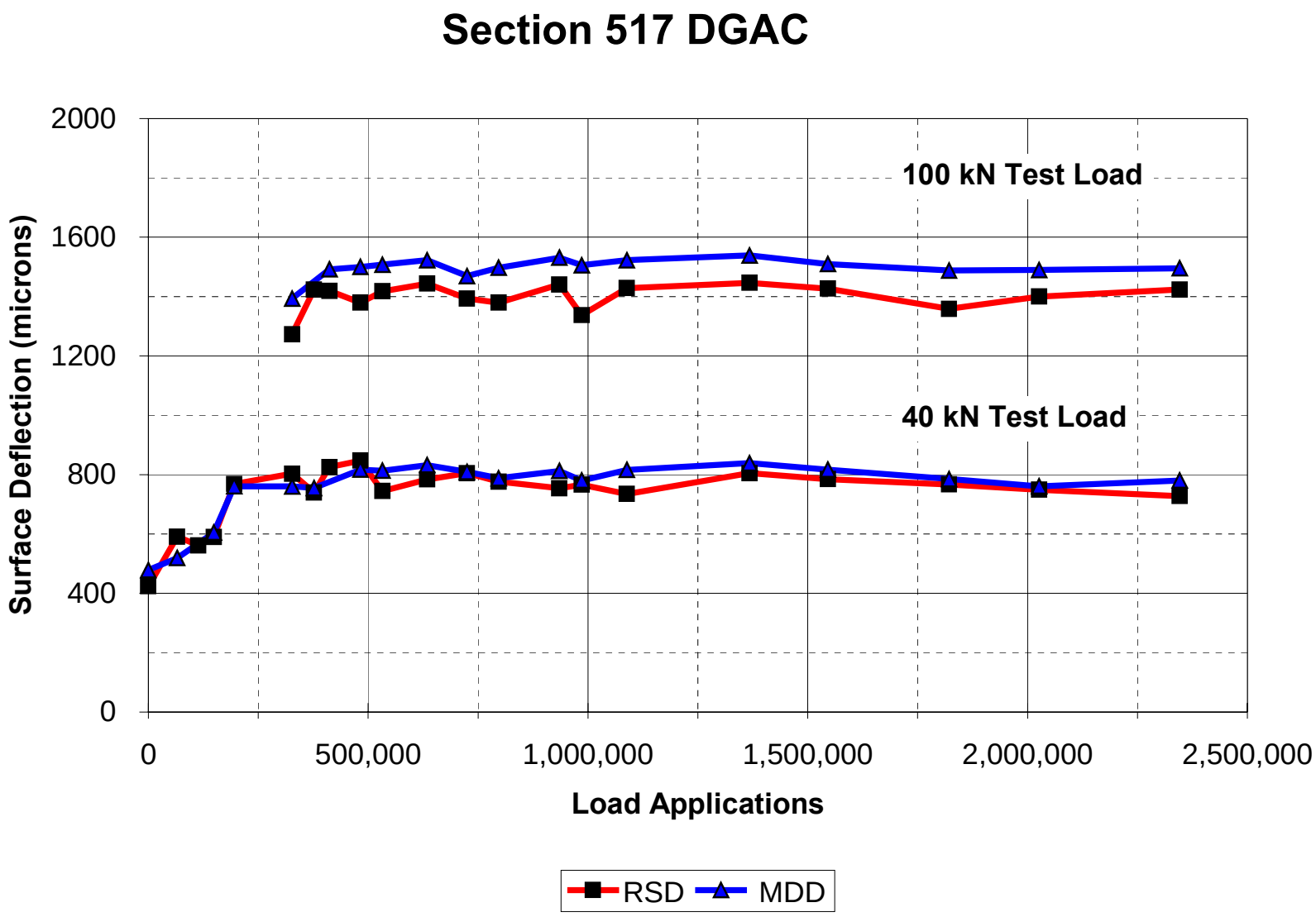

Figure 3.64. MDD and RSD surface deflections in Section 517 (undrained, DGAC overlay).

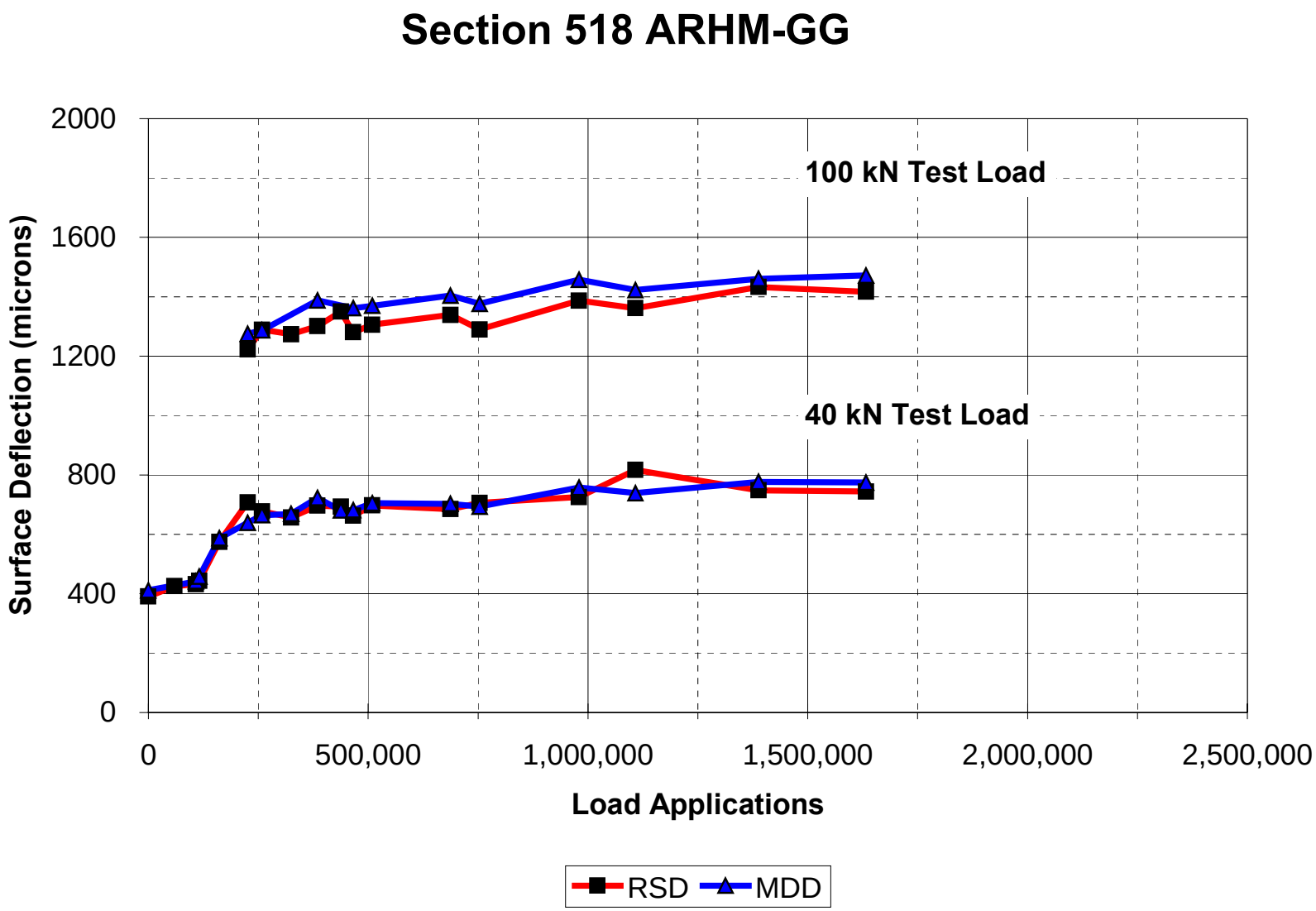

Figure 3.65. MDD and RSD surface deflections in Section 518 (undrained, ARHM-GG overlay).

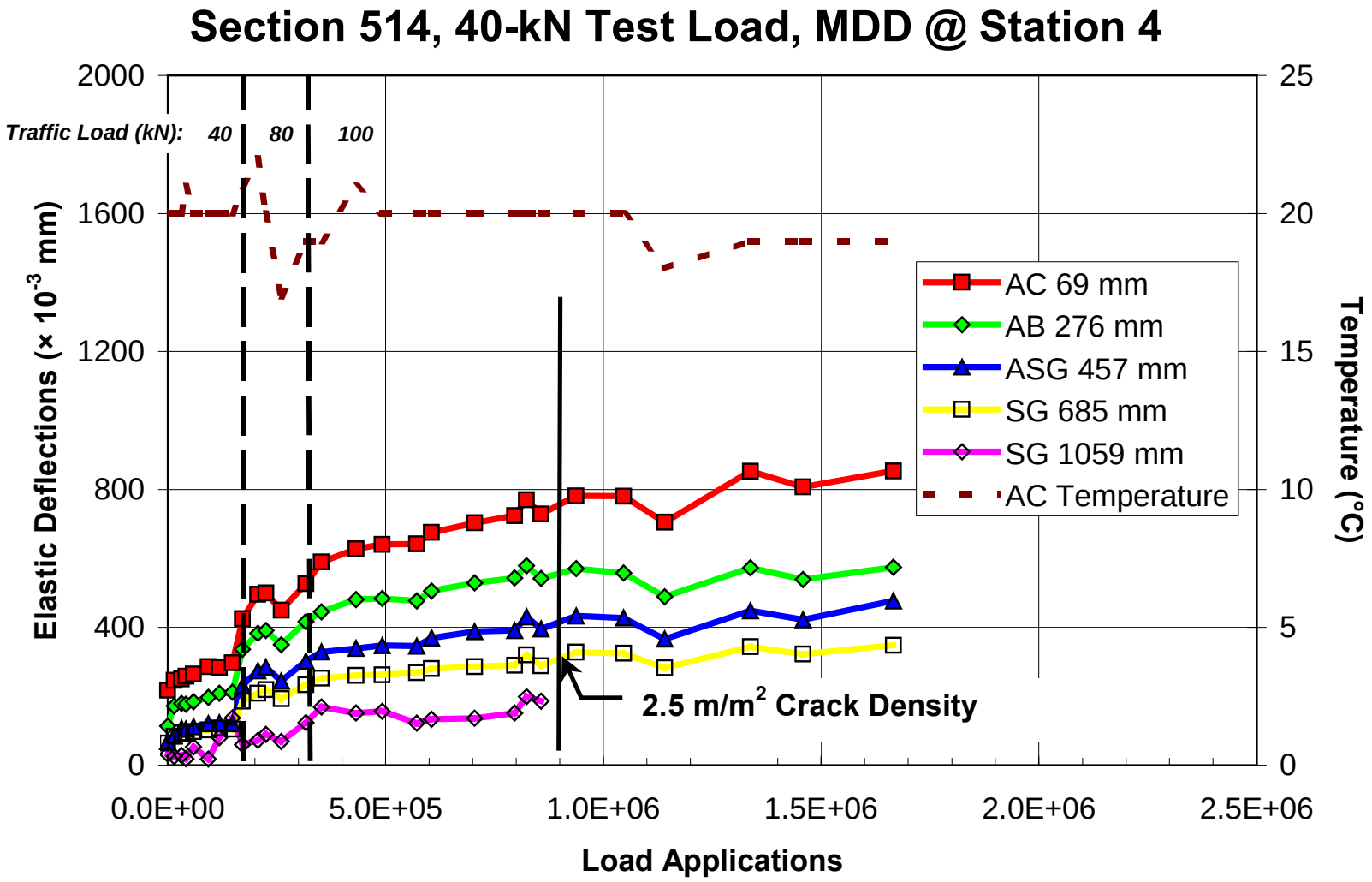

Figure 3.66. In-depth elastic deflections at Station 4, Section 514 (drained, DGAC overlay), 40-kN test load.

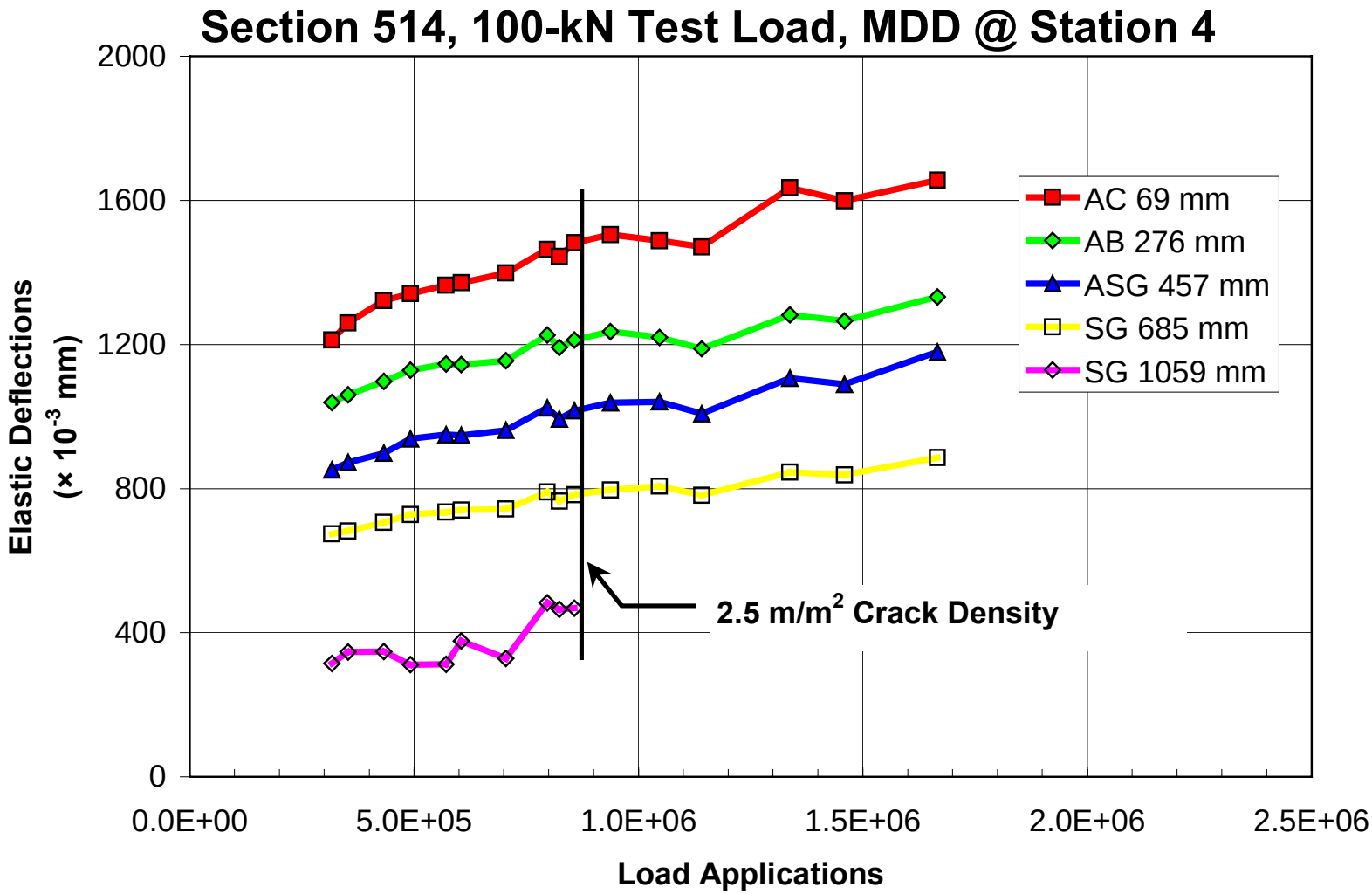

Figure 3.67. In-depth elastic deflections at Station 4, Section 514 (drained, DGAC overlay), 100-kN test load.

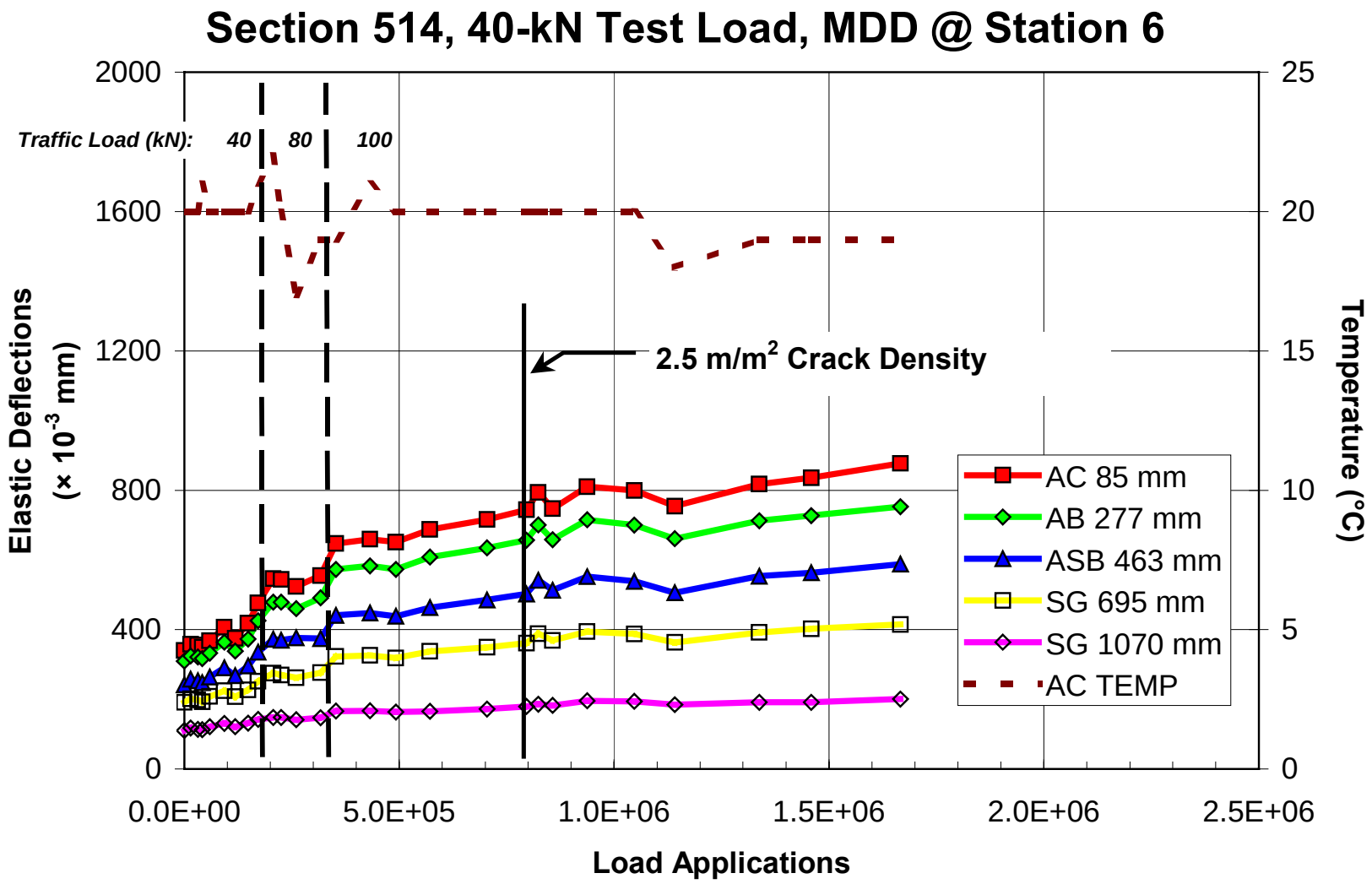

Figure 3.68. In-depth elastic deflections at Station 6, Section 514 (drained, DGAC overlay), 40-kN test load.

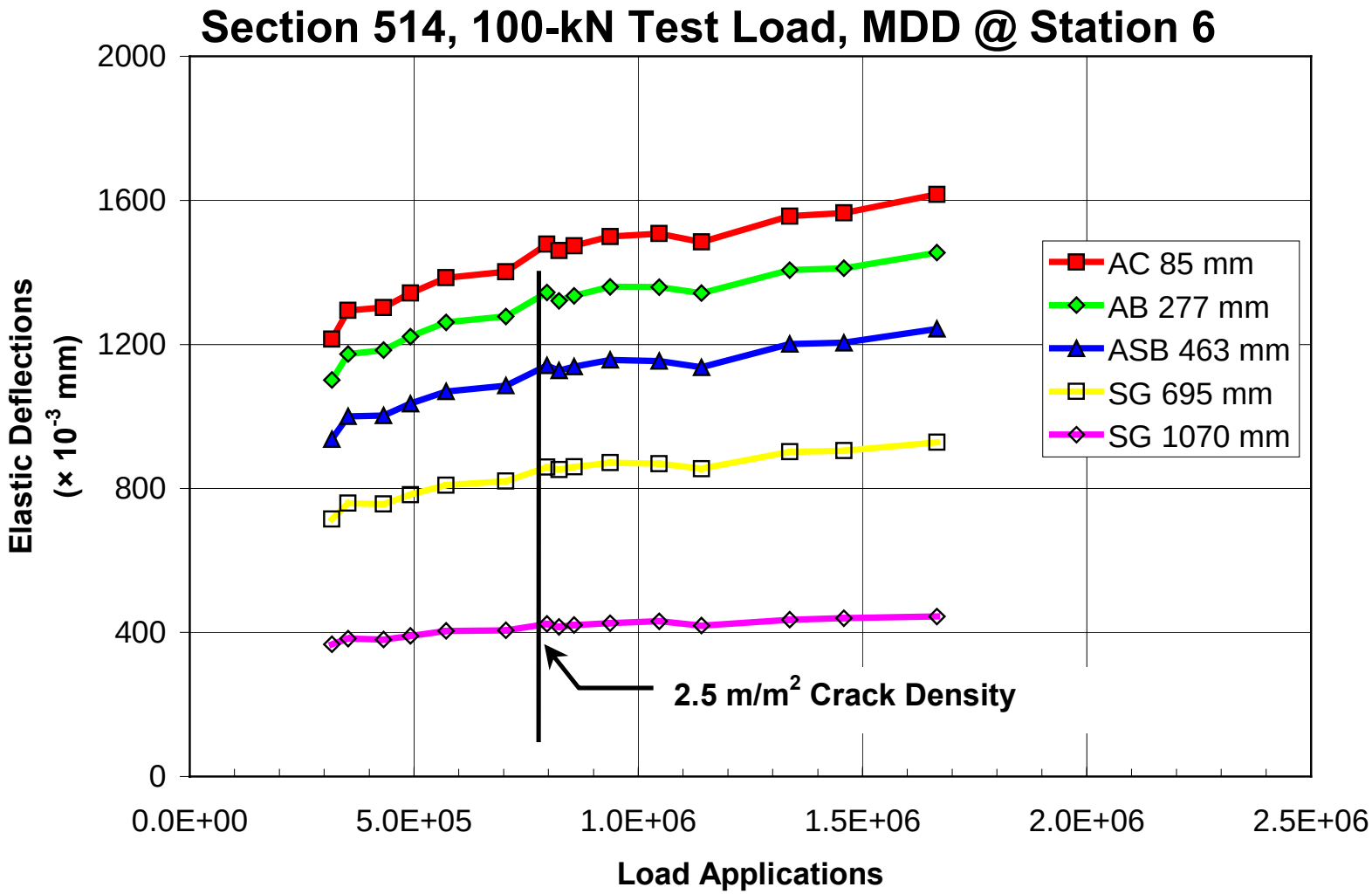

Figure 3.69. In-depth elastic deflections at Station 6, Section 514 (drained, DGAC overlay), 100-kN test load.

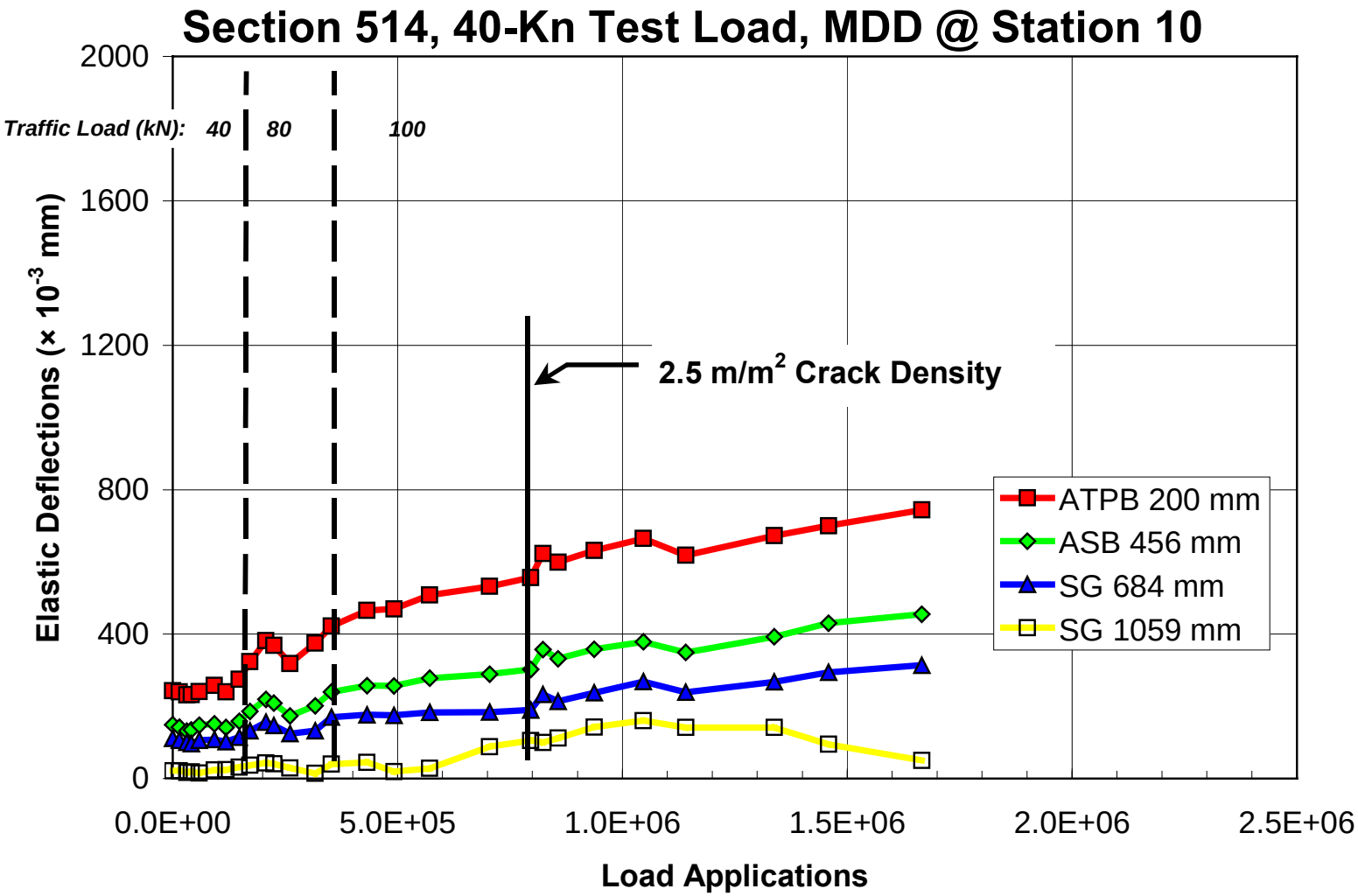

Figure 3.70. In-depth elastic deflections at Station 10, Section 514 (drained, DGAC overlay), 40-kN test load.

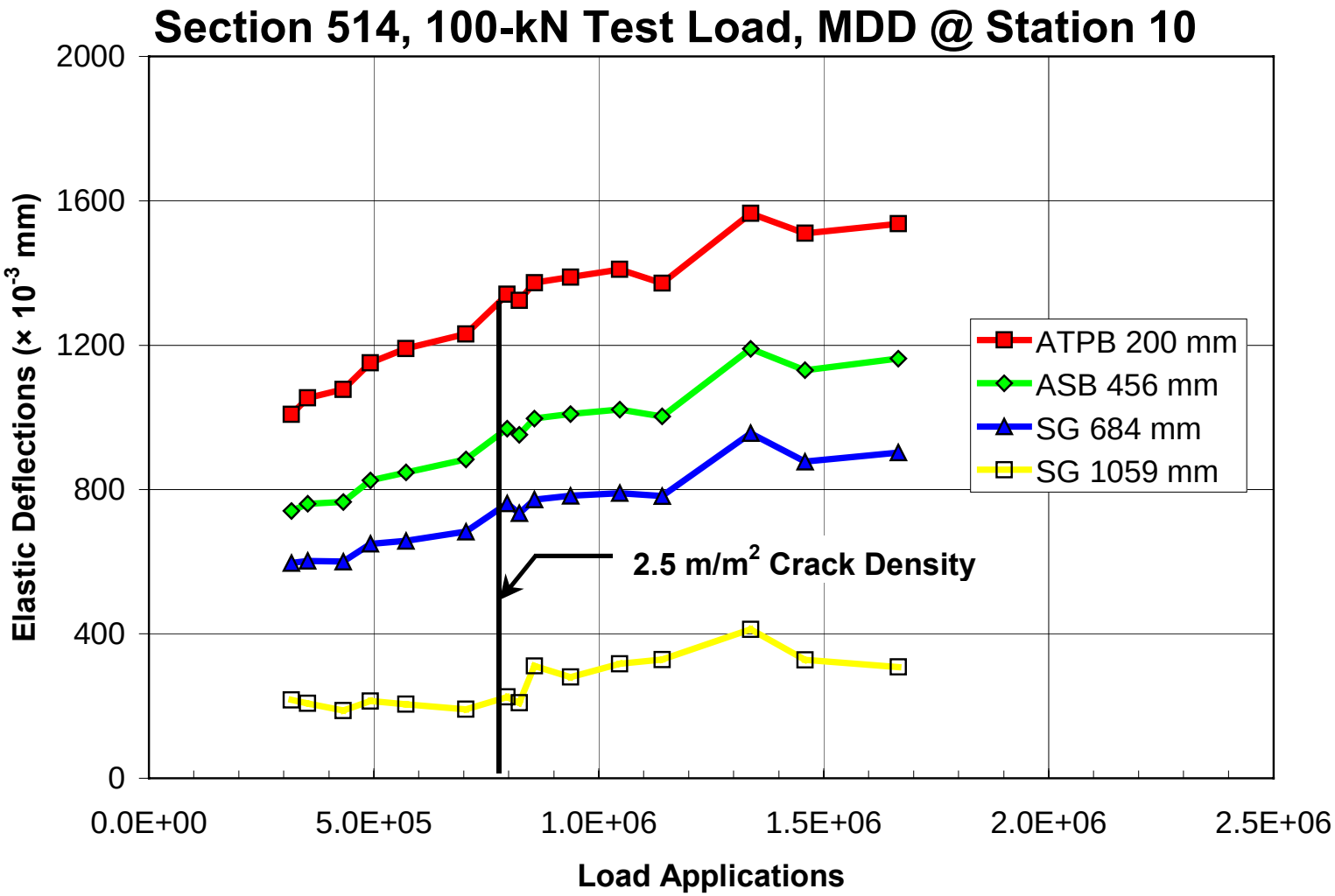

Figure 3.71. In-depth elastic deflections at Station 10, Section 514 (drained, DGAC overlay), 100-kN test load.

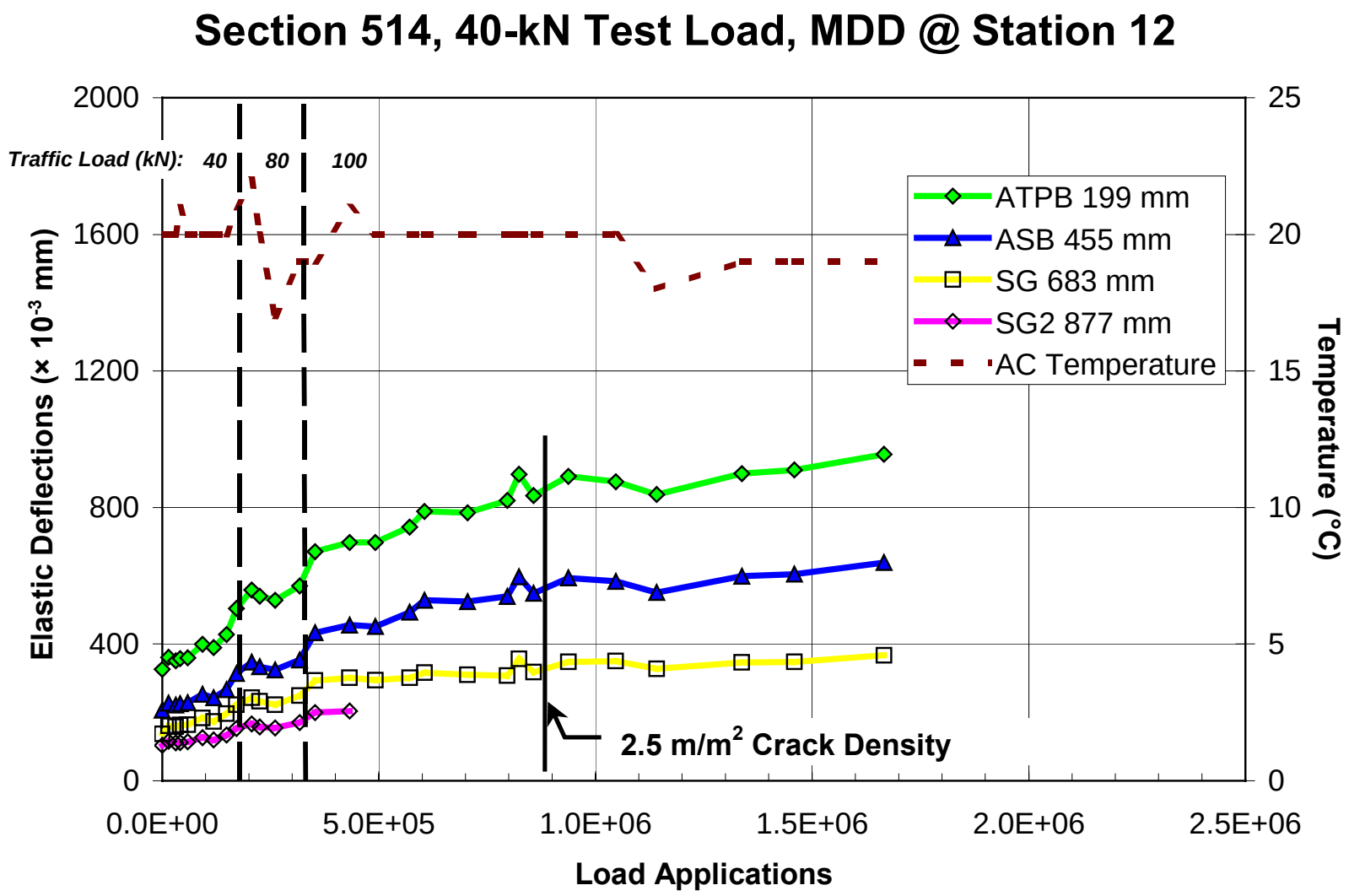

Figure 3.72. In-depth elastic deflections at Station 12, Section 514 (drained, DGAC overlay), 40-kN test load.

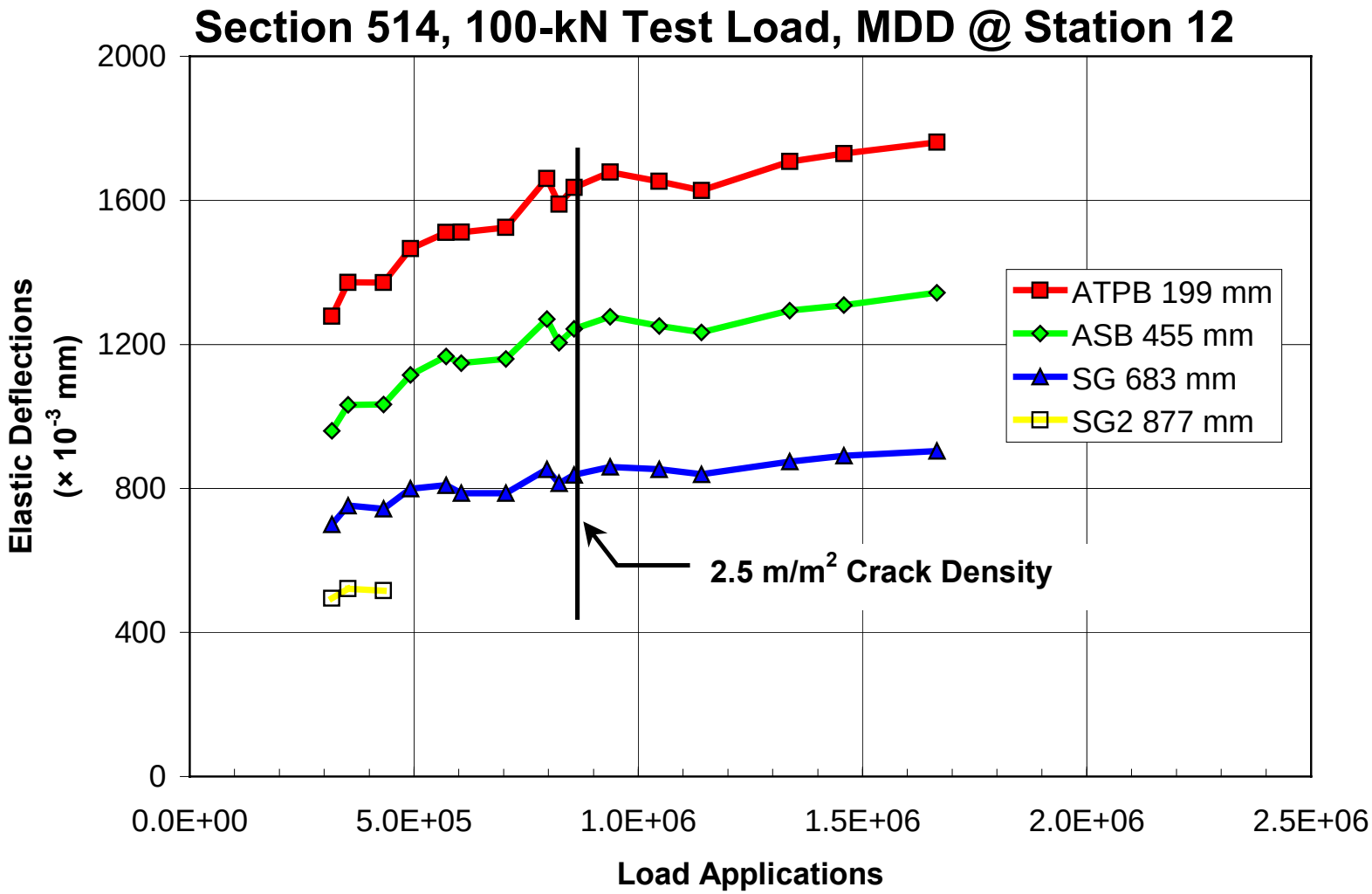

Figure 3.73. In-depth elastic deflections at Station 12, Section 514 (drained, DGAC overlay), 100-kN test load.

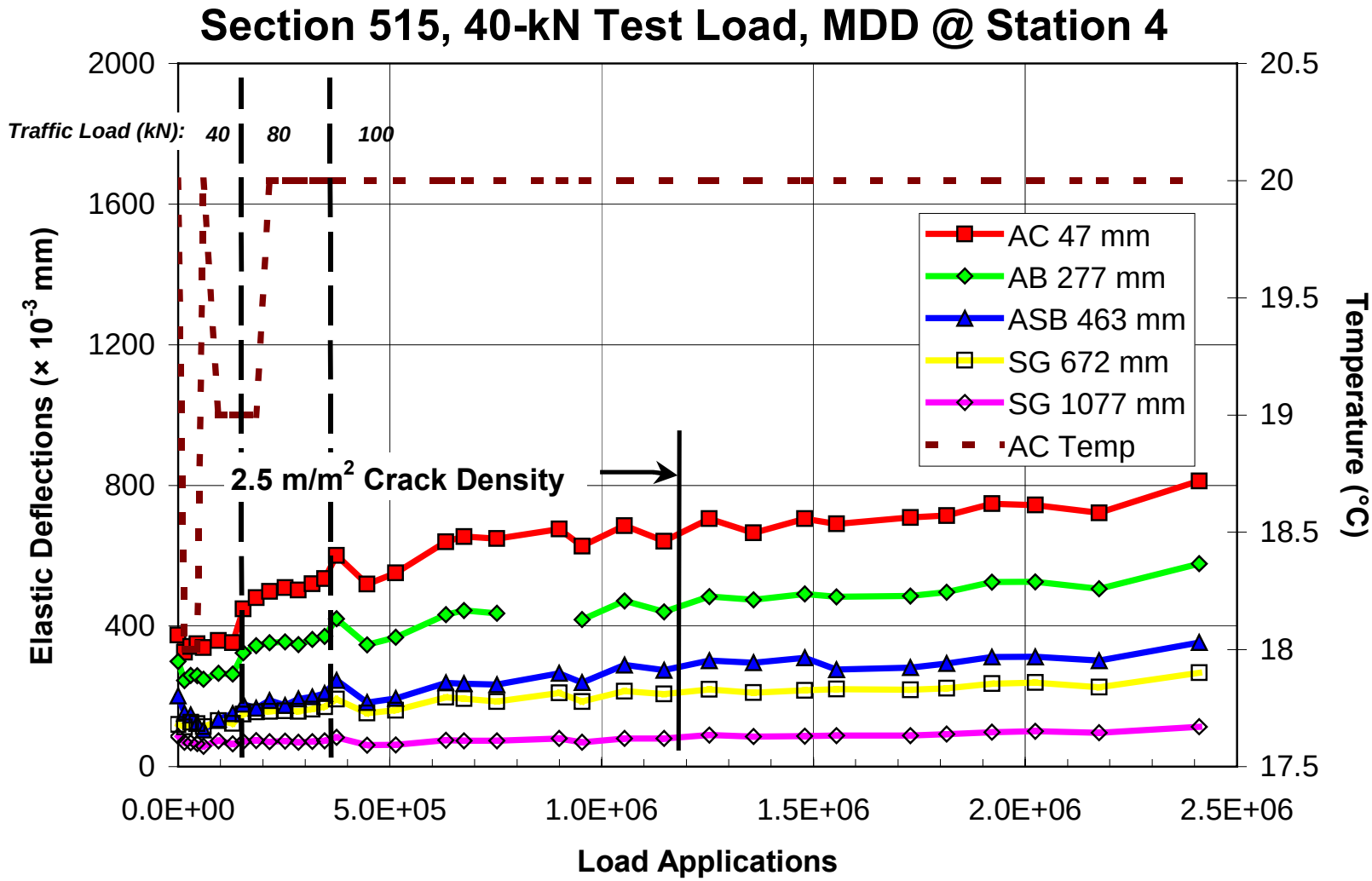

Figure 3.74. In-depth elastic deflections at Station 4, Section 515 (drained, ARHM-GG overlay), 40-kN test load.

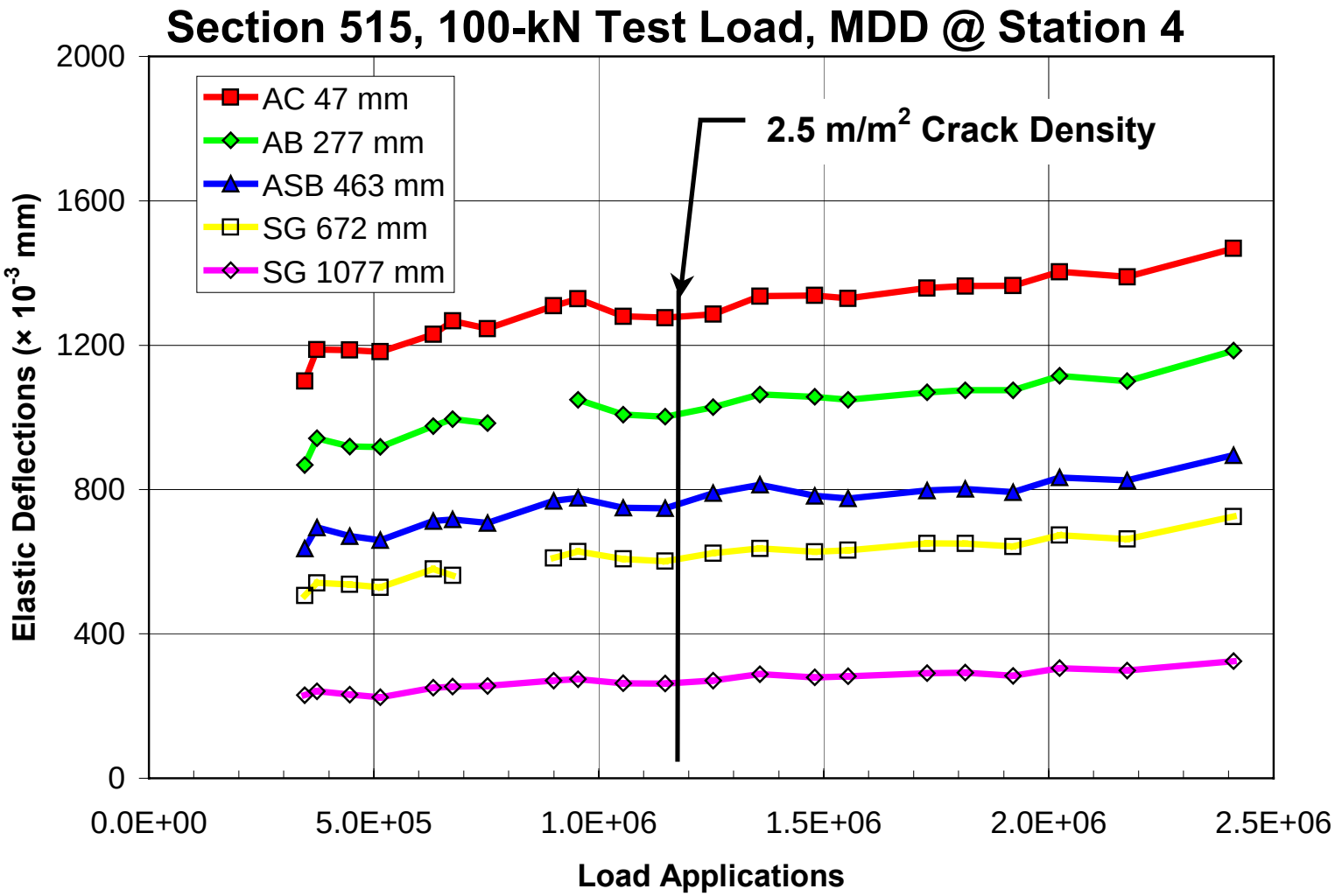

Figure 3.75. In-depth elastic deflections at Station 4, Section 515 (drained, ARHM-GG overlay), 100-kN test load.

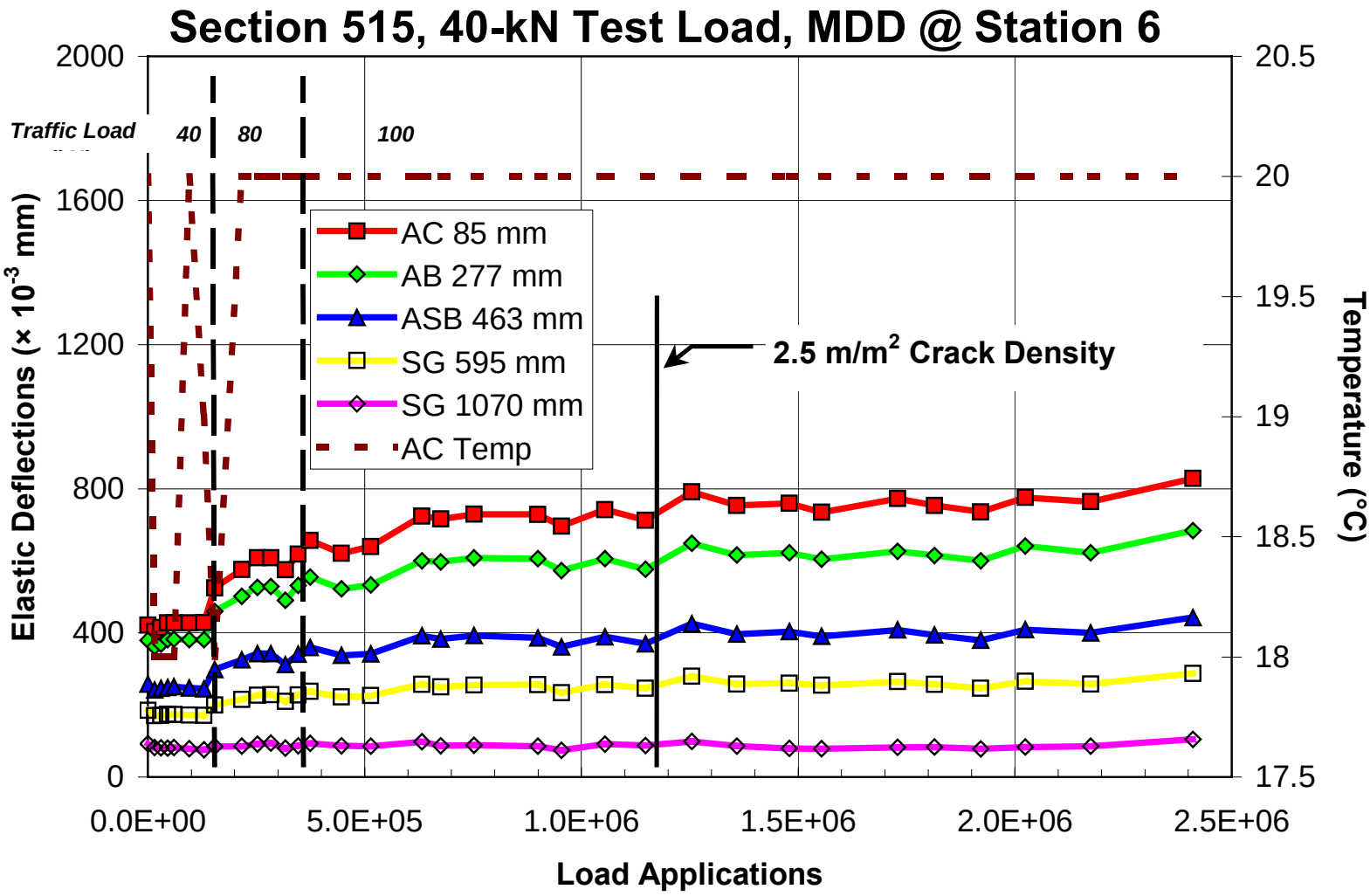

Figure 3.76. In-depth elastic deflections at Station 6, Section 515 (drained, ARHM-GG overlay), 40-kN test load.

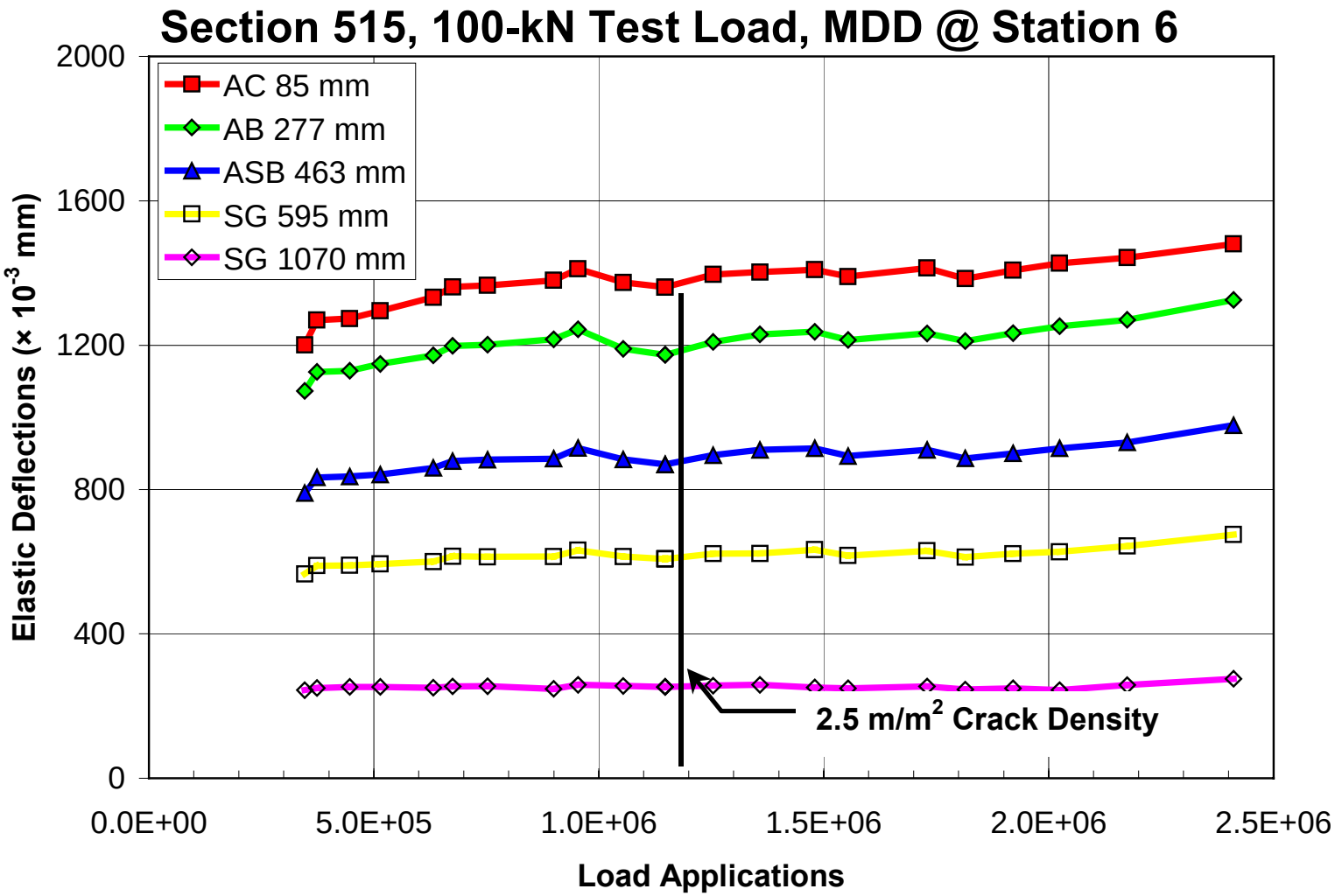

Figure 3.77. In-depth elastic deflections at Station 6, Section 515 (drained, ARHM-GG overlay), 100-kN test load.

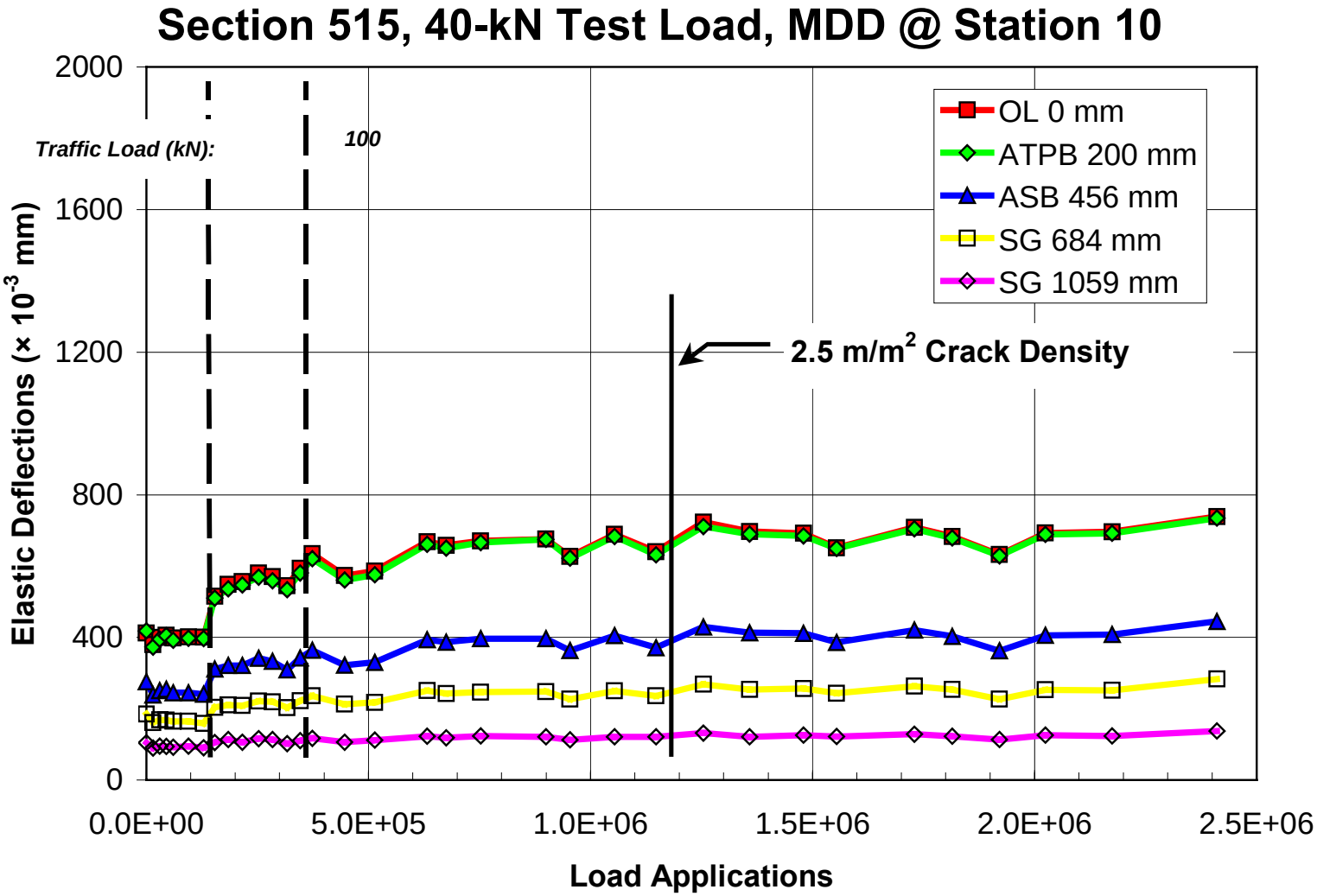

Figure 3.78. In-depth elastic deflections at Station 10, Section 515 (drained, ARHM-GG overlay), 40-kN test load.

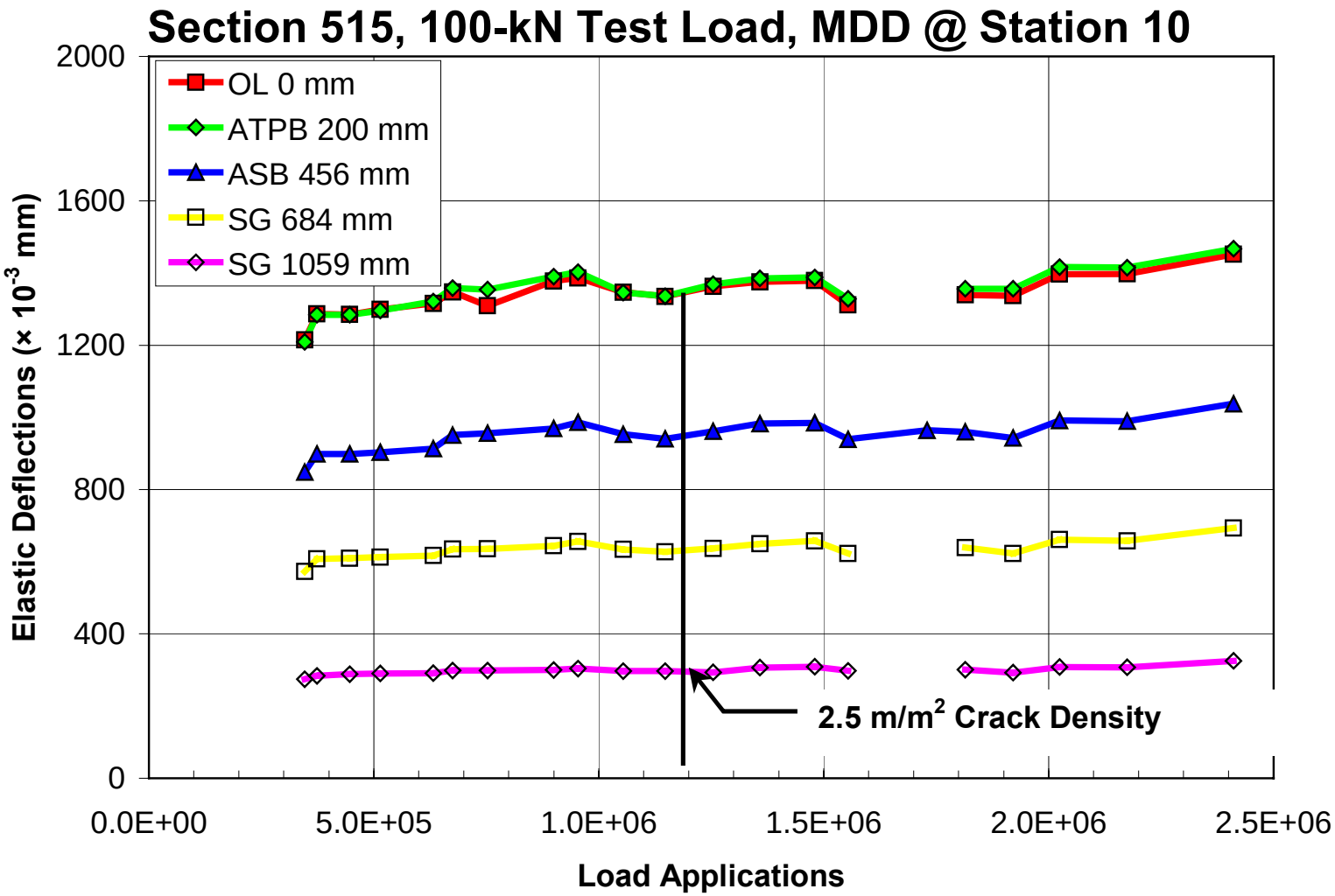

Figure 3.79. In-depth elastic deflections at Station 10, Section 515 (drained, ARHM-GG overlay), 100-kN test load.

content decreased from 30 to 25 percent, yet did not affect the in-depth elastic deflections measured in the subgrade.

Average in-depth elastic deflections in Sections 514 and 515 under the 40-kN and 100-kN test loads are presented in Figures 3.80–3.83. Overall, in-depth elastic deflections are higher in Section 514 than in Section 515. In-depth elastic deflections at the beginning and end of testing are presented in Table 3.15 for the 40-kN test load.

Table 3.15 In-Depth Elastic Deflection under 40-kN Test Load in Drained Sections

Pavement Layer	Elastic Deflections in Section (microns)			
	514 DGAC		515 ARHM-GG	
	Start	End	Start	End
Overlay	303	921	344	747
AC	279	865	381	782
ATPB	285	850	396	713
Aggregate Base	211	663	321	597
Aggr. Subbase	149	471	228	392
Subbase	117	356	155	262

Coefficients of variation of in-depth elastic deflections are presented in Table 3.16. These coefficients of variation are more meaningful for the deflections measured on top of the unbound layers given that multiple MDD instruments were installed at these layers. In-depth elastic deflections recorded in Section 514 at Stations 4 and 6 were somewhat different from those recorded at Stations 10 and 12. In-depth elastic deflection variability can be attributed to variations in layer thickness, material density, and level of bonding between the bound layers.

Table 3.16 Coefficients of Variation for In-Depth Deflections in Drained Sections

Pavement Layer	Test Section			
	514 (DGAC)		515 (ARHM-GG)	
	40-kN Test Load	100-kN Test Load	40-kN Test Load	100-kN Test Load
Aggregate Base	16	7	20	10
Aggregate Subbase	23	11	21	10
Subgrade	30	6	11	2

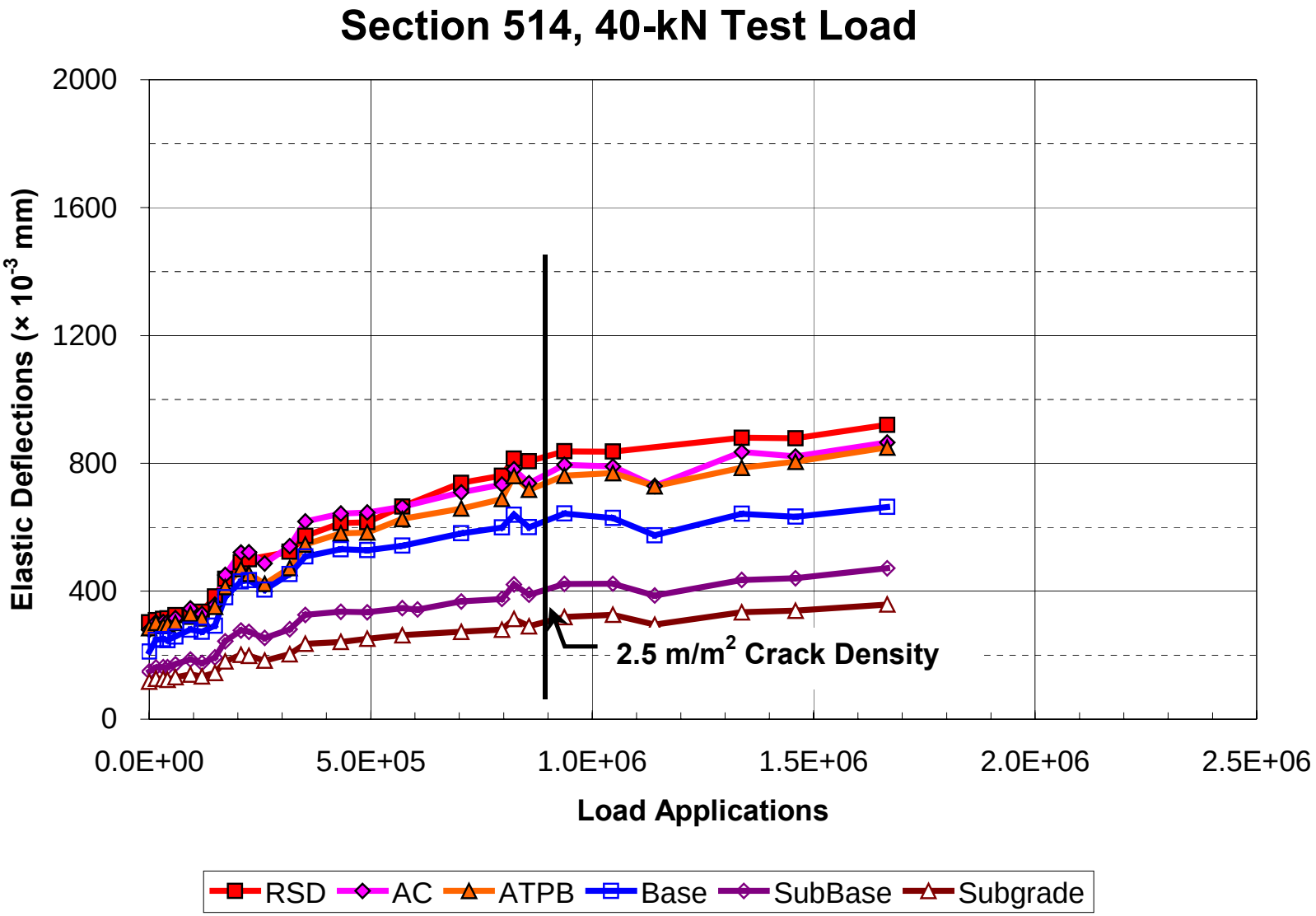

Figure 3.80. Average in-depth deflections for Section 514 (drained, DGAC overlay), 40-kN test load.

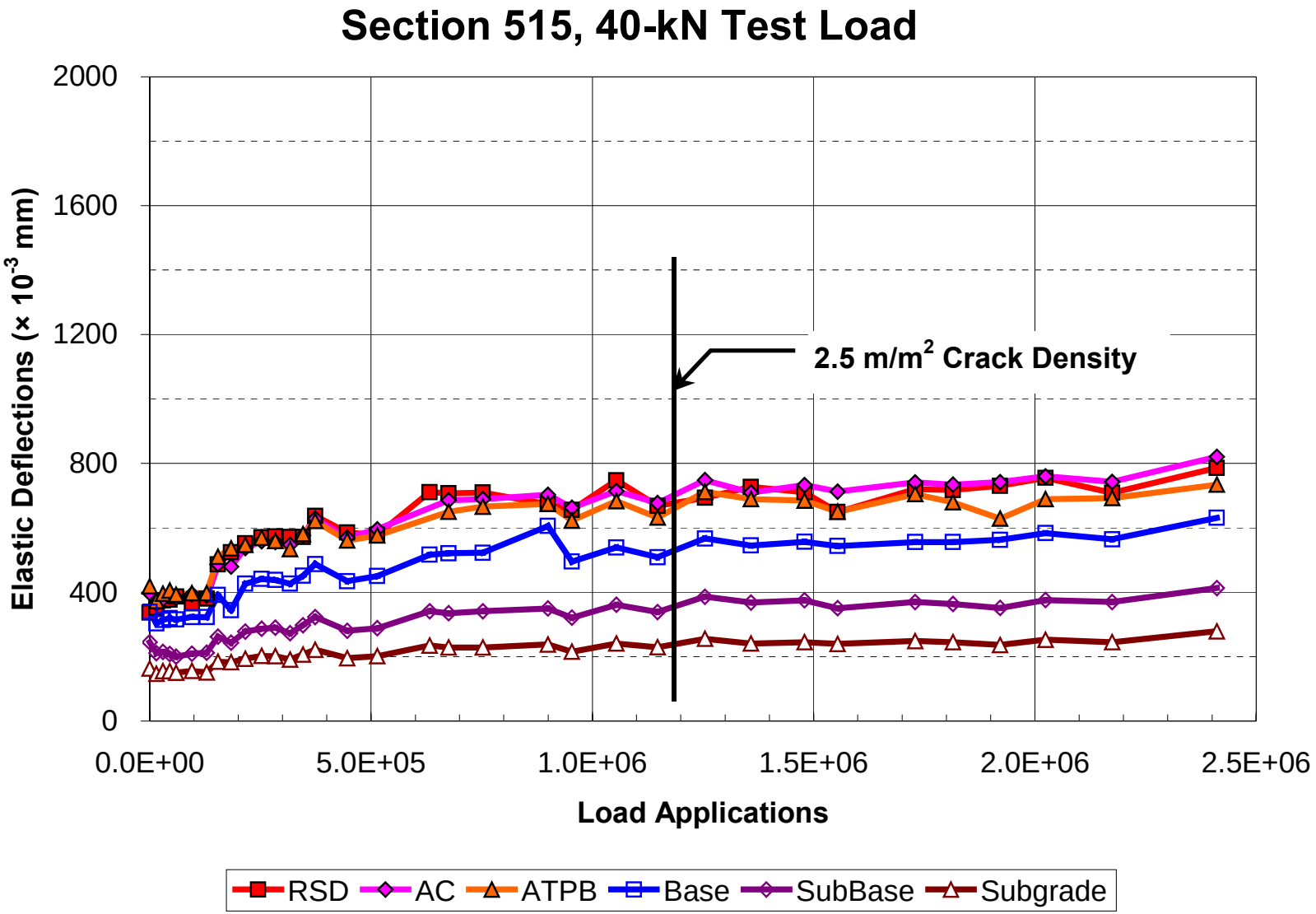

Figure 3.81. Average in-depth deflections for Section 515 (drained, ARHM-GG overlay), 40-kN test load.

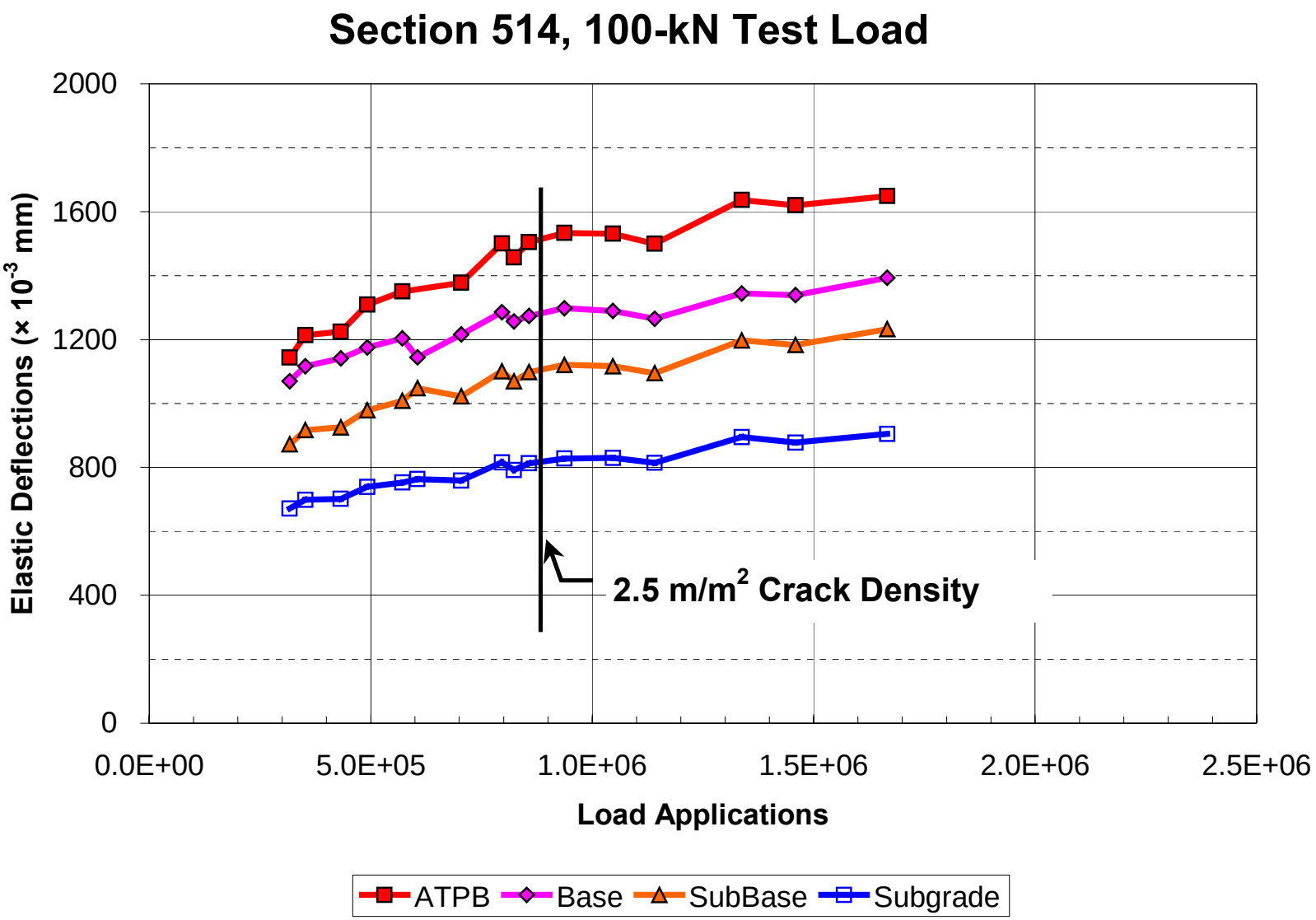

Figure 3.82. Average in-depth deflections for Section 514 (drained, DGAC overlay), 100-kN test load.

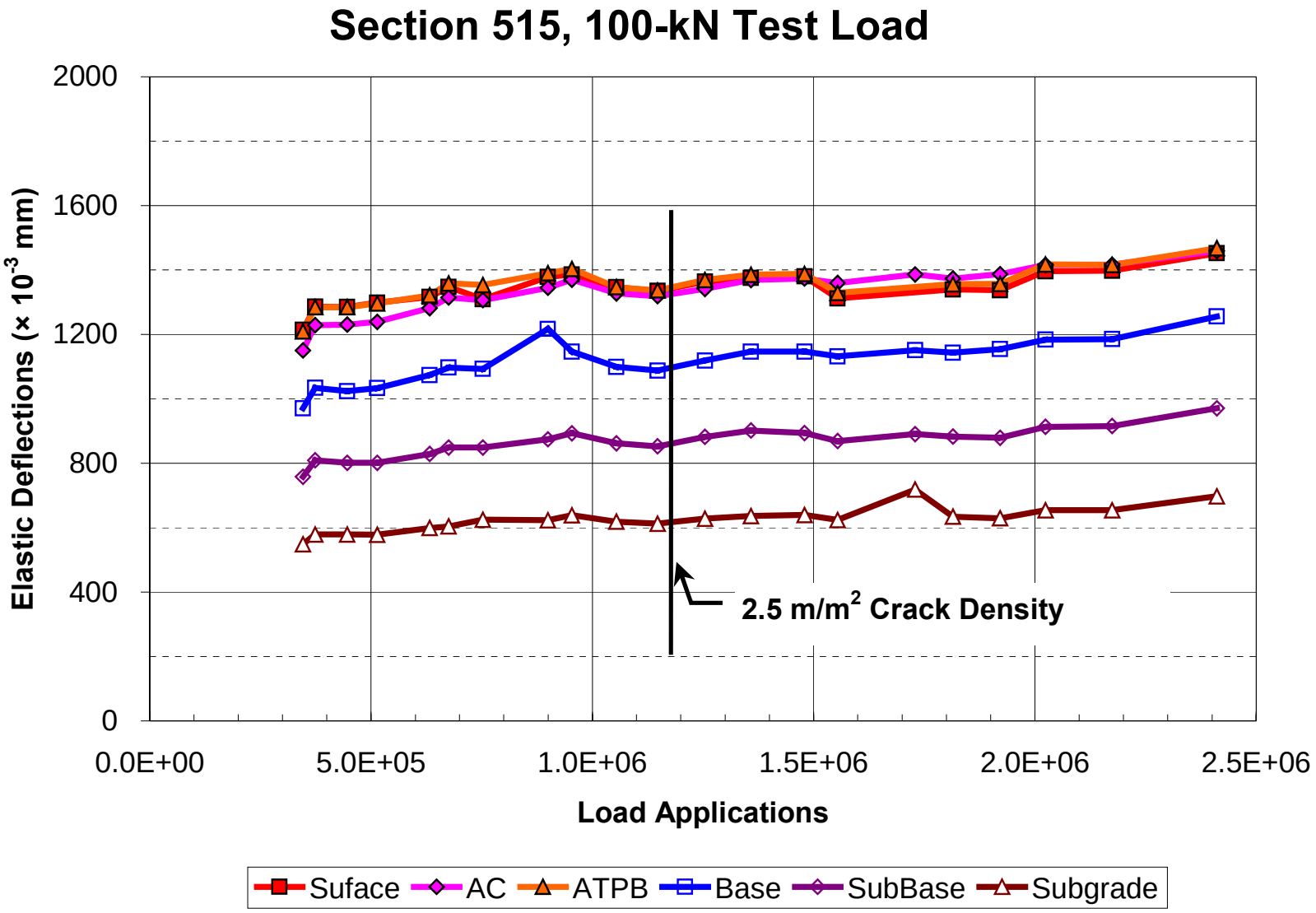

Figure 3.83. Average in-depth deflections for Section 515 (drained, ARHM-GG overlay), 100-kN test load.

The contribution of each pavement layer and the subgrade to the total surface elastic deflection based on the average data is presented in Table 3.17. The elastic contribution of the bound layers varied from 18 to 28 percent in Section 514 and 15 to 22 percent in Section 515 under the 40-kN test load. The elastic contribution of the bound and unbound layers in both sections is similar. The trend of incremental elastic contribution in the bound layers with number of load applications suggests that pavement damage can be attributed to cracking in the overlay and/or by loss of stiffness in the ATPB layer. The approximately constant moisture content in the unbound layers suggests that moisture content has little effect in the increased elastic deflections of these layers. A discussion of elastic deflections and non-linear response is presented in Section 3.5.4.

Table 3.17 Contribution of Pavement Layer Deflection to Surface Deflection in Drained Sections

Pavement Layer	Contribution to Surface Deflections (percent)							
	40-kN Test Load				100-kN Test Load			
	514 DGAC		515 ARHM-GG		514 DGAC		515 ARHM-GG	
	Start	End	Start	End	Start	End	Start	End
Overlay	6*	9*	15*	8*	4*	2*	3	2
AC							16*	14*
ATPB	12	19		14		17		
Aggregate. Base	28	22	29	28	18	10	18	21
Aggreg. Subbase	13	12	17	17	18	18	17	18
Subgrade	40	39	42	34	60	53	45	46

* These values represent the combined contribution of the applicable pavement layers.

3.4.3 In-Depth Pavement Deflections in the Undrained Sections

In-depth elastic deflection data for the 40-kN and 100-kN test loads are presented in Figures 3.84–3.89 for Section 517 and in Figures 3.90–3.93 for Section 518. In-depth elastic deflections for Section 518 are presented for Stations 6 and 10 only.

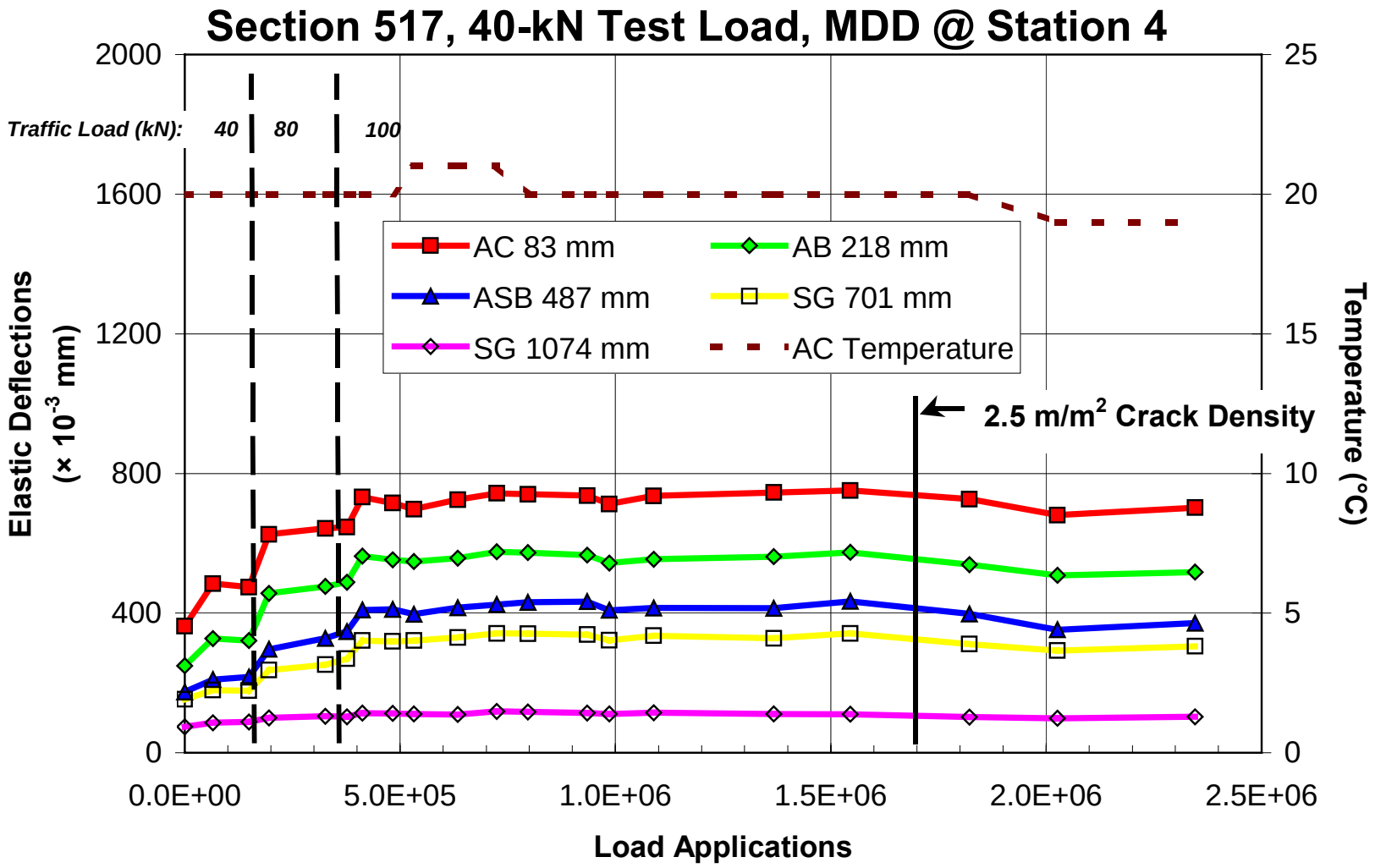

Figure 3.84. In-depth elastic deflections for at Station 4, Section 517 (undrained, DGAC overlay), 40-kN test load.

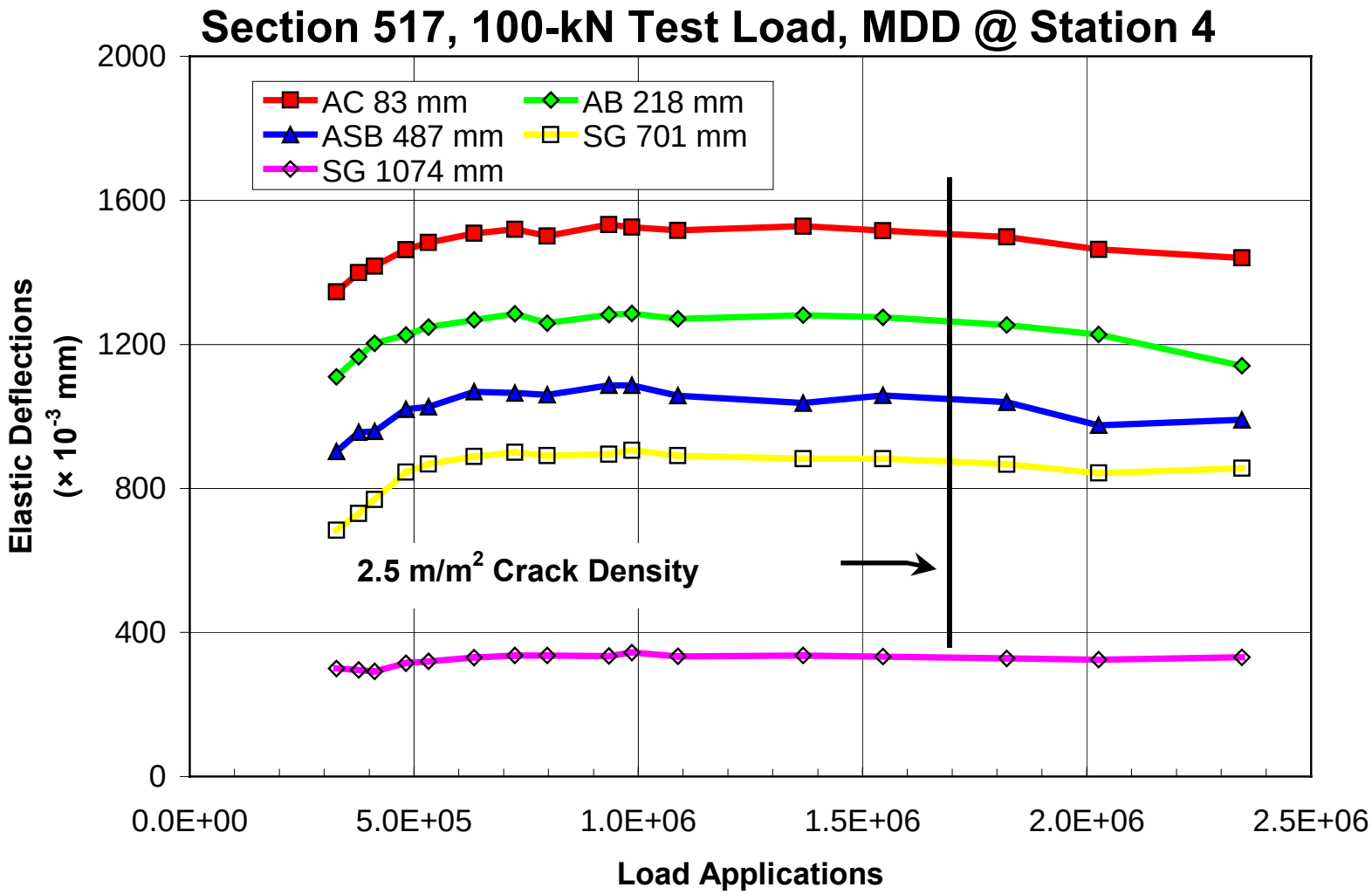

Figure 3.85. In-depth elastic deflections at Station 4, Section 517 (undrained, DGAC overlay), 100-kN test load.

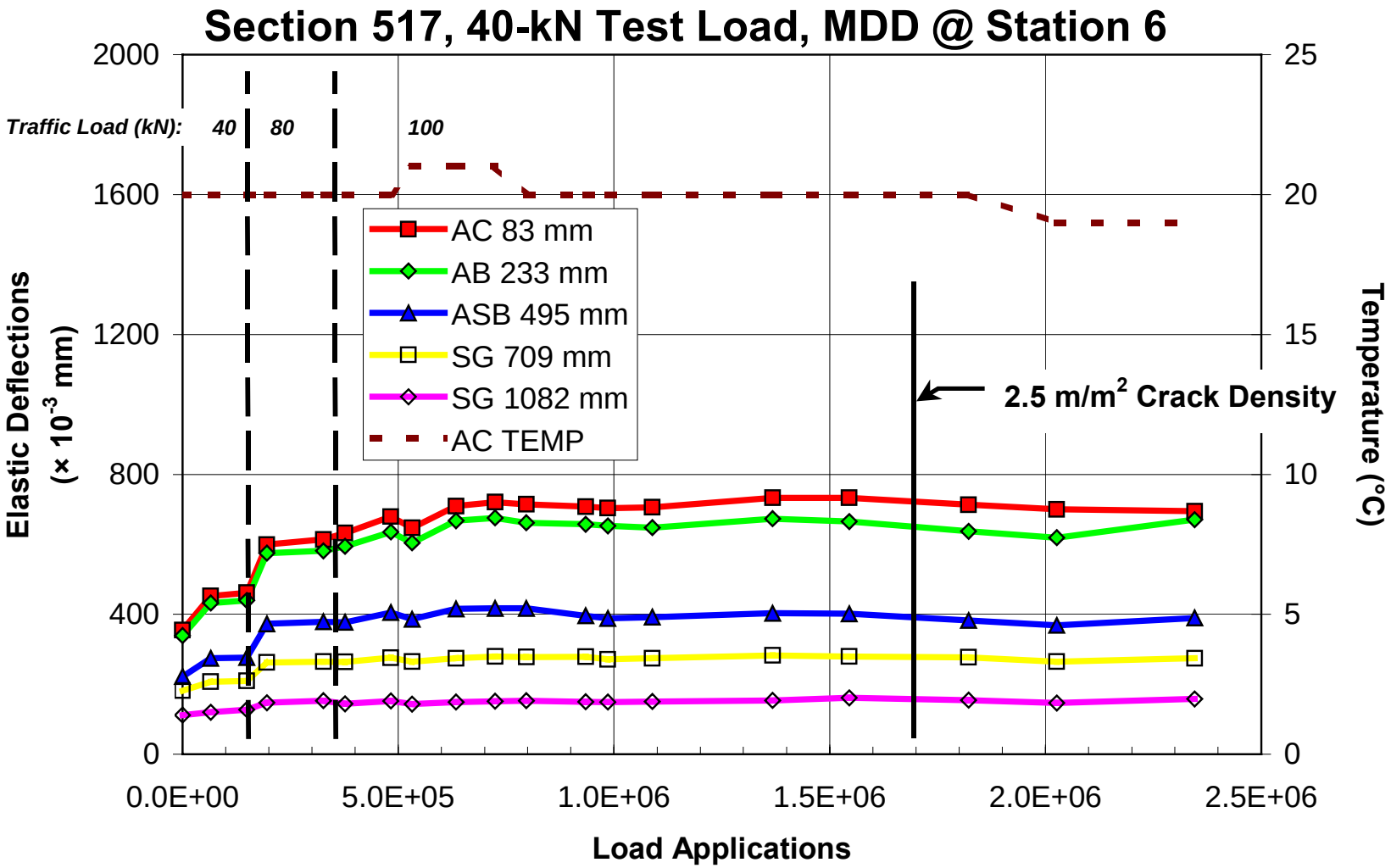

Figure 3.86. In-depth elastic deflections at Station 6, Section 517 (undrained, DGAC overlay), 40-kN test load.

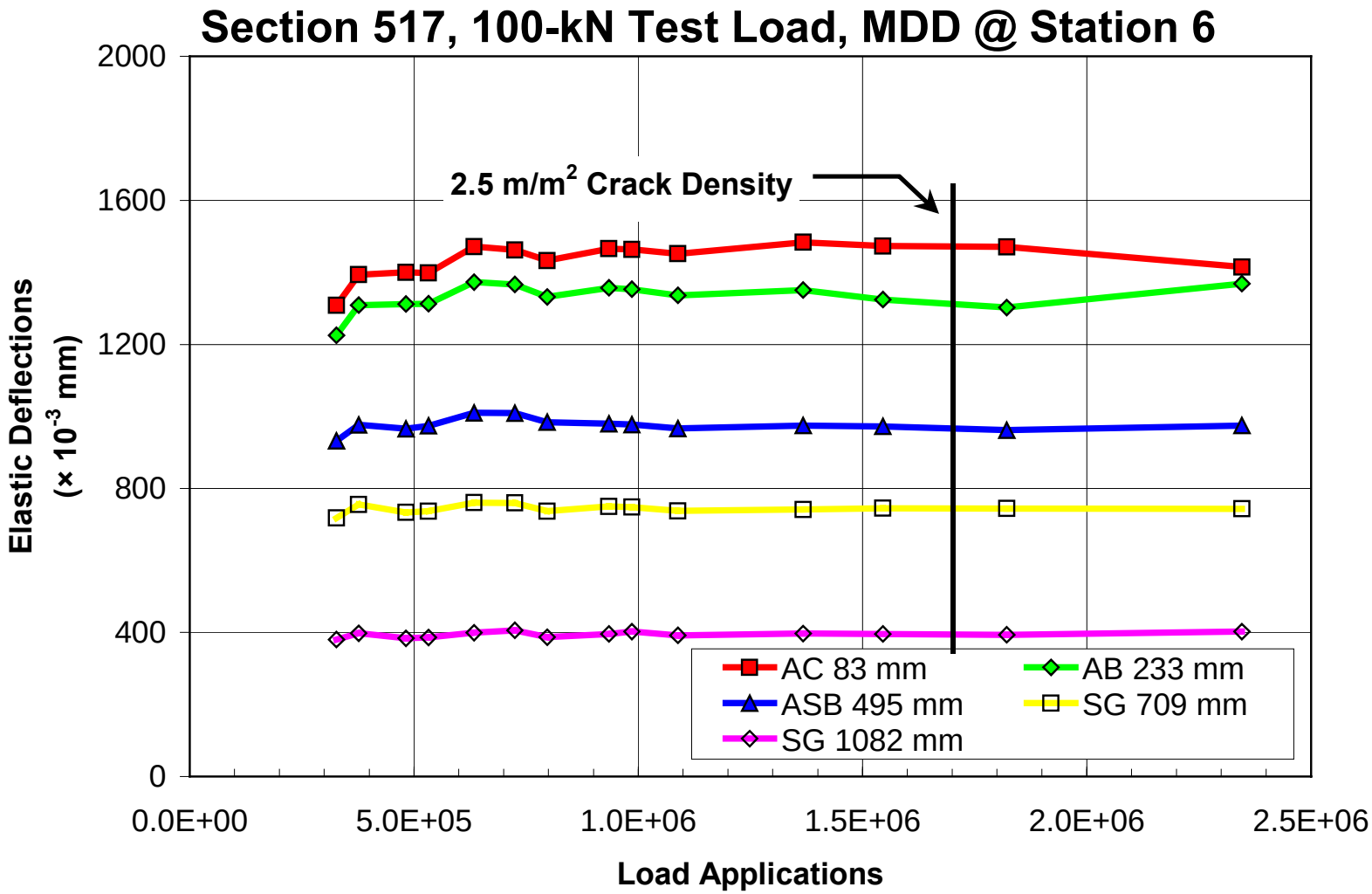

Figure 3.87. In-depth elastic deflections at Station 6, for Section 517 (undrained, DGAC overlay), 100-kN test load.

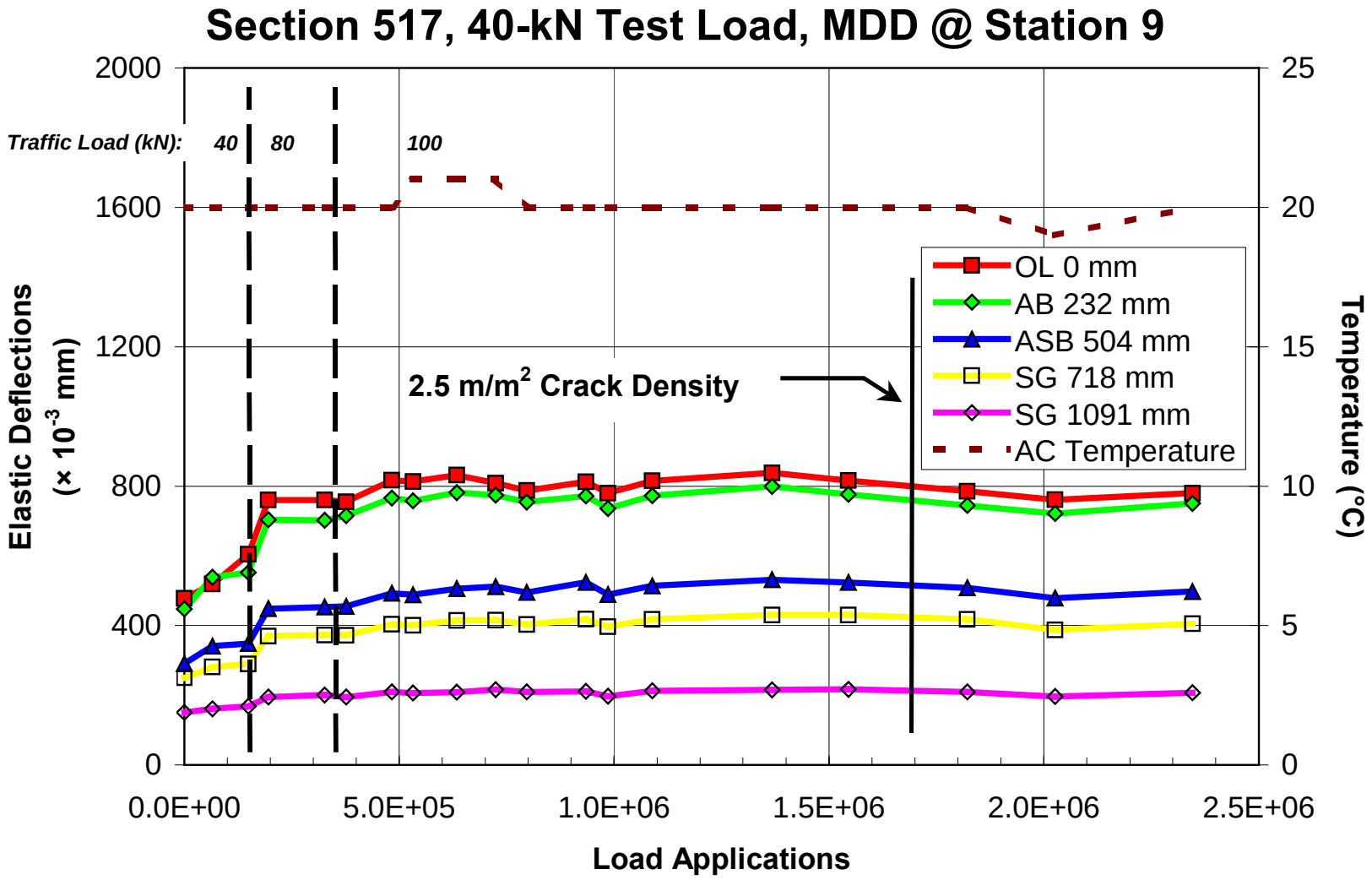

Figure 3.88. In-depth elastic deflections at Station 9, Section 517 (undrained, DGAC overlay), 40-kN test load.

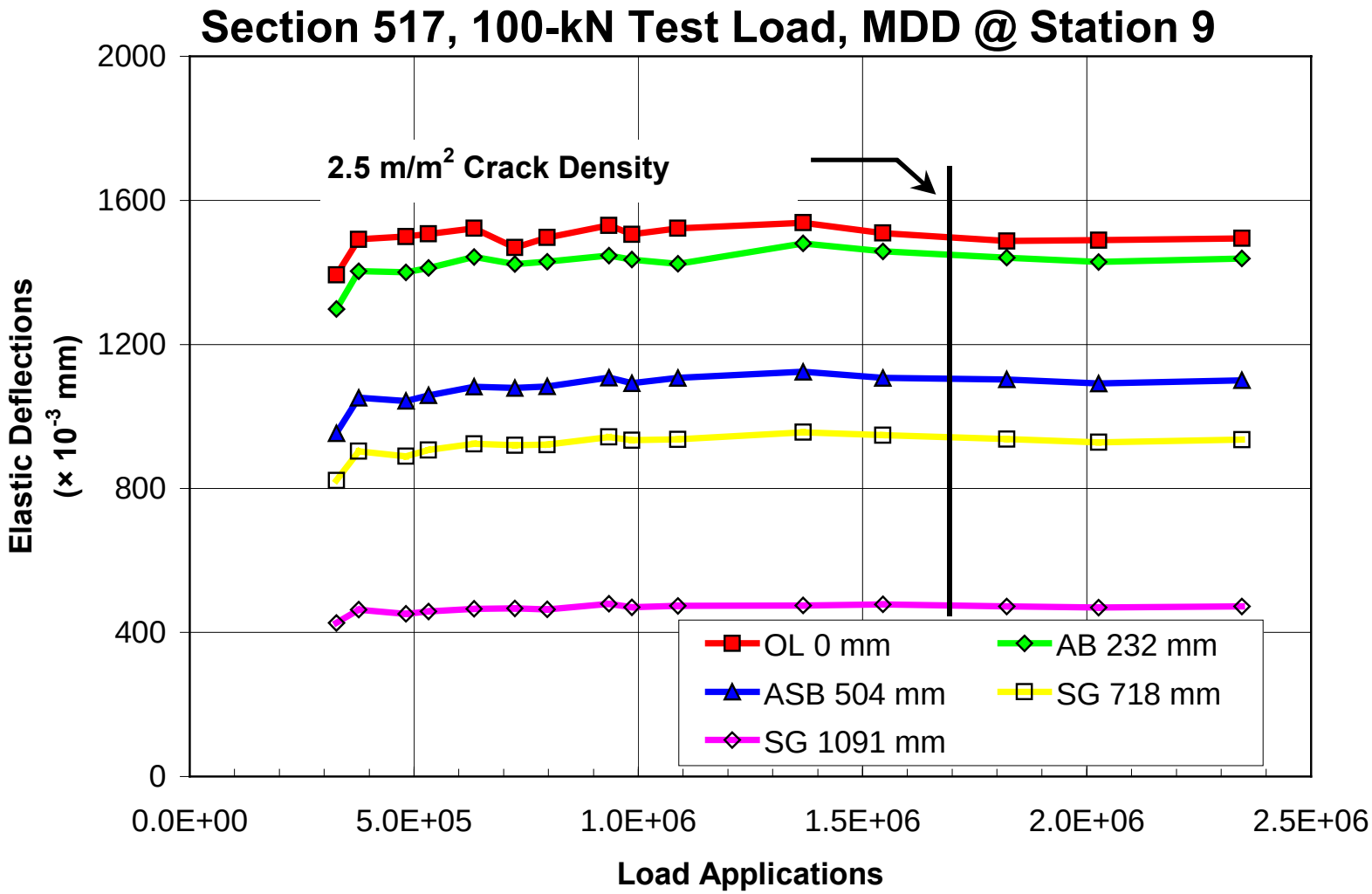

Figure 3.89. In-depth elastic deflections at Station 9, Section 517 (undrained, DGAC overlay), 100-kN test load.

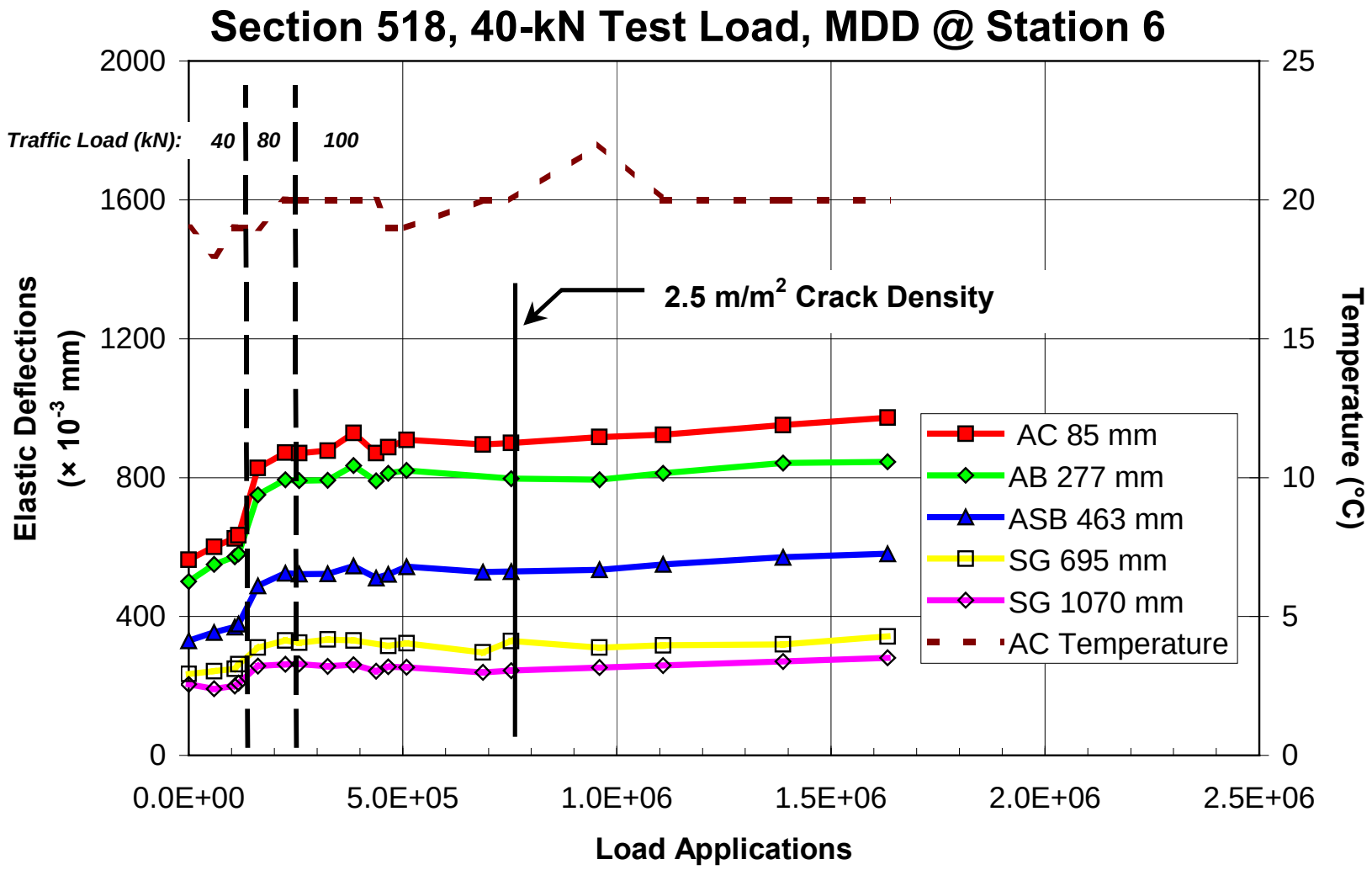

Figure 3.90. In-depth elastic deflections at Station 6, Section 518 (undrained, ARHM-GG overlay), 40-kN test load.

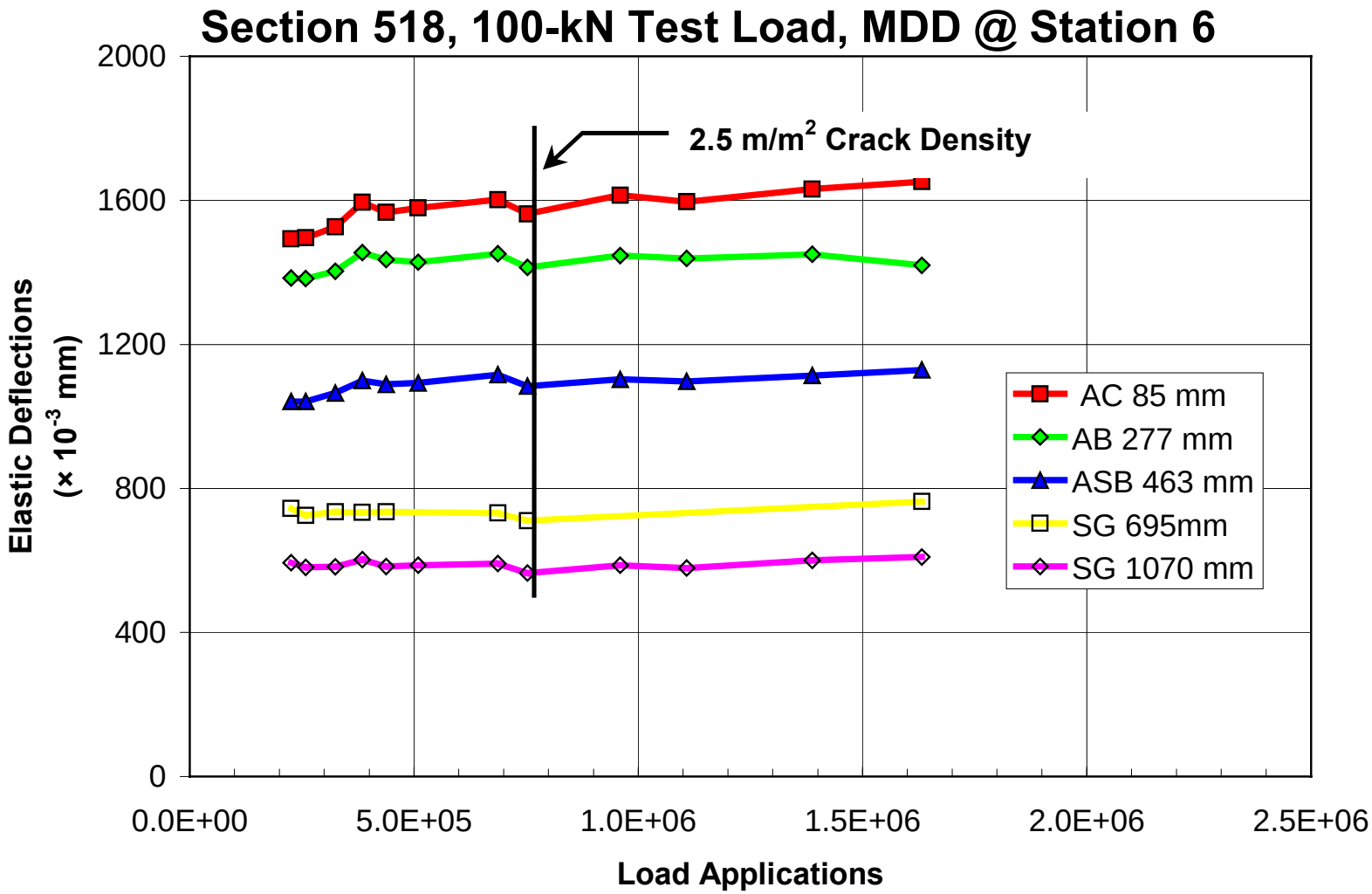

Figure 3.91. In-depth elastic deflections at Station 6, Section 518 (undrained, ARHM-GG overlay), 100-kN test load.

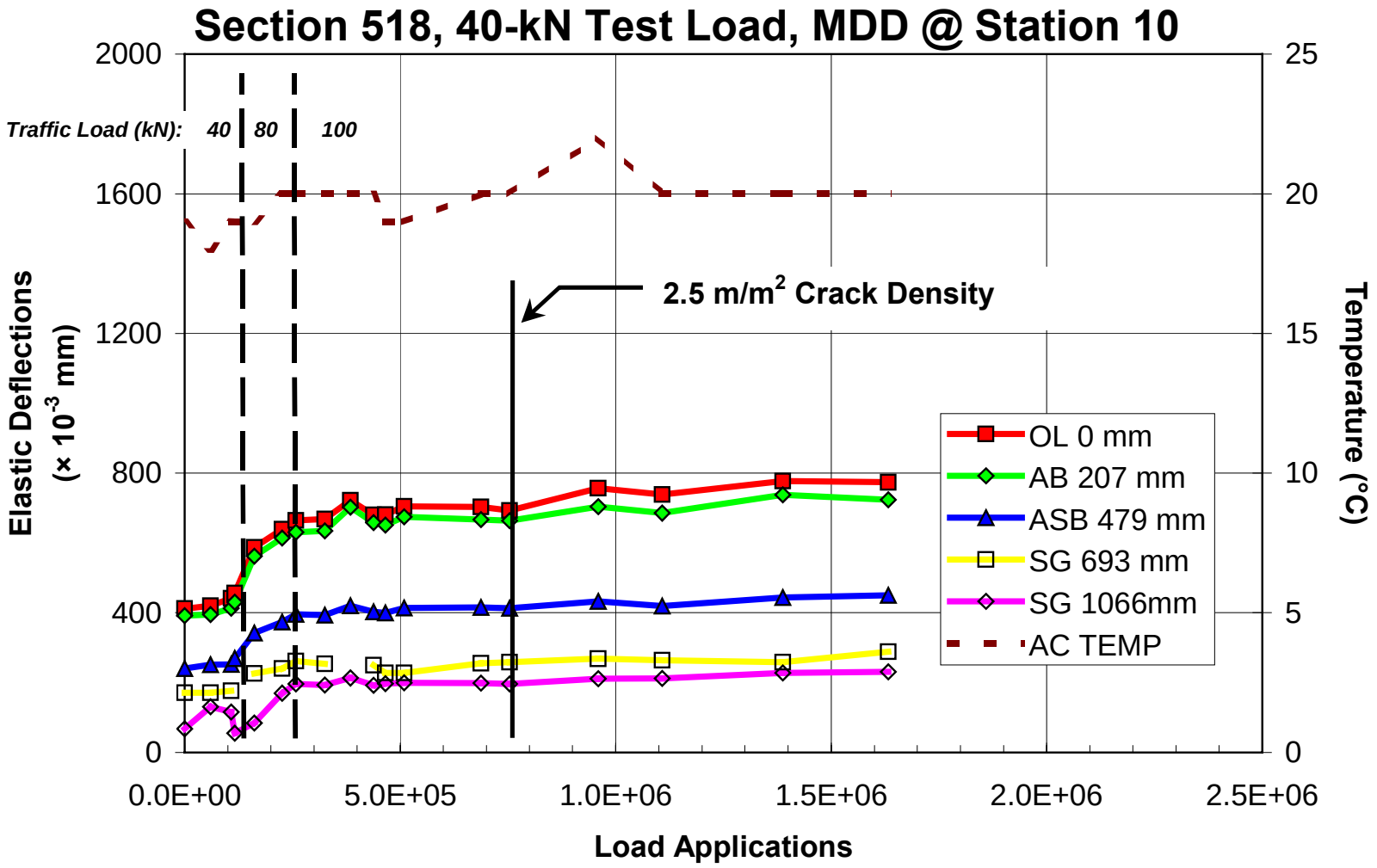

Figure 3.92. In-depth elastic deflections at Station 10, Section 518 (undrained, ARHM-GG overlay), Station 10, 40-kN test load.

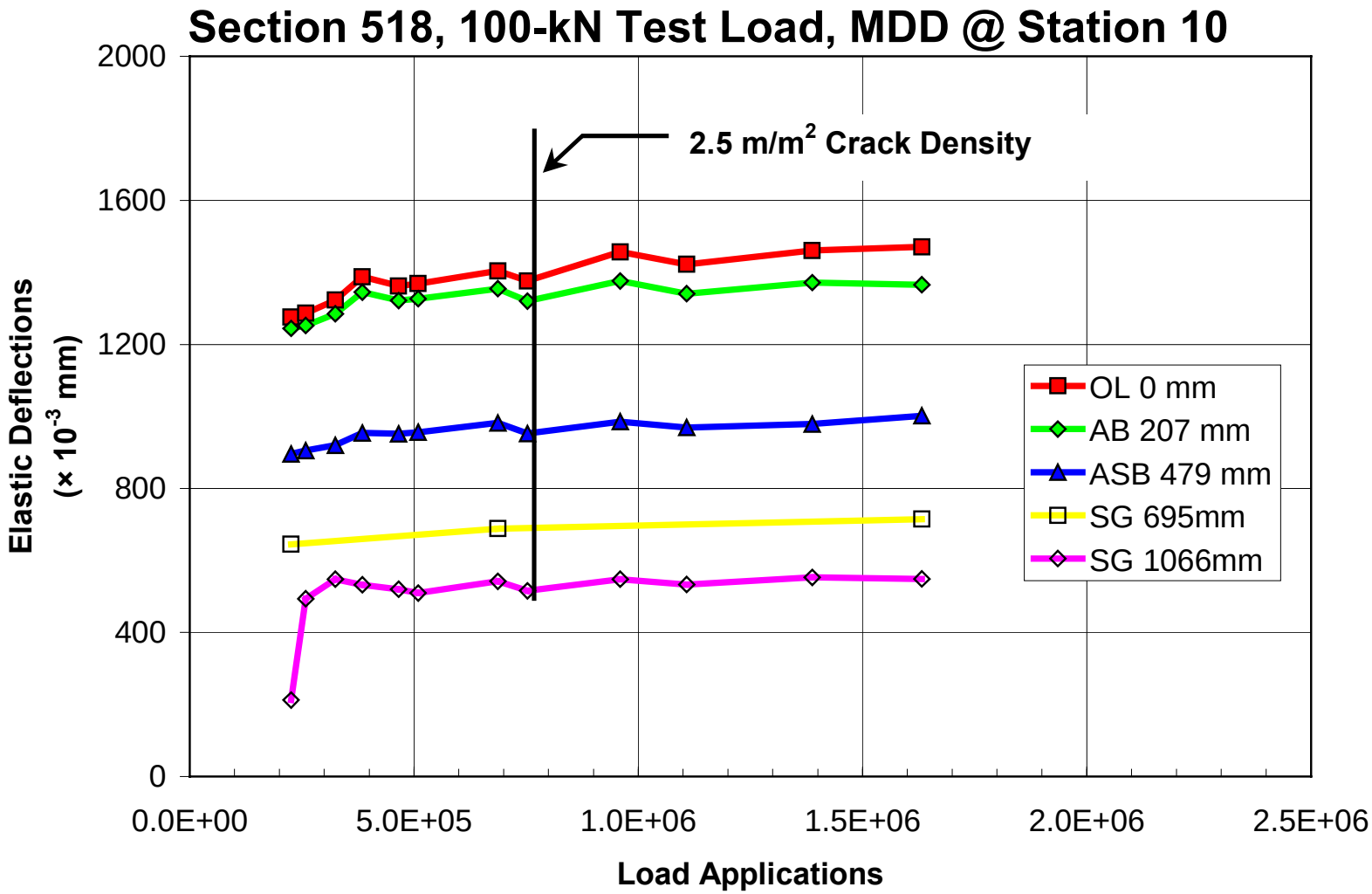

Figure 3.93. In-depth elastic deflections at Station 10, Section 518 (undrained, ARHM-GG overlay), 100-kN test load.

As with the drained sections, the data show the progressive increase in elastic deflection of all pavement layers and the subgrade with traffic loading. Pavement temperature variations were minimal at the time of data collection.

Average in-depth elastic deflections in Sections 517 and 518 under the 40-kN and 100-kN test loads are presented in Figures 3.94–3.97. Overall, in-depth elastic deflections are higher in Section 518 than in Section 517. In-depth elastic deflections at the beginning and end of testing are presented in Table 3.18 for the 40-kN test load. Deflection data for Section 518 was not averaged in Table 3.18.

Table 3.18 In-Depth Elastic Deflection under 40-kN Test Load in Undrained Sections

Pavement Layer	Elastic Deflections in Section (microns)					
	517 (DGAC)		518 (ARHM-GG)			
	Start	End	Start		End	
			MDD Station		MDD Station	
			6	10	6	10
Overlay	499	771	n/a	411	n/a	774
AC	413	695	563	n/a	972	n/a
Aggregate Base	389	631	500	392	845	723
Aggregate Subbase	271	428	330	240	580	450
Subbase	213	339	235	171	342	288

Coefficients of variations for these sections are presented in Table 3.19. These coefficients of variation are more meaningful for the deflections measured in the unbound layers given that multiple MDD instruments were installed at these layers. In-depth elastic deflections recorded in Section 518 at Station 6 were somewhat different from those recorded at Station 10. Variability in in-depth elastic deflection can be attributed to variations in layer thickness, material density, and level of bonding between the asphalt-bound layers.

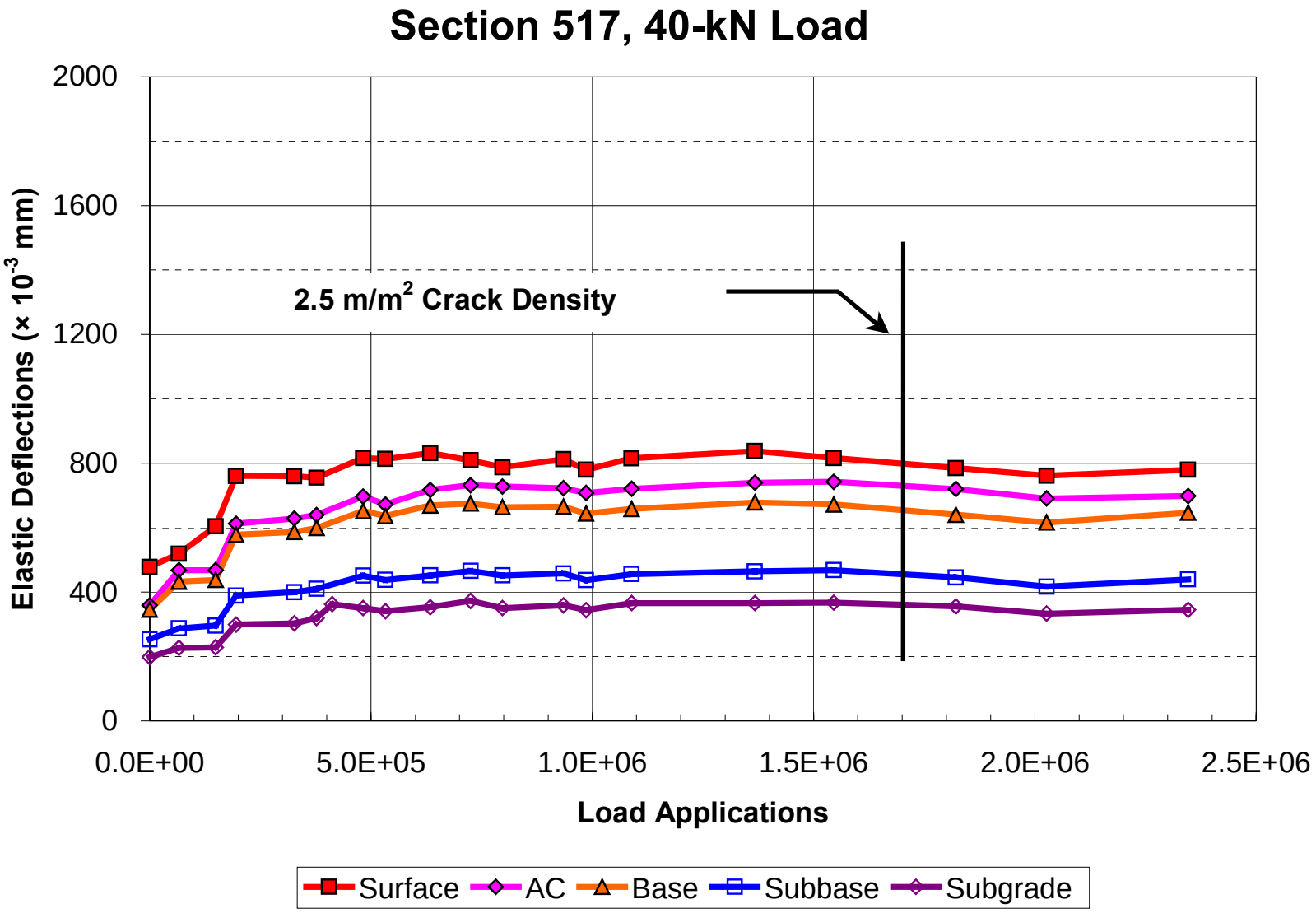

Figure 3.94. Average in-depth defelctions in Section 517 (undrained, DGAC overlay), 40-kN test load.

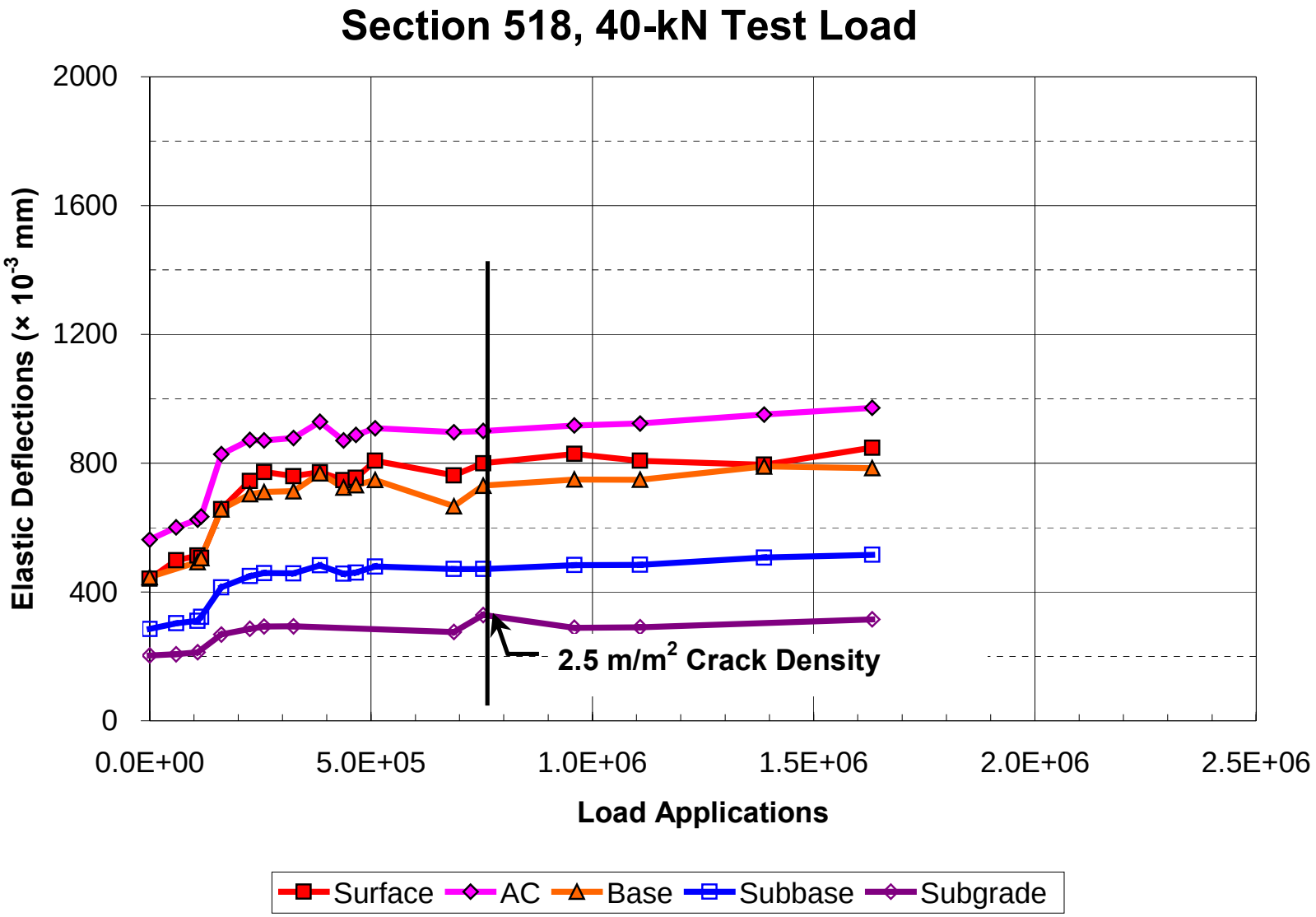

Figure 3.95. Average in-depth deflections in Section 518 (undrained, ARHM-GG overlay), 40-kN test load.

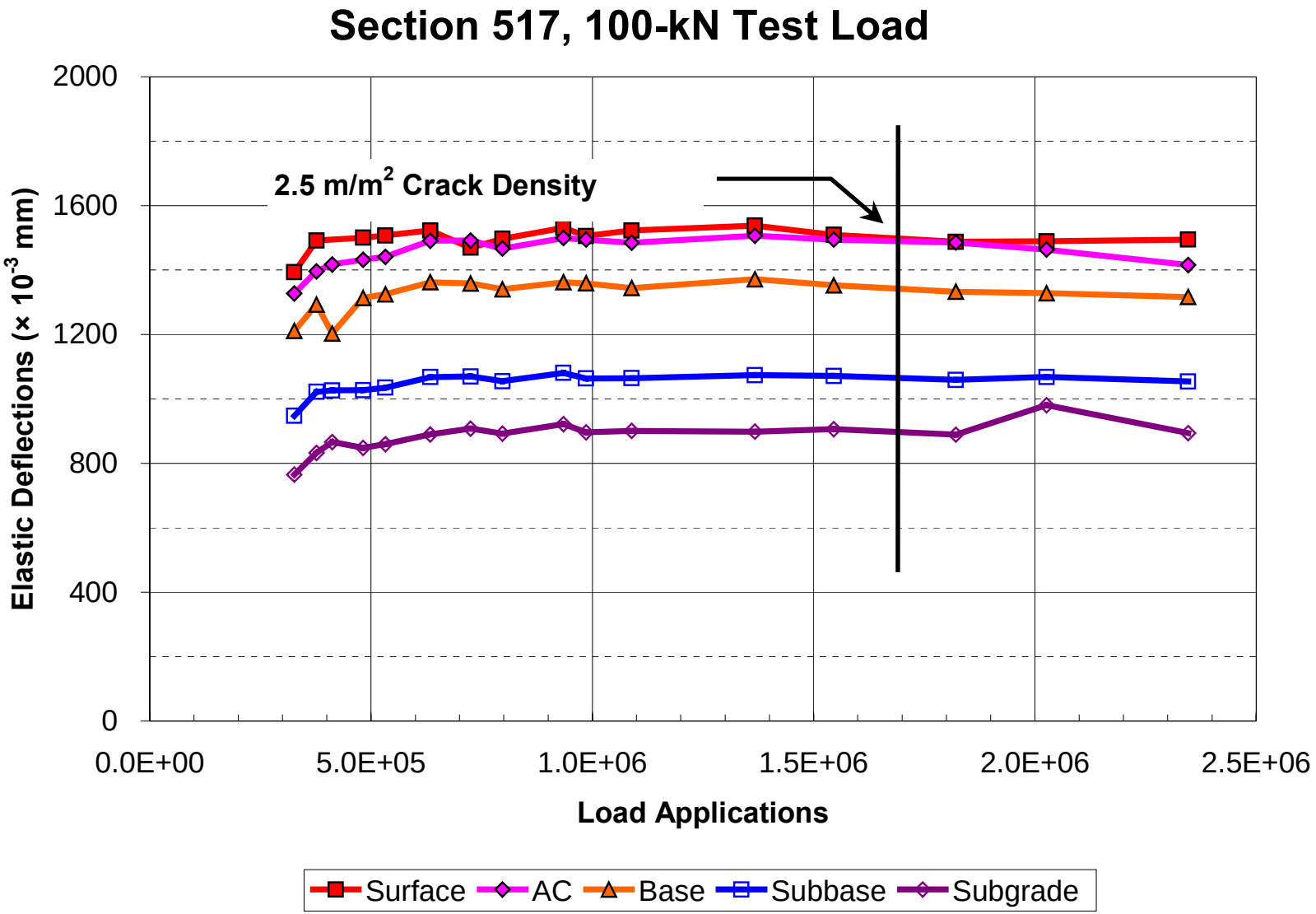

Figure 3.96. Average in-depth defelctions in Section 517 (undrained, DGAC overlay), 100-kN test load.

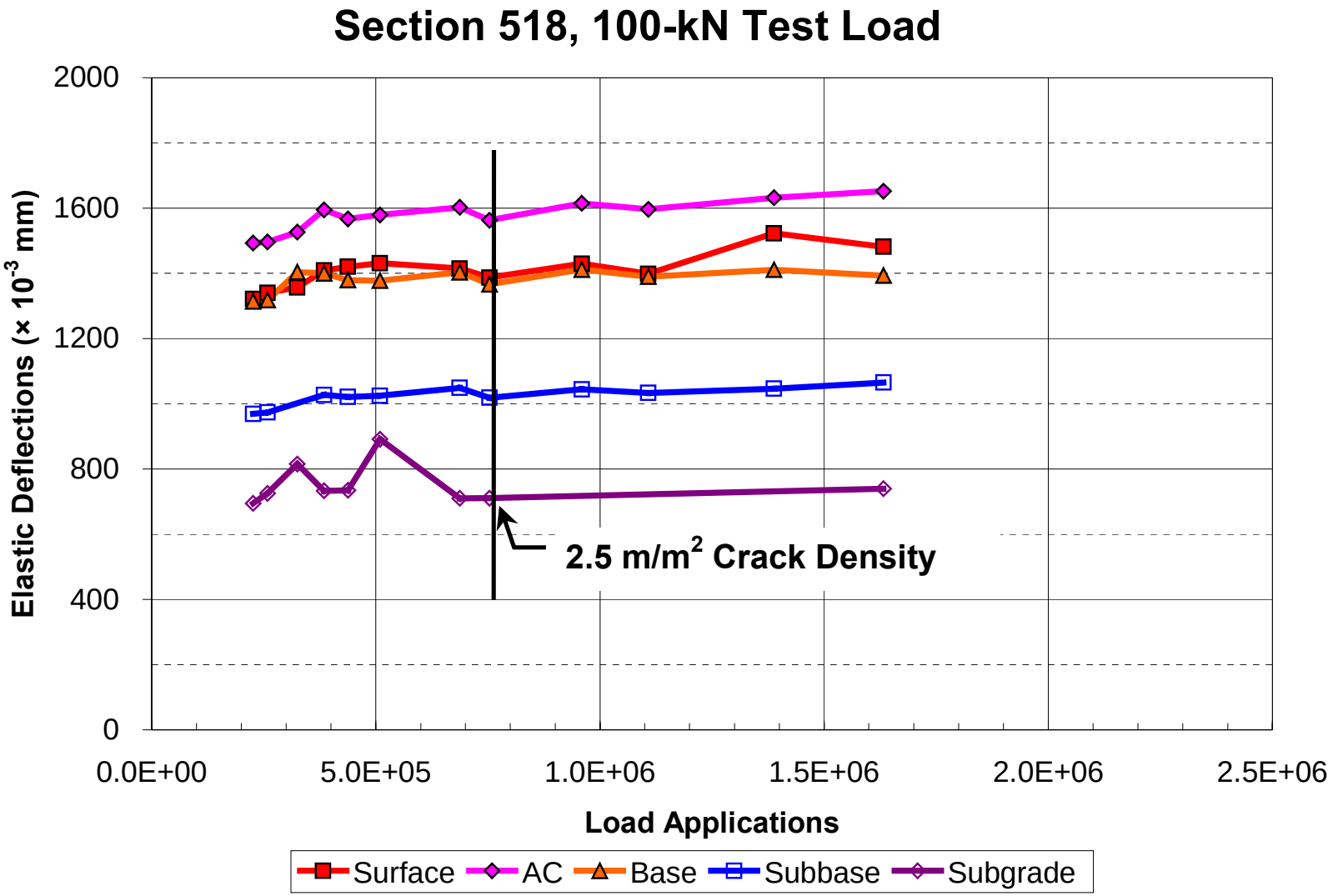

Figure 3.97. Average in-depth deflections in Section 518 (undrained, ARHM-GG overlay), 100-kN test load.

Table 3.19 Coefficients of Variation for In-Depth Deflections in Undrained Sections

Pavement Layer	Test Section			
	517 (DGAC)		518 (ARHM-GG)	
	40-kN Test Load	100-kN Test Load	40-kN Test Load	100-kN Test Load
Aggregate Base	18	7	15	5
Aggregate Subbase	15	6	20	9
Subgrade	19	13	18	8

The contribution of each pavement layer and the subgrade to the total surface elastic deflection based on the average data is presented in Table 3.20. The elastic contribution of the asphalt-bound layers varied from 18 to 24 percent in Section 517 and 7 to 9 percent in Section 518 under the 40-kN test load.

Table 3.20 Contribution of Pavement Layer Deflection to Surface Deflection in Undrained Sections

Pavement Layer	Contribution to Surface Deflection (percent)							
	40-kN Test Load				100-kN Test Load			
	517 DGAC		518 ARHM-GG		517 DGAC		518 ARHM-GG	
	Start	End	Start	End	Start	End	Start	End
Overlay AC	24	18	7	9	14	11	3	8
Aggregate Base	24	26	34	32	19	18	25	23
Aggregate Subbase	11	12	18	23	13	9	20	21
Subgrade	41	44	41	36	55	62	50	48

The percent contribution to elastic deflection of the bound layers in the undrained sections was lower than that of the bound layers in the drained sections. This is due to the total thickness of the bound layers in the undrained sections being thinner than that of the drained sections. A brief discussion regarding the elastic deflections and non-linear response of these sections continues in Section 3.4.4.

3.4.4 Discussion of Elastic Deflections and Non-Linear Response of Goal 3 Sections

Figure 3.98 presents in-depth elastic deflections as a function of pavement depth at various stages of load application under the 40-kN test load for all test sections. The progressive decrease in the slope of the line connecting the deflection measured between two adjacent MDDs indicates a reduction in stiffness of the layer between the two MDDs.

The reduction in stiffness of the AC layer is mainly due to fatigue cracking of this layer. Because the temperature control box maintained a uniform temperature in the sections, temperature variation caused little effect in the stiffness reduction.

The AB and ASB layers also showed a reduction in stiffness. Given that water content was constant throughout testing, moisture did not have a significant role in reducing the stiffness of these layers. Figure 3.98 shows that as the AC layer lost stiffness, so did the AB and ASB layers. The stiffness of the AB and ASB depends significantly on the confinement provided by the AC layer. Therefore, as the AC cracks, the confinement around the granular layer is reduced, thus reducing its stiffness.

Figure 3.99 shows elastic deflections as a function of the test load at the end of HVS testing. The results demonstrate the non-linear response of the paving materials. The dashed lines in Figure 3.99 indicate a linear response. The elastic deflections on top of the subgrade show a linear response. The AB and ASB are non-linear, especially at high load levels.

3.4.5 Falling Weight Deflectometer (FWD) Maximum Deflections

A series of Falling Weight Deflectometer (FWD) measurements were periodically obtained on the Goal 3 sections. The FWD measurements taken on April 27, 1997 covered all the sections prior to HVS trafficking (Figure 3.100). The FWD measurement taken on January

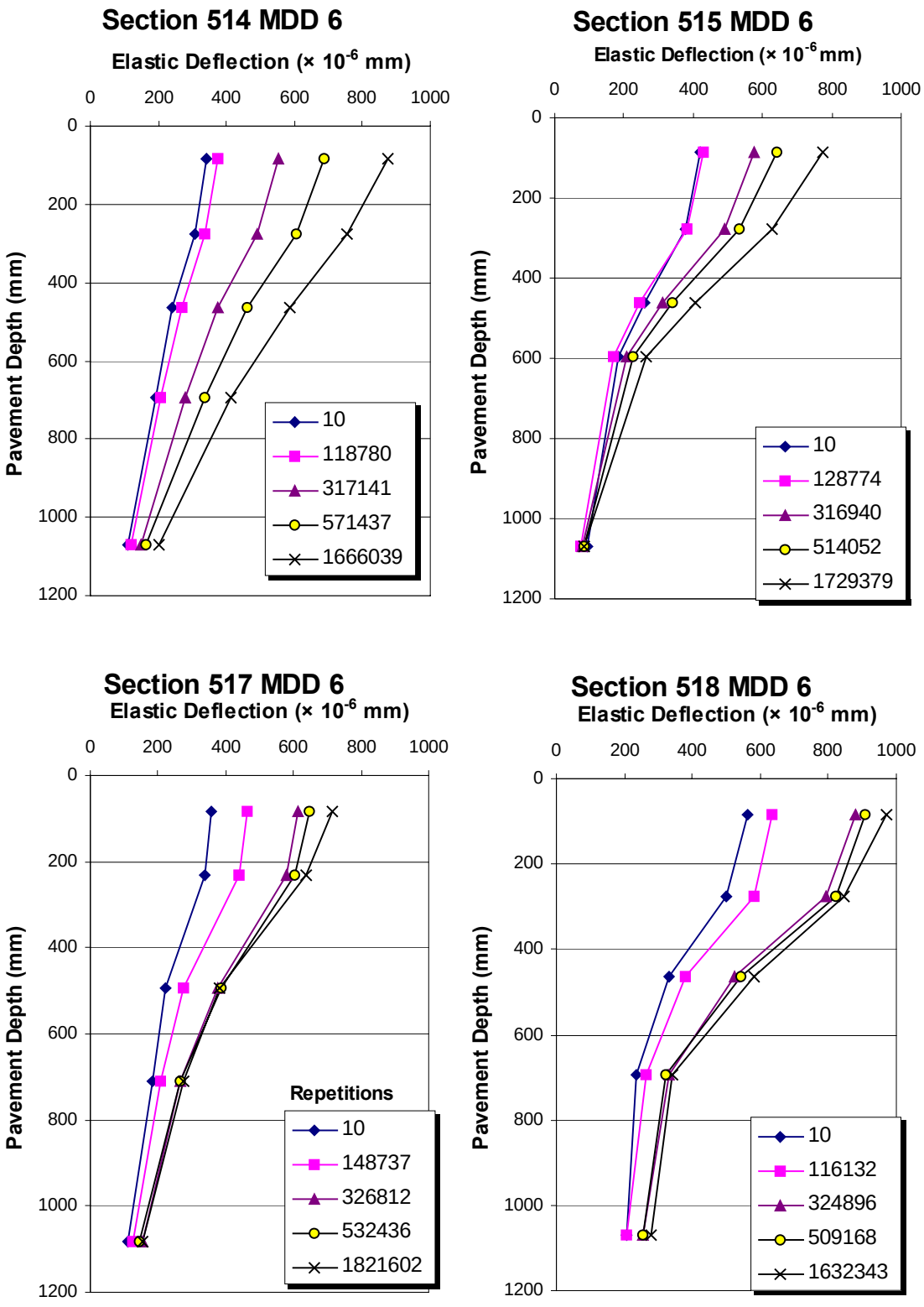

Figure 3.98. Elastic deflections with depth for all four overlay sections.

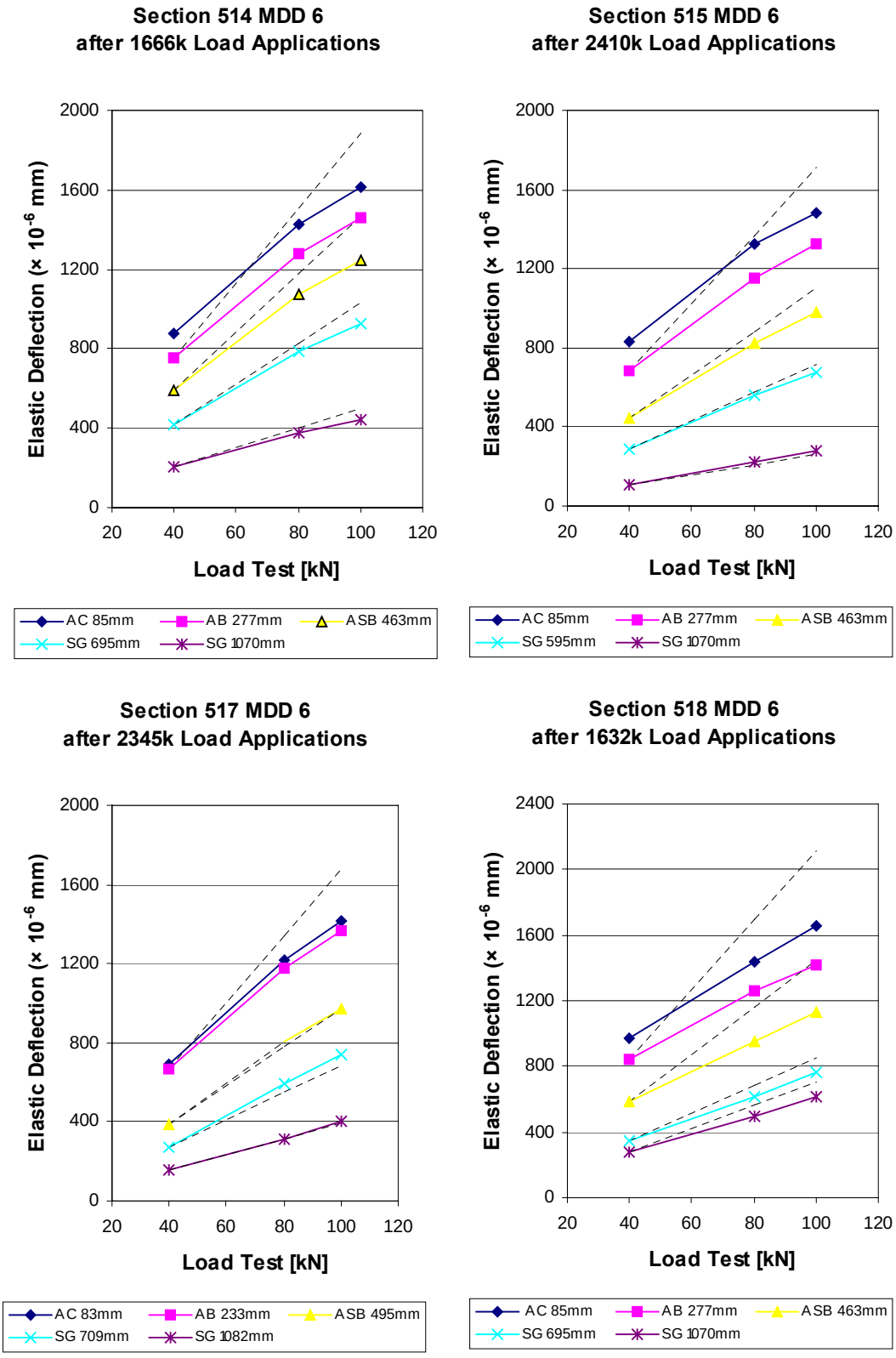

Figure 3.99. Non-linear response of pavement layers for all four overlay sections.

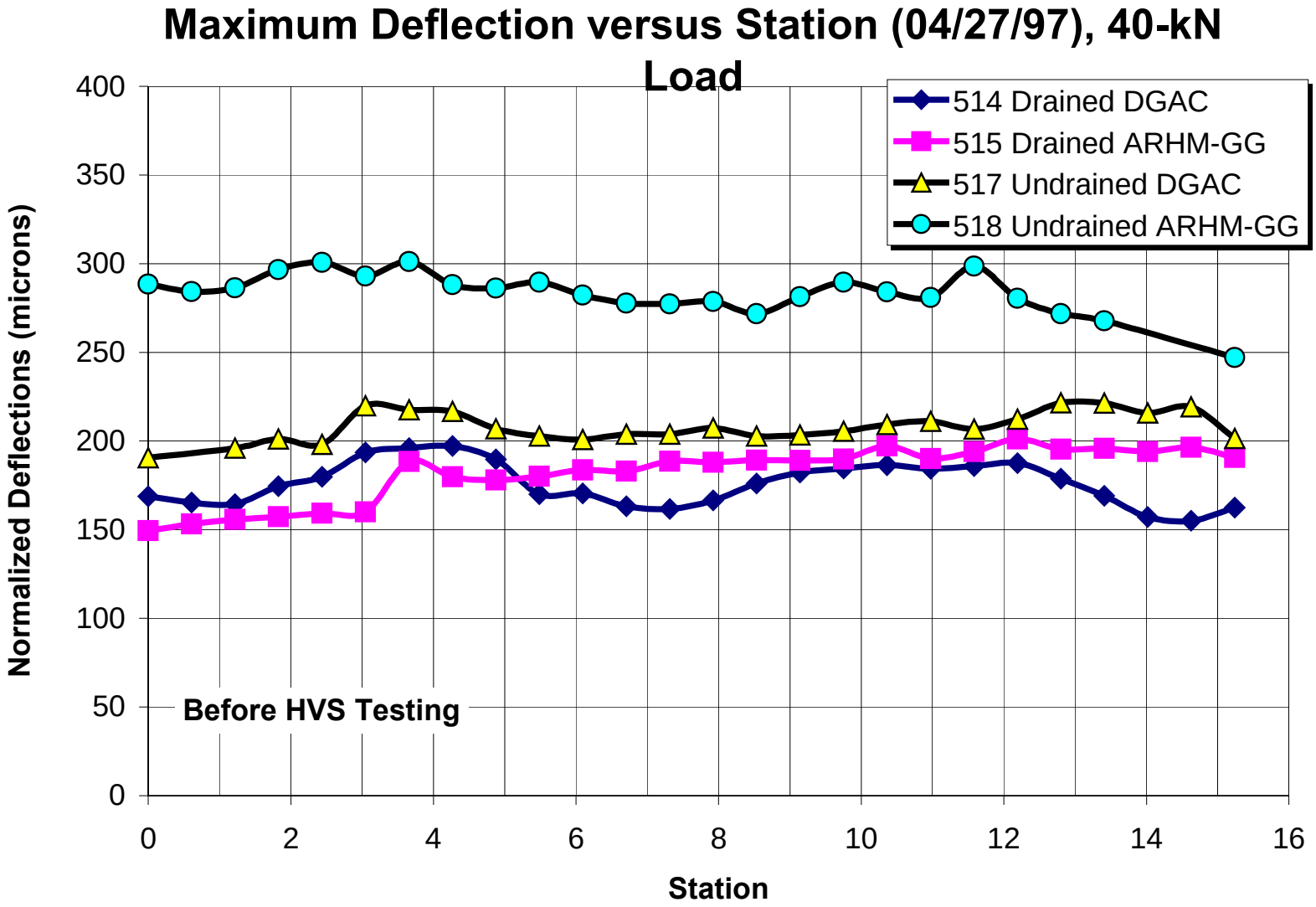

Figure 3.100. FWD maximum deflections before HVS testing, March 1997.

6, 1998 covered Section 514 after HVS trafficking and prior to HVS trafficking for the remaining sections. The FWD measurements taken on May 11, 1999 covered Sections 517 and 518 after HVS testing. Table 3.21 summarizes maximum FWD deflections obtained on the Goal 3 sections.

Table 3.21 Normalized 40-kN Maximum FWD Deflections

Section	Date	Deflections (microns)		
		Average	Standard Deviation	80th Percentile
514 Drained DGAC	4/27/97	179	12	188
	1/6/98	275	43	304
	5/11/99			
515 Drained ARHM-GG	4/27/97	185	12	294
	1/6/98	129	11	136
	5/11/99			
517 Undrained DGAC	4/27/97	209	7	217
	1/6/98	145	5	150
	5/11/99	208	13	221
518 Undrained ARHM-GG	4/27/97	285	10	294
	1/6/98	190	6	195
	5/11/99	317	19	331

FWD measurements made after HVS testing.

Table 3.21 shows that prior to HVS testing, FWD deflections decreased from April 1997 to January 1998. The reduction in elastic deflections is due to temperature changes. Pavement temperatures averaged 18ºC on January 6, 1998 and 26ºC on April 27, 1997.

Using the April 1997 data, Table 3.21 shows that before HVS testing, Section 514 had the lowest deflections followed by Sections 515, 517, and 518, respectively. Sections 514, 515, and 517 had similar deflections, averaging 174 microns with a standard deviation of 15. Elastic deflections in Section 518 were 62 percent larger than those of the other sections.

FWD deflections at the end of HVS testing increased 91, 12, and 26 percent from the April 1997 deflections for Sections 514, 517, and 518, respectively. Figure 3.101 shows that FWD deflections were more variable for Section 514 than for the other sections.

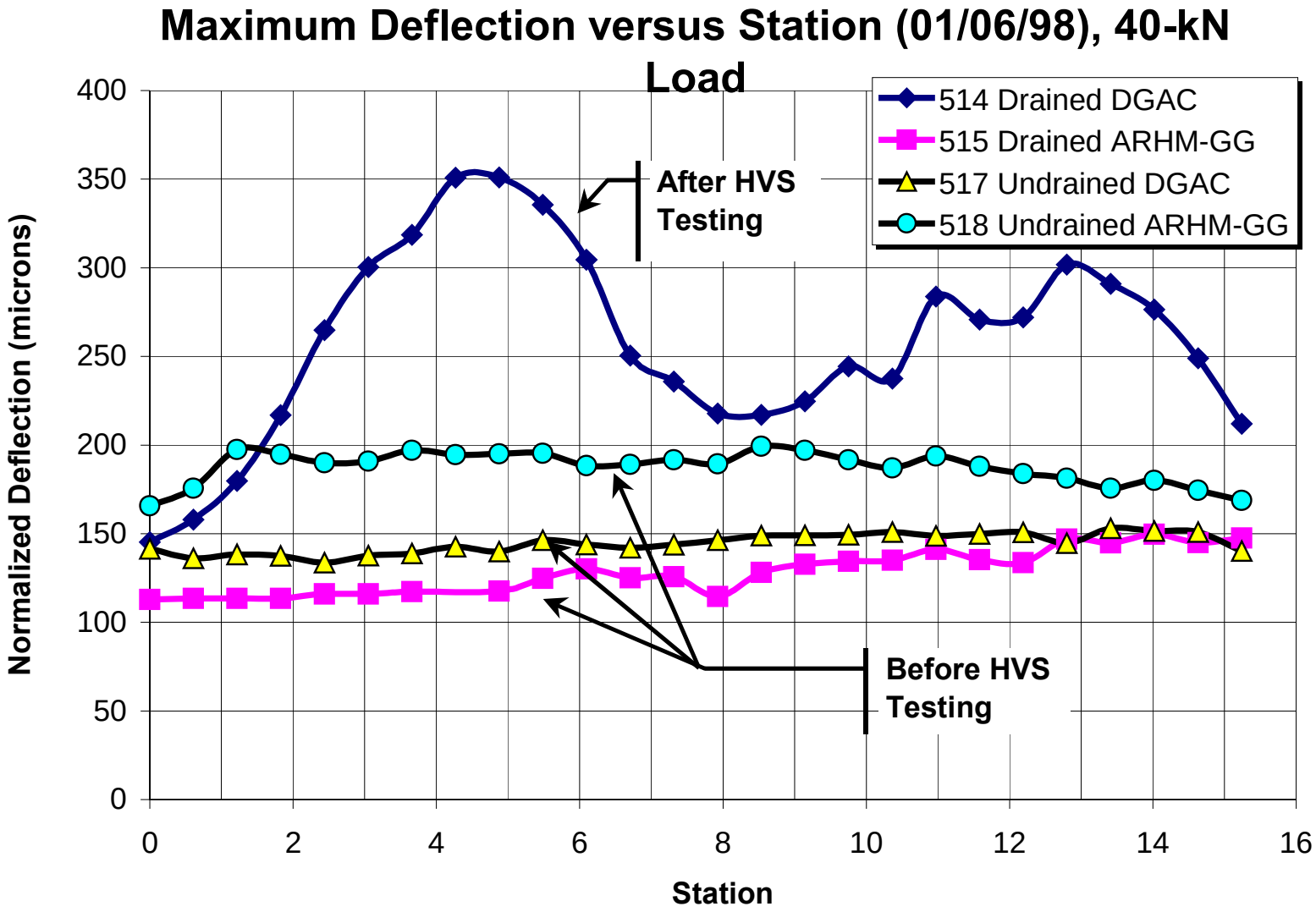

Figure 3.101. FWD maximum deflections, January 1998 (Section 514 tested, Sections 515–518 not yet tested).

On Section 514, the peak deflections were obtained between Stations 4 and 6 and between Stations 12 and 14. The peak deflection measured at Stations 4 and 6 was 46 percent larger than that measured at Stations 12 and 14. The lowest elastic deflection was obtained between Stations 7 and 10. The variation in elastic deflection along the section was influenced by the level of bonding between the two AC lifts.

FWD deflections on Sections 517 and 518 are presented in Figure 3.102. Deflections on Section 518 are about 67 percent greater than those measured on Section 517. It is important to note that FWD deflections on Section 517 were obtained approximately 5 months after HVS testing was completed. This rest period may have had an influence on the FWD deflections measured on this section.

3.4.5.1 RSD versus FWD

Table 3.22 compares the surface deflections obtained with the Road Surface Deflectometer and the Falling Weight Deflectometer. The difference in surface deflections measured by these two devices is evident: RSD deflections are 2.4 to 3.5 times greater than FWD deflections. RSD deflections reflect a slow moving load with the load moving towards the measuring point while the FWD applies a transient dynamic load pulse of 25 to 35 milliseconds duration simulating a fast-moving wheel load.

Table 3.22 Comparison of RSD and FWD Deflections at the Completion of Trafficking

Test Section	**Surface Deflections (microns) under 40-kN Test Load**	
	RSD	**FWD**
514 Drained DGAC	900	275
515 Drained ARHM-GG	747	
517 Undrained DGAC	708	208
518 Undrained ARHM-GG	821	317

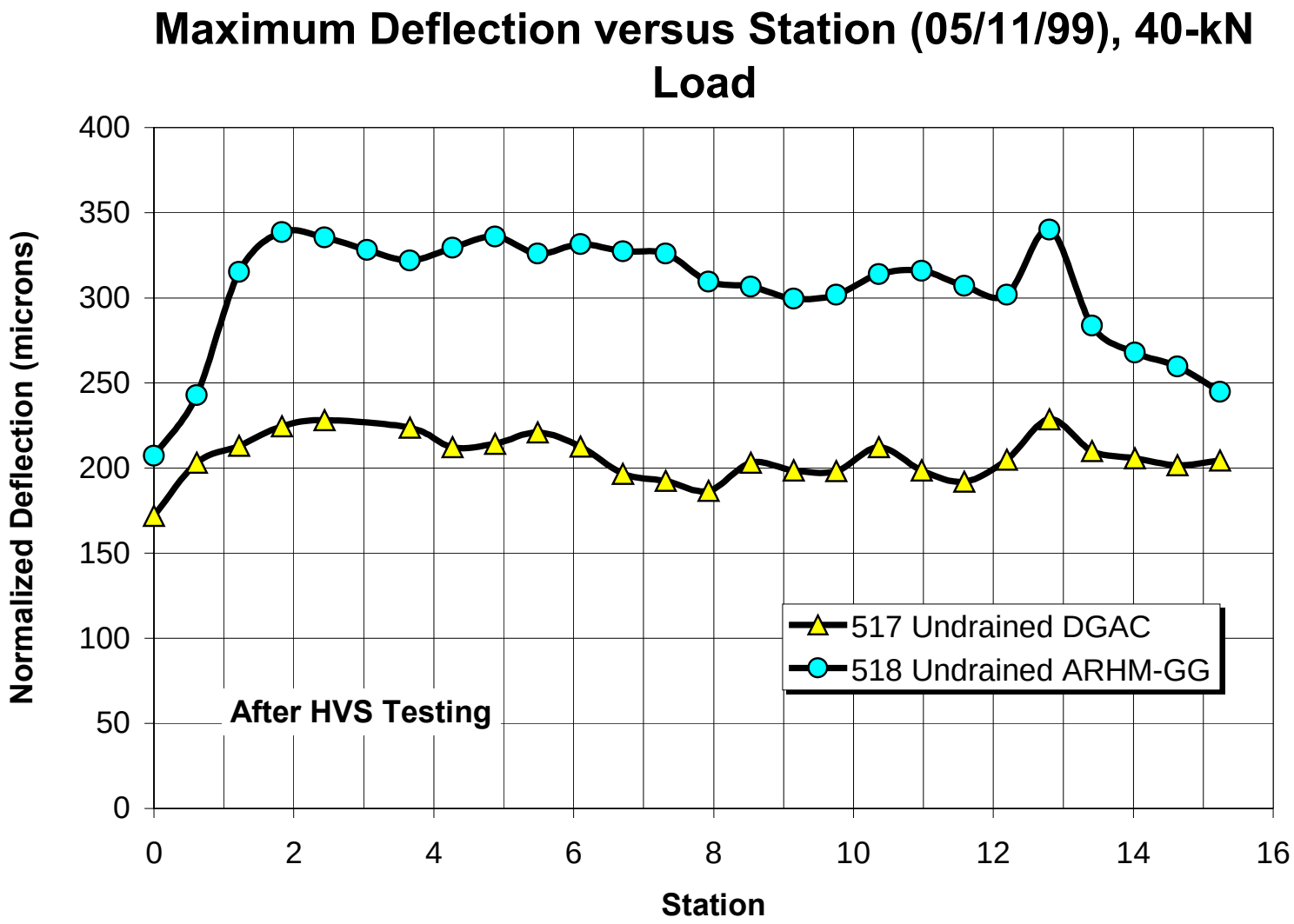

Figure 3.102. FWD maximum deflections after HVS testing, May 1999.

3.5 Dynamic Cone Penetrometer (DCP) Results

Table 3.23 summarizes Dynamic Cone Penetrometer (DCP) penetration rates for the Goal 3 sections taken inside and outside the traffic area. The shaded columns correspond to measurements taken inside the traffic area. The DCP data are presented in Figures 3.103–3.106 for all four test sections. The data show that there is not a significant statistical difference between DCP measurements taken inside and outside the traffic area at the end of HVS traffic.

Table 3.23 Summary of DCP Penetration Rates (mm/blow)

Section	Layer	Average Penetration Rate (mm/blow)	
		Inside Trafficked Area	Outside Trafficked Area
Section 514	***AB***	4.4	4.2
	ASB	1.9	1.4
	SG	22.4	19.4
Section 515	***AB***	1.3	
	ASB	0.8	
	SG	2.0	
Section 517	***AB***	1.2	1.9
	ASB	1.3	2.0
	SG	16.4	10.0
Section 518	***AB***	2.0	2.2
	ASB	1.1	1.8
	SG	15.9	11.3

Table 3.24 shows DCP penetration rates obtained 10 days after constructing the AB.(*12*) Except for Section 514, the penetration rates seem to have decreased considerably in the AB and ASB layers since construction.

Table 3.24 DCP Penetration Rates 10 Days after Construction of AB

Layer	Penetration Rate (mm/blow)
Aggregate Base	2.3
Aggregate Subbase	3.4
Subgrade	17.7

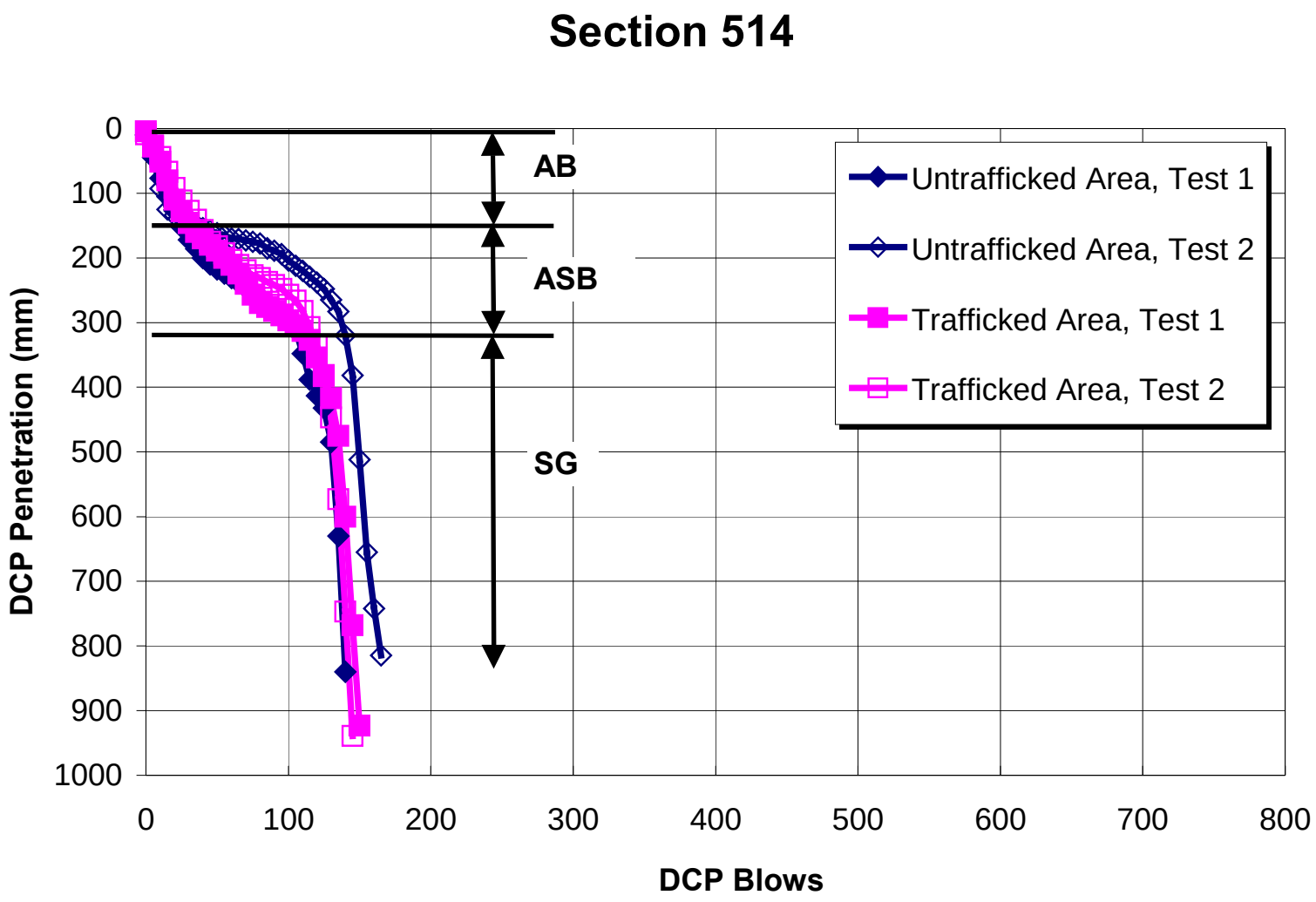

Figure 3.103. DCP results, Section 514 (drained, DGAC overlay).

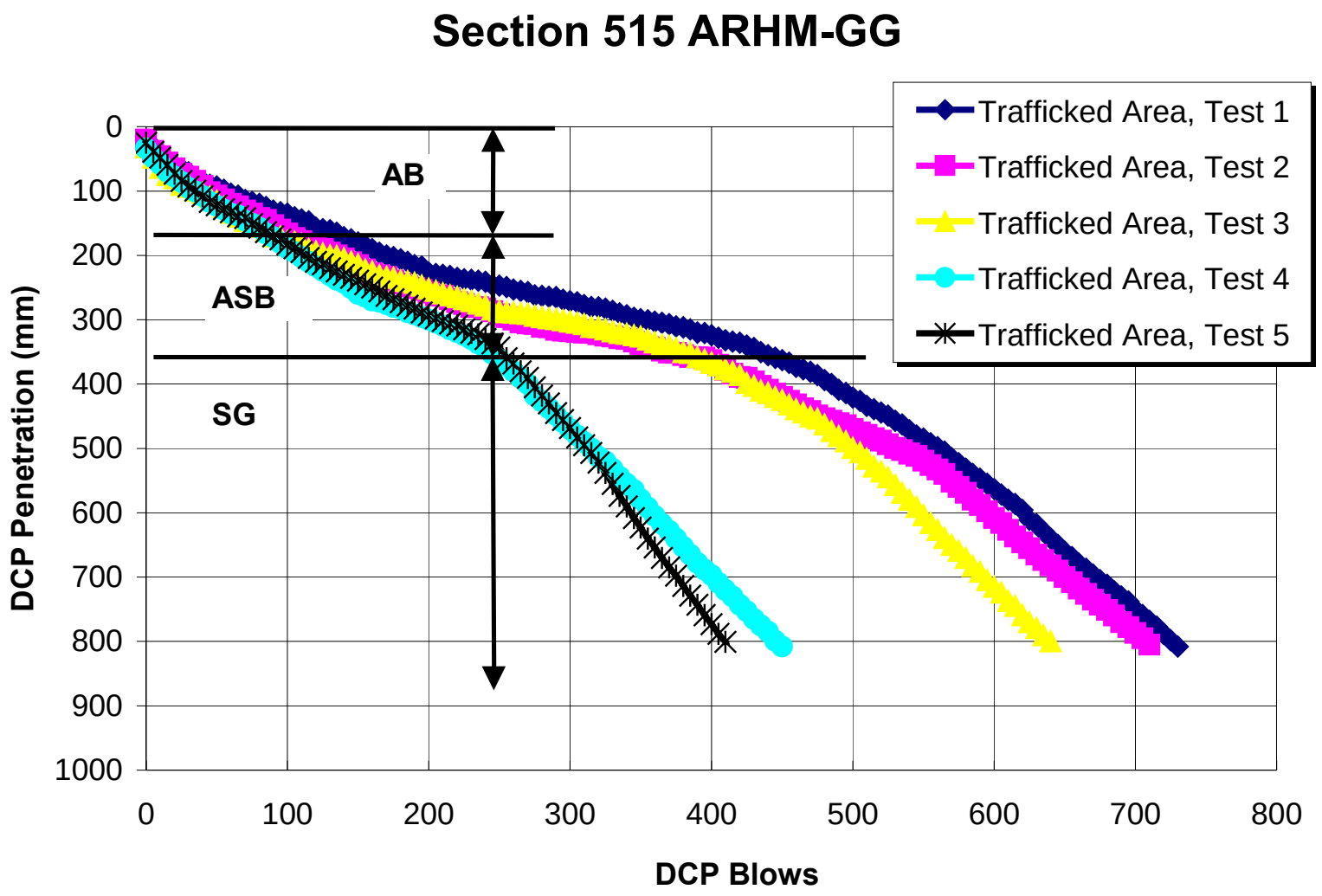

Figure 3.104. DCP results, Section 515 (drained, ARHM-GG overlay).

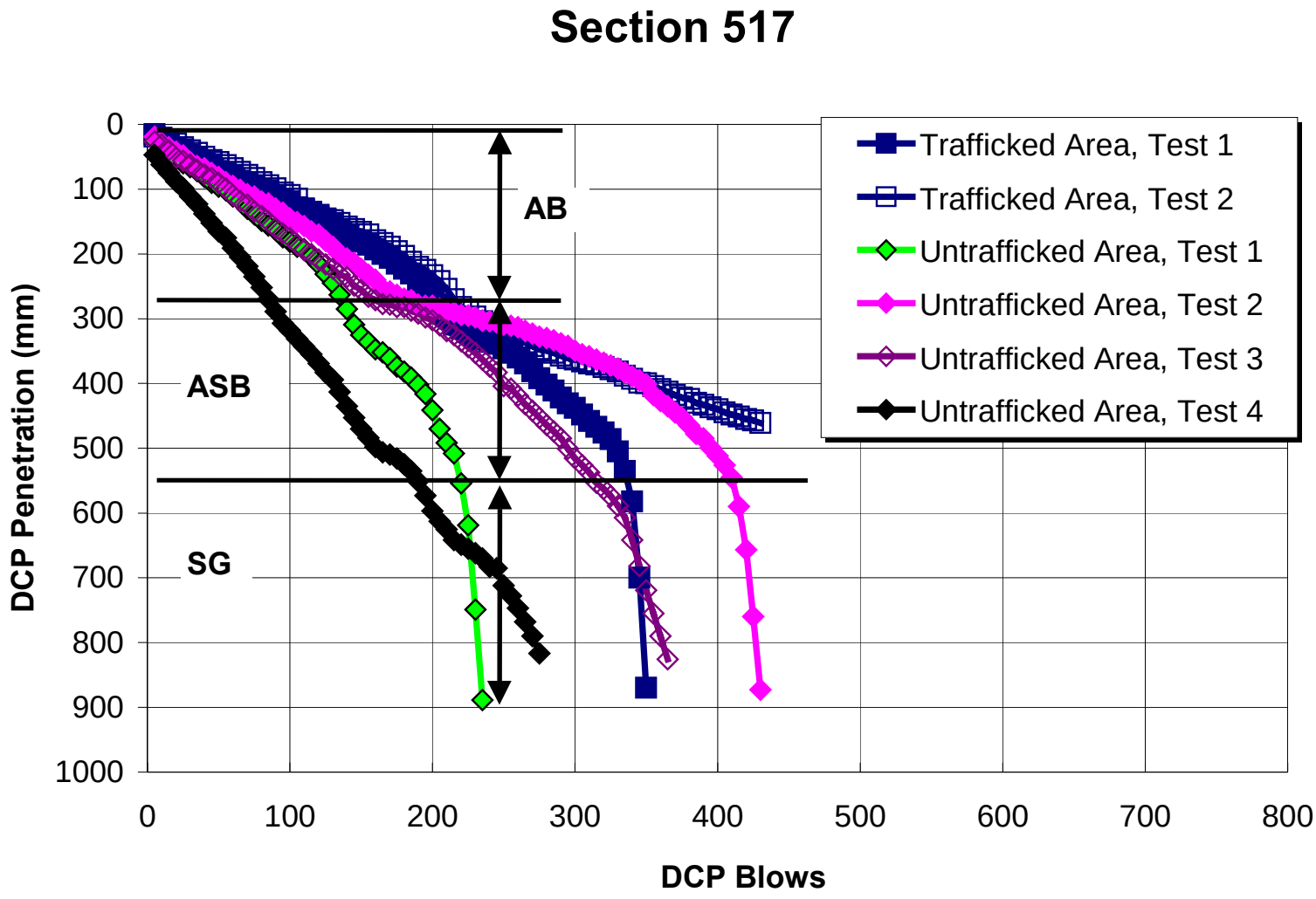

Figure 3.105. DCP results, Section 517 (undrained, DGAC overlay).

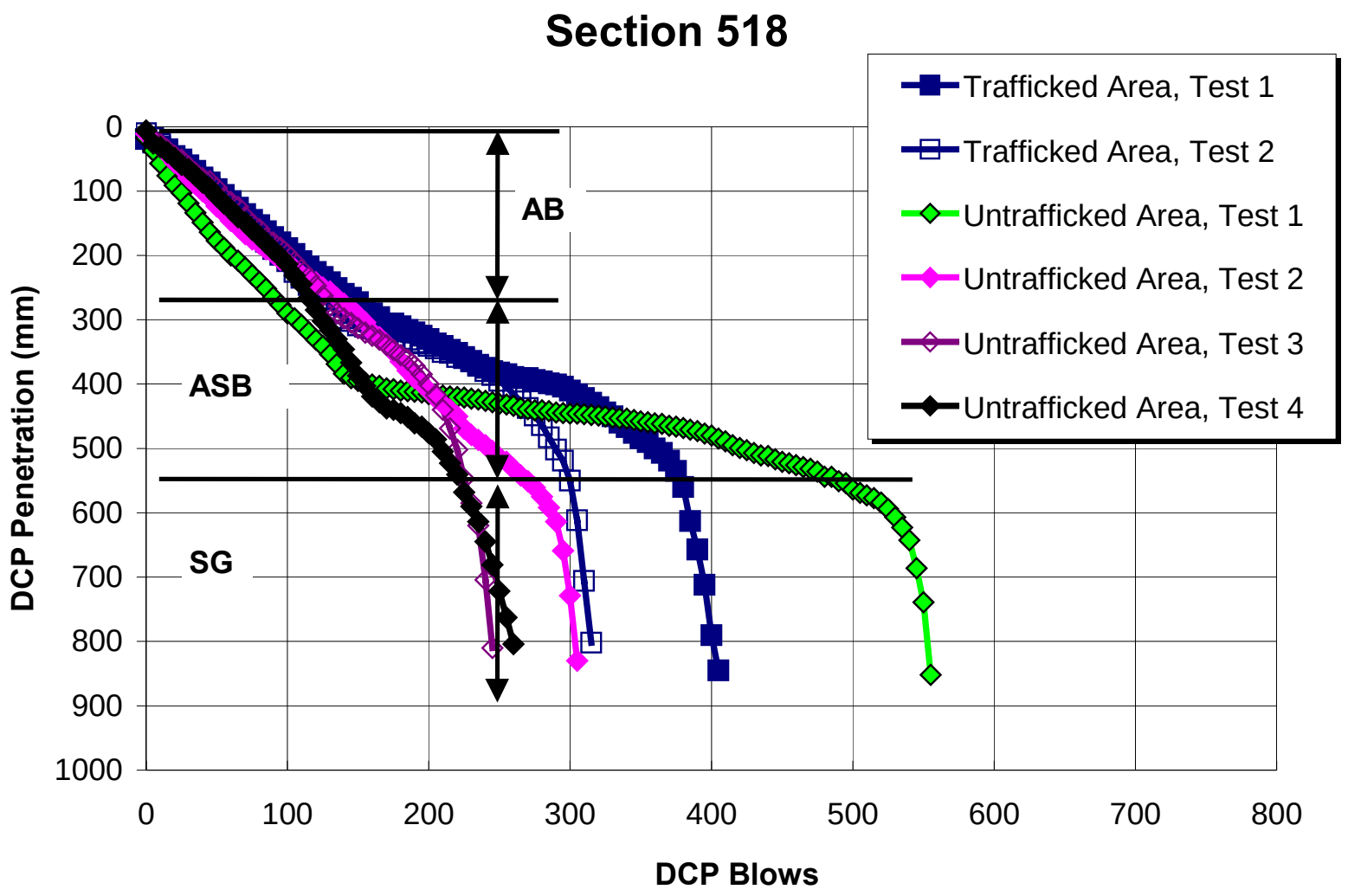

Figure 3.106. DCP results, Section 518 (undrained, ARHM-GG overlay).

The DCP penetration rates also indicate strength variability in the unbound layers. Possible reasons for this variability are material quality, grading compaction effort, and moisture content throughout the test sections, and the variability of the test itself.

Average DCP penetration rates for the AB in Sections 515, 517 and 518 ranged from 1.3 to 2.1 mm/blow. Section 514 had a DCP penetration rate of 4.3 mm/blow in the AB. Average DCP penetration rates for the ASB in all the sections were less variable and lower than those for the AB layer, averaging from 0.8 to 1.8 mm/blow.

DCP penetration rates for the subgrade present significant variability from one section to another. DCP measurements for Section 514 were taken in February 1999. DCP measurements for the other sections were obtained in July 1999. Figures 3.11 and 3.12 show that the subgrade had a higher moisture content in February 1999 than in July 1999. This is reasonable considering that February is a peak rainfall month and July is one of the driest months of the year.

Although DCP measurement for Sections 515, 517, and 518 were made in July 1999, the data show a significant variability in the subgrade among the sections. For example, Section 515 had subgrade penetration rates comparable to those of the AB and ASB. Section 517 had penetration rates that ranged from 2.7 to 28.8 mm/blow; Section 518 had penetration rates that ranged from 7.7 to 19.0 mm/blow. These results are reasonable considering the varying subgrade conditions encountered in test pits under the pavements in 1994.(*12*) At that time, different lenses of subgrade materials were encountered at different locations and depths.

3.6 Crack Monitoring Results

Crack monitoring was an essential part of data collection because fatigue and reflection cracking in asphalt pavement manifest themselves in the form of surface cracks. Crack

monitoring included direct measurement of crack length, photographic documentation and digital image analysis of the cracking process, crack activity meter (CAM) data collection, and coring to examine the propagation of cracks with depth.

3.6.1 Visual Inspection of Cracks

Table 3.25 shows when the first cracks were detected in the Goal 3 sections during HVS traffic. Regular crack inspections were made from the time of first crack detection through to the end of testing. The observed cracks were hairline cracks (approximately 0.2 mm maximum crack width) and were sometimes difficult to detect visually. These hairline cracks did not spall or increase in width during testing. The lack of crack deterioration is attributed to the lack of water and mineral particles on the pavement surfaces and to the good support provided by the uncracked bottom AC lift to the cracked top AC lift and overlay layers. The observed cracks were marked with a lumber crayon and photographed for later digital image analysis.

Table 3.25 Load Applications to Crack Density

Section		**Load Applications to Crack Density (thousands)**	
		0.5 m/m^2	**2.5 m/m^2**
Drained	514 DGAC	648	890
	515 ARHM-GG	810	1,190
Undrained	517 DGAC	1,060	1,700
	518 ARHM-GG	492	750

3.6.2 Digital Image Analysis of Cracks

Figures 3.107–3.110 illustrate the sequences of surface crack patterns versus number of load applications for Sections 514, 515, 517, and 518, respectively. The figures show that there were more longitudinal cracks in Section 514 (drained, DGAC overlay) than for the other sections.

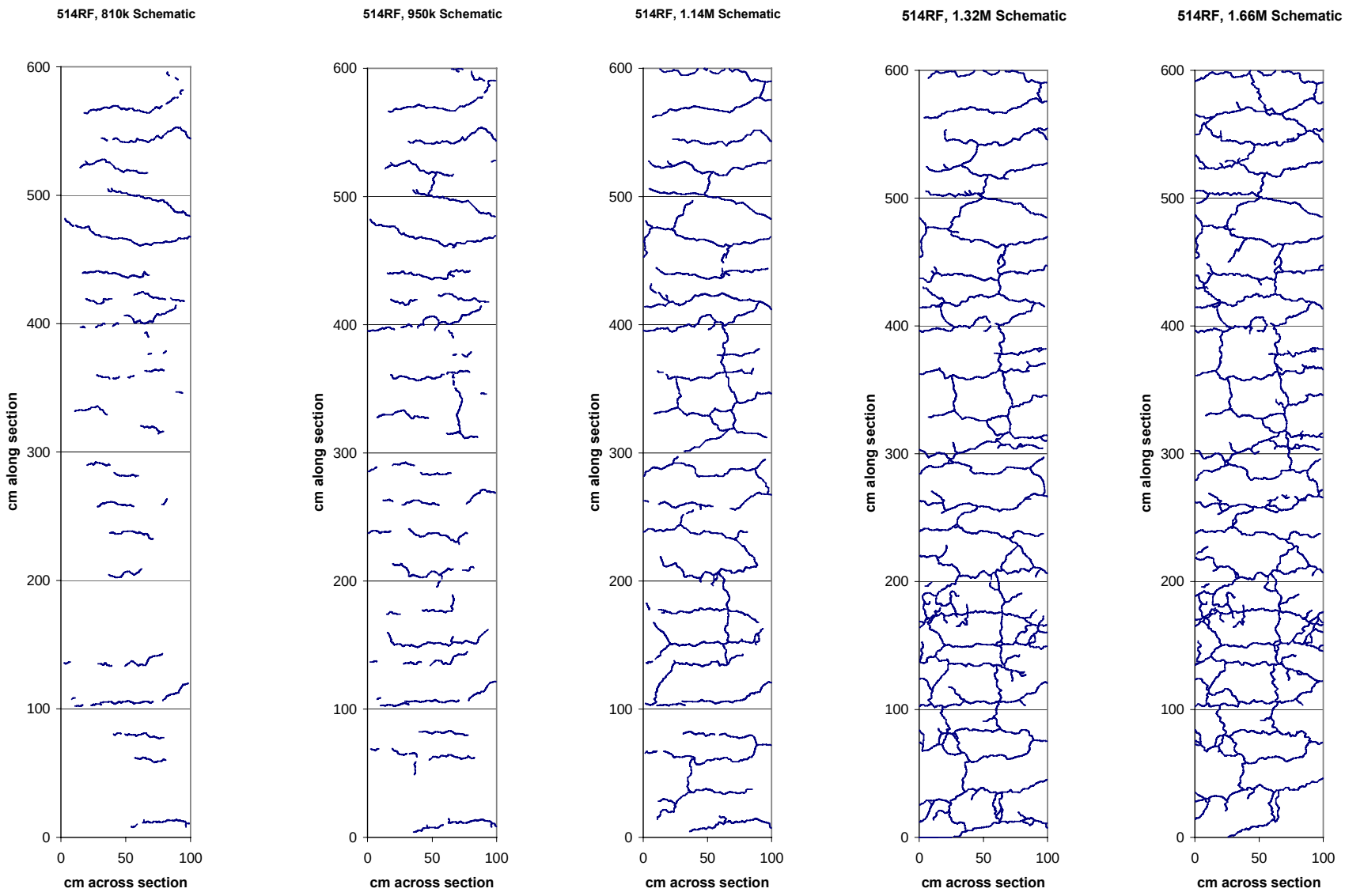

1.8 m/m^2 2.6 m/m^2 4.0 m/m^2 5.9 m/m^2 8.2 m/m^2

Figure 3.107. Crack development in Section 514 (drained, DGAC overlay).

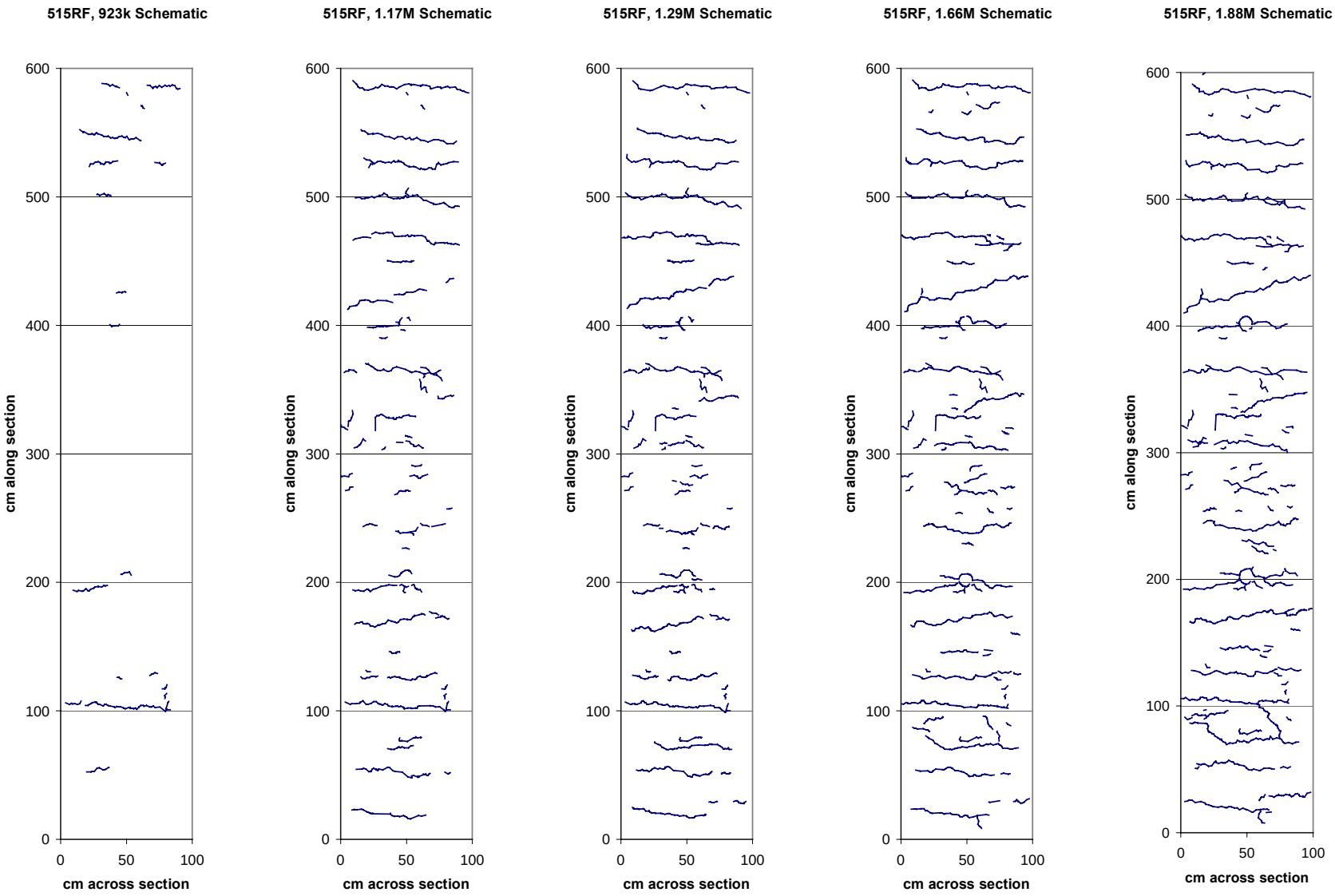

0.6 m/m^2 2.5 m/m^2 2.9 m/m^2 3.6 m/m^2 4.1 m/m^2

Figure 3.108. Crack development in Section 515 (drained, ARHM-GG overlay).

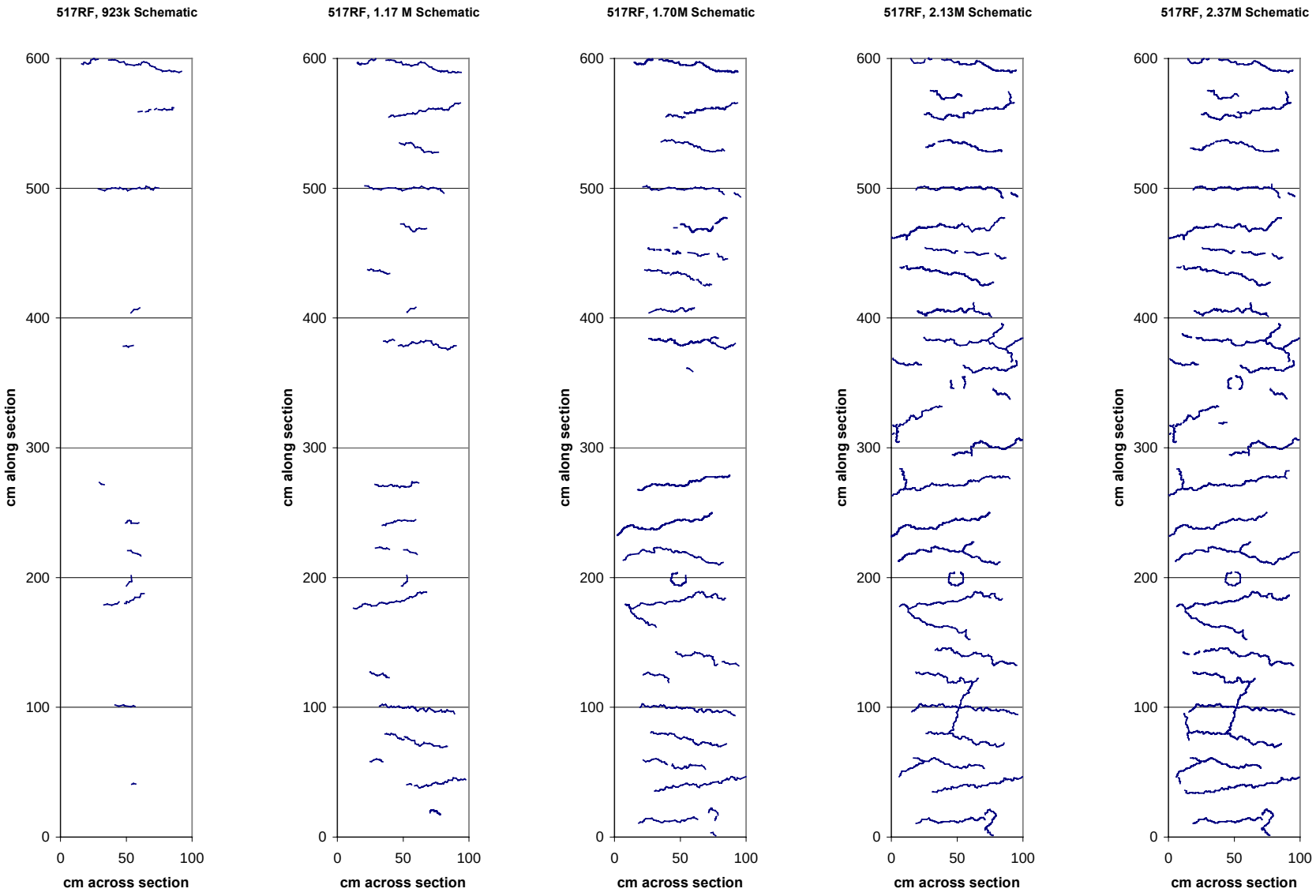

0.4 m/m^2 1.2 m/m^2 2.5 m/m^2 3.8 m/m^2 4.1 m/m^2

Figure 3.109. Crack development in Section 517 (undrained, DGAC overlay).

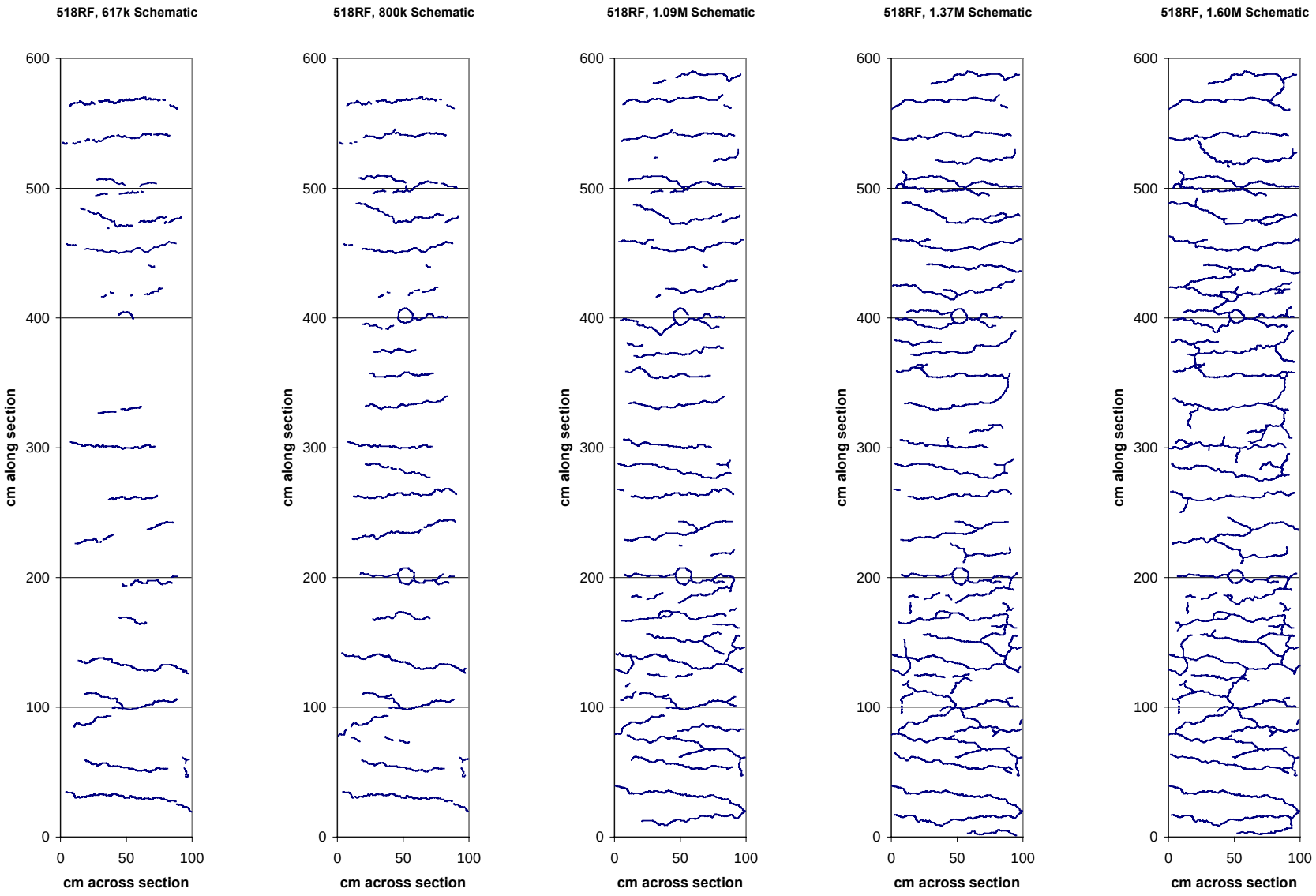

Figure 3.110. Crack development in Section 518 (undrained, ARHM-GG overlay).

Using digital image analysis, it was possible to quantify crack progression. Figure 3.111 shows the progress of crack accumulation and crack density for all four test sections. Two distinctive pavement cracking statistics should be noted: Sections 514 (drained, DGAC overlya) and 518 (undrained, ARHM-GG overlay) both displayed approximately double the crack lengths of Sections 515 and 517 after about 1.5 million load applications.

Figure 3.112 shows the variation in Road Surface Deflectometer (RSD) deflections with respect to crack density under the 40-kN test load. Except for Section 514, there is no significant increase in RSD deflections with crack density. The results indicate that once the cracks appeared on the surface of the overlay, significant damage had already occurred.

Figures 3.113 and 3.114 show the crack patterns obtained at the end of Goal 1 (initial sections) and at the end of Goal 3 (overlays) in the undrained sections transposed over one another. The figure shows that cracks at the end of Goal 1 and at the end of Goal 3 mostly occurred in the same locations, indicating that reflection cracking is the mechanism of failure in the Goal 3 overlay.

Figure 3.115 compares of the amount of cracking for the Goal 1 and Goal 3 sections.

The Section 514 DGAC overlay exhibited a number of cracks of greater length than were observed on the underlying Section 500. It is possible that a significant number of surface cracks were not measured when collecting data on the Goal 1 section.

Of the four overlay sections, Section 517 (DGAC overlay) reflected the least number of cracks from the underlying pavement (Section 502), even though Section 502 had the highest degree of cracking of the four underlying pavements.

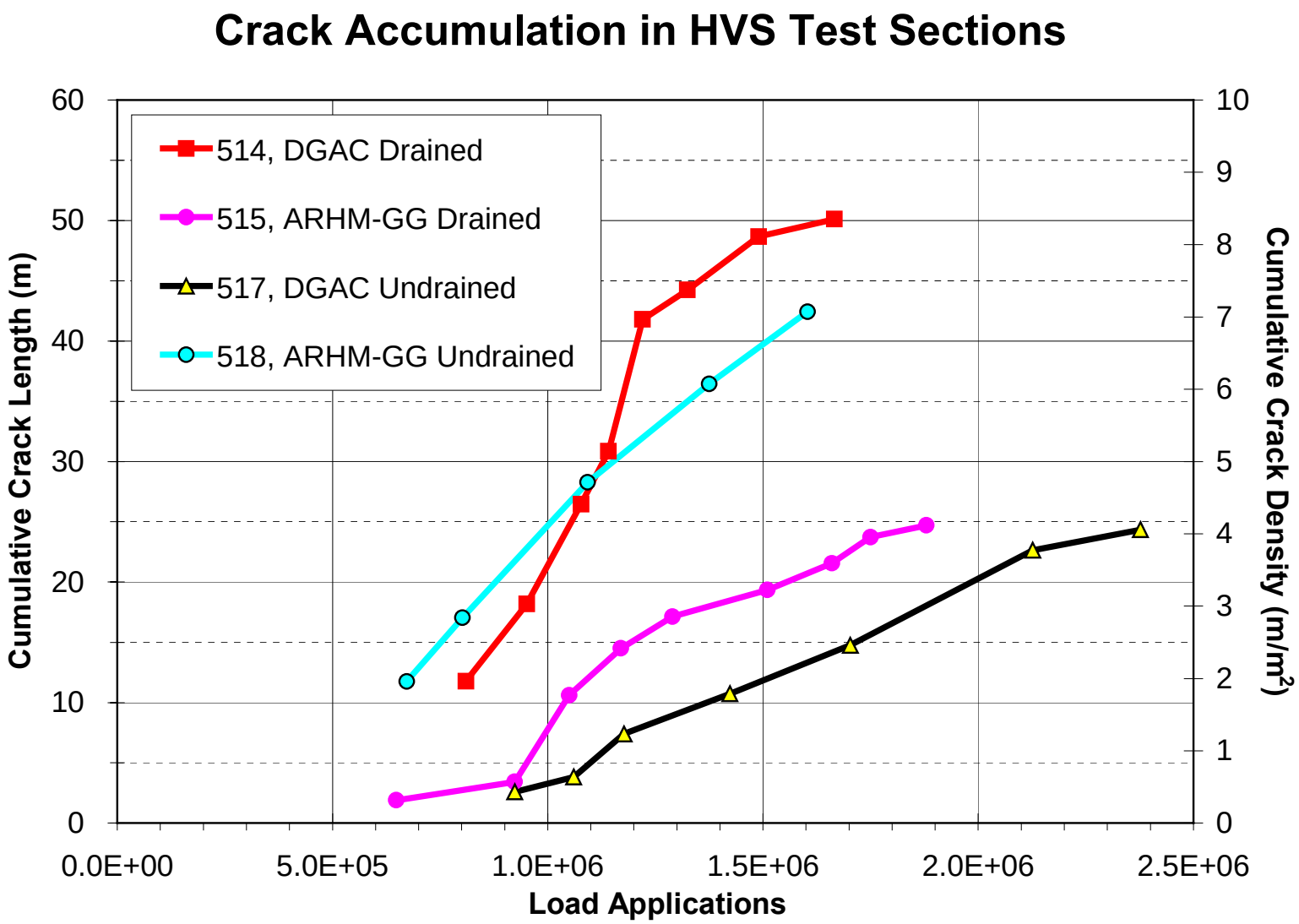

Figure 3.111. Crack accumulation in HVS test sections.

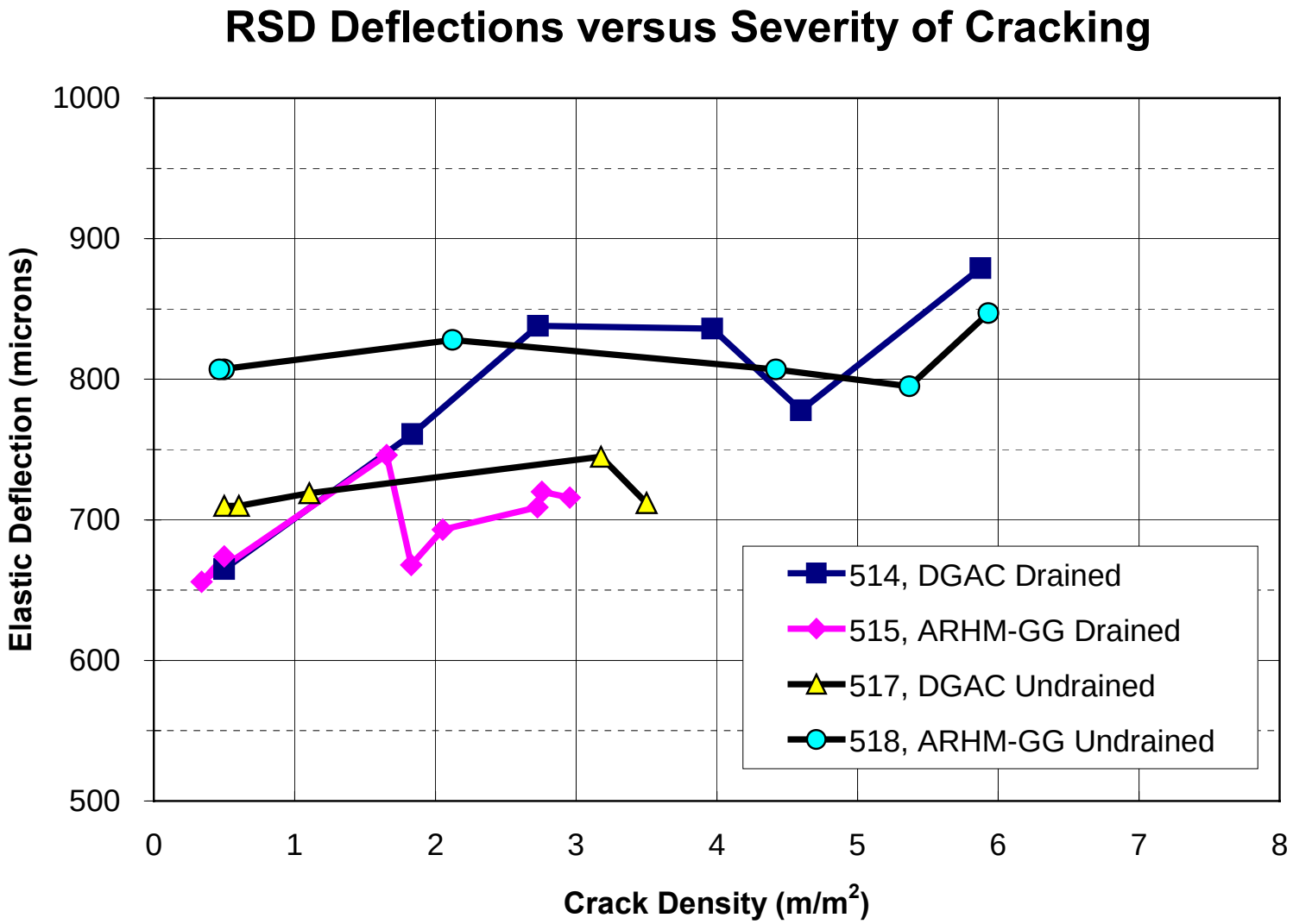

Figure 3.112. Variation of RSD maximum deflections with crack length density under 40-kN test load.

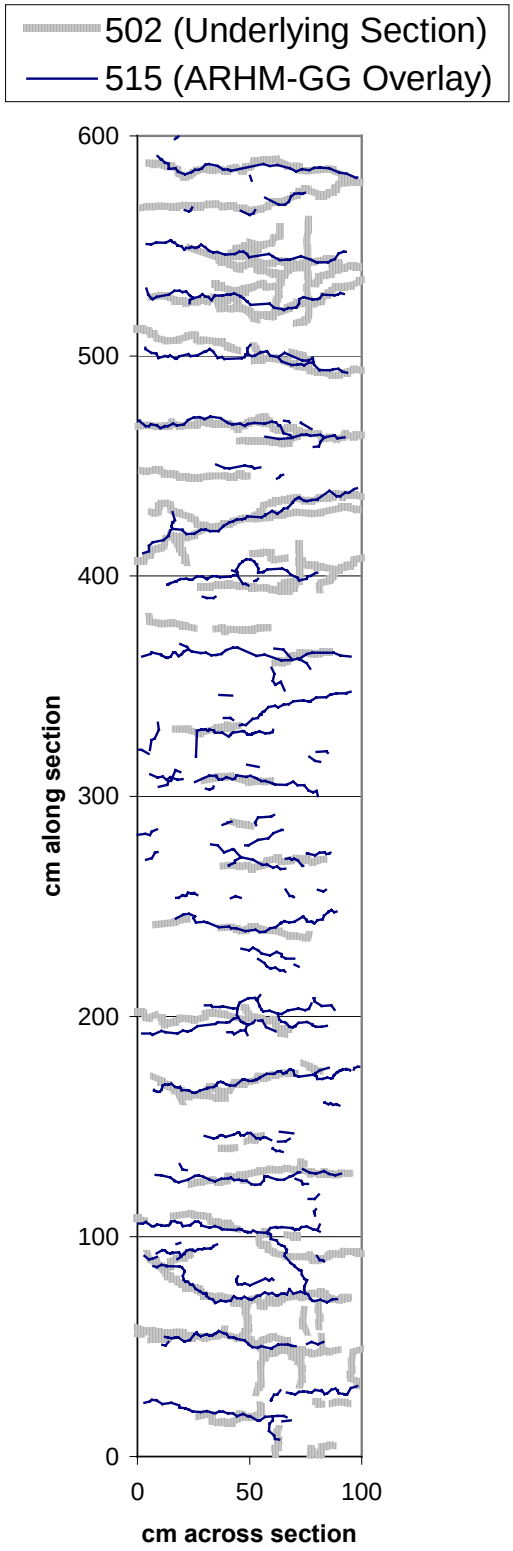

Figure 3.113. Crack reflection in Section 502/515.

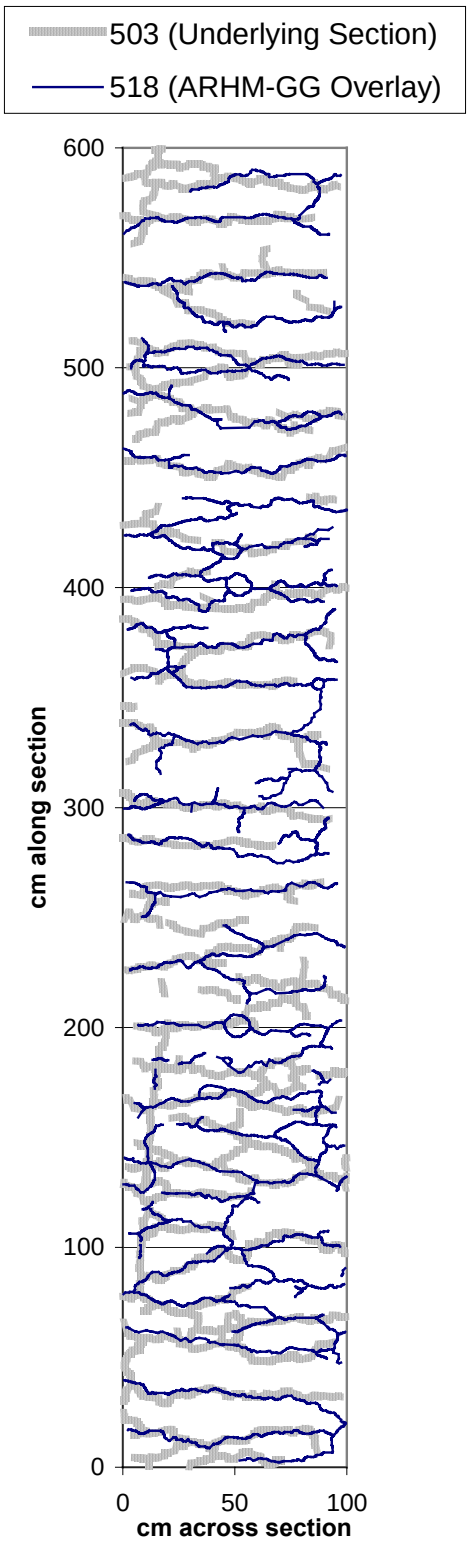

Figure 3.114. Crack reflection in Section 503/518.

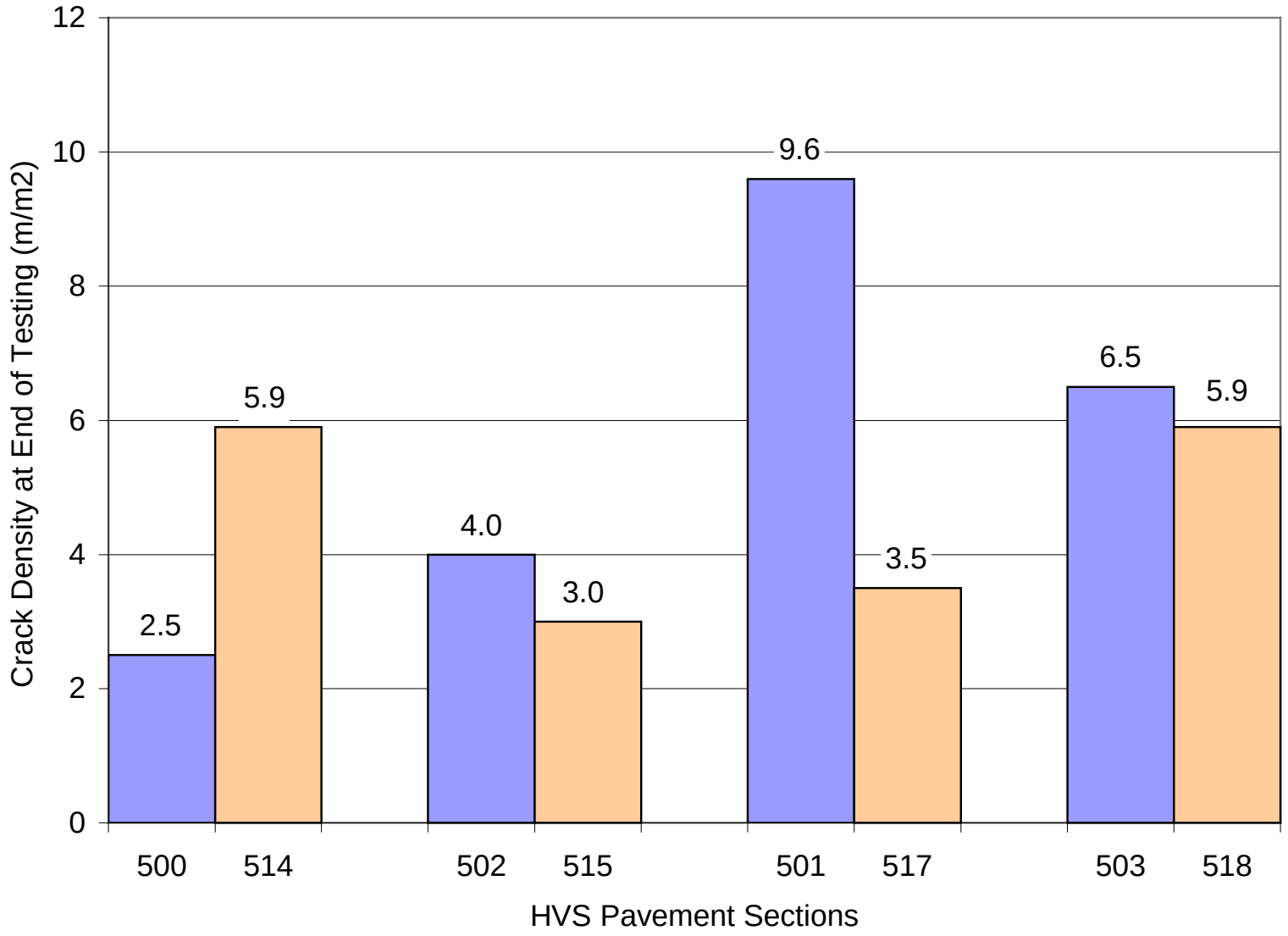

Figure 3.115. Comparison of crack density for Goal 1 and Goal 3 test sections at end of HVS testing.

3.6.3 Crack Activity Meter (CAM)

The Crack Activity Meter (CAM) was used to measure crack displacements on selected cracks on each test section. Figure 3.116 shows typical CAM data collected as the HVS dual wheel approached the point of measurement and passed over it. The vertical and horizontal displacements were obtained simultaneously. A positive relative horizontal displacement indicates that the faces of the beams that compose the crack are approaching (closing the crack gap). A positive relative vertical displacement indicates that the trailing beam moves up in relation to the leading beam.

Figures 3.117–3.120 show total vertical and horizontal activity under the 40-kN test load for the four test sections.

The data show that the total horizontal displacements were larger than the total vertical displacements in the drained sections (Sections 514 and 515). The total horizontal displacements in the DGAC overlay (Section 514) were approximately 75 percent larger than the total horizontal displacements in the ARHM-GG overlay (Section 515).

In the undrained sections (Sections 517 and 518), total vertical crack displacements tended to be higher than the total horizontal displacements. One reason for this compared to the drained sections is that the cracked asphalt concrete layer in the undrained section did not have the additional support provided by the ATPB in the drained sections. The total vertical displacements tented to be slightly larger in Section 517 (DGAC overlay) than in Section 518 (ARHM-GG overlay) while total horizontal displacement tended to be slightly larger in Section 518 (ARHM-GG) than in Section 517 (DGAC).

Figures 3.121–3.124 show the crack response under the 100-kN test load for the four test sections.

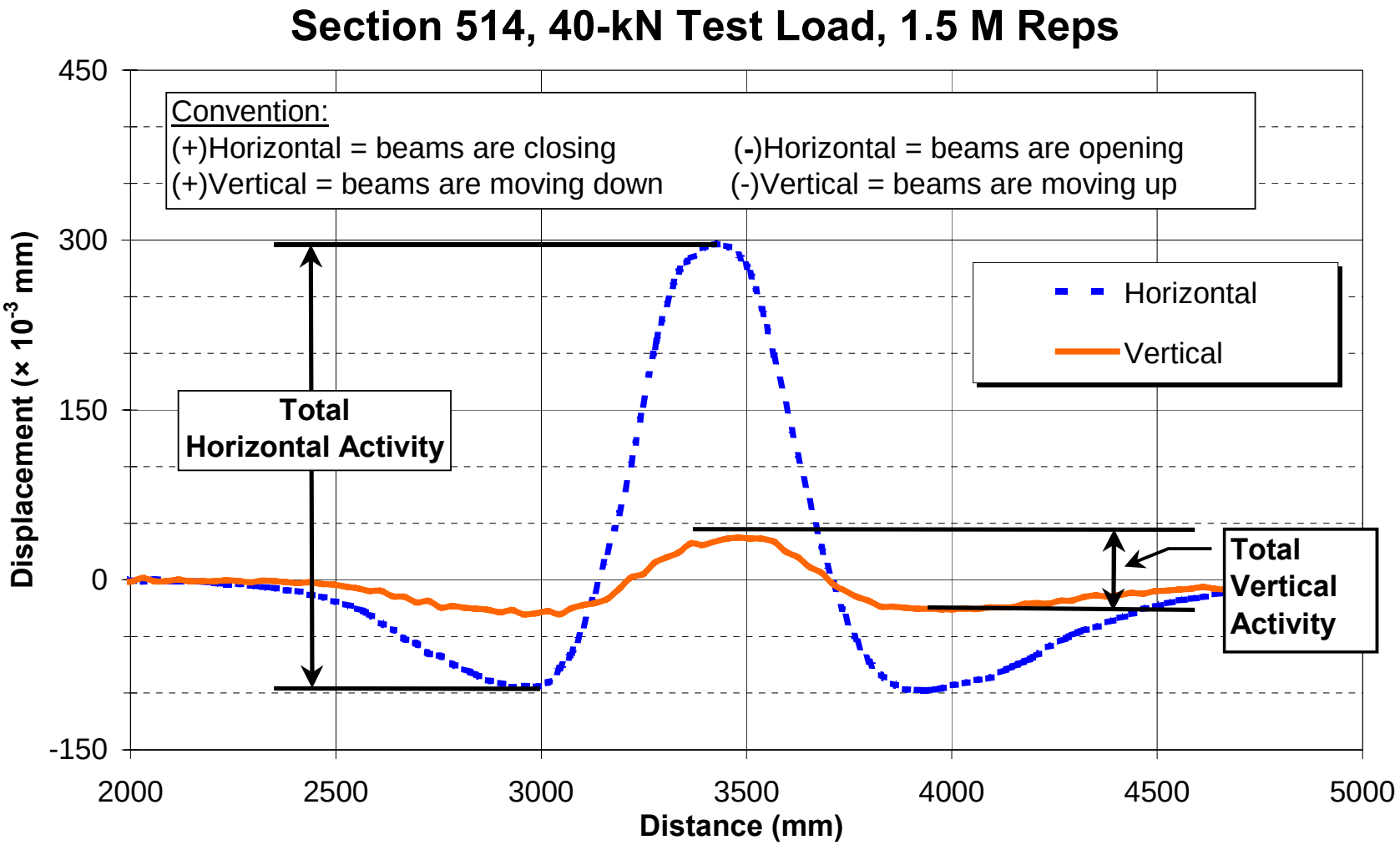

Figure 3.116. Example of typical CAM data.

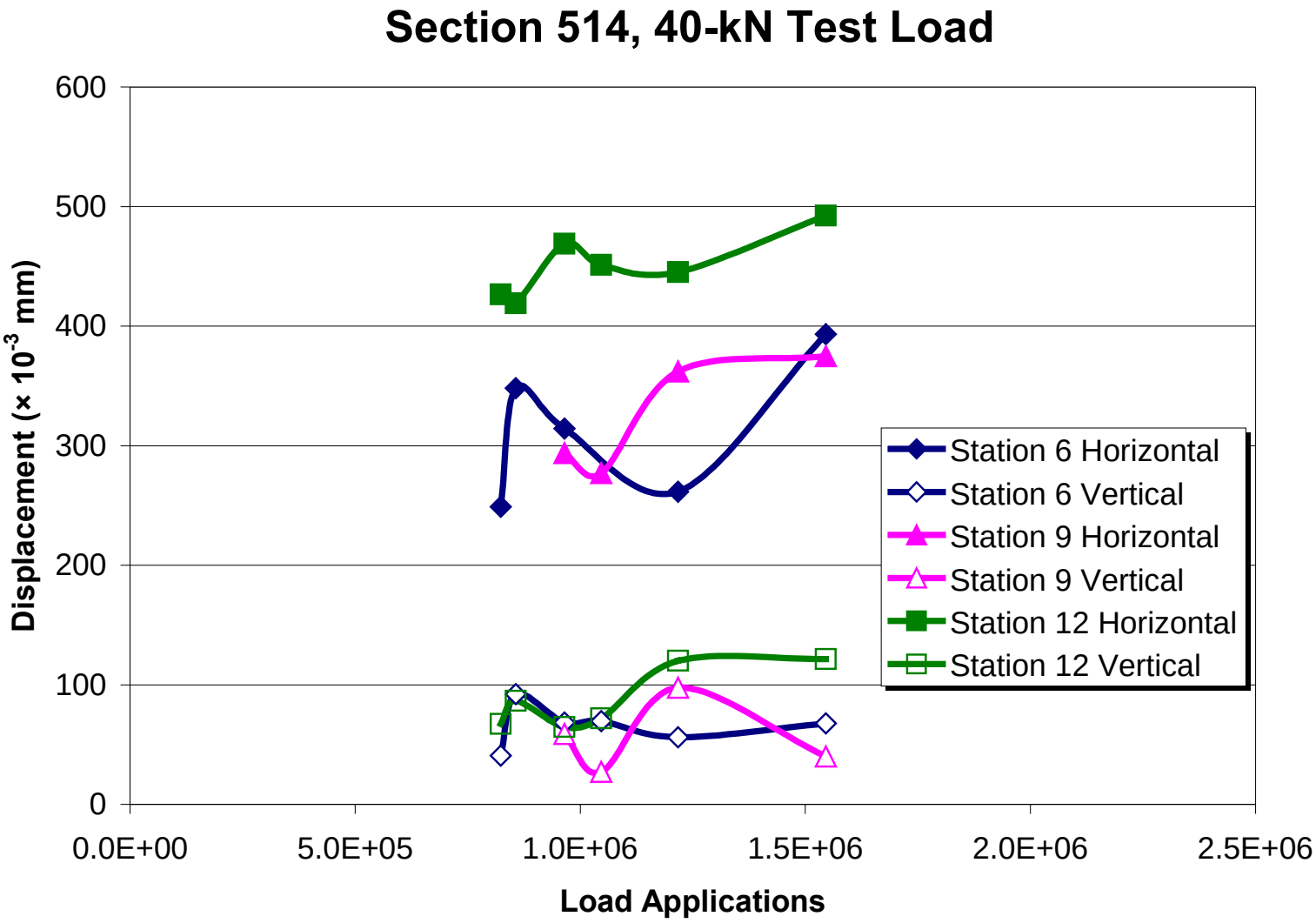

Figure 3.117. Crack activity in Section 514 (drained, DGAC overlay), 40-kN test load.

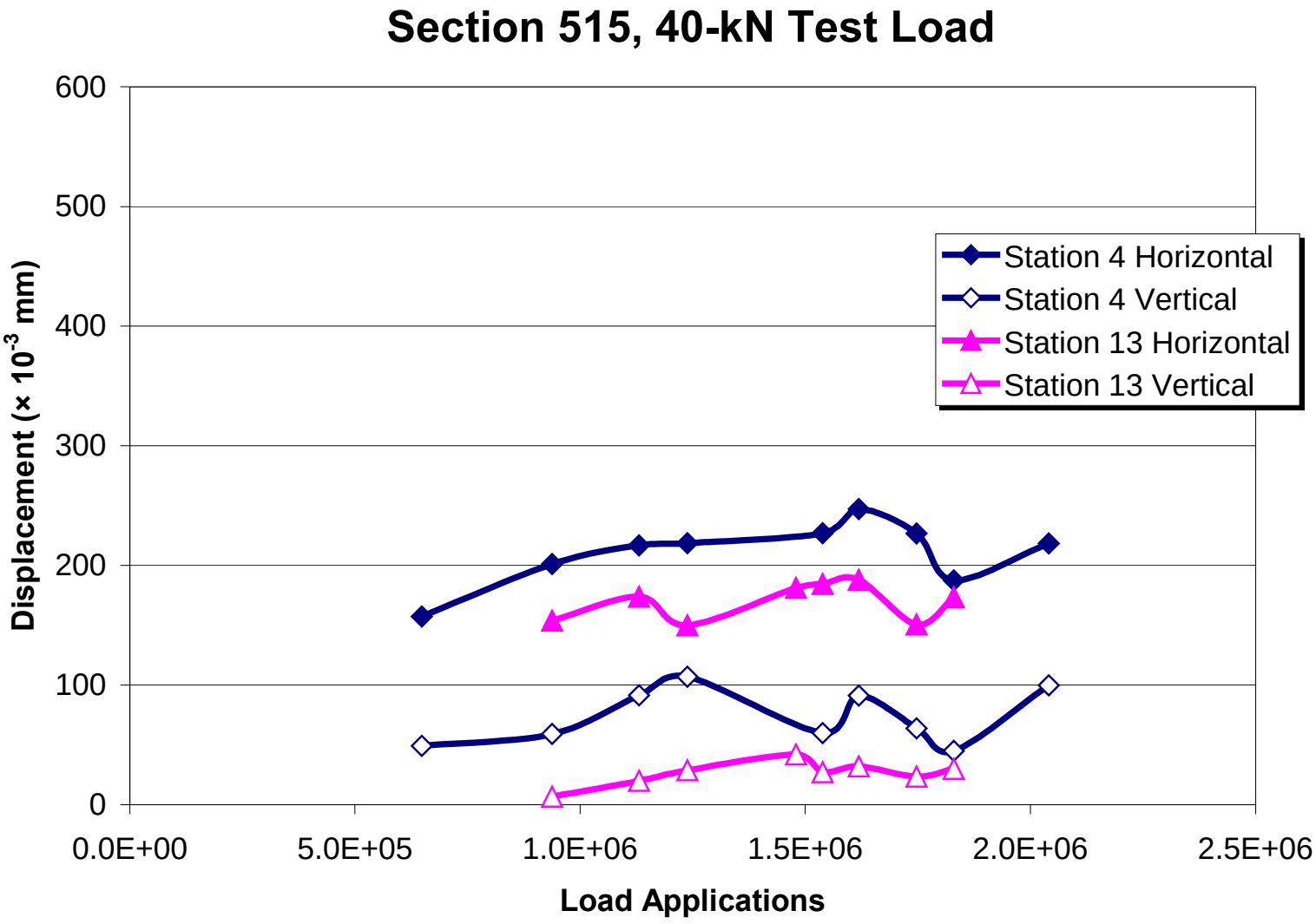

Figure 3.118. Crack activity in Section 515 (drained, ARHM-GG overlay), 40-kN test load.

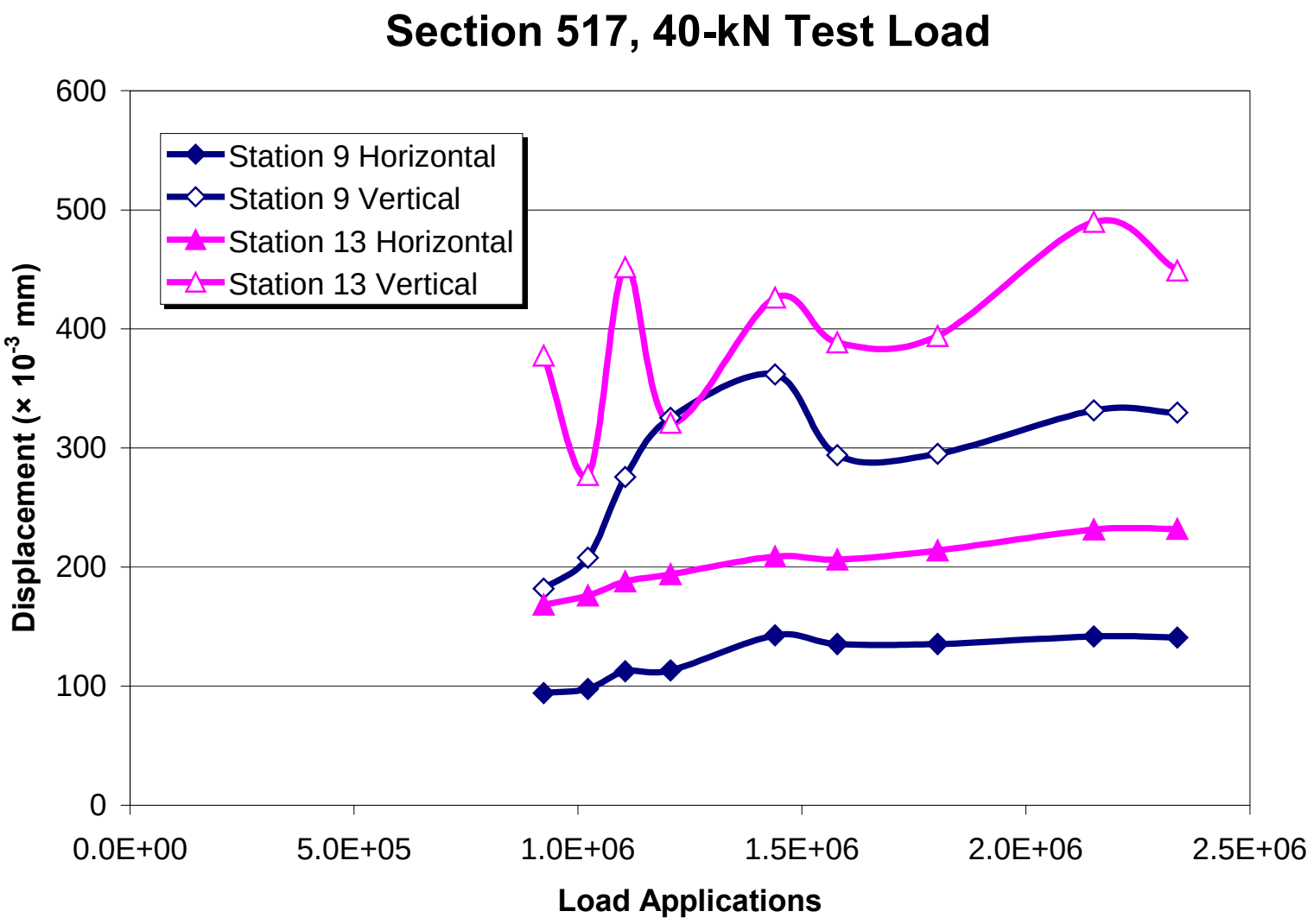

Figure 3.119. Crack activity in Section 517 (undrained, DGAC overlay), 40-kN test load.

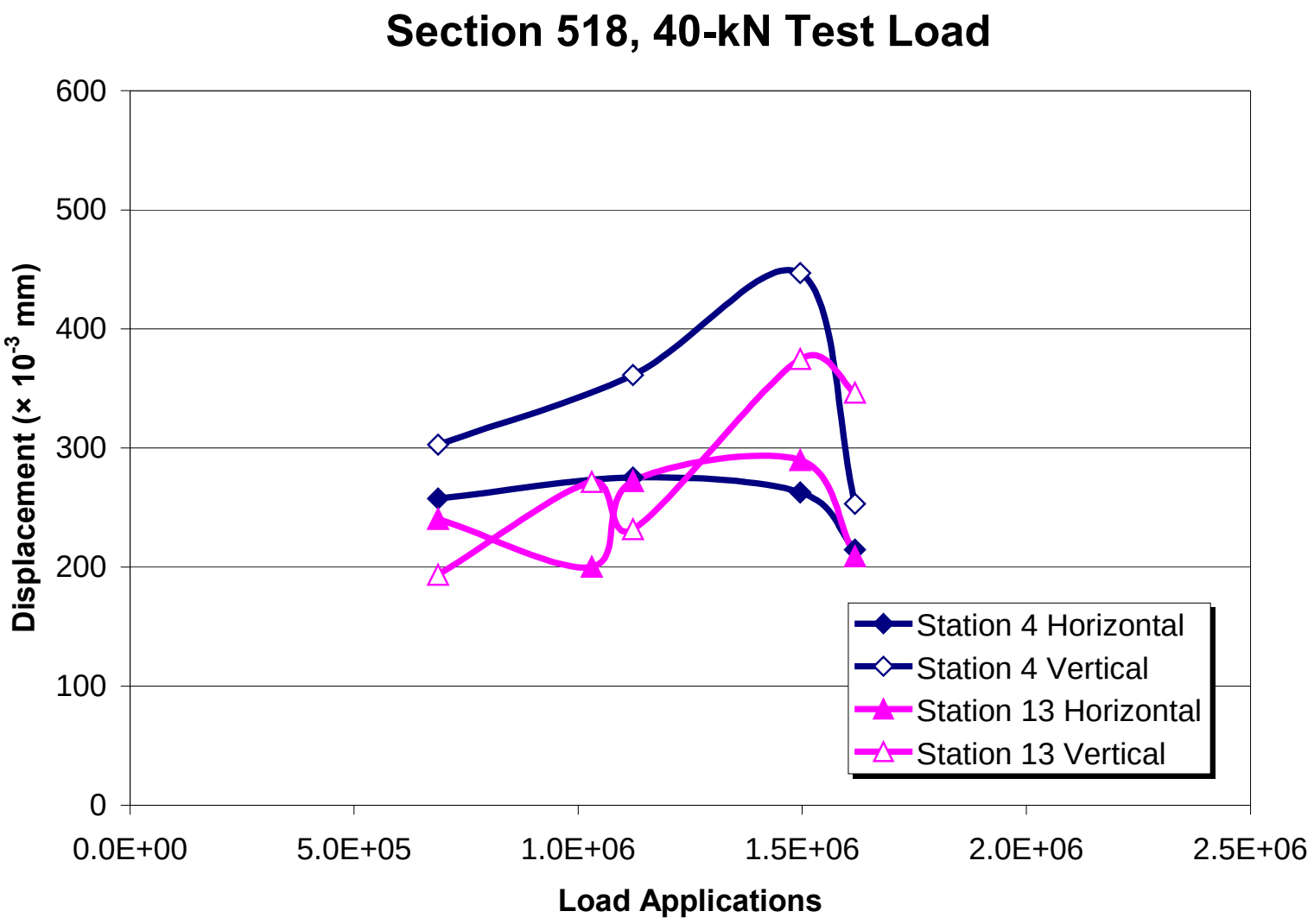

Figure 3.120. Crack activity in Section 518 (undrained, ARHM-GG overlay), 40 kN test load.

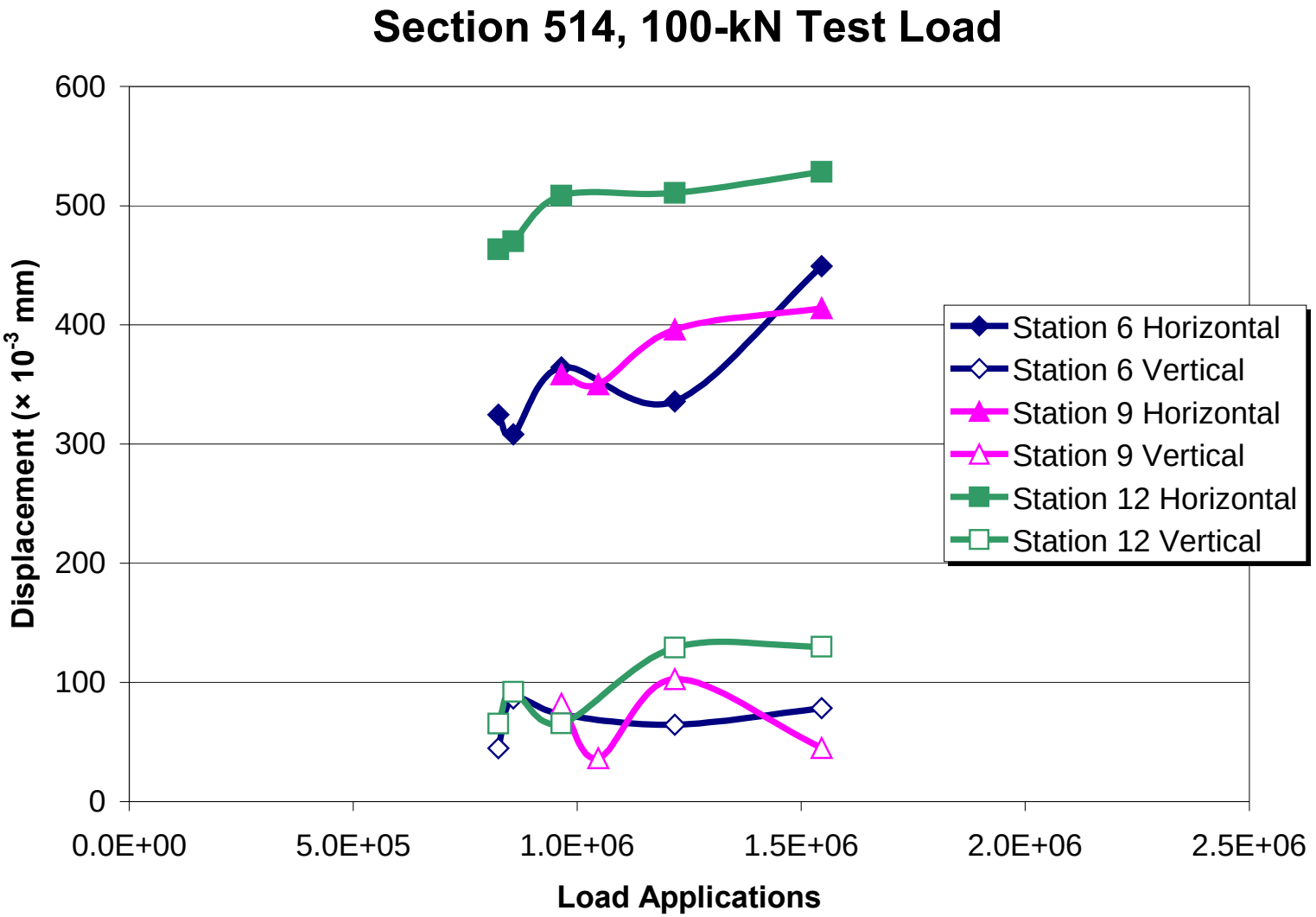

Figure 3.121. Crack activity in Section 514 (drained, DGAC overlay), 100-kN test load.

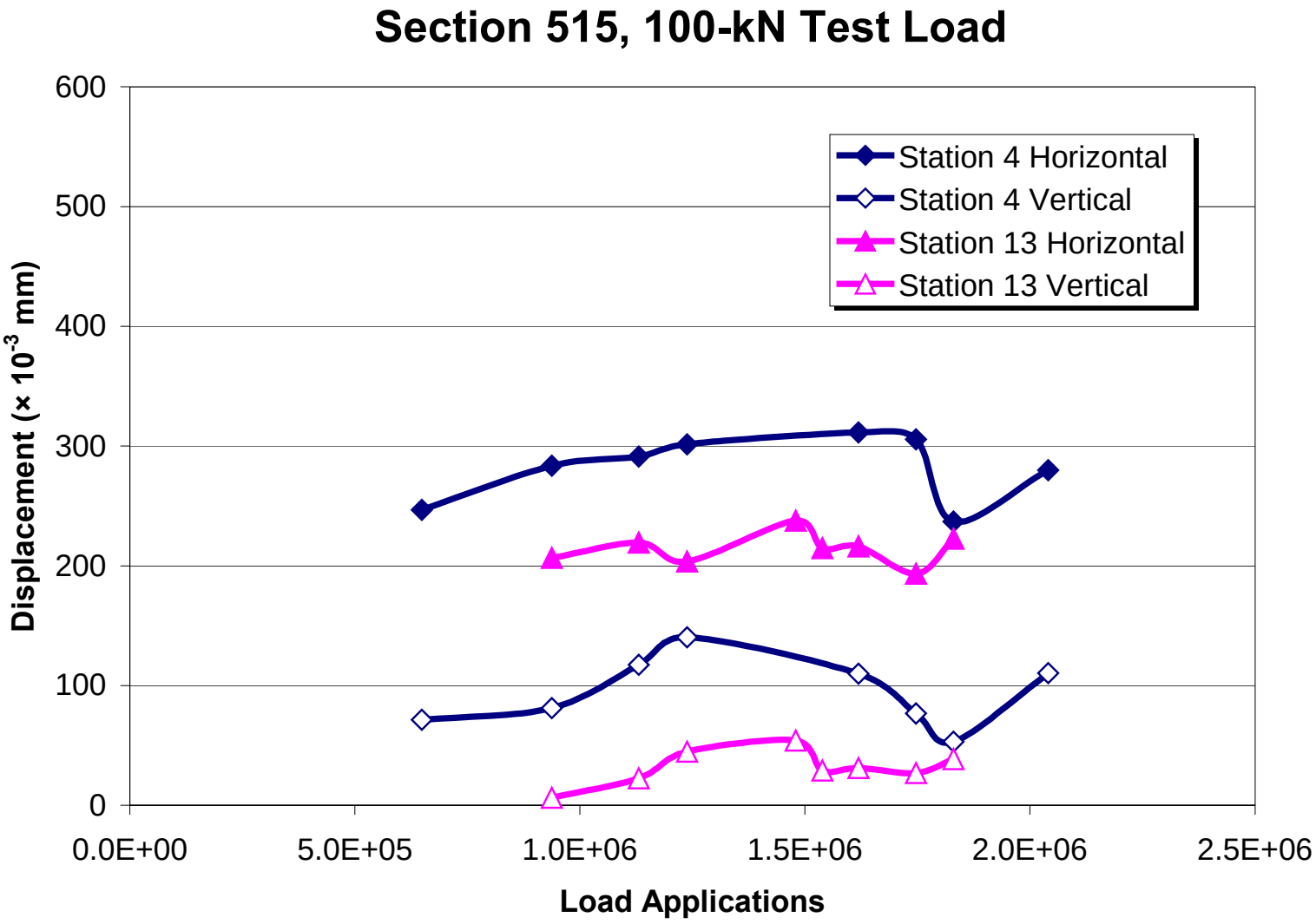

Figure 3.122. Crack activity in Section 515 (drained, ARHM-GG overlay), 100-kN test load.

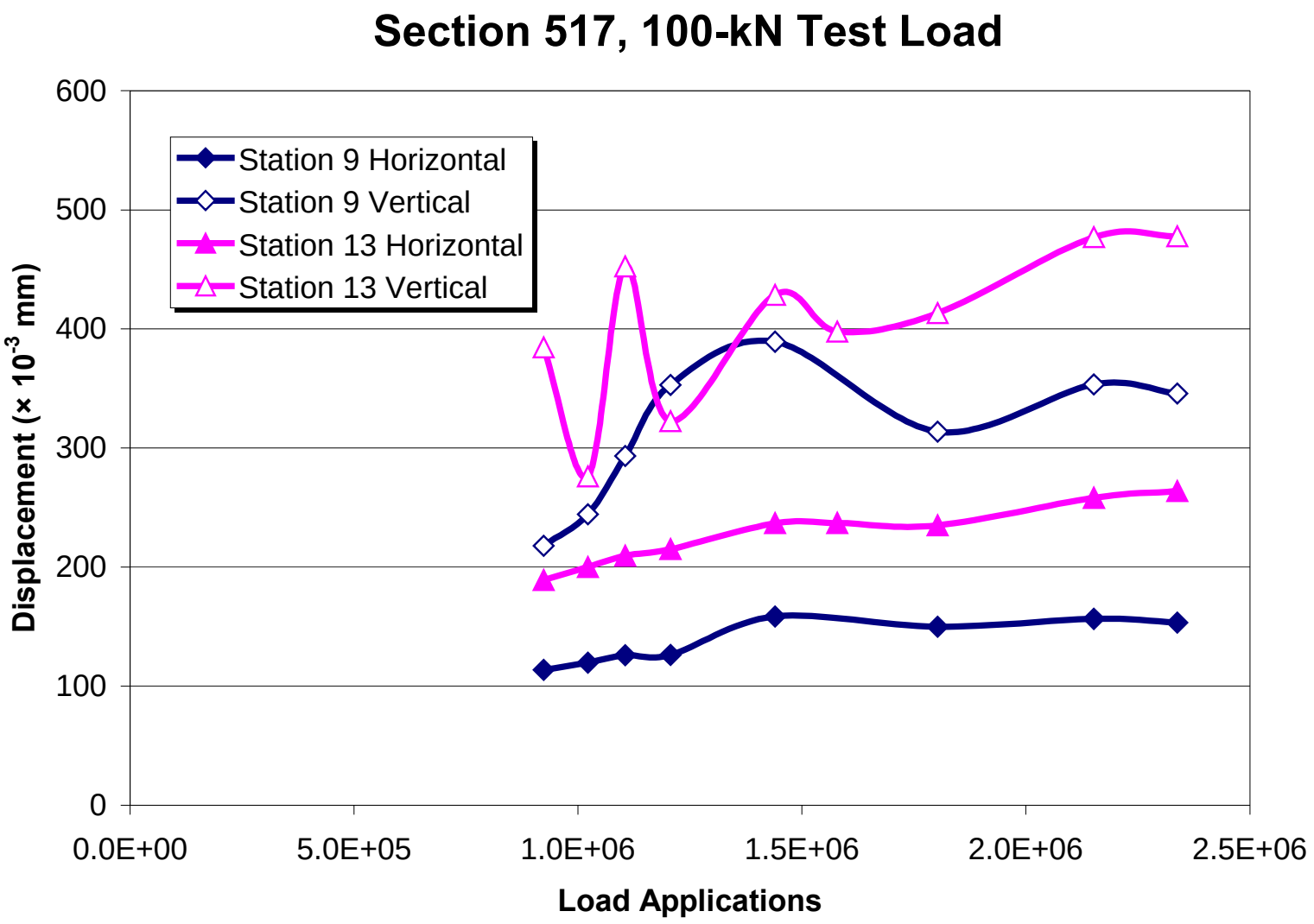

Figure 3.123. Crack activity in Section 517 (undrained, DGAC overlay), 100-kN test load.

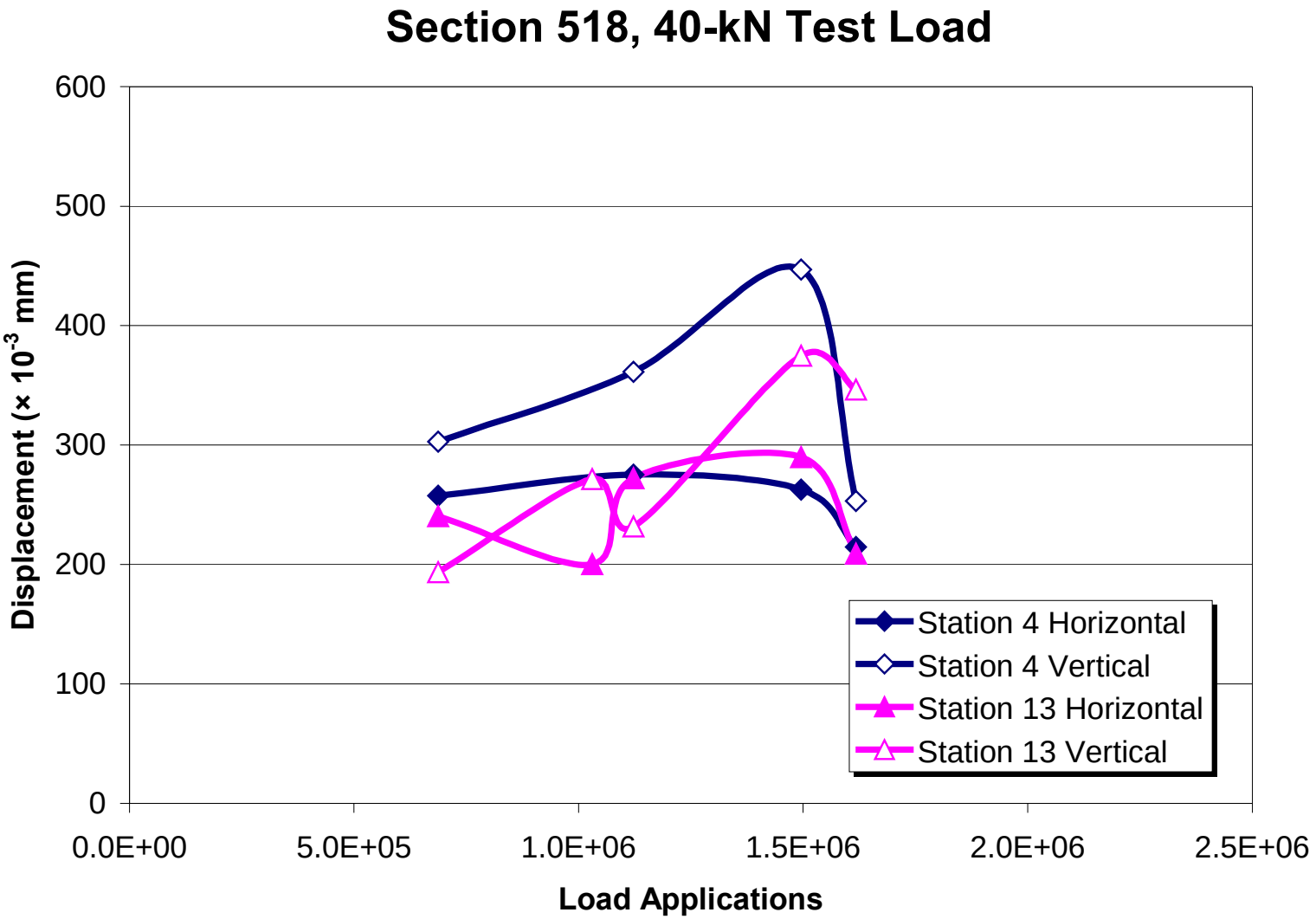

Figure 3.124. Crack activity in Section 518 (undrained, ARHM-GGoverlay), 100-kN test load.

In the drained sections (Sections 514 and 515), total horizontal displacements were approximately 15 percent greater under the 100-kN test load compared to the 40-kN test load. Total vertical displacements were not significantly different. In the undrained sections (Sections 517 and 518), total displacements under the 100-kN test load were not significantly greater than those of the 40-kN test load.

The movement of the cracks on all of the sections is complex because of the presence of the generally uncracked bottom AC lift beneath the top AC lift and overlay , and the lack of bonding between the top and bottom AC lifts.

4.0 PERFORMANCE EVALUATION AND MECHANISTIC ANALYSES

The results of the Goal 3 HVS testing program permit the verification of current procedures and the development of new methodologies for pavement design and rehabilitation. In this chapter, the mechanistic analyses are based on the elastic layer theory and are used to relate the response of the pavement sections to their performance under the Heavy Vehicle Simulator (HVS).

4.1 Caltrans Overlay Design Method

The Caltrans method for rehabilitation of flexible pavements is based on elastic surface deflection criteria as measured with a Benkelman Beam or Traveling Deflectometer under an 80-kN single axle load. Deflections on the Goal 1 test sections were measured using a Dynaflect, Falling Weight Deflectometer (FWD), and Road Surface Deflectometer (RSD). All deflection measurements were taken at a pavement surface temperature of approximately 20ºC.

Overlay thicknesses were designed using California Test Method 356. Calculations were based on 80th percentile deflections, a Traffic Index of 9 [1 million Equivalent Single Axle Loads (ESALs)], and an asphalt thickness of 150 mm. The 80th percentile deflections used for overlay design were obtained from Sections 500 and 501 in the Goal 1 test program (overlaid as Sections 514 and 517 under the Goal 3 program). Table 4.1 summarizes the 80th percentile deflections used for overlay design. Per CTM 356, the estimated tolerable deflection was 355 microns, which yielded an estimated percent reduction in deflection of 52 and 60 percent for the drained and undrained sections, respectively.

The final overlay thicknesses were chosen to reduce deflections to the tolerable deflections are summarized in Table 4.2. Details of the thickness designs are presented in the construction report for the Goal 3 test program.(*10*)

Table 4.1 80th Percentile Deflections for Overlay Design

Section	80th Percentile Deflection (microns)		
	Dynaflect	FWD	RSD
500 Drained	203	229	737
501 Undrained	254	584	889

Table 4.2 Final Overlay Design Thicknesses

Test Section	Overlay Thickness, mm	Overlay Material
514/500	75*	Dense Graded AC
515/502	37	Asphalt Rubber Hot Mix
517/501	75	Dense Graded AC
518/503	37	Asphalt Rubber Hot Mix

* Includes 15-mm of 9.5-mm maximum size aggregate asphalt concrete to "level up" the rutted pavement.

4.1.1 Comparison of Estimated and Actual Reduction in Deflections After Overlay

A summary of the actual 80th percentile deflections obtained under the RSD before and after overlay is presented in Table 4.3. The 80th percentile deflections obtained with the overlays at the start of HVS testing show reductions in deflections of 60 percent for the drained sections and 52 percent for the undrained sections, with the drained sections having initial deflections near or within the estimated tolerable deflection. Section 514 was within the tolerable deflections. Section 515 had deflections 4 percent higher than the tolerable limit. The undrained sections had deflections 20 to 34 percent higher than the tolerable deflection of 355 microns.

The results indicate that thicker overlays would be required for these undrained sections to decrease the deflections to the tolerable deflection according to CTM 356.

Table 4.3 RSD 80th Percentile Deflections before and after Overlay

Test Section	Surface Deflections, microns		Percent Reduction after overlay
	Before Overlay (After Goal 1 Trafficking Complete)	After Overlay (Before HVS Goal 3 Trafficking Begun)	
514/500 DGAC	774	330	57
515/502 ARHM-GG	944	368	61
517/501 DGAC	906	426	53
518/503 ARHM-GG	974	478	50

4.1.2 Performance Evaluation

For use in performance evaluations, the number of loads applied by the HVS, the 80- and 100-kN dual-wheel loads (160- and 200-kN axle loads, respectively) are converted to equivalent 80-kN single axle loads (ESALs) using a load equivalency exponent of 4.2 per Caltrans. The number of ESALs produced by these loads is computed as:

$$ESALs = N_{Load}\left(\frac{Axle\ Load}{80kN}\right)^{4.2} \quad \textbf{(4.1)}$$

where, N_{Load} is the number of applications under a given load level, and *Axle Load* is two times the load on the dual-wheels of the HVS. Table 4.4 shows the approximate number of 80-kN ESALs applied to the four pavement sections using the 4.2 load equivalency exponent.

Table 4.4 Applied ESALs

Section		Load Applications (thousands)			ESALs Applied during Goal 3 (millions)	ESALs Applied during Goal 1 and Goal 3 (millions)
		40kN	80kN	100kN		
Drained	514 DGAC	172	145	1350	66	178
	515 ARHM-GG	128	218	2065	101	218
Undrained	517 DGAC	148	179	2019	98	157
	518 ARHM-GG	116	110	1406	68	149

The deflection-based performance was evaluated in terms of the RSD deflections at a crack density of 2.5 m/m^2. The number of HVS load applications, the corresponding number of ESALs and the RSD 80th percentile elastic deflections at a crack density of 2.5 m/m^2 are summarized in Table 4.5.

Table 4.5 Deflections and Load Repetitions to Crack Density of 2.5 m/m^2

Section	80th Percentile RSD Deflections (microns)	HVS Load Applications (thousands)	Estimated ESALs using 4.2 factor (millions)
514 DGAC	901	890	29.6
515 ARHM-GG	696	1,190	43.8
517 DGAC	785	1,700	67.7
518 ARHM-GG	846	750	26.6

Table 4.5 shows that the performance of all the overlays exceeded the expected performance of 1.0 million ESALs. The average ESALs at a cracking density of 2.5 m/m^2 are similar for Sections 514 (drained, DGAC) and 518 (undrained, ARHM-GG), followed by Section 515 (drained, ARHM-GG) and Section 517 (undrained, DGAC). The results do not show a clear trend indicating that a specific type of section (drained or undrained) with a specific overlay strategy (DGAC or ARHM-GG) is a superior pavement. However, before cracking appeared, the RSD deflections on the drained sections were similar and larger than the RSD deflections on the undrained sections, as shown in Figure 3.51–3.54.

4.1.3 Statistical Analysis

The conditions of the pavement before overlay and the thickness of the overlays can explain the performance of the overlays to a given level of surface cracking. The aforementioned can be express as:

$$Overlay\ Performance \approx Condition\ Before\ Overlay + Overlay\ Thickness \quad \textbf{(4.2)}$$

The condition before overlay can be established in terms of deflections, if deflections are used to determine overlay requirements. The overlay thickness variable must be able to implicitly consider type of overlay by incorporating a structural equivalency factor. The

following linear model mathematically express the relation between overlay performance and the variables affecting overlay performance:

$$ESALs\ to\ failure = a * def + b * t * EF + c \quad \textbf{(4.3)}$$

where, *a*, *b*, and *c* are linear regression constants, *ESALs* is the number of equivalent single axle loads to failure, *def* is the measured deflections before overlay, *t* is the thickness of the overlay, and *EF* is the structural factor for the overlay type.

Current Caltrans design procedures indicate that ARHM-GG overlay thicknesses are typically half of the equivalent DGAC overlay. Based on this, an equivalent structural factor *EF* of 1 and 2 can be assumed for the DGAC and ARHM-GG overlays, respectively.

Using the results of the Goal 1 and Goal 3 testing programs summarized in Tables 4.2–4.5, the resulting model for the performance of the overlay in terms of deflection is:

$$\begin{aligned} &ESALs\ to\ failure\ (2.5m/m^2\ cracl\ density) = 256\text{-}0.85 * def + 6.72 * t * EF \\ &R\text{-}squared = 0.780 \qquad\qquad SEE^* = 15.1\ million\ ESALs \end{aligned} \quad \textbf{(4.4)}$$

$^*SEE$ = Standard Error of Estimate

where *ESALs* is millions of equivalent single axle loads, *def* is the 80th percentile RSD deflections in microns at 20ºC before overlay, and *t* is the thickness of the overlay in mm.

4.1.4 Verification of ARHM-GG Equivalent Overlay Thickness

Per Caltrans design procedures, the ARHM-GG overlay thicknesses are typically half of the equivalent DGAC overlay thickness. Using Equation 4.3, it is possible to find a mathematical solution for the equivalent factor *EF* for the ARHM-GG overlay so that the R-squared value of the model represented in Equation 4.3 is maximized. The results indicate an *EF* for the ARHM-GG overlay of 2.14, which yielded an R-squared value of 1.0. The analysis

shows that the half thickness approach used in the design of the ARHM-GG overlay for the Goal 3 sections is appropriate.

4.2 Moduli Backcalculated from Elastic Deflections

The moduli of the various pavement layers were back-calculated from in-depth elastic deflections obtained with the MDDs and from FWD data collected before and after HVS testing.

4.2.1 Moduli from In-Depth Deflections

MDD peak in-depth elastic deflections obtained at the surface or near the surface, the top of the AB, the top of the ASB, and the top of the subgrade were used to estimate effective layer moduli of the asphalt bound layers (including the ATPB), aggregate base, aggregate subbase, and subgrade. The process was performed using an elastic layer program that back-calculates moduli from in-depth elastic deflections. The results of the process are presented in Figures 4.1–4.4.

Figures 4.1–4.4 show the progressive decrease of the effective moduli of the AC, AB, ASB, and SG layers with HVS trafficking under a 40-kN test load. The reductions in moduli were significant when the 80-kN traffic loads were applied and continued to decrease under the 100-kN test loads until they reached an asymptotic value.

Table 4.6 summarizes the effective asphalt moduli for the Goal 3 sections at the beginning of testing, at a crack length density of 2.5 m/m^2, and at the end of HVS testing. The effective AC moduli for the drained sections included the overlay, the two lifts of dense graded asphalt concrete, and the ATPB layer. Under the 40-kN test load, the initial effective AC moduli of the sections with the DGAC overlay are higher than those with the ARHM-GG overlay. At a crack length density of 2.5 m/m^2, the effective AC moduli in Sections 514, 515, and 517 were

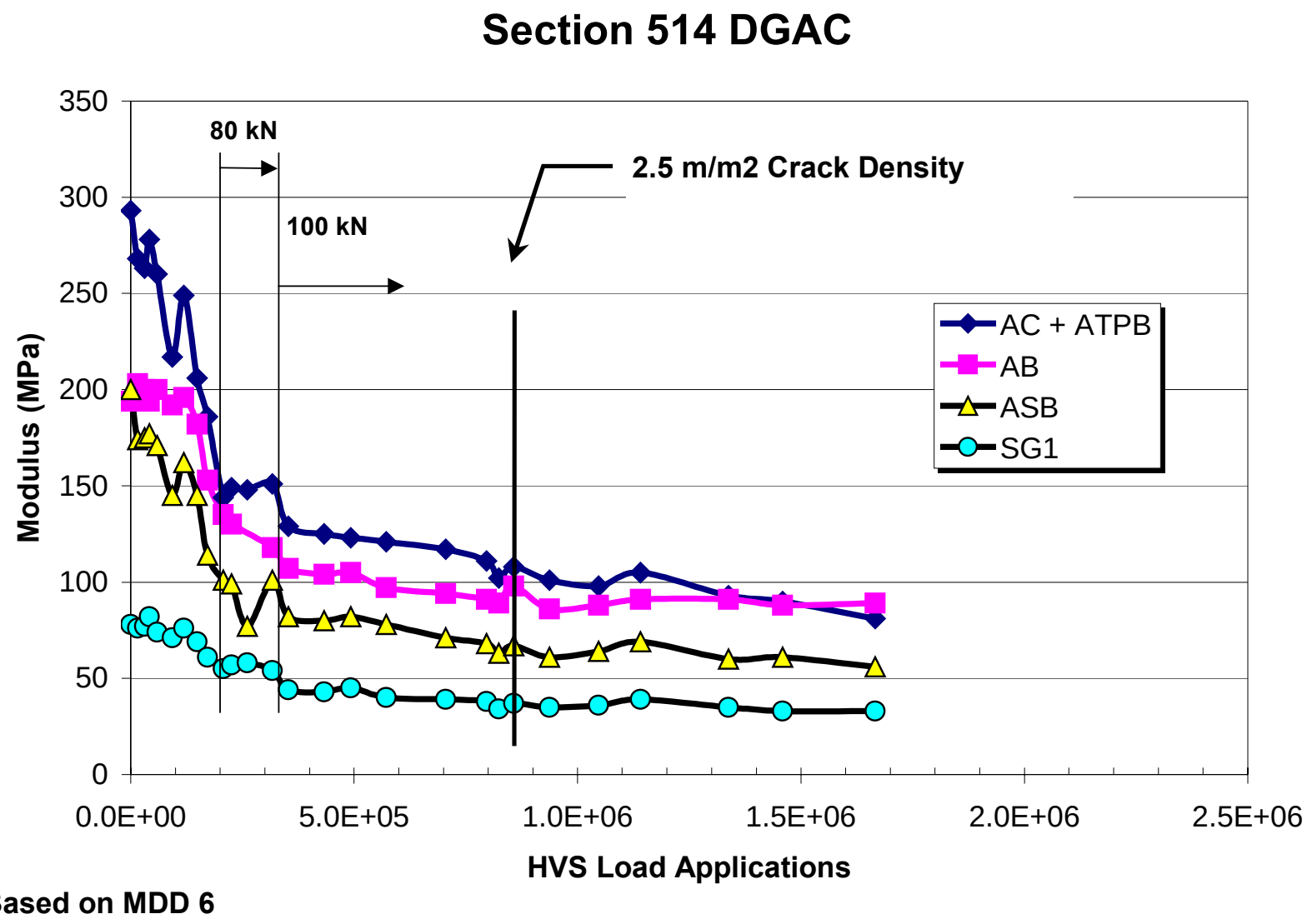

Figure 4.1. Effective moduli for Section 514 (drained, DGAC overlay), 40-kN test load.

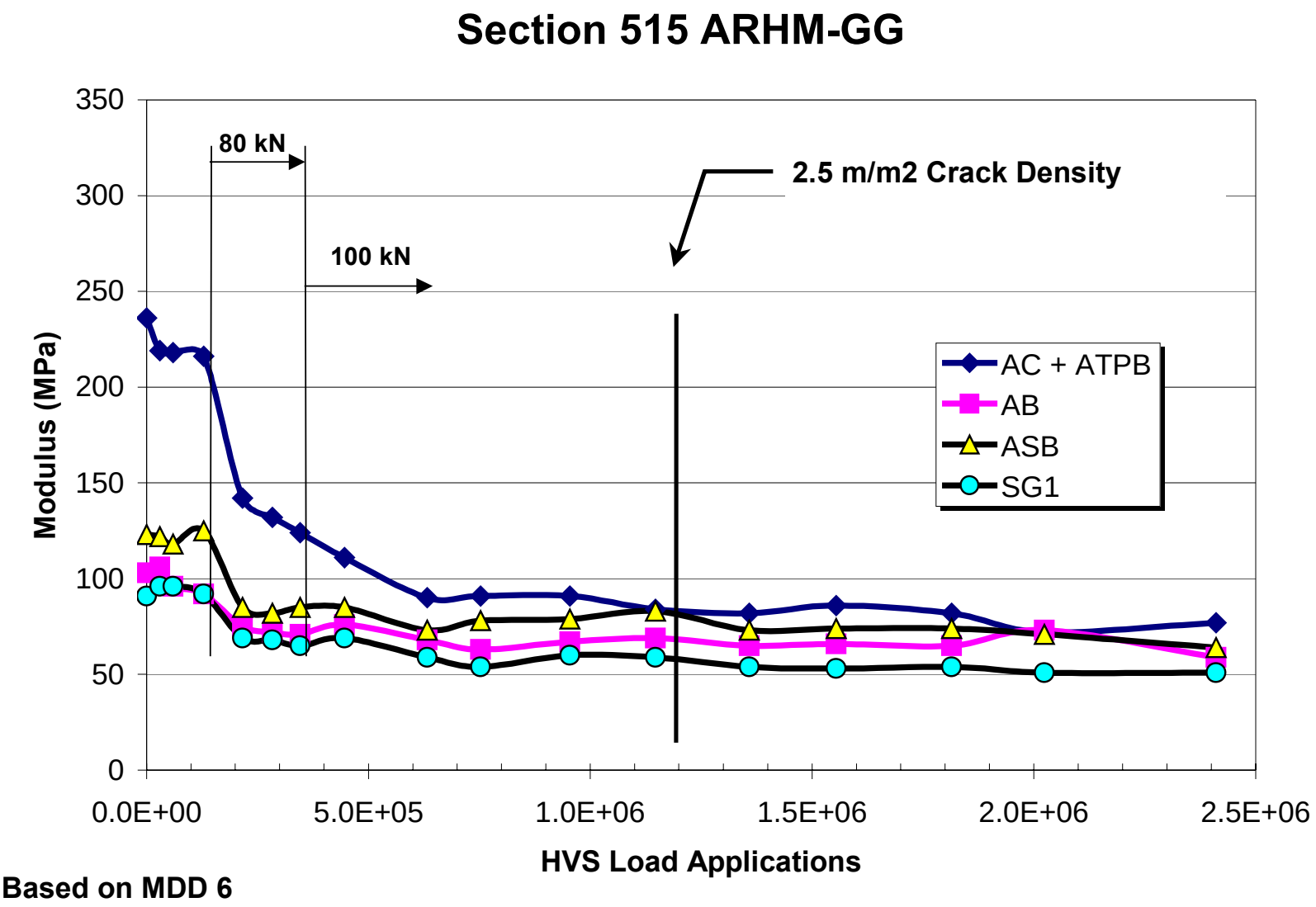

Figure 4.2. Effective moduli for Section 515 (drained, ARHM-GG overlay), 40-kN test load.

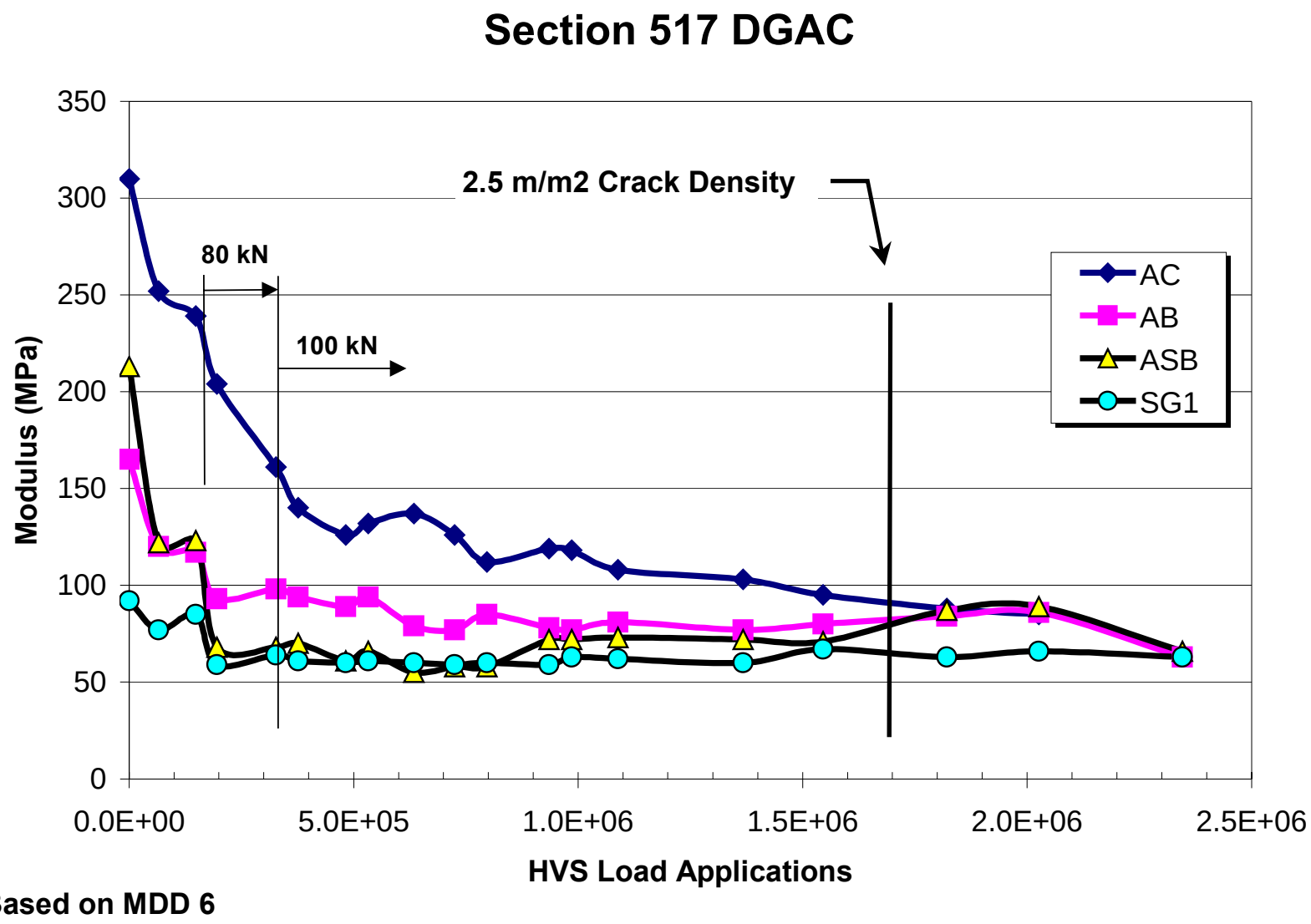

Figure 4.3. Effective moduli for Section 517 (undrained, DGAC overlay), 40-kN test load.

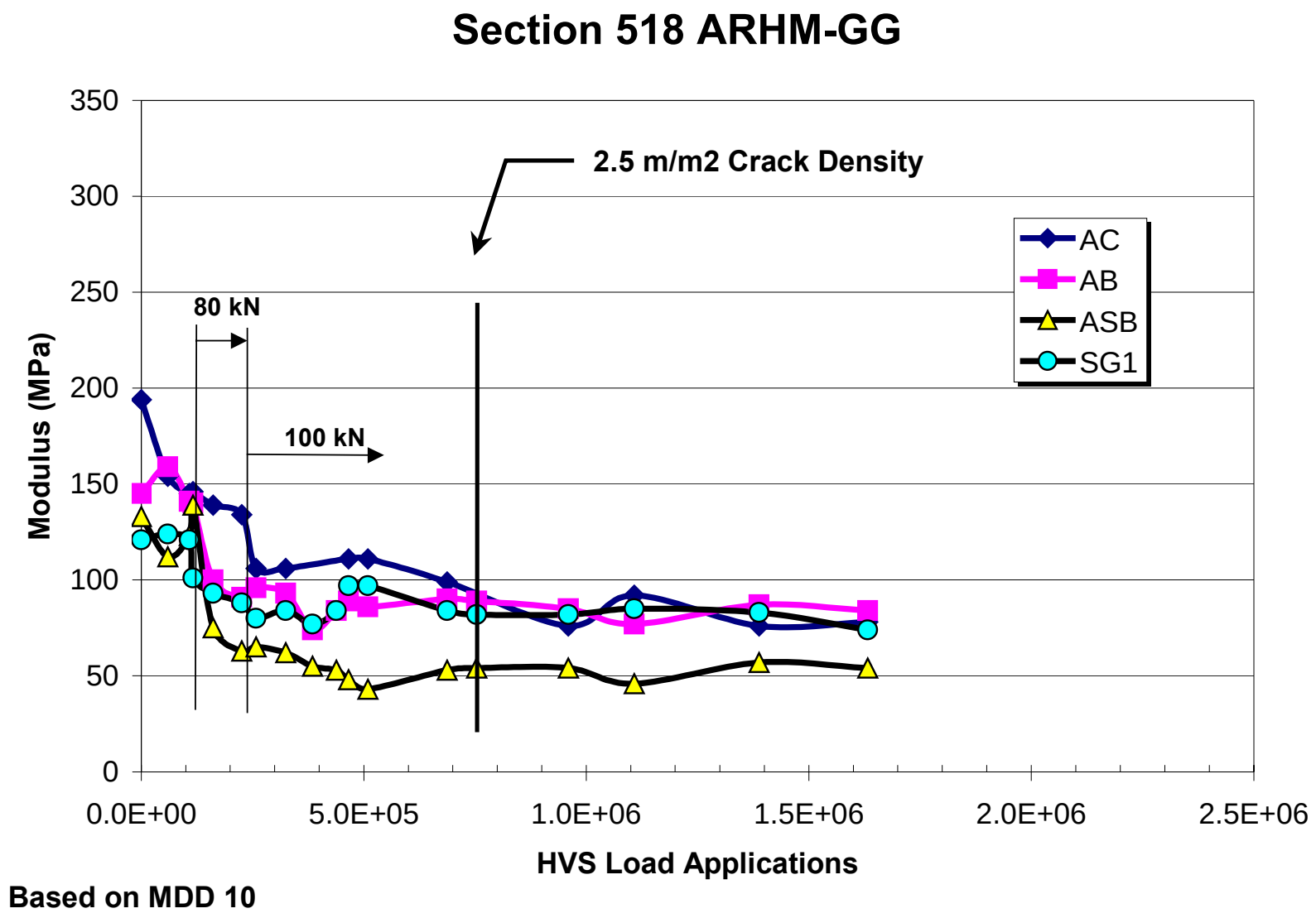

Figure 4.4. Effective moduli for Section 518 (undrained, ARHM-GG overlay), 40-kN test load.

reduced by approximately 65 percent of the initial moduli. Section 518, which had the lowest initial effective AC moduli, had a reduction of 48 percent.

Table 4.6 Effective Back-Calculated AC Moduli under 40- and 100-kN Test Loads

Section	Effective AC Moduli (MPa)				
	After 10 Applications	At a Crack Density of 2.5 m/m^2		At End of HVS Testing	
	40-kN load	40-kN load	100-kN load	40-kN load	100-kN load
514 DGAC	293	108	388	81	325
515 ARHM-GG	236	83	330	77	330
517 DGAC	310	94	300	89	280
518 ARHM-GG	194	99	260	74	224

Under the 100-kN load test, the effective AC moduli were about 3 times higher than those under the 40-kN test load. The asymptotic values for the effective AC moduli were from 80 to 100 MPa under the 40-kN test load and from 220 to 330 MPa under the 100-kN test load. Figures 4.5–4.8 show the effective moduli under the 100-kN test load.

Effective moduli for the unbound materials varied with HVS load applications. Figures 4.1–4.4 show that high effective moduli were obtained at the initial stage of traffic. As the effective moduli of the asphalt bound materials decreased, the effective moduli of the unbound materials also decreased. The average effective moduli for each unbound layer at the asymptotic values under the 40-kN and 100-kN test loads are presented in Table 4.7. The table shows that the effective moduli of the AB increased as the test load was increased, and the effective moduli of the ASB and subgrade decreased as the test load was increased.

Table 4.7 Effective Moduli of Unbound Materials

Section	Effective Moduli of Unbound Materials (MPa)					
	40-kN Test Load			100-kN Test Load		
	AB	ASB	Subgrade	AB	ASB	Subgrade
514 DGAC	91	65	36	144	56	25
515 ARHM-GG	66	74	55	76	61	46
517 DGAC	80	71	62	114	65	36
518 ARHM-GG	86	38	66	148	41	56

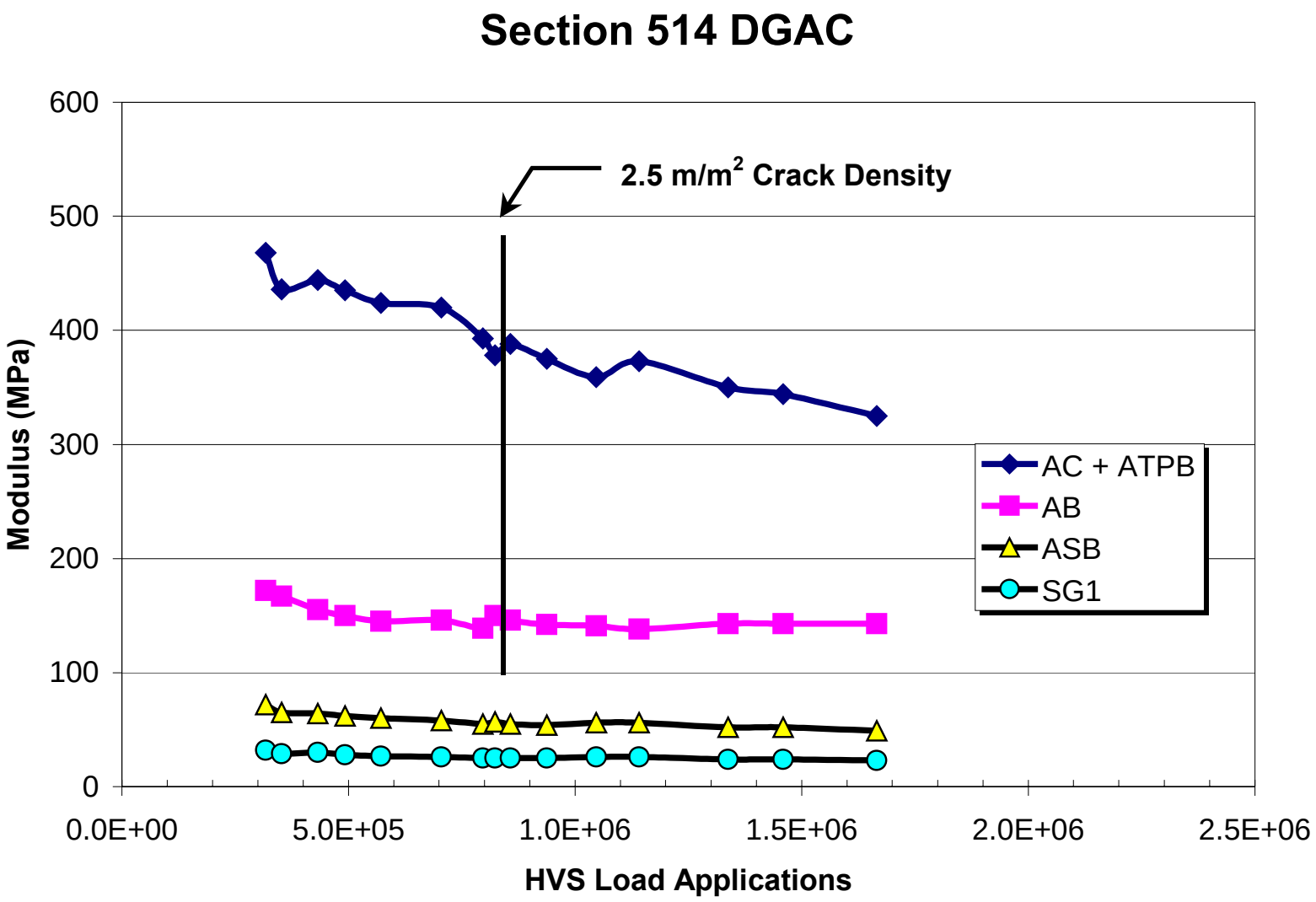

Figure 4.5. Effective moduli for Section 514 (drained, DGAC overlay), 100-kN test load.

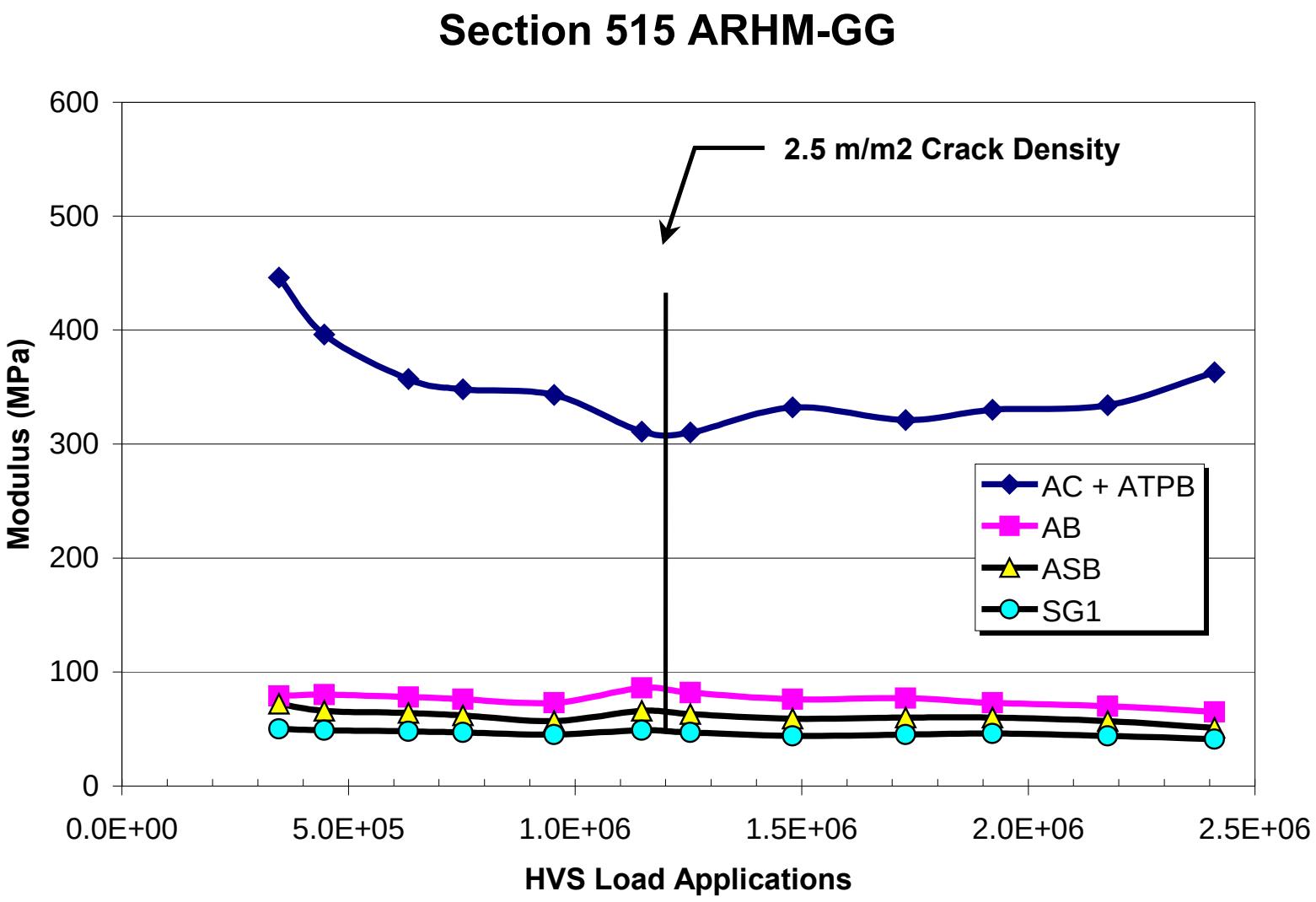

Figure 4.6. Effective moduli for Section 515 (drained, ARHM-GG overlay), 100-kN test load.

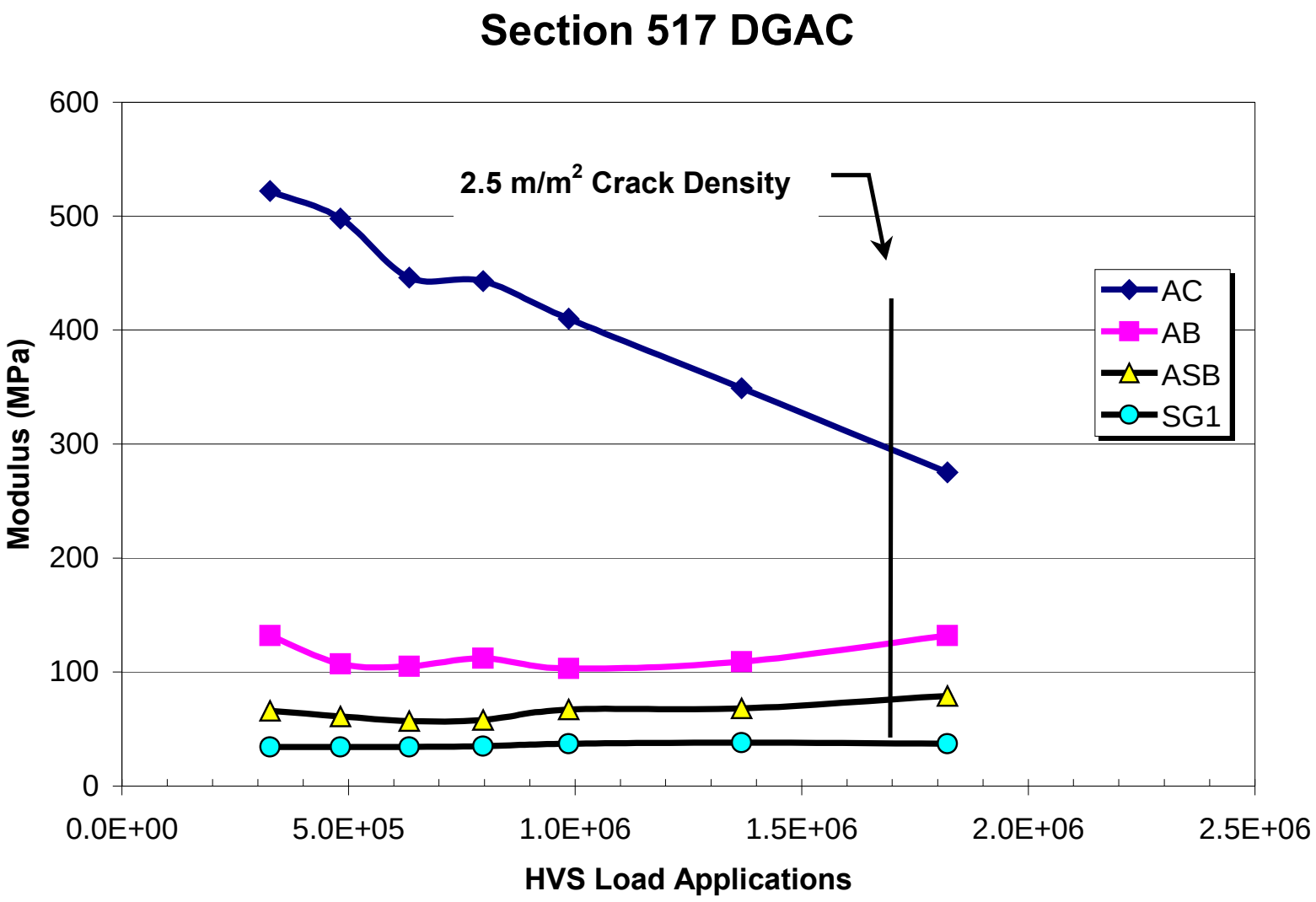

Figure 4.7. Effective moduli for Section 517 (undrained, DGAC overlay), 100-kN test load.

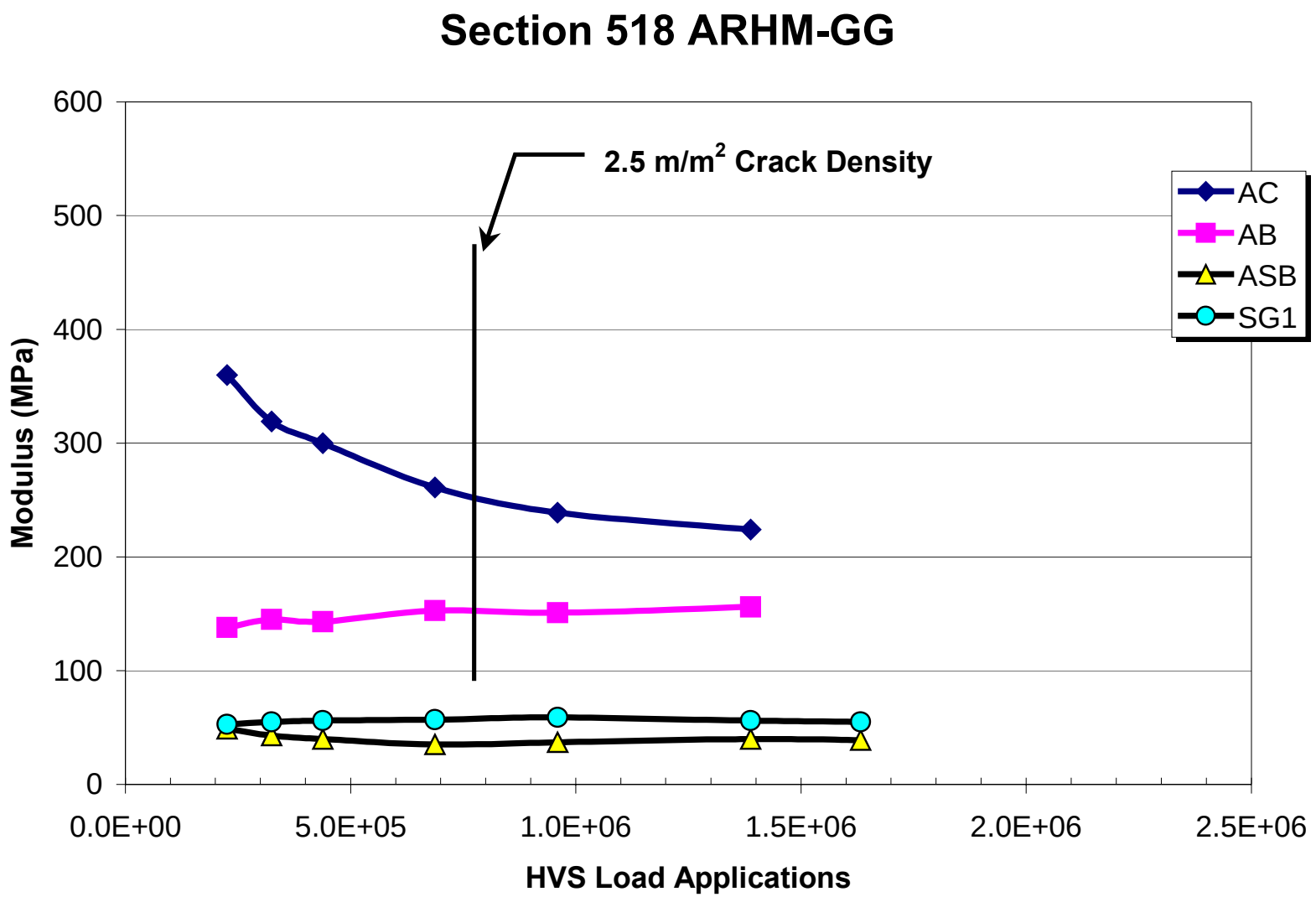

Figure 4.8. Effective moduli for Section 518 (undrained, ARHM-GG overlay), 100-kN test load.

An increase in the effective moduli of the AB may be produced by an increase in the stress state in this layer. The decrease in the effective stiffness of the ASB can be associated with a reduction in the stress state in this layer. The elastic layer theory could not be used to examine the stress state in these layers because it assumes that the granular layers are continuous materials that can resist tension.

4.2.2 Moduli from FWD Deflections

The FWD deflections reported in Chapter 3 were used to determine layer moduli in the test sections. Layer moduli were back-calculated using the ELMOD program.(*22*) Average moduli are summarized in Table 4.8. In this analysis, the various layers in the pavement sections were simplified into a three layer system in which the asphalt-bound layers were combined in one layer, the base and subbase another layer, and the subgrade was the semi-infinite layer. The combined layer thicknesses were obtained from the trench data summarized in Table 3.10. A Poisson's ratio of 0.35 was assumed for all layers.

The data illustrate the effect of temperature on the AC moduli. The moduli obtained in January 1998 during lower temperatures are higher than those back-calculated from the deflections obtained in April 1997 when the temperatures were higher. (See Sections 3.1.1 and 3.1.2 for discussion of air and pavement temperatures during the tests.)

The moduli obtained from FWD deflections are higher than those obtained from the MDD deflections with a slow moving HVS test wheel. The rates of loading produced by these two methods are different, and in turn affect the material properties of the asphalt concrete. The MDD measurements reflect a slow moving load deflection with the wheel load moving towards the measuring point at a speed of 8 km/h. The FWD applies a transient dynamic load pulse of 25 to 35 ms duration.

Table 4.8 Moduli Back-Calculated from FWD Deflections

Section	Moduli in MPa					
	Asphalt Bound		Aggregate Bases		Subgrade	
	Average	Standard Deviation	Average	Standard Deviation	Average	Standard Deviation
April 27, 1997						
514	3393	623	279	61	82	5
515	2997	698	331	36	131	12
517	2850	323	407	33	85	7
518	1958	194	249	25	118	15
January 6, 1998						
514	1660	519	161	37	44	8
515	6074	1527	465	73	109	13
517	6054	387	570	50	84	9
518	4212	431	388	34	88	8
May 11, 1999						
517	3151	964	413	113	197	14
518	1997	286	109	25	175	10

Higlighted data in the table are back-calculated moduli from after HVS testing.

4.3 Pavement Response

Pavement responses are used in mechanistic-based procedures to estimate pavement life. The back-calculated layer moduli discussed in Section 4.2 are used as material property inputs to an elastic layer program that calculates pavement responses. The tensile strain at the bottom of the combined AC layer and the vertical strain at the top of the subgrade are the pavement responses of interest. In current mechanistic approaches, the tensile strain at the bottom of the AC and the compressive vertical strain on the top of the subgrade are used to estimate pavement fatigue life and pavement rutting, respectively.

Table 4.9 summarizes tensile strains under the 40-kN and 100-kN loads. Under the 40-kN load, the tensile strains at the bottom of the asphalt bound layers are largest for the sections with the ARHM-GG overlay. Under the 100-kN load, tensile strains at the beginning of the 100-kN traffic loading were also largest for the sections with the ARHM-GG overlay. At the end of

testing, the sections had tensile strains greater than 560 microstrain under the 40-kN load and greater than 700 microstrain under the 100-kN load.

Table 4.9 Computed Tensile Strain at the Bottom of the Asphalt-Bound Layers under the 40-kN and 100-kN Test Loads

Test Load	Stage of Traffic	Strains ($\times 10^{-6}$)			
		Drained Sections		Undrained Sections	
		514 DGAC	515 ARHM-GG	517 DGAC	518 ARHM-GG
40 kN	Beginning	238	403	315	443
	End	560	821	721	638
100 kN	Beginning	581	847	737	860
	End	744	1048	850	812

Table 4.10 summarizes computed vertical compressive strains on top of the subgrade under the 40-kN and 100-kN loads. At the beginning of HVS testing, vertical strains under the 40-kN test load were from 260 to 360 microstrain. At the completion of the HVS testing the drained sections had a higher increase in the vertical strain than the undrained sections. Under the 100-kN load, vertical strains ranged from 1000 to 1800 microstrain.

Table 4.10 Computed Vertical Strain at the Top of the Subgrade Layers under the 40-kN and 100-kN Test Loads

Test Load	Stage of Traffic	Strains ($\times 10^{-6}$)			
		Drained Sections		Undrained Sections	
		514 DGAC	515 ARHM-GG	517 DGAC	518 ARHM-GG
40 kN	Beginning	306	338	264	360
	End	815	675	439	510
100 kN	Beginning	1276	1121	1245	1026
	End	1775	1387	1217	1026

Pavement responses under the 40-kN plate load FWD tests are summarized in Table 4.11. The table shows the effect of temperature in the pavement responses. Lower tensile strains and vertical compressive strains were obtained for the colder temperatures of January 1998. The data presented in Table 4.11 also shows the effect of rate of loading on the calculated responses.

Lower strain responses were obtained from the FWD than from the MDD measurements with the slow moving wheel.

Table 4.11 Pavement Responses Before and After Testing under FWD Testing

Section	Test No.	Test Date	Strain ($\times 10^{-6}$)	
			AC Tensile	Subgrade Compressive
Before HVS Testing				
514 DGAC	1	04/27/97	81.5	183.5
515 ARHM-GG	1	04/27/97	91.9	152.1
	2	01/06/98	55.7	126.8
517 DGAC	1	04/27/97	84.6	131.7
	2	01/06/98	49.8	99.2
518 ARHM-GG	1	04/27/97	166.6	155.4
	2	01/06/98	98.8	139.2
After HVS Testing				
514 DGAC	1	01/06/98	156.4	351.3
517 DGAC	1	05/11/99	78.5	82.6
518 ARHM-GG	1	05/11/99	237.9	126.6

The results demonstrate the effect of temperature and rate of loading in the tensile strain and compressive strain responses. The proper characterization of the material to obtain pavement responses is very important for the prediction of pavement life.

5.0 SUMMARY, CONCLUSIONS, AND RECOMMENDATIONS

5.1 Summary

This report describes the results of the Goal 3 HVS tests conducted on four pavement test sections at the Institute of Transportation Studies Pavement Research Center located at the Richmond Field Station at the University of California, Berkeley. The main objective of the CAL/APT Goal 3 Program was the evaluation of the performance of two rehabilitation strategies: 1) conventional Dense Graded Asphalt Concrete (DGAC) overlay, and; 2) Asphalt Rubber Hot Mix Gap-Graded (ARHM-GG) overlay.

The thickness of the DGAC overlay was calculated based on deflection measurements following Caltrans Test Method 356. The ARHM-GG overlay thickness was half that of the DGAC as per Caltrans procedures. These overlays represent typical pavement structures currently in use throughout California.

Goal 3 HVS Test traffic was initiated in September 1997 on Section 514 and completed in May 1999 on Section 518. Table 5.1 summarizes the number of load applications and estimated number of ESALs on the pavement sections.

Table 5.1 Total HVS Load Repetitions and ESALs Applied

Section		Load Applications (thousands)				ESALs Applied (millions)
		40 kN	80 kN	100 kN	Total	
Drained	514 DGAC	172	145	1350	1667	66
	515 ARHM-GG	128	218	2065	2411	101
Undrained	517 DGAC	148	179	2019	2346	98
	518 ARHM-GG	116	110	1406	1632	68

During HVS testing, load-associated cracks and surface rutting were present on the pavement sections. The pavement sections failed by reflection cracking, with crack length densities exceeding the failure criterion of 2.5 m/m^2. Table 5.2 summarizes the number of HVS load repetitions and ESALs associated with the first cracks (0.5 m/m^2) and with the amount of cracks present at the failure criterion of 2.5 m/m^2.

Table 5.2 Load Applications to Crack Density

Section		Load Applications to Crack Density			
		0.5 m/m^2 Crack Density		2.5 m/m^2 Crack Density	
		HVS Repetitions ($\times 10^3$)*	ESALs ($\times 10^6$)*	HVS Repetitions ($\times 10^3$)*	ESALs ($\times 10^6$)*
Drained	514 DGAC	648	11	890	30
	515 ARHM-GG	810	22	1,190	44
Undrained	517 DGAC	1,060	35	1,700	68
	518 ARHM-GG	492	13	750	27

* The non-linearity in the relationship of HVS repetitions to ESALs is explained in Section 4.1.2.

The average maximum rut depth in the sections did not exceed the criterion of 13 mm. Rutting was attributed to all pavement layers with degrees of rutting contribution varying depending on section type (drained or undrained) and overlay strategy (DGAC or ARHM-GG).

The estimated number of ESALs carried by the overlays exceeds the estimated pavement life of one million ESALs (Traffic Index of 9) assumed during the overlay design activities.

5.2 Conclusions

The following conclusions result from the HVS tests and associated analyses on the test sections:

1. Deflection reductions predicted by CTM 356 were adequate for the drained sections but greater than actually occurred for the undrained sections. The data show that the

undrained sections before overlay had higher cracking density than the drained sections.

2. The overlay thicknesses reduced the elastic deflections on the previously cracked sections to levels near the estimated tolerable deflection in the drained sections and to 20 to 30 percent higher than the estimated tolerable deflection in the undrained sections.
3. Based on the load equivalency exponent of 4.2 per Caltrans, both overlay strategies significantly exceeded the expected performance of 1.0 million ESALs. The significant difference between overlay design and HVS testing is that the conditions under the HVS are ideal—construction variability is minimal, environmental conditions include constant temperature with minimal moisture effects, load and tire pressure conditions are controlled, and only two overlay mixes were tested.
4. The results at the cracking failure criterion of 2.5 m/m^2 do not show a clear trend indicating that a specific type of section (drained or undrained) with a specific overlay strategy (DGAC or ARHM-GG) is a superior pavement.
5. Before cracking appeared, the RSD deflections on the drained sections were lower than the undrained sections regardless of overlay type.
6. Statistical analyses of the HVS data indicate that the overlay performance is inversely related to the elastic deflections before overlay and directly related to overlay thickness.
7. The statistical analyses also verify the Caltrans procedure for ARHM-GG overlay design thickness as half the equivalent the DGAC overlay thickness. Based on the

test data, the ARHM-GG overlay has the same performance as a DGAC overlay that is 2.1 times thicker.

8. The elastic deflections obtained for determining overlay requirements are significantly influenced by the rate of loading and temperature. Higher deflections are obtained under slow moving wheels and warmer temperatures. Given that elastic deflections are used to back-calculate layer moduli in order to estimate pavement responses and predict pavement performance, these pavement responses are also significantly influenced by the rate of loading and temperature.
9. The mechanistic analyses indicate that the granular base and subbase layers and the subgrade exhibit a stress dependency response. The aggregate base tended to stiffen and the subgrade tended to soften under increasing stress levels. The non-linear response of these layers was evident during HVS testing.
10. Plastic deformation was not a critical issue in the Goal 3 sections, but the results indicated that the overlay and the ATPB layers significantly contributed to surface rutting. The test sections with the DGAC overlay had more rutting than the sections with the ARHM-GG overlay. A possible influence for this is the thickness of the DGAC overlay: it was thicker than the ARHM-GG overlay, and therefore contained more material not previously hardened by traffic and aged by the environment.
11. The plastic deformation of the unbound materials was not significant. However, the data indicate that the plastic deformation of the unbound materials continued at approximately the same rate as was observed at the end of trafficking during the Goal 1 testing program. The assumption that these layers behave as if they were

untrafficked after overlay is not correct. These results are important for addressing the rutting potential of sections in need of rehabilitation.

5.3 Recommendations

The following recommendations are made to Caltrans based on the results and conclusions presented in this report:

1. Evaluate the proportion of overlays being placed by Caltrans that fail due to reflection cracking instead of fatigue cracking. Develop criteria for determining when reflection cracking is expected to occur, based on improved methods of pavement characterization. These criteria will likely include
   a. the type and severity of cracking in the existing pavement,
   b. the climate region,
   c. expected traffic,
   d. stiffnesses and thicknesses of existing pavement layers, with stiffnesses determined from deflections collected using Falling Weight Deflectometers and back-calculation using methods similar to those used in Chapter 4 of this report, and thicknesses determined using the Dynamic Cone Penetrometer and a limited number of asphalt concrete cores.
2. Require the use of Life Cycle Cost Analysis (LCCA) for selection of overlay type for each project. If the failure type is determined to likely be reflection cracking, and life cycle costing indicates that ARHM-GG has a lower life cycle cost, then ARHM-GG overlays should be required in place of DGAC. A simplified process for LCCA needs to be developed and made available to Caltrans pavement designers, and Maintenance programmers.

3. Investigate the use of recycled ARHM-GG in hot mix, or for use as shoulder backing or other pavement material.
4. Develop QC/QA processes for ARHM-GG to reduce the air-void contents to those regularly obtained with DGAC.
5. Continue research into the process of reflection cracking, and develop better procedures for determining the appropriate thickness of DGAC and ARHM-GG overlays.
6. Move towards the use of mechanistic-empirical methods to select overlay thickness for fatigue cracking, and away from the current method that is based on different pavement structures from those currently typically encountered by pavement designers.

6.0 REFERENCES

1. Maintenance Program, Maintenance and Transportation Programming. *Ten-Year State Highway System Rehabilitation Plan, 1997-1998 through 2007-2008*. California Department of Transportation, Sacramento, February 1, 1998.

2. Shatnawi, S. 1999. *Performance of Asphalt Rubber Mixes in California*. Submitted to the International Journal of Road Materials and Pavement Design, Hermes Science Publications, Paris, France, July.

3. Maintenance Program, Pavement Management Information Branch. *1997 State of the Pavement*. California Department of Transportation, Sacramento, November, 1999.

4. Maintenance Program, Pavement Management Information Branch. *1995 State of the Pavement*. California Department of Transportation, Sacramento, November 1997.

5. Office of Office Engineer, Division of Construction. *1993 Contract Cost Data*. California Department of Transportation, Sacramento.

6. Rust, F., L. du Plessis, B. Verhaeghe and J. Grobler, Heavy Vehicle Simulator Testing of Trial Sections for Caltrans, Report prepeared for Caltrans, DPVT C/255, SCIR, Pretoria, South Africa, October, 1993.

7. Harvey, J. and L. Popescu, "Rutting of Caltrans Asphalt concrete and Asphalt-Rubber Hot Mix Under Different Wheels, Tires and Temperatures – Accelerated Pavement Testing Evaluation", Draft Report for the California Department of Transportation, Institute of Transportation Studies, University of California, Berkeley, January, 2000.

8. *Standard Tests*, California Department of Transportation, Sacramento, 1995.

9. Division of New Technology, Materials, and Research. *Design Guide for ARHM-GG (Interim)*. California Department of Transportation, Sacramento, February 28, 1992.

10. Harvey, J., N. Coetzee and L. Louw, Design and Construction of CAL/APT Goal 3 DGAC and ARHM-GG Overlays, and Review of Caltrans Design and Construction Methods, Draft Report prepared for California Department of Transportation. CAL/APT Program, Pavement Research Center, Institute of Transportation Studies, University of California, Berkeley, December, 1999.

11. University of California Berkeley Pavement Research Center; Dynatest Consulting, Inc.; Division of Roads and Transport Technology, CSIR. 1997. *Test Plan for CAL/APT Goal 3*. Test Plan prepared for the California Department of Transportation, 1997.

12. Harvey, J., L. du Plessis, F. Long, S. Shatnawi, C. Scheffy, B. Tsai, I, Guada, D. Hung, N. Coetzee, M. Reimer, and C. L. Monismith, Initial CAL/APT Program: Site Information, Test Pavement Construction, Pavement Materials Characterizations, Initial CAL/HVS Test

Results, and Performance Estimates, Pavement Research Center, CAL/APT Program, Institute of Transportation Studies, University of California, Berkeley, June 1996.

13. Harvey, J., L. du Plessis, F. Long, J. Deacon, I, Guada, D. Hung, and C. Scheffy, CAL/APT Program: Test Results from Accelerated Test on Pavement Structure Containing Asphalt Treated Permeable Base (ATPB)—Section 500RF, Pavement Research Center, CAL/APT Program, Institute of Transportation Studies, University of California, Berkeley, June 1997.

14. Harvey, J., J. Prozzi, J. Deacon, D. Hung, I. Guada, L. du Plessis, F. Long and C. Scheffy, CAL/APT Program: Test Results from Accelerated Pavement Test on Pavement Structure Containing Aggregate Base (AB) - Section 501RF, Report for the California Department of Transportation, Institute of Transportation Studies, University of California, Berkeley, April, 1999 (Draft submitted September, 1997).

15. Harvey, J., I, Guada, C. Scheffy, L. Louw, J. Prozzi, and D. Hung, CAL/APT Program: Test Results from Accelerated Pavement Test on Pavement Structure Containing Asphalt Treated Permeable Base—Section 502CT, Draft Report, Pavement Research Center, CAL/APT Program, Institute of Transportation Studies, University of California, Berkeley, February 1998.

16. Harvey, J., D. Hung, J. Prozzi, L. Louw, C. Scheffy, and I. Guada, CAL/APT Program: Test Results from Accelerated Pavement Test on Pavement Structure Containing Untreated Aggregate Base—Section 503RF, Draft Report, Pavement Research Center, CAL/APT Program, Institute of Transportation Studies, University of California, Berkeley, December 1997.

17. de Beer, M. and C. Fisher, Contact Stresses of Pneumatic Tires Measured with the Vehicle-Road Surface Pressure Transducer Army (VRSPTA) System for the University of California at Berkeley (UCB) and The Nevada Automotive Test Center (NATC). Vols. 1 and 2., Transportek, CSIR, South Africa, June 1997.

18. Ardila-Coulson, M., D. Coulson, and P. Sebaaly, Extent of Use and Performance Traits of Super-Single Tires, Draft report prepared for the National Cooperative Highway Research Program, University of Nevada, Reno, February, 1998.

19. Bell, C., and S. Randhawa, Truck Tire Issues: Evaluation of Impacts of High Pressure Tires and Single-Tired Axles in Oregon, Transportation Research Report 92-17, Transportation Research Institute, Oregon State University, Corvallis, November, 1992.

20. Scheffy, C., E. Diaz. “Asphalt Concrete Fatigue Crack Monitoring and Analysis Using Digital Image Analysis Techniques,” *Proceedings from the Accelerated Pavement Testing International Conference*. Reno, Nevada, October 18-20, 1999.

21. Optimas Corporation. *Optimas Program Version 5.2*, Bothell, Washington, November 1995.

22. Dynatest Engineering A/S. *ELMOD/ELCON Evaluation of Layer Moduli and Overlay Design User’s Manual.* Denmark, March 1990.

7.0 TEST PLANS

HVS Test Plan	Updated 1/10/97	514RF (Overlay of 500RF)
SECTION DESCRIPTION	Drained section with 15-mm patch and 60-mm DGAC overlay	
TIRE PRESSURE	720 kPa (105 psi)	
TRAFFIC LOAD	40 kN, 80 kN, 100 kN	
TIRE TYPE	Radial dual	
TEMPERATURE CONTROL	16-24°C	

POSITION OF THERMOCOUPLES	Position 4, 8, 12	Depth 0, 50, 134, 200, 270 mm
POSITION OF MDD	MDD 4:	69, 276, 457, 685, 1059 mm
	MDD 6:	85, 277, 463, 685, 1070 mm
	MDD 10:	0, 200, 456, 684, 1059 mm
	MDD 12:	199, 455, 683, 877, 1057 mm

REPS	LOAD (kN)	PROF POINT 0-16	MDD 6, 10	MDD 4, 12, between wheels	MDD 4, 12, under wheels	RSD CL POINT 4,6,8,10,12	RSD 200 CS, 200 TS 4,8,12	TEMP HOURLY	CAM	NDG Surface	NDG In depth	Photos
10	40	yes	40	40	40	40	40	yes		yes	yes	yes
15000 (daily)	40	yes	40	40		40		yes				
30000	40	yes	40	40	40	40		yes				
45000	40	yes	40	40		40		yes				
60000	40	yes	40	40	40	40		yes				
90000	40	yes	40	40		40		yes				
120000	40	yes	40	40	40	40		yes				
150000	40	yes	40	40	40	40		yes				yes
170000	40 to 80	yes	40	40	40	40	40	yes				
205000	80	yes	40	40	40	40	40	yes				
225000	80	yes	40	40		40		yes				
260000	80	yes	40	40		40		yes				
317000	80 to 100	yes	40, 80, 100	40, 80, 100	40, 80, 100	40, 80, 100	40, 80, 100	yes		yes	yes	yes
353000	100	yes	40, 80, 100	40, 80, 100	40, 80, 100	40, 80, 100	40, 80, 100	yes				
400000	100	yes	40, 100	40, 100		40, 100	40, 100	yes				
450000	100	yes	40, 100	40, 100		40, 100	40, 100	yes				
500000	100	yes	40, 100	40, 100	40, 100	40, 100	40, 100	yes				
If steady state phase has been reached weekly readings can be made, if not continue at 50,000 rep intervals												
weekly until failure	100	yes	40, 100	40, 100	40, 80	40, 100	40, 100 every 2nd week	monthly		monthly	every 2nd month	every 2nd week until close to target and then weekly
Crack initiation	100	yes	40, 80, 100	40, 80, 100	40, 80, 100	40, 80, 100	40, 80, 100	yes	yes	yes	yes	yes
Take complete set of readings after crack initiation and reduce interval between data capture to daily for 2 days												
Failure	100	yes	40, 80, 100	40, 80, 100	40, 80, 100	40, 80, 100	40, 80, 100	yes	yes	yes	yes	yes

HVS Test Plan	Updated 1/10/97	515RF (Overlay of 502CT)
SECTION DESCRIPTION	Drained Section with 38-mm ARHM-GG overlay	
TIRE PRESSURE	720 kPa (105 psi)	
TRAFFIC LOAD	40 kN, 80 kN, 100 kN	
TIRE TYPE	Radial dual	
TEMPERATURE CONTROL	16-24°C	

POSITION OF THERMOCOUPLES	Position 4, 8, 12	Depth 0, 50, 108, 193, 270 mm
POSITION OF MDD	MDD 4:	47, 277, 463, 595, 1070 mm
	MDD 6:	85, 277, 463, 595, 1070
	MDD 10:	0, 200, 456, 684, 1059
	MDD 12:	50, 200, 456, 684, 1059

REPS	LOAD (kN)	PROF POINT 0-16	MDD 6, 10	MDD 4, 12, between wheels	MDD 4, 12, under wheels	RSD CL POINT 4,6,8,10,12	RSD 200 CS, 200 TS 4,8,12	TEMP HOURLY	CAM	NDG Surface	NDG In depth	Photos
10	40	yes	40	40	40	40	40	yes		yes	yes	yes
15000 (daily)	40	yes	40	40		40		yes				
30000	40	yes	40	40	40	40		yes				
45000	40	yes	40	40		40		yes				
60000	40	yes	40	40	40	40		yes				
95612	40	yes	40	40		40		yes				
128774	40 to 80	yes	40, 80	40, 80	40, 80	40, 80	40, 80	yes				
153785	80	yes	40	40		40		yes				yes
184030	80	yes	40	40	40	40		yes				
200000	80	yes	40	40		40		yes				
225000	80	yes	40	40	40	40		yes				
250000	80 to 100	yes	40, 80, 100	40, 80, 100	40, 80, 100	40, 80, 100	40, 80, 100	yes		yes	yes	yes
275000	100	yes	40, 80, 100	40, 80, 100	40, 80, 100	40, 80, 100	40, 80, 100	yes				
300000	100	yes	40, 100	40, 100		40, 100	40, 100	yes				
350000	100	yes	40, 100	40, 100		40, 100	40, 100	yes				
400000	100	yes	40, 100	40, 100	40, 100	40, 100	40, 100	yes				
If steady state phase has been reached weekly readings can be made, if not continue at 50,000 rep intervals												
weekly until failure	100	yes	40, 100	40, 100	40, 80	40, 100	40, 100 every 2nd week	monthly		monthly	every 2nd month	every 2nd week until close to target and then weekly
Crack initiation	100	yes	40, 80, 100	40, 80, 100	40, 80, 100	40, 80, 100	40, 80, 100	yes	yes	yes	yes	yes
Take complete set of readings after crack initiation and reduce interval between data capture to daily for 2 days												
Failure	100	yes	40, 80, 100	40, 80, 100	40, 80, 100	40, 80, 100	40, 80, 100	yes	yes	yes	yes	yes

HVS Test Plan			Updated July 1998						517RF (Overlay of 501RF)			
SECTION DESCRIPTION			Undrained section with 75-mm DGAC overlay									
TIRE PRESSURE			720 kPa (105 psi)									
TRAFFIC LOAD			40 kN, 80 kN, 100 kN									
TIRE TYPE			Radial dual									
TEMPERATURE CONTROL			16-24°C									
POSITION OF THERMOCOUPLES			Position 4, 8			Depth 0, 50, 75, 141, 207 mm						
POSITION OF MDD			MDD 4:			83, 218, 487, 701, 1074 mm						
			MDD 6:			83, 233, 495, 709, 1082 mm						
			MDD 9:			0, 232, 504, 718, 1091 mm						
			MDD 12:			219, 491, 705, 877, 1078 mm						
REPS	LOAD (kN)	PROF POINT 3-13	MDD 6, 9	MDD 4, 12	RSD CL POINT 4,6,8,10,12	RSD 200 CS, 200 TS 4,8,12	TEMP HOURLY	CAM	NDG Surface	NDG In depth	Photos	
10		40 yes		40	40	40	40 yes		yes	yes	yes	
15000 (daily)		40 yes					yes					
30000		40 yes					yes					
60000 (2 days)		40 yes		40	40	40	40 yes					
every 2nd day		40 yes					yes					
etc		40 yes					yes					
stable phase	40 to 80	yes		40	40	40	40 yes					
next day		80 yes					yes					
3rd day		80 yes		40	40	40	40 yes					
every 2nd day		80 yes					yes					
stable phase	80 to 100	yes	40, 80, 100	40, 80, 100	40, 80, 100	40, 80, 100	yes		yes	yes	yes	
day 1		100 yes					yes					
day 2		100 yes	40, 100	40, 100	40, 100	40, 100	yes					
every 2nd day		100 yes	40, 100	40, 100	40, 100	40, 100	yes					
flattens out		100 yes	40, 80, 100	40, 80, 100	40, 80, 100	40, 80, 100	yes					
If steady state phase has been reached weekly readings can be made, if not continue at 50,000 rep intervals												
every 2nd week to cracking		100 yes	40, 100	40, 100	40, 100	40, 100 every 4th week	yes					
Crack initiation		100 yes	40, 80, 100	40, 80, 100	40, 80, 100	40, 80, 100	yes	yes	yes	yes	yes	
Take complete set of readings after crack initiation and reduce interval between data capture to daily for 2 days, weekly for 2 weeks and then every 2nd week again and take pictures every time CAM readings are taken (every 2nd week)												
every 2nd week		100 yes	40, 100	40, 100	40, 100	40, 100 every 4th week	yes	yes			yes when doing CAM	
Failure		100 yes	40, 80, 100	40, 80, 100	40, 80, 100	40, 80, 100	yes	yes	yes	yes	yes	

HVS Test Plan			Updated July 1998						518RF (Overlay of 503RF)			
SECTION DESCRIPTION			Undrained section with 75-mm DGAC overlay									
TIRE PRESSURE			720 kPa (105 psi)									
TRAFFIC LOAD			40 kN, 80 kN, 100 kN									
TIRE TYPE			Radial dual									
TEMPERATURE CONTROL			16-24°C									
POSITION OF THERMOCOUPLES			Position 4, 8									
POSITION OF MDD			MDD 4: MDD 6: MDD 9: MDD 12:									
REPS	LOAD (kN)	PROF POINT 3-13	MDD 6, 9		MDD 4, 12	RSD CL POINT 4,6,8,10,12	RSD 200 CS, 200 TS 4,8,12	TEMP HOURLY	CAM	NDG Surface	NDG In depth	Photos
10	40	yes		40		40	40	yes		yes	yes	yes
15000 (daily)	40	yes						yes				
30000	40	yes						yes				
60000 (2 days)	40	yes		40		40	40	yes				
every 2nd day	40	yes						yes				
etc	40	yes						yes				
stable phase	40 to 80	yes		40		40	40	yes				
next day	80	yes						yes				
3rd day	80	yes		40		40	40	yes				
every 2nd day	80	yes						yes				
stable phase	80 to 100	yes	40, 80, 100		40, 80, 100	40, 80, 100	40, 80, 100	yes		yes	yes	yes
day 1	100	yes						yes				
day 2	100	yes	40, 100		40, 100	40, 100	40, 100	yes				
every 2nd day	100	yes	40, 100		40, 100	40, 100	40, 100	yes				
flattens out	100	yes	40, 80, 100		40, 80, 100	40, 80, 100	40, 80, 100	yes				
If steady state phase has been reached weekly readings can be made, if not continue at 50,000 rep intervals												
every 2nd week to cracking	100	yes	40, 100		40, 100	40, 100	40, 100 every 4th week	yes				
Crack initiation	100	yes	40, 80, 100		40, 80, 100	40, 80, 100	40, 80, 100	yes	yes	yes	yes	yes
Take complete set of readings after crack initiation and reduce interval between data capture to daily for 2 days, weekly for 2 weeks and then every 2nd week again and take pictures every time CAM readings are taken (every 2nd week)												
every 2nd week	100	yes	40, 100		40, 100	40, 100	40, 100 every 4th week	yes	yes			yes when doing CAM
Failure	100	yes	40, 80, 100		40, 80, 100	40, 80, 100	40, 80, 100	yes	yes	yes	yes	yes